



The  
University  
Of  
Sheffield.

**Multilayer poly(glycerol sebacate urethane) scaffold with biomimetic properties for oral mucosa tissue engineering**

**By:**

Andreas Samourides

A thesis submitted in partial fulfilment of the requirements for the degree of  
Doctor of Philosophy

The University of Sheffield  
Faculty of Engineering  
Department of Materials Science and Engineering

September 2018

## **Declaration**

I hereby declare that this thesis is my own work and effort, and that this thesis has not been submitted to another university in full or in part for another degree or qualification. Where other sources of information have been used, they have been acknowledged. Permission has been granted from copyright holders to replicate figures or data within this thesis.

Andreas Samourides

Sheffield, September 2018

This thesis is dedicated to my parents.

## **Acknowledgments**

I would like to thank my supervisors, Dr Vanessa Hearnden and Professor Biqiong Chen, for their enormous help and support to develop the necessary research skills and critical thinking. I would also like to thank my initial supervisor Dr Chuh K Chong and the University of Sheffield for securing me the University of Sheffield Tuition fee waiver that allowed me to perform this research. Despite the difficulties that I had at the beginning of my PhD, Professor Biqiong Chen and Dr Vanessa Hearnden, provided me with all the knowledge and expertise required to finish my PhD.

Thank you to Dr Martin Frydrych for mentoring me through almost everything I know about polymer synthesis and freeze drying, which without his knowledge and techniques I would not achieve what I present in this thesis. Thank you to Dr Le Ma for training me on using scanning electron microscopy that played a major role in my experiments. I would also like to thank Ben Palmer that he trained me in Fourier transform infrared spectroscopy, differential scanning calorimetry and thermal gravimetric analysis. Thanks also go to Dr Sabiniano Roman that helped me for my initial mechanical testing, live/dead and Sirius red assays. I would also like to thank my assessors, Dr Ihtesham ur Rehman and Dr Gwendolen Reilly, that guided me towards the correct path during my first- and second-year viva.

My huge thanks go to Dr Vanessa Hearnden that taught me cell isolation and culture routines for human primary cells. Vanessa introduced me and passed me all her knowledge and expertise in tissue processing, wax embedding, sectioning and staining for histology and immunohistochemistry.

I am very grateful to Professor Biqiong Chen for supporting my ideas and allowing me to experiment while always providing me with valuable feedback. Biqiong

provided me with the facilities and the know-how to synthesise, fabricate and characterise the physical properties of my samples.

Sincere thanks go to Natalie Shirley and all my friends for always supporting me throughout my academic years and making my life as amazing as it is.

Finally, I would like to thank and recognise all the help and love from my parents, Demetres Samourides, Eleni Samouridou, and my sister Sonia Samouridou. Without them I would not be able to achieve what I achieved. Thank you very much.

## **Abstract**

Defects in the oral cavity, caused from gingival recessions, trauma, chronic infections and oral cancer, have demonstrated a great challenge to treat because of the limitation of donor oral tissue. Oral mucosa tissue engineering is a science that aims to engineer a three-dimensional oral mucosa able to reconstruct the native oral mucosa tissue to treat defects in the oral cavity. Within the tissue engineering field biomaterials are used, called scaffolds, to support and promote the cell growth. Until now, no synthetic scaffolds have been used for oral mucosa tissue engineering clinically. Thus, the aim of this thesis was to develop synthetic poly(glycerol sebacate urethane) (PGSU) scaffolds that mimic the native oral mucosa's structure for potential oral mucosa tissue graft.

Large three-dimensional PGSU scaffolds were successfully fabricated, demonstrating high porosity and water permeability. The freeze drying protocol was characterised, illustrating that the pore size, pore structure and mechanical properties can vary significantly between different protocols. However, the porosity and water permeability were not affected by the freeze drying protocol. The scaffolds were sterilised and found that these scaffolds were not affected by the sterilisation method, however, the microstructure and mechanical properties of the scaffold were not suitable for tissue engineering oral mucosa tissue.

To optimise both the microstructure and mechanical properties of the scaffold the polymer concentration was altered and the freeze drying technique improved. It was found that the pore size and porosity of the scaffolds could be closely controlled using these techniques which led to the generation of scaffolds with improved mechanical properties. The scaffolds made with higher polymer concentration had smaller pore

sizes and porosity but higher mechanical properties. The enhanced mechanical properties of the scaffolds were closer to the oral mucosa's biomechanical properties and it was demonstrated that the shape and strength of the scaffolds can be recovered after loading. During *in vitro* cell culture the cell metabolic activity significantly increased over time and the microstructure did not affect the metabolic activity but did affect the cell distribution. The cells could not penetrate the smaller pore size scaffolds; therefore the cell distribution was poor. Cells deposited significantly more collagen in scaffolds with higher porosity compared to those which were less porous during *in vitro* cell culture.

In the final chapter more complex scaffold structures were fabricated by combining freeze drying, mould technology and airbrushing fabrication techniques. Novel PGSU isotropic, anisotropic and hierarchical multilayer scaffolds were developed by altering the freeze drying mould while a two-layer scaffold with a layer that mimics the basement membrane of the oral mucosa was generated using airbrushing. The basement membrane-like layer of the scaffold successfully acted as a cell barrier with limited infiltration from the epithelium layer and a multilayer epithelium was evident after co-culture with oral fibroblasts. The collagen production from the multilayer scaffold was higher than the one-layer scaffolds characterised previously in this study.

In this thesis we fabricated a synthetic, elastomeric, biomimetic PGSU scaffold with potential to be used in oral mucosa tissue engineering and other areas of soft tissue engineering.

# Contents

Declaration .....	i
Acknowledgments.....	iii
Abstract .....	v
List of figures .....	xii
List of tables.....	xxvi
List of abbreviations.....	xxviii
Chapter 1 Literature Review .....	1
1.1. INTRODUCTION .....	1
1.2. ORAL MUCOSA .....	2
1.2.1. Structure of oral mucosa .....	2
1.2.2. Ultrastructure of oral mucosa .....	3
1.2.3. Biomechanical properties of oral mucosa .....	5
1.2.4. Reconstruction of oral mucosa defects.....	7
1.2.4.1. Graft source.....	7
1.2.4.2. Epithelial cell sheet engineering .....	7
1.2.4.3. 3D Tissue engineered oral mucosa .....	9
1.3. SCAFFOLDS IN TISSUE ENGINEERING .....	15
1.3.1. General properties .....	15
1.3.2. Scaffold characterisation .....	17
1.3.2.1. External morphology .....	18
1.3.2.2. Surface properties .....	18
1.3.2.3. Scaffold architecture: Pore size, shape, porosity and interconnectivity.....	19
1.3.2.3.1. Mimicking basement membrane matrices .....	21
1.3.2.4. Degradation rate.....	23
1.3.2.5. Mechanical properties.....	24
1.3.3. Oral mucosa scaffold properties.....	25
1.3.4. Biomaterials .....	26
1.3.4.1. Natural biomaterials.....	26
1.3.4.2. Synthetic biomaterials.....	28
1.3.4.3. Natural vs synthetic biomaterials.....	31
1.4. POLY(GLYCEROL SEBACATE).....	33



1.4.1. Introduction to poly(glycerol sebacate).....	33
1.4.2. Poly(glycerol sebacate) scaffold preparation techniques .....	36
1.4.3. Poly(glycerol sebacate) modifications .....	43
1.4.4. Poly(glycerol sebacate urethane).....	44
1.5. SCAFFOLD FABRICATION .....	49
1.5.1. Freeze-drying .....	49
1.5.2. Airbrushing.....	52
1.6. SUMMARY OF LITERATURE REVIEW.....	52
1.7. AIMS AND OBJECTIVES .....	54
Chapter 2 Poly(glycerol sebacate urethane) synthesis, scaffold fabrication and effect of sterilisation method.....	57
2.1. INTRODUCTION .....	57
2.2. MATERIALS AND METHODS.....	58
2.2.1. Materials.....	58
2.2.2. Methods.....	59
2.2.2.1. Pre-PGS synthesis.....	59
2.2.2.2. Gel permeation chromatography of pre-PGS.....	59
2.2.2.3. PGSU-film and PGSU-2.5% fabrication .....	60
2.2.2.4. Scaffold sterilisation .....	63
2.2.2.5. Porous scaffold characterisation .....	63
2.2.2.5.1. Fourier transform infrared spectroscopy .....	63
2.2.2.5.2. Scanning electron microscopy.....	64
2.2.2.5.3. Porosity measurement.....	65
2.2.2.5.4. Mechanical testing.....	65
2.2.2.5.5. <i>In vitro</i> enzymatic degradation testing .....	65
2.2.2.5.6. Water contact angle .....	66
2.2.2.5.7. Permeability testing.....	67
2.2.2.6. Validation of cytocompatibility and sterilisation method.....	68
2.2.2.6.1. L929 cell culture.....	68
2.2.2.6.2. Sample preparation and cell seeding .....	69
2.2.2.6.3. Cell metabolic activity assays.....	69
2.2.2.6.3.1. MTT assay.....	70
2.2.2.6.3.2. Resazurin reduction assay .....	70
2.2.2.7. Statistical analysis.....	72
2.3. RESULTS.....	72

2.3.1. Pre-PGS and PGS characterisation.....	72
2.3.2. PGSU-2.5% scaffold characterisation.....	73
2.3.3. PGSU-2.5% fabrication characterisation – freezing temperature .....	79
2.3.4. PGSU scaffold - sterilisation effect.....	85
2.3.4.1. Physical properties .....	85
2.3.4.2. Cell metabolic activity .....	88
2.3.4.2.1. MTT assay .....	88
2.3.4.2.2. Resazurin reduction assay .....	89
2.4. DISCUSSION.....	91
2.5. CONCLUSION.....	100
Chapter 3 Biocompatible poly(glycerol sebacate urethane) scaffolds with controllable porous structures and mechanical properties .....	103
3.1. INTRODUCTION .....	103
3.2. MATERIALS AND METHODS.....	104
3.2.1. Materials.....	104
3.2.2. Methods.....	104
3.2.2.1. Pre-PGS synthesis.....	104
3.2.2.2. PGSU-5, 10, 15% scaffolds .....	105
3.2.2.2.1. Aluminium tray mould .....	105
3.2.2.2.2. Random orientation PGSU scaffolds.....	105
3.2.2.3. Porous scaffold characterisation .....	107
3.2.2.4. Microstructure effect on cell viability.....	108
3.2.2.4.1. Sample preparation and cell seeding .....	108
3.2.2.4.2. Resazurin reduction assay .....	108
3.2.2.5. Histology.....	109
3.2.2.6. Sirius red staining .....	109
3.2.2.7. Statistical analysis.....	110
3.3. RESULTS.....	110
3.3.1. Characterisation of PGSU scaffold .....	110
3.3.1.1. ATR-FTIR of PGSU scaffolds.....	110
3.3.1.2. Microstructure of the PGSU scaffolds .....	111
3.3.1.3. Mechanical Properties.....	114
3.3.1.4. <i>In vitro</i> enzymatic degradation .....	115
3.3.1.5. Scaffold permeability .....	116
3.3.2. Long term cell culture .....	117

3.3.2.1. Cell activity .....	118
3.3.2.2. Collagen content .....	120
3.4. DISCUSSION.....	122
3.5. CONCLUSIONS .....	132
Chapter 4 Hierarchical multilayer poly(glycerol sebacate urethane) scaffolds to replicate native tissues .....	134
4.1. INTRODUCTION .....	134
4.2. MATERIALS AND METHODS.....	137
4.2.1. Materials.....	137
4.2.2. Methods.....	137
4.2.2.1. Pre-PGS synthesis.....	137
4.2.2.2. PGSU-5, 10, 15% scaffolds .....	137
4.2.2.2.1. Aluminium tray with PTFE mould .....	138
4.2.2.2.2. Controlled orientation PGSU scaffolds .....	138
4.2.2.2.3. Multilayer PGSU scaffolds.....	139
4.2.2.2.4. Mould characterisation – polymer solution freezing rate .....	141
4.2.2.2.5. Multilayer scaffold characterisation .....	142
4.2.2.3. Oral mucosa <i>in vitro</i> cell culture experiments .....	142
4.2.2.3.1. OKF6 cell culture .....	142
4.2.2.3.2. Normal oral keratinocytes cell culture.....	143
4.2.2.3.3. Normal tonsil fibroblasts cell culture .....	144
4.2.2.3.4. Oral cells co-culture.....	144
4.2.2.3.4.1. OKF6 attachment on PGSU-film .....	144
4.2.2.3.4.1.1. Live/Dead staining .....	144
4.2.2.3.4.2. NOK attachment on PGSU-film.....	145
4.2.2.3.4.3. PGSU-BM sample preparation.....	145
4.2.2.3.4.4. Preparation of de-epithelialised dermis.....	146
4.2.2.3.5. Histology .....	147
4.2.2.3.6. Immunohistochemistry .....	147
4.2.2.4. Statistical analysis.....	148
4.3. RESULTS.....	148
4.3.1. Mould characterisation – polymer solution freezing rate.....	148
4.3.2. Microstructure of PGSU scaffolds .....	151
4.3.3. Oral mucosa <i>in vitro</i> cell culture .....	170
4.3.3.1. OKF6 cell attachment on PGSU-film .....	170

4.3.3.2. NOK attachment on PGSU-films.....	174
4.3.3.3. Dynamic seeding.....	174
4.3.3.4. Human oral cells co-culture .....	176
4.4. DISCUSSION.....	178
4.5. CONCLUSION.....	187
Chapter 5 Conclusions and suggestions for future work .....	189
5.1. CONCLUSIONS.....	189
5.2. FUTURE WORK.....	194
References .....	198

## List of figures

- Figure 1.1: Schematic of the general structure of oral mucosa; A) histological sample of oral mucosa taken from human patients and B) tissue engineered oral mucosa constructs using de-epithelialised dermis [2]. (ECM = extracellular matrix) Scale bar is 200  $\mu\text{m}$ . Reprinted by permission from Springer Nature, Colley et al. [2], copyright 2011.....3
- Figure 1.2: Schematic of the epidermal basement membrane. Adapted from Stanely et al. [11] with permission from Elsevier, copyright 1982. ....5
- Figure 1.3: Oral Mucosa tissues from the lingual and buccal aspects of human lower jaw.....7
- Figure 1.4: Oral mucosa epithelial cell sheet using temperature-responsive culture dish. Source: <http://www.dentistry.bham.ac.uk/admissions/page1.asp> ....9
- Figure 1.5: *Ex vivo* produced oral mucosa equivalent (EVPOME) illustrating its tensile strength. Adapted from Izumi et al. [1] with permission from Elsevier, copyright 2003. ....10
- Figure 1.6: Schematic of oral mucosa and skin demonstrating the similarities between tissue layers. Adapted from Evans et al. [47] with permission from Elsevier, copyright 2017. ....15
- Figure 1.7: (a) Images of tissue development in three-dimensional matrix channels. Actin stress fibres were stained with phalloidin-FITC and visualised using confocal microscopy. (i) Triangular (ii) Square (iii) hexagonal and (iv) circular shape. (b) shows with red dotted lines the tissue development at three time point (1 = early time point and 3 = latest time point). Adapted from Rumpler et al. [77] with permission from Royal Society, copyright 2008.....21

Figure 1.8: Schematic showing the summary of biocompatibility pathways between biomaterial and the defensive, target and interfering cells with their relevant clinical outcomes. Adapted from Williams D. [117] with permission from Elsevier, copyright 2014. ....	32
Figure 1.9: The synthesis and chemical structure of PGS. Reprinted from Li et al. [121] with permission from SAGE JOURNALS, copyright 2014.. ....	33
Figure 1.10: SEM images of PGS scaffolds fabricated with micromoulding. (A) Top view, (B) 60° angle view, (C) pore view at 30° angle and (D) edge view at 60° angle. Reprinted from Neeley et al. [125] with permission from Elsevier, copyright 2008. ....	39
Figure 1.11: SEM images of (a) accordion-like, (b) square and (c) rectangular honeycomb PGS scaffolds made using laser microablation. Scale bar is 100 µm. Reprinted with permission from Springer Nature: Engelmayr et al. [134], copyright 2008. ....	40
Figure 1.12: Micro-CT (a,b) and digital (c,d) images of PGS scaffold fabricated using solid freeform fabrication. (a) side view, (b) top view, (c) side view, (d) top view. Reprinted from Kemppainen et al. [143] with permission from John Wiley and Sons, copyright 2010. ....	41
Figure 1.13: SEM image of PGS/PLLA core/shell nanofibres. Reprinted from Yi et al. [133], with permission from John Wiley and Sons, copyright 2008. ....	42
Figure 1.14: SEM image of PGS scaffold fabricated using porogen leaching. Reprinted from Radisic et al. [139], with permission from John Wiley and Sons, copyright 2007. ....	42

Figure 1.15: *In vitro* enzymatic degradation of PGSU films synthesised using different reactants ratio and cured PGS. Reprinted from Pereira et al. [147], with permission from John Wiley and Sons, copyright 2012. ....44

Figure 1.16: (A) FTIR spectroscopy analysis of PGS and PGSU, (B) summary of the mechanical properties of PGSU, (C) representative stress-strain curves of PGSU and cured PGS, (D) stress-strain curve of PGSU during 100 cyclic loading cycles. PGSU-SF = solvent free synthesis, PGSU-S = with solvent synthesis, YM = Young’s modulus, UTS = ultimate tensile strength, EL = elongation at break. Reprinted from Pereira et al. [147], with permission from John Wiley and Sons, copyright 2012.....45

Figure 1.17: Ultimate Tensile strength of PGSU obtained from literature. Horizontal lines indicate the maximum and minimum UTS of oral mucosa dependent on the location. Data used in this figure were obtained from [16, 147] and plotted by the author.....46

Figure 1.18: Young’s modulus of PGSU obtained from literature. Horizontal lines indicate the maximum and minimum Young’s Modulus of oral mucosa dependent on the location. Data used in this figure were obtained from [16, 147] and plotted by the author. ....46

Figure 1.19: *In vivo* subcutaneous and cardiac biocompatibility and biodegradation of PGSU films. (A) Histological images and anti-CD68 stained subcutaneous tissue, comparison between PGSU and PLGA. (B) characterisation of foreign body response during *in vivo* study (0 mean no infiltration and 4 severe infiltration). (C) *in vivo* biodegradation of PGSU at different reactant ratios, (D) Cross section SEM images during degradation (scale bar = 50  $\mu$ m). (E) H&E stained sections during myocardium implantation

(M = myocardium). (F) Cardiac function before and after PGSU implantation. Reprinted from Pereira et al. [147], with permission from John Wiley and Sons, copyright 2012.....	48
Figure 1.20: Normal freeze drying cycle during scaffold fabrication. The schematic is not scaled.....	50
Figure 1.21: Three-phase diagram of water derived from the data provided from National Institute of Standards and Technology (NIST, <a href="https://webbook.nist.gov/cgi/cbook.cgi?ID=C7732185&amp;Units=SI&amp;Mask=4#Thermo-Phase">https://webbook.nist.gov/cgi/cbook.cgi?ID=C7732185&amp;Units=SI&amp;Mask=4#Thermo-Phase</a> ). $T_{tp}$ : Triple point temperature, $P_{tp}$ : Triple point pressure. ....	51
Figure 2.1: Pre-PGS synthesis setup. ....	59
Figure 2.2: Synthesis of pre-PGS and PGSU polymer. ....	60
Figure 2.3: Freeze drying cycle for PGSU-2.5% scaffolds. The 1,4-dioxane/polymer solution was frozen at 3 different temperatures, 0 °C, -20 °C or -50 °C, and lyophilised the same way. ....	62
Figure 2.4: Three-phase diagram of 1,4-dioxane derived from the data provided from National Institute of Standards and Technology (NIST, <a href="https://webbook.nist.gov/cgi/cbook.cgi?ID=C123911&amp;Mask=4#Thermo-Phase">https://webbook.nist.gov/cgi/cbook.cgi?ID=C123911&amp;Mask=4#Thermo-Phase</a> ). $T_{tp}$ : Triple point temperature, $P_{tp}$ : Triple point pressure. The purple circle shows the temperature and pressure of the 1,4-dioxane during primary drying in the freeze drier. ....	62
Figure 2.5: Schematic of synthesis and fabrication method for PGSU-2.5% scaffolds. ....	63



Figure 2.6: Example of pore size measurements using ImageJ. A) Shows an example of how the scale of the SEM image is set into the software and (B) is a representation of how the pores were selected using the freehand tool.	64
Figure 2.7: Schematic of permeability test setup using the constant head method. dH <sub>2</sub> O is distilled water, H is constant head length, L is scaffold thickness and Q is flow rate. The schematic is not scaled.	68
Figure 2.8: Macroscopic images of (A) pre-PGS and (B) cured PGS film.	72
Figure 2.9: FTIR spectra of pre-PGS and cured PGS. (A) vertically shifted and (B) overlapped spectra. n=3	73
Figure 2.10: Macroscopic images of PGSU-2.5% scaffolds. (A) Top, (B) cross section and (C) bottom.	74
Figure 2.11: ATR-FTIR spectra of pre-PGS and PGSU-2.5% scaffolds. Scaffolds were examined before prior ethanol extraction and post ethanol extraction and compared between them and against pre-PGS that served as a control. FTIR was also carried out for the HDI. n=3.	75
Figure 2.12: SEM images of PGSU-2.5% scaffolds taken from A1-2) top, B1-2) cross and C1-2) bottom section.	76
Figure 2.13: PGSU-2.5% scaffold cross section from top to bottom.	76
Figure 2.14: Pore size of PGSU-2.5% scaffolds. Results are shown as mean ± standard deviation. (n=50 and *** when p < 0.001)	77
Figure 2.15: Representative tensile strength - strain curve of PGSU-2.5% scaffolds.	78
Figure 2.16: PGSU film and scaffold enzymatic degradation over 28 days period. Results are shown as mean ± standard deviation. (n=3, *** when p < 0.001 compared with PBS and PGSU-film)	79

Figure 2.17: SEM images of PGSU-2.5% scaffolds frozen at 0 °C taken from A1-2) top, B1-2) cross and C1-2) bottom section. ....80

Figure 2.18: SEM images of PGSU-2.5% scaffolds frozen at -50 °C taken from A1-2) top, B1-2) cross and C1-2) bottom section .....81

Figure 2.19: Pore sizes of PGSU-2.5% scaffolds frozen at different temperature, 0 °C, -20 °C and -50 °C. Results are shown as mean ± standard deviation. n=50, \*\*\* when  $p < 0.001$  between groups and ### when  $p < 0.001$  within groups (colours are used for # to distinguish the groups). .....82

Figure 2.20: Mechanical properties of PGSU-2.5% scaffolds frozen at different temperatures, 0 °C, -20 °C and -50 °C. Results are shown as mean ± standard deviation. (n=5, \*\* when  $p < 0.01$ , \*\*\* when  $p < 0.001$ ).....83

Figure 2.21: Water contact angle of cured PGS film, PGSU-film and PGSU-2.5% scaffold over a period of 60 seconds. A1-2) Cured PGS-film, B1-2) PGSU-film, C1-2) PGSU-2.5% scaffold and D) measured water contact angle. The water contact angle of PGSU-2/5% scaffold was 0° at 60 seconds. Results are shown as mean ± standard deviation. (n=3, \*\*\* when  $p < 0.001$ ) .....84

Figure 2.22: Permeability results measured from PGSU-2.5% scaffolds frozen at different temperature, 0 °C, -20 °C and -50 °C. Results are shown as mean ± standard deviation. n=3. ....85

Figure 2.23: FTIR spectra of PGSU-2.5% compared against their sterilisation method. ....86

Figure 2.24: Mechanical properties obtained from the porous PGSU-2.5% scaffolds compared against their sterilisation method. A) Representative tensile strength - strain curves, B) Young's modulus, C) ultimate tensile strength

and D) elongation at break. NS = non sterilised, EtOH = 70% ethanol, PAA = 0.1% paracetic acid. Results are shown as mean  $\pm$  standard deviation. n=5.....87

Figure 2.25: Permeability of PGSU-2.5% compared against their sterilisation method. Results are shown as mean  $\pm$  standard deviation. n=3.....88

Figure 2.26: MTT assay of (A) PGSU-2.5% scaffolds (B) and films normalised against the TCP. Results are shown as mean  $\pm$  standard deviation. n=3, \* when  $p < 0.05$ .....89

Figure 2.27: Normalised absorbance from the resazurin assays of PGSU-film and PGSU-2.5%. A) Metabolic activity of cells seeded on the PGSU-film. B) Metabolic activity from cells seeded on the PGSU-scaffold. Results are shown as mean  $\pm$  standard deviation. n=3, \*\* when  $p < 0.01$ , \*\*\* when  $p < 0.001$ .....90

Figure 2.28: Seeding efficiency achieved from seeding PGSU-2.5% scaffold and films. The asterisks signify the significant difference between PGSU-2.5% scaffold and film. Results are shown as mean  $\pm$  standard deviation, n=3, \* when  $p < 0.05$ .....90

Figure 3.1. Aluminium tray mould with 6 wells for random orientation (mould-random) scaffold fabrication. Scale bar is 5 cm..... 105

Figure 3.2. Synthesis and fabrication method schematic for PGSU scaffolds..... 106

Figure 3.3: Three-phase diagram of 1,4-dioxane derived from the data provided from National Institute of Standards and Technology (NIST, <https://webbook.nist.gov/cgi/cbook.cgi?ID=C123911&Mask=4#Thermo-Phase>). Ttp: Triple point temperature, Ptp: Triple point pressure. The

purple circle shows the temperature and pressure of the 1,4-dioxane during primary drying in the freeze drier. ....	106
Figure 3.4. Freeze drying cycle during the PGSU porous scaffolds fabrication procedure.....	107
Figure 3.5: ATR-FTIR spectra of pre-PGS and the PGSU scaffolds. All three polymer concentrations were examined and compared against pre-PGS that served as a control. FTIR was also carried out for the HDI. n=3. ....	111
Figure 3.6: Measured (A) pore size (n=50) and (B) porosity (n=5) of the PGSU scaffolds from three different sections. Results are shown as mean ± standard deviation, (A) n=5, *** when $p < 0.001$ between groups and ### when $p < 0.001$ within groups (colours are used for # to distinguish the groups); (B) n=5, *** when $p < 0.001$ . ....	112
Figure 3.7: SEM images of porous (A1-6) PGSU-5%, (B1-6) PGSU-10% and (C1-6) PGSU-15% scaffolds. ....	113
Figure 3.8: (A) Representative stress-strain curve, (B) Young’s modulus, (C) ultimate tensile strength, (D) elongation at break, (E) cyclic loading, and (F) suture retention strength of the PGSU scaffolds. Results are shown as mean ± standard deviation, n=5, * when $p < 0.05$ . ....	115
Figure 3.9: In-vitro enzymatic degradation of PGSU5%, 10% and 15% scaffolds. Samples were degraded in PBS as a control. Results are shown as mean ± standard deviation, n=3, *** when $p < 0.001$ . ....	116
Figure 3.10: Scaffold water permeability using the constant head method and Darcy's law. Results are shown as mean ± standard deviation, n=3, *** when $p <$ 0.001.....	117

- Figure 3.11: Resazurin assay of multiple cell seeding densities at day 1. Results are shown as mean  $\pm$  standard deviation, n=3, \* when  $p < 0.001$ ..... 118
- Figure 3.12: Seeding efficiency experiment calculated by the cell metabolic activity found on the scaffolds normalised against the TCP (positive control) on day 3 using resazurin assay. The statistical significance is shown against the TCP. Results are shown as mean  $\pm$  standard deviation, n=3, \*\*\* when  $p < 0.001$ ..... 118
- Figure 3.13: Cell activity of L929 cells seeded on PGSU-5%, 10% and 15% scaffolds measured by resazurin assay. (n=3, \*\*\* when  $p < 0.001$ ) ..... 119
- Figure 3.14: Histological analysis (H&E staining) of the cell seeded PGSU scaffolds for all three concentrations (A) PGSU-5%, (B) PGSU-10% and (C) PGSU-15% after 15 days L929 culture..... 120
- Figure 3.15: Standard curve of Sirius red on known amounts of collagen type I isolated from rat tail. A magnification of the standard curve is also shown to indicate with a vertical dotted line where the limit of detection (LOD) and limit of quantitation (LOQ) are. (n=3) ..... 120
- Figure 3.16: (A) Collagen content as a percentage of the dry sample's mass deposited by L929 cells after 15 days of culture. SEM images of (B) PGSU-5%, (C) PGSU-10% and (D) PGSU-15% from the cross section area of the scaffolds after culture. Results are shown as mean  $\pm$  standard deviation, n=3, \*\* when  $p < 0.01$ ..... 122
- Figure 3.17: Representative images showing the scaffolds after picosirius red staining, which stains collagen with red dye A shrinkage is observed for the PGSU-5%, due to its weaker mechanical properties and higher

collagen content. Negative control were acellular scaffolds. Scale bar is 10 mm..... 122

Figure 4.1. Inhouse designed moulds with aluminium base and PTFE walls for multiple orientation scaffold fabrication. (A) Top view of the mould-vertical, (B) side view of mould-vertical, (C) top view of mould-horizontal and (D) side view of mould-horizontal. Scale bar is 5 cm. .... 138

Figure 4.2: Schematic showing the moulds and the locations that the temperature probes were placed to quantify the freezing rate of the polymer solution. A) is the mould-random (asterisk: red = 0 mm, green = 5 mm, blue = 10 mm), B) is the mould-vertical (asterisk: red = 0 mm, green = 5 mm, blue = 10 mm) and C) is the mould-horizontal (asterisk: red = 0 mm, green = 20 mm, blue = 40 mm). The schematic is not scaled. .... 142

Figure 4.3: Image showing the PGSU-BM ready for dynamic seeding. The scaffolds are fixed in a surgical stainless-steel ring and overlaid with cell/media suspension. The well-plate was then placed in a sterile plastic bag with a syringe and a syringe filter to sterilise the returning air while ventilating. .... 146

Figure 4.4: Thermal profile of the PGSU/1,4-dioxane solution during freezing using the mould-random.  $T_m$  = melting point of 1,4-dioxane. The schematic represents the mould and the freezing direction of the polymer solution (schematic is not scaled). .... 149

Figure 4.5: Thermal profile of the PGSU/1,4-dioxane solution during freezing using the mould-vertical.  $T_m$  = melting point of 1,4-dioxane. The schematic represents the mould and the freezing direction of the polymer solution (schematic is not scaled). .... 150

Figure 4.6: Thermal profile of the PGSU/1,4-dioxane solution during freezing using the mould-horizontal.  $T_m$  = melting point of 1,4-dioxane. The schematic represents the mould and the freezing direction of the polymer solution (schematic is not scaled). ..... 151

Figure 4.7: SEM images of the PGSU-random scaffolds. A1-2) Top section, B1-2) bottom section and C1-2) cross section. The schematic demonstrates the plywood structure of the scaffold..... 152

Figure 4.8: SEM images of PGSU-vertical. A1-2) Top section and B1-2) cross section. The schematic demonstrates the plywood structure of the scaffold. .... 153

Figure 4.9: PGSU-vertical pore size measured from the top and cross section. Results are shown as mean  $\pm$  standard deviation, n=50, \* when  $p < 0.05$ ..... 154

Figure 4.10: Water permeability of the PGSU-vertical. The anisotropic structure of the scaffold was examined by measuring the permeability parallel (longitudinal) and perpendicular to the pore direction. Results are shown as mean  $\pm$  standard deviation, n=3..... 154

Figure 4.11: SEM images of PGSU-horizontal. A1-2) Top section, B1-2) bottom section and C1-2) cross section. The schematic demonstrates the plywood structure of the scaffold..... 156

Figure 4.12: PGSU-horizontal pore size measured from the top, cross section and bottom of the scaffold. Results are shown as mean  $\pm$  standard deviation, n=50..... 157

Figure 4.13: Water permeability of PGSU-horizontal. The anisotropic structure was examined by measuring the permeability parallel (longitudinal) and perpendicular to the pore direction. Results are shown as mean  $\pm$  standard deviation, n=3, \*\*\* when  $p < 0.001$ ..... 157

Figure 4.14: SEM images of PGSU-bilayer. A1-2) Top section, B1-2) bottom section and C1-3) cross section (C2 = PGSU-15% and C3 = PGSU-10%). The schematic demonstrates the plywood structure of the scaffold..... 159

Figure 4.15: PGSU-bilayer pore size measured from the top, cross section (CS) and bottom. Since it is consisted of two layers the top and bottom layers of the scaffold were measured separately. Results are shown as mean  $\pm$  standard deviation, n=50, \*\*\* when  $p < 0.001$ ..... 160

Figure 4.16: Water permeability of PGSU-bilayer measured longitudinal to the scaffold. Results are shown as mean  $\pm$  standard deviation, n=3..... 160

Figure 4.17: PGSU-BM fabricated with different airbrushing techniques. (A1-2) 1 ml of polymer solution was sprayed and frozen at  $-20^{\circ}\text{C}$  before freeze drying (PGSU-BM(1)), (B1-2) 1 ml polymer solution was sprayed and frozen in liquid nitrogen before freeze drying (PGSU-BM(2)), (C1-2) 1 ml of polymer solution was sprayed and left in room temperature to dry (PGSU-BM(4)), (D1-2) 2 ml of polymer solution was sprayed and frozen in liquid nitrogen before freeze drying (PGSU-BM(3)) and (E1-2) 2 ml of polymer solution was sprayed and left in room temperature to dry (PGSU-BM(5)). The schematic demonstrates the plywood structure of the scaffold. .... 163

Figure 4.18: SEM images of PGSU-BM(4). A1-2) Top section, B1-2) Bottom section and C1) cross section. The schematic demonstrates the plywood structure of the scaffold..... 164

Figure 4.19: PGSU-BM pore size was measured from the cross section and bottom of the scaffold. Results are shown as mean  $\pm$  standard deviation, n=50... 165

Figure 4.20: Water permeability of the PGSU-BM measured longitudinal to the scaffold. Results are shown as mean  $\pm$  standard deviation, n=3..... 165



Figure 4.21: SEM images of PGSU-trilayer. A1-2) Top section, B1-2) Bottom section and C1-4) cross section. (C3 = PGSU-15% and C4 = PGSU-10%). The schematic demonstrates the plywood structure of the scaffold..... 167

Figure 4.22: PGSU-trilayer pore size was measured from the cross section (CS) and bottom. Since the scaffold is consisted of three layers and the first layer is low porosity, the other two layers were measured and plotted separately. CS = cross section. Results are shown as mean  $\pm$  standard deviation, n=50, \*\*\* when  $p < 0.001$ ..... 168

Figure 4.23: Water permeability of the PGSU-trilayer measured longitudinal to the scaffold. Results are shown as mean  $\pm$  standard deviation, n=3. .... 168

Figure 4.24: Water permeability of all PGSU scaffolds fabricated for this chapter. Statistical significance was found in all multiple comparison cases, except PGSU-trilayer vs PGSU-bilayer. Results are shown as mean  $\pm$  standard deviation, n=3, \*\*\* when  $p < 0.001$ ..... 169

Figure 4.25: PGSU films seeded with OKF6. (A) The absorbance obtained from OKF6 cultured on PGSU films and TCP which served as the positive control; (B) Normalised absorbance against the positive control (TCP) of the resazurin assay for all 9 days, Results are shown as mean  $\pm$  standard deviation, n=3 in triplicates, \*\*\* when  $p < 0.001$ ..... 171

Figure 4.26: Images taken from the samples after resazurin assay at each time point. A) day 3, B) day 6 and C) day 9. PC = positive control, cells cultured on TCP; NC = negative control, acellular films..... 171

Figure 4.27: OKF6 cells cultured on PGSU-film for 9 days and stained with live/dead assay. A1-2) TCP, B1-2) PGSU-film, C1-2) NC, D1-2) autofluorescence

of TCP and E1-2) autofluorescence of PGSU with the corresponding excitation/emission wavelengths. The scale bars are 200  $\mu\text{m}$ ..... 173

Figure 4.28: PGSU films seeded with NOK cells. (A) The absorbance obtained from NOK cultured on PGSU films and TCP which served as the positive control; (B) Normalised absorbance against the positive control (TCP) of the resazurin assay for all 9 days, Results are shown as mean  $\pm$  standard deviation, n=3 in triplicates, \*\*\* when  $p < 0.001$ ..... 174

Figure 4.29: Histology (H&E) of PGSU-10% scaffolds seeded with L929 fibroblasts using (A1 and A2) Static (B1 and B2) Vacuum seeding. Scale bar is 50  $\mu\text{m}$ . n=3. .... 175

Figure 4.30: Collagen produced on the scaffolds measured using Sirius red and standardised using the standard curve in chapter 3. The results are demonstrated as a percentage of collagen mass per dry sample's mass. Results are shown as mean  $\pm$  standard deviation, n=3..... 176

Figure 4.31: Collagen produced on the scaffolds measured using Sirius red and standardised using the standard curve in Chapter 3. The results are demonstrated as percentage of collagen mass against the scaffolds dry mass. PGSU-5% is from Chapter 3 and is there for comparison reasons. Results are shown as mean  $\pm$  standard deviation, n=3, \*\*\* when  $p < 0.001$ . .... 177

Figure 4.32: Representative sections from PGSU-BM samples after cell co-culture with NTF and NOK. A1-2) are PGSU-BM stained with H&E, B1-2) immunohistochemically stained PGSU-BM with AE1/AE3. n=3. Scale bar is 100  $\mu\text{m}$ ..... 178

## List of tables

Table 1.1: The tensile properties and stress relaxation data obtained from Gakto et al. studying Porcine Oral Soft Tissue [16]. The results are shown as mean $\pm$ SD at n=9.....	6
Table 1.2: Summary of the results from the scaffolds tested in Moharamzadeh et al. [30]. PET = Poly(ethylene terephthalate) membrane (pore size 3.0 $\mu$ m); PC = Polycarbonate membrane (pore size 3.0 $\mu$ m); PLLA = Poly L-lactic acid scaffold; PS = Polystyrene scaffold; CGC = Collagen-glycosaminoglycan-chitosan scaffold. Adapted by permission from Moharamzadeh et al. [30]: Springer Nature, copyright 2007. ....	12
Table 1.3: PGS scaffold fabrication techniques review table. ....	39
Table 2.1: Gel permeation chromatography results from pre-PGS. <i>Mn</i> , <i>Mw</i> and PDI are number average molecular weight, weight average molecular weight and polydispersity index respectively. ....	72
Table 2.2: Pore size and porosity of PGSU-2.5% scaffolds. Results are shown as mean $\pm$ standard deviation. (n=50 for pore size and n=3 for porosity, *** when $p < 0.001$ ) .....	77
Table 2.3: Porosity of PGSU-2.5% scaffolds frozen at different temperatures. Results are shown as mean $\pm$ standard deviation. n=3.....	82
Table 3.1: Collagen content and dry sample mass measured on each sample group. The ratio was then calculated and demonstrated as collagen concentration per dry sample mass. Results are shown as mean $\pm$ standard deviation, n=3, ** when $p < 0.01$ .....	122
Table 4.1: PGSU-BM airbrushing conditions.....	140
Table 4.2: Antibodies and antigen retrieval conditions used in this study.....	148

Table 4.3: Summary of the different moulds and scaffolds demonstrated in this  
chapter.....169

## List of abbreviations

2D	Two-dimensional
3D	Three-dimensional
AE1/3	Cytokeratin antibody
AM	Amniotic membrane
AT	Achilles tendon
ATE	Adipose tissue engineering
ATR	Attenuated total reflection
bFGF	basic Fibroblast growth factors
BM	Basement membrane
BS EN ISO	British, European and International standards
CS	Cross section
DAB	3'-diaminobenzidine tetrahydrochloride
DED	De-epithelialised dermis
DMEM	Dulbecco's modified eagle's medium
ECM	Extra cellular matrix
EDTA	Ethylenediaminetetraacetic
EGF	Epidermal growth factors
EVPOME	Ex vivo produced oral mucosa equivalent
FCS	Fetal calf serum
FDA	Food and Drug Administration
FT-IR	Fourier transform infrared spectroscopy
GPC	Gel permeation chromatography
H&E	Haematoxylin and eosin

HDI	Hexamethylene diisocyanate
i3T3	Irradiated mouse fibroblasts
ISO	International organization for standardization
KSFM	Keratinocyte - SFM media
L929	Immortalised mouse fibroblast cell line
Mould-horizontal	Mould to produce horizontal anisotropic scaffolds
Mould-random	Mould to produce isotropic scaffolds
Mould-vertical	Mould to produce vertical anisotropic scaffolds
MSCs	Mesenchymal stem cells
MTT	3-(4,5-dimethylthiazol-2-yl)-2,5-diphenyltetrazolium bromide
NEAA	Non-essential amino acids
NOK	Normal oral keratinocytes
NTF	Normal tonsil fibroblasts
OD	Optical density
OKF6	Immortalised human oral keratinocytes
OMTE	Oral mucosa tissue engineering
P/S	Penicillin-streptomycin
PAA	Poly(acrylic acid)
PAA	Paracetic acid
PBS	Phosphate-buffered saline
PCL	Poly( $\epsilon$ -caprolactone)
PDI	Polydispersity index
PDMS	Polydimethylsiloxane
PEG	Poly(ethylene glycol)

PEGT/PBT	Poly(ethylene glycol terephthalate)-poly(butylene terephthalate) co-polymer
PGA	Poly(glycolic acid)
PGS	Poly(glycerol sebacate)
PGS/PLLA	Poly(glycerol sebacate)/polylactic acid polymer blend
PGSA	Poly(glycerol sebacate) acrylate
PGSM	Poly(glycerol sebacate) methacrylate
PGSU	Poly(glycerol sebacate urethane)
PGSU-2.5%	Poly(glycerol sebacate urethane) scaffold with 2.5% polymer concentration(w/v%)
PGSU-5%	Poly(glycerol sebacate urethane) scaffold with 5% polymer concentration(w/v%)
PGSU-10%	Poly(glycerol sebacate urethane) scaffold with 10% polymer concentration(w/v%)
PGSU-15%	Poly(glycerol sebacate urethane) scaffold with 15% polymer concentration(w/v%)
PGSU-bilayer	Poly(glycerol sebacate urethane) two-layer scaffold
PGSU-BM	Poly(glycerol sebacate urethane) two-layer scaffold with basement membrane like layer
PGSU-film	Poly(glycerol sebacate urethane) film
PGSU-horizontal	Poly(glycerol sebacate urethane) scaffold with horizontal anisotropic porous structure
PGSU-random	Poly(glycerol sebacate urethane) scaffold with random isotropic porous structure
PGSU-trilayer	Poly(glycerol sebacate urethane) three-layer scaffold

PGSU-vertical	Poly(glycerol sebacate urethane) scaffold with vertical anisotropic porous structure
PHBV	Poly(hydroxybutyrate-co-hydroxyavalerate)
PI	Propidium iodide
PLA	Poly(lactic acid)
PLGA	Poly(lactic-co-glycolic acid)
PLLA	Poly(lactic acid)
Pre-PGS	Poly(glycerol sebacate) prepolymer
PTFE	Polytetrafluoroethylene
PU	Polyurethane
PVA	Poly(vinyl alcohol)
SAM	Self-assembling monolayers
SD	Standard deviation
SEM	Scanning electron microscopy
TCP	Tissue culture plastic
TE	Tissue engineering
THF	Tetrahydrofuran
TIPS	Thermal induced phase separation
UTS	Ultimate tensile strength



## Chapter 1 Literature Review

### 1.1. Introduction

Tissue Engineering (TE) is a multidisciplinary field, aiming towards regenerating or replacing disordered and malfunctioned tissues or organs [3]. This field is based on the ability of the cells to adhere, migrate, proliferate and metabolise to a specific tissue *in vivo* and *in vitro*. In addition, a synthetic and/or biological biomaterial, known as scaffold, is used to provide the cells with a three-dimensional (3D) structure for the cells to be seeded within their structure and apply their physiological/biological ability. The cells will then start developing their extra cellular matrix which will replace the biodegradable scaffold [4]. Both cells and scaffold have been and still are under extensive research on how they affect the tissue generation and the method that the cell seeded scaffold is being cultured *in vitro* is of critical importance. Both parameters, cells and scaffold, depend on the tissue that is being engineered, because dissimilar tissues are constructed with different cells, different structure and under different biological environment. In this project the focus is on oral mucosa tissue engineering (OMTE). The development of a tissue engineered oral mucosa will aid in replacing soft tissue defects found in the oral cavity such as gingival recessions or defects resulting from trauma, chronic infections and oral cancer. Treating wounds in the oral cavity has been a challenge due to limitation of donor oral tissue. Since this science aims to replace dysfunctional or damaged organs, it is of critical importance to mimic the properties of the native tissue. The optimum objective of multiple research groups is to engineer a 3D oral mucosa able to reconstruct the native oral tissue when needed. To do this a scaffold that is biocompatible, biodegradable and

mechanically stable is necessary. This project will investigate a polymer based on poly(glycerol sebacate) (PGS) because of its physical and biological properties.

## 1.2. Oral mucosa

### 1.2.1. Structure of oral mucosa

Oral mucosa is the lining of the oral cavity. It consists of a thick stratified squamous epithelium that overlies the lamina propria, which is attached at the basement membrane. The epithelium functions by protecting the underlying tissue from mechanical damage as it can withstand considerable friction [5]. The lamina propria is comprised of fibroblasts, capillaries, inflammatory cells and extra cellular matrix (ECM), and it functions by providing resistance to tear and compression forces maintaining the integrity of the tissue. The native structure of oral mucosa is shown in Figure 1.1, along with histology images of human oral mucosa and a tissue engineered oral mucosa made using de-epithelialised dermis (DED). Another important function of oral mucosa is that when injured it produces antimicrobial peptides called defensins, not allowing the entry of microorganisms and toxic substances into the body [6]. Oral mucosa at different regions of the oral cavity has different properties, for example, more strength is required at the hard palate and gingiva, and more elasticity at lips, cheek and floor of the mouth. Additionally, depending on the function of the region, the epithelium of oral mucosa is keratinised (masticatory mucosa), non-keratinised (lining mucosa) or both (specialised mucosa) for example the dorsum of the tongue. The keratinisation is there to give extra protection against abrasion during eating, and it is found on gingiva, hard palate and the dorsum of the tongue. The non-keratinised regions are those that require flexibility as mentioned previously [7, 8].

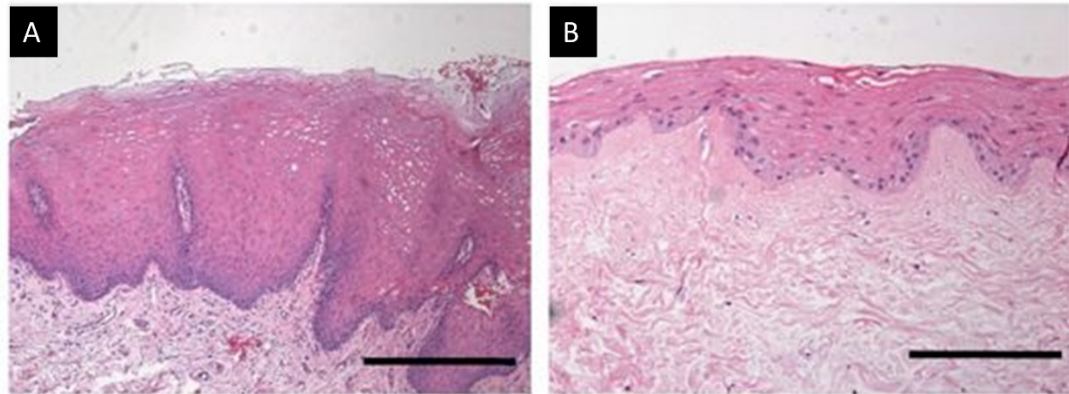
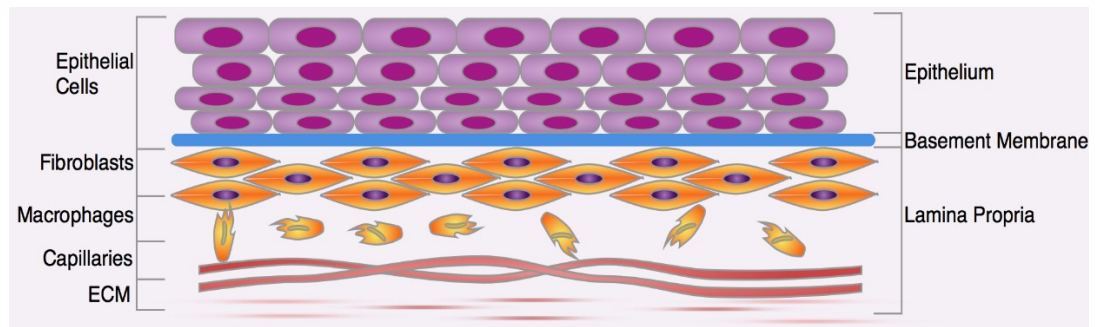


Figure 1.1: Schematic of the general structure of oral mucosa; A) histological sample of oral mucosa taken from human patients and B) tissue engineered oral mucosa constructs using de-epithelialised dermis [2]. (ECM = extracellular matrix) Scale bar is 200  $\mu\text{m}$ . Reprinted by permission from Springer Nature, Colley et al. [2], copyright 2011.

## 1.2.2. Ultrastructure of oral mucosa

The epithelium of oral mucosa is composed by different cell layers that have various degrees of differentiation called basal layer, spinous layer, granular or intermediate layer (keratinised or non-keratinised epithelium) and keratinised layer [8]. The cells within the basal layer of the epithelium are responsible for cell division and production. These cells are the smallest ones and least differentiated forming one or two layers in the epithelium. While the cells differentiate, they move to the spinous layer where they increase in size and change shape obtaining more desmosomes and keratin filaments. For the granular or intermediate layer the cells are flattened and have a high percentage of keratin filaments [8]. Again, depending on the location of the oral mucosa the epithelium's thickness is different. The mucosa lining the cheek has the

## Chapter 1

thickest epithelium,  $540 \pm 90 \mu\text{m}$ , where the thickness of the hard palate and the floor of the mouth is  $310 \pm 50 \mu\text{m}$  and  $190 \pm 40 \mu\text{m}$  respectively [9].

The basement membrane is the location where the epithelium and the lamina propria attach. The epithelium is attached by hemidesmosomal attachment of the basal cells to a basal lamina, where the lamina propria is attached by anchoring fibrils (collagen VII) to collagen fibres of lamina propria [9]. Its functionality is to orchestrate growth factor-mediated extracellular communication, cellular adhesion, migration and differentiation [10]. The basement membrane consists of two layers, the lamina lucida and lamina densa, shown in Figure 1.2. The lamina lucida is responsible for cell attachment and acts as a permeability barrier, whereas lamina densa is responsible for structure support [11]. Lamina lucida is 15 – 65 nm thick and is mainly composed of laminin, a large asymmetric molecule containing three A chains and one B chain, that facilitates cell attachment [11, 12]. The lamina densa is 15 – 125 nm thick and is mainly composed of proteoglycan and collagen IV, which proteoglycan blocks the passage of some anionic macromolecules and collagen IV provide the basic scaffold of the basement membrane [11-13]. The effect that fibroblasts have on the basement membrane formation was studied in Ghalbzouri et al. [14] and they showed that fibroblasts induced the expression of a great variety of basement membrane proteins, including collagen IV and laminin [14]. Furthermore, it was found that laminin is expressed by keratinocytes only when fibroblasts are present, signifying the importance of co-culture for tissue generation [14].

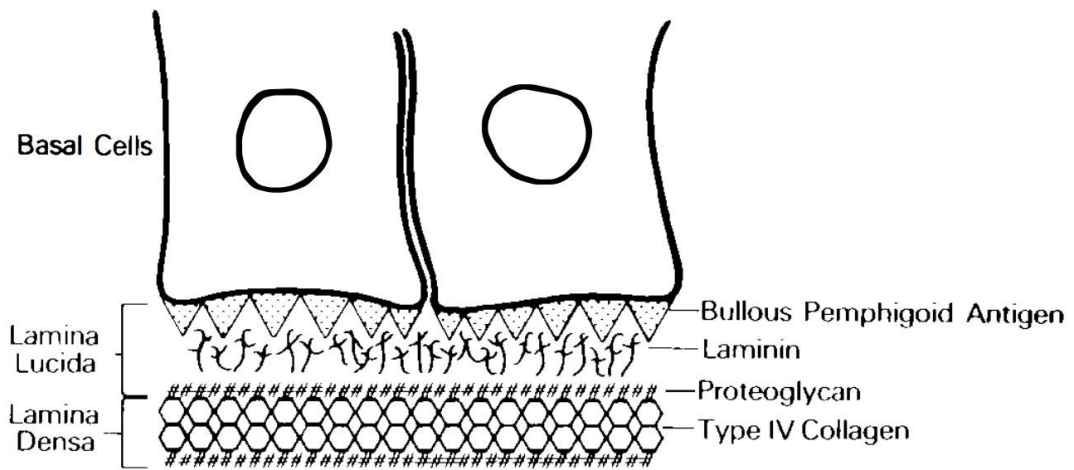


Figure 1.2: Schematic of the epidermal basement membrane. Adapted from Stanely et al. [11] with permission from Elsevier, copyright 1982.

Last, the lamina propria is comprised of fibroblasts and occasionally macrophages, plasma cells, mast cells and lymphocytes [15]. The fibroblasts function by producing collagen type I, III, V and VI fibres [8].

### 1.2.3. Biomechanical properties of oral mucosa

Oral mucosa tissue is subjected to a variety of mechanical forces such as compression, elongation, friction and hydrodynamic forces. These forces are generated by normal everyday actions, including mastication, teeth brushing, speech and saliva flow. These mechanical properties are dependent on the location of the mucosa. There is limited descriptive analysis published describing the biomechanical properties of oral mucosa. However, Goktas et al, have investigated the mechanical behaviour of porcine oral soft tissues, that morphologically and histologically resemble human oral soft tissue [16]. They showed that the attached gingiva, which is firmly attached to the underlying cementum and alveolar bone, is significantly stiffer and has higher resistance to stress, than in other regions. This occurs because the attached oral mucosa is keratinised. Table 1.1, shows the biomechanical properties obtained from the above-mentioned study, and Figure 1.3 is a diagram of the oral cavity indicating the location of the

# Chapter 1

lingual and buccal mucosae mentioned in the table. The highest ultimate tensile strength (UTS) and Young's modulus is found on buccal attached gingiva ( $3.94 \pm 1.19$  MPa and  $19.75 \pm 6.20$  MPa respectively) which is located at the side gum. The lowest UTS and Young's modulus ( $1.06 \pm 0.10$  MPa and  $2.48 \pm 0.37$  MPa respectively) is observed on buccal mucosa, the tissue located immediately adjacent to the side lips.

Table 1.1: The tensile properties and stress relaxation data obtained from Gakto et al. studying Porcine Oral Soft Tissue [16]. The results are shown as mean  $\pm$  SD at n=9.

<u>Region</u>	<u>Tensile Properties</u>			<u>Stress Relaxation Data</u>	
	Failure Load (N)	Tensile Strength (MPa)	Young Modulus (MPa)	Initial Stress (MPa)	Equilibrium Stress (MPa)
Lingual attached gingiva	$10.89 \pm 2.74$	$2.83 \pm 0.99$	$18.83 \pm 5.98$	$1.88 \pm 0.11$	$0.97 \pm 0.08$
Buccal attached gingiva	$19.74 \pm 5.04$	$3.94 \pm 1.19$	$19.75 \pm 6.20$	$1.84 \pm 0.23$	$0.96 \pm 0.14$
Lingual alveolar mucosa	$10.54 \pm 2.18$	$1.72 \pm 0.51$	$4.79 \pm 2.54$	$0.25 \pm 0.03$	$0.1 \pm 0.01$
Buccal alveolar mucosa	$8.93 \pm 2.06$	$1.29 \pm 0.19$	$5.74 \pm 1.15$	$0.21 \pm 0.02$	$0.09 \pm 0.01$
Buccal mucosa	$9.08 \pm 1.66$	$1.06 \pm 0.10$	$2.48 \pm 0.37$	$0.39 \pm 0.03$	$0.19 \pm 0.03$

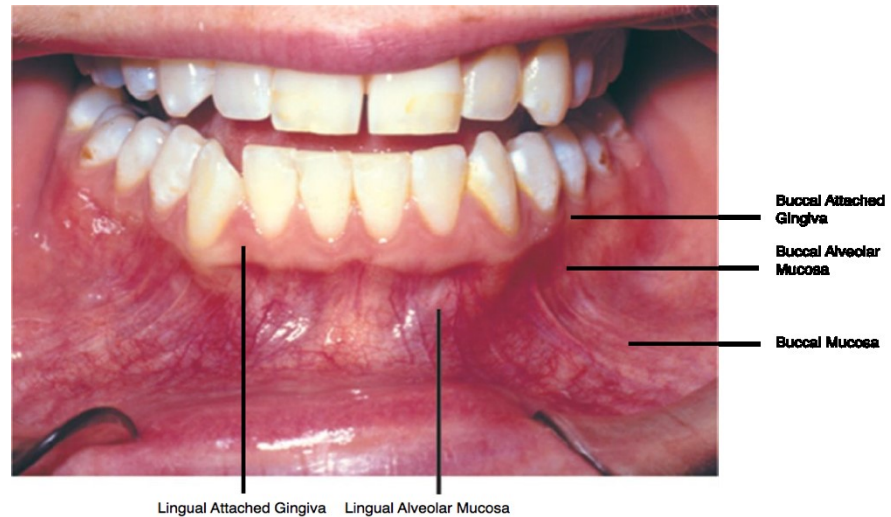


Figure 1.3: Oral Mucosa tissues from the lingual and buccal aspects of human lower jaw.

## 1.2.4. Reconstruction of oral mucosa defects

### 1.2.4.1. Graft source

Usually to reconstruct oral mucosa defects, transplants obtained from the inner cheek and the palate are used [17]. The transplantation is done by firstly dissecting the diseased or injured mucosa using CO<sub>2</sub> gas laser and then securing the transplants onto the defect using 7-0 nylon sutures [18]. However as mentioned previously the oral tissue is limited in size and quantity, hence when extensively needed, skin tissue and intestinal mucosa are commonly used. Using this alternative grafts has two disadvantages, the donor site morbidity and negligible assimilation [19]. This assimilation occurs because of the difference between properties of the skin and oral mucosa, such as the pattern of keratinisation and hair growth [20]. These disadvantages produced the need of an alternative defect reconstruction approach, which tissue engineering researchers are currently investigating.

### 1.2.4.2. Epithelial cell sheet engineering

Following success of epidermal cell sheets fabricated for skin defects, researchers started applying similar techniques to grow oral epithelial cell sheets *in vitro*. Cell

## Chapter 1

sheet engineering is a TE methodology without using a scaffold. There are multiple techniques for oral mucosa cell sheet engineering; the most popular are culturing on amniotic membranes (AM), on collagen membranes and on temperature responsive culture dishes [18, 21, 22].

Amniotic membrane attracted a high interest as a cell culture substrate. It was found multiple times that it can excellently facilitate *in vitro* cell proliferation, differentiation and functional organisation [18]. AM is a thin parenchymal tissue that surrounds the surface of placenta, that has distinctive characteristics such as anti-infection and anti-inflammatory properties [23, 24]. It was used as a cell culture substrate by Amemiya et al. [18]. They cultured oral mucosal epithelial cells and they used them as grafts to five patients. A 12-month follow-up study showed good cell differentiation and the cells had stratified from five to seven layers. This indicates that AM based epithelial cell sheets can be a useful method for oral mucosa reconstruction [18], however, more research is necessary.

The epithelial cell sheets, made from any of the above cell culture substrates, have the great advantage of having high regenerative capabilities allowing a rapid healing without forming a scar [25]. It has been reported that epithelial sheets were formed in 12 days and maintained *in vitro* for 30 days [26]. Results obtained from clinical trials were again successful in accelerating healing of oral mucosa defects having a smooth keratinised region. For example, a cultured epithelial sheet was used to cover the mouth floor after partial resection due to tongue cancer, and 10 days after normal oral mucosa was formed [20]. In another study, epithelial cell sheets cultured *in vitro* for 14 days with autologous oral cells were used to transplant on the palatal mucosa, and 3 weeks later there were no clinical differences observed. The same observation was



## Chapter 1

further evaluated 3 months after transplantation. Additionally, in both studies mentioned no infections or scar contractions were found [20, 27].

Nevertheless, the epithelial cell sheets have a disadvantage of being fragile, making them difficult to handle and not possible to fill deep defects [28]. Therefore, bioengineers moved on to developing 3D oral mucosa equivalents.

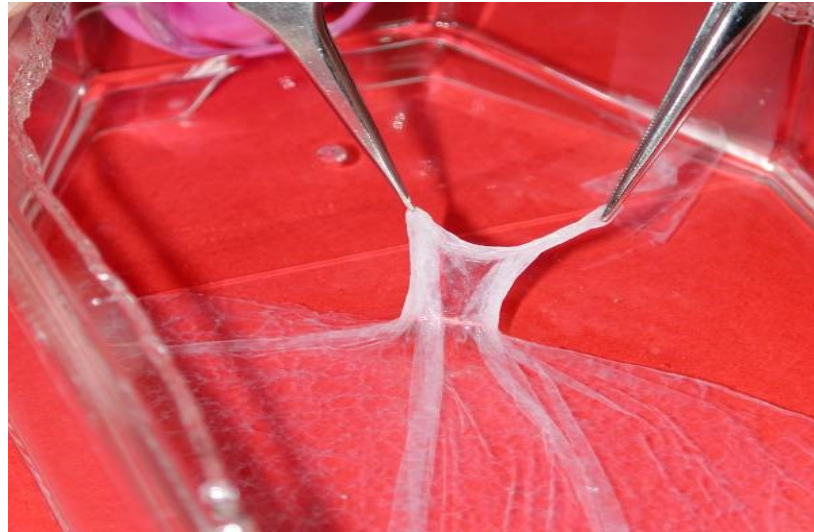


Figure 1.4: Oral mucosa epithelial cell sheet using temperature-responsive culture dish. Source: <http://www.dentistry.bham.ac.uk/admissions/page1.asp>

### 1.2.4.3. 3D Tissue engineered oral mucosa

3D tissue engineered grafts are usually fabricated using a scaffold seeded with oral keratinocytes and fibroblasts. In this case these 3D models can fill deep defects, resembling the complex structure of the oral mucosa's native tissue, having epithelium, lamina propria and a basement membrane between them, high degree of differentiation and ability to histologically assess the tissue development process [29]. These 3D tissue engineered grafts are substantially superior in terms of their tensile

strength compared to the epithelial cell sheets mentioned previously, which can be seen comparing Figure 1.4 and Figure 1.5.



Figure 1.5: *Ex vivo* produced oral mucosa equivalent (EVPOME) illustrating its tensile strength. Adapted from Izumi et al. [1] with permission from Elsevier, copyright 2003.

Multiple scaffolds have been used for reconstructing full-thickness oral mucosa, including animal dermis, acellular cadaver dermis from human skin and synthetic polymeric scaffolds [28, 30-32]. The animal dermis and cadaver scaffolds lacked fibroblasts, and this affected the lamina propria development. Additionally, it was found that fibroblasts promote epithelial cells to grow and differentiate, along with the formation of a basement membrane [29, 33]. An *in vivo* study has been attempted by Ophof et al. [34] using acellular dermis and autologous epithelial cells, transplanted in dogs. During their study they concluded that probably due to insufficient vascularisation of the graft the healing was not better compared to control incisions. A clinically successful tissue engineered oral mucosa graft was demonstrated by Izumi et al [1]. Their *ex vivo* produced oral mucosa equivalent (EVPOME) was composed using AlloDerm® (or allogenic human acellular dermis) with autologous epithelial cells, shown in Figure 1.5. The result was better and faster healing compared to AlloDerm® alone. Non-keratinised oral mucosa was also developed using epithelial cells isolated from the cheek based on collagen-glycosaminoglycan-chitosan scaffold

## Chapter 1

[35]. They demonstrated that a 9-10 layers thick epithelium was developed under specific culture conditions, which were 7 days culture with their sample fully submerged in media followed by 14 days culture at the air-liquid interface [35]. They also concluded that this biomimicity was obtained because of the interaction between fibroblasts of lamina propria and epithelial cells of oral mucosa.

These full thickness oral mucosa equivalents have also been used for *in vitro* cytotoxicity testing of oral care products, and even for urethral reconstruction with successful results [36, 37]. Another study aiming to generate a tissue engineered oral mucosa equivalent, compared three different commercially available scaffolds, Tissufoil E (collagen membrane from purified collagen I), dermal regeneration template (porous matrix of fibres made from crosslinked bovine tendon collagen and glycosaminoglycan) and Vicryl (woven polyglycin which is the copolymer of glycolide and lactide) [38]. To test these scaffolds, they cultured human oral cells, keratinocytes and fibroblasts, up to 20 days and examined the tissue development using histology and immunohistochemistry. They concluded that the dermal regeneration template scaffold was more suitable for generating an oral mucosa tissue equivalent, due to better combination of fibroblast cell growth and keratinocytes stratification [38]. Aiming to develop a full-thickness oral mucosa model for biological assessment of dental biomaterials, Moharamzadeh et al. [30] compared the suitability of 10 different scaffolds (shown in Table 1.2 below) evaluating their biocompatibility, biostability, porosity, and ability to mimic native oral mucosa morphology. Their conclusions were that collagen-glycosaminoglycan-chitosan (CGC) scaffold demonstrated a differentiated and reproducible oral mucosa model which reflected native oral mucosa [30].

# Chapter 1

Table 1.2: Summary of the results from the scaffolds tested in Moharamzadeh et al. [30]. PET = Poly(ethylene terephthalate) membrane (pore size 3.0  $\mu\text{m}$ ); PC = Polycarbonate membrane (pore size 3.0  $\mu\text{m}$ ); PLLA = Poly L-lactic acid scaffold; PS = Polystyrene scaffold; CGC = Collagen-glycosaminoglycan-chitosan scaffold. Adapted by permission from Moharamzadeh et al. [30]: Springer Nature, copyright 2007.

Scaffold	Biocompatibility	Biostability	Porosity/thickness	Epithelial morphology
<b>Collagen type I</b>	Good	Less than 2 weeks	Poor fibroblast infiltration into scaffold	Multi-layer on compact areas and epithelial islands on porous areas
<b>Cross-linked collagen type I</b>	Good	Good	Same as above	Same as above
<b>Bilayer collagen types I and III</b>	Good	Less than 3 weeks	Too thick	Keratinocyte multi-layer
<b>Collagen-elastin</b>	Good	Good	Very poor porosity	Thin epithelial layer
<b>PET and PC membrane</b>	Good	Good	No 3D matrix for fibroblast support	2-3 layers of keratinocytes
<b>Electrospun PLLA</b>	Good	Good	Good	Multi-layer in laminated scaffold, island formation in non-laminated scaffold

<b>Electrospun PS</b>	Good	Good	Larger pore size than PLLA	Thin epithelial layer
<b>Agarose gel</b>	Poor cell adhesion	N/A	N/A	No epithelium present
<b>CGC</b>	Good	Good	Good	Multi-layer stratified epithelium

Simsek et al. [39], fabricated three synthetic scaffolds and compared them with natural dermis (Euroskin). Using electrospinning they fabricated scaffolds composed of either microfibrinous poly(lactic acid) (PLA); nanofibrous poly(3-hydroxybutyrate-co-3-hydroxyvalerate) (PHBV); and a micro-/nanofibrous trilayer of PLA-PHBV-PLA. These three synthetic scaffolds and Euroskin were seeded with oral keratinocytes and fibroblasts and in terms of metabolic activity there was no significant difference between them during the 28 days *in vitro* cell culture [39]. They concluded their work by suggesting that their trilayer (PLA-PHBV-PLA) scaffold presented a good alternative to allodermis because it was suitable for oral keratinocyte and fibroblast growth with good cell viability and minimal contraction as well as it had good mechanical properties [39].

Due to large similarities of oral mucosa and skin (Figure 1.6) it is worth mentioning some of the advances in skin TE. Skin is the largest organ of the human body. Its functionality is to protect the human body from the surrounding environment by forming a barrier that keeps pathogens and microorganisms from entering the body [40]. The majority of skin TE applications are involved into healing acute and chronic wounds [41]. Due to its role the skin tissue is constantly exposed to microbes, thermal and mechanical stimuli and for this reason skin is composed from three layers,

## Chapter 1

epidermis, dermis and hypodermis. The epidermis is separated by a basement membrane from the dermis, and has a compact surface to permit water retention and reduce dehydration as well as protect itself from infection [42]. Skin tissue and oral mucosa have similar functions and epithelial structure. Both function as a protective barrier and are comprised from a stratified squamous epithelium and an underlying connective tissue. The oral mucosa has higher concentration of vasculature and permeability compared to skin and there is an absence of hair follicles and sweat glands [6]. The mechanical properties and cell architecture of the oral mucosa vary according to its location and functionality [6].

Developing scaffolds for skin tissue engineering is one of the most researched areas in tissue engineering [43-45]. Poly (ethyleneglycolterephthalate)- poly (butylene terephthalate) (PEGT/PBT) co-polymer was used in skin tissue engineering [45]. This biodegradable scaffold showed good mechanical properties, however the seeding of the scaffold was not ideal and fibroblast-populated collagen or fibrin was required to seed into the pores of the scaffold. To compare natural and synthetic dermal matrices a dermal scaffold composed of knitted poly(lactic-co-glycolic acid) (10:90)-poly( $\epsilon$ -caprolactone) (PLGA-PCL) mesh was fabricated. Human dermal fibroblasts were cultured on it for over 3 weeks. The synthetic mesh has demonstrated a better cell distribution and tissue formation compared to three natural scaffolds, equine collagen foam (TissuFleece®), acellular dermal replacement (Alloderm®) and chitosan scaffold. From these results they showed that physical characteristics such as porosity and mechanical stability are important to determine the success of dermal matrix material [46].

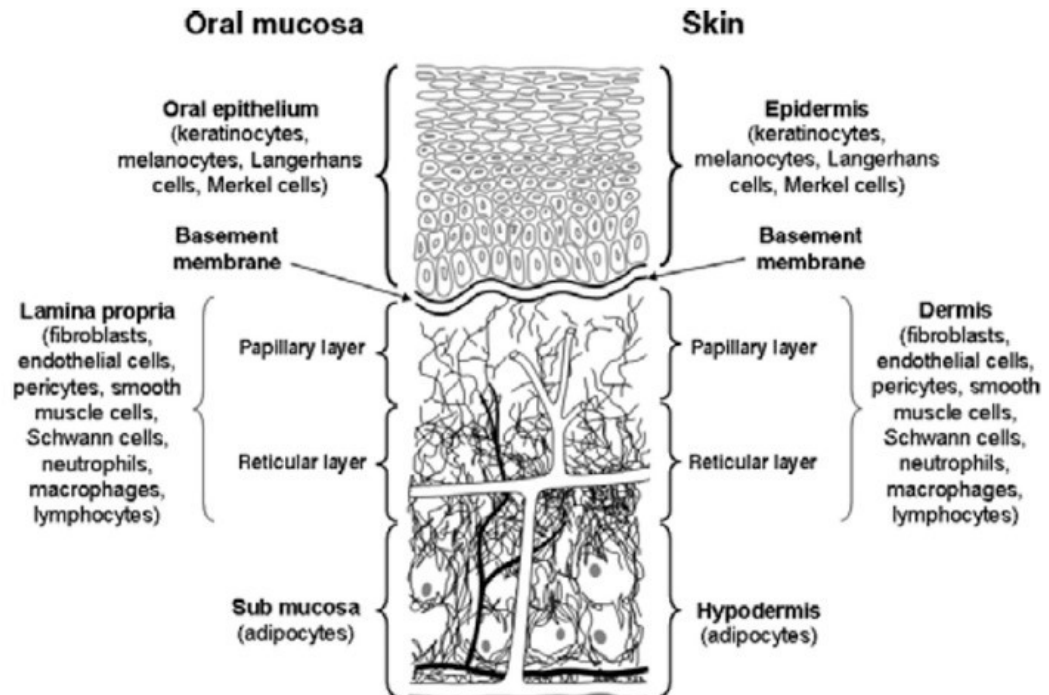


Figure 1.6: Schematic of oral mucosa and skin demonstrating the similarities between tissue layers. Adapted from Evans et al. [47] with permission from Elsevier, copyright 2017.

## 1.3. Scaffolds in tissue engineering

From the previous sections it was understood that the success of oral mucosa TE is somehow depended on the scaffold and its properties. Therefore, understanding individually each scaffold property is important when developing scaffolds for TE.

### 1.3.1. General properties

Several biomaterials have been used to produce scaffolds for TE and researchers have developed skin [45], oral mucosa [35], cartilage and bone [48], blood vessels [49], bladder [50], pancreas [51], nerves [52], adipose tissue [53] and various other soft tissues using synthetic, natural or combination scaffolds. All these scaffolds are designed so they possess the following properties:

- i) Biocompatible

## Chapter 1

This property is a primary criterion that all scaffolds should have. The scaffolds should be biocompatible without causing any toxic and inflammatory effects *in vivo*, promote cell adhesion, cell-biomaterial interaction and ECM deposition. The term biocompatible biomaterial has been changing over the past 50 years because it depends heavily on the intended application of the biomaterial. The 1<sup>st</sup> generation definition of biocompatibility was that a material is biocompatible when the material is less reactive chemically [54]. The 2<sup>nd</sup> generation definition of biocompatibility was derived after realising that (i) the response to specific materials could vary from one application site to another; (ii) sometimes the material should react with the tissue rather than be inert; and (iii) some applications required the material to be biodegradable. Therefore, they defined biocompatibility as “Biocompatibility refers to the ability of a material to perform with an appropriate host response in a specific situation” [54]. This definition was adequate to define both 2<sup>nd</sup> and 3<sup>rd</sup> generation biomaterials that included materials that could mimic physical and biological properties of tissues. However, due to the emergence of multiple uses of biomaterials (e.g. regenerative medicine, drug delivery, gene delivery etc) a new definition of biocompatibility has been proposed from Williams [54] stating that “Biocompatibility refers to the ability of a biomaterial to perform its desired function with respect to a medical therapy, without eliciting any undesirable local or system effects in the recipient or beneficiary of that therapy, but generating the most appropriate beneficial cellular or tissue response in that specific situation, and optimising the clinically relevant performance of that therapy” [54].

### ii) Biodegradable

As mentioned earlier, the scaffolds provide a temporary structure to the cells allowing them to produce their own ECM to replace it. Therefore, it should be biodegradable, ideally degrading at a rate that can vary to synchronise with the tissue development.



### iii) Mechanical properties

The scaffold should also be mechanically stable to be manipulated during surgical implantation. Additionally, it is beneficial when the scaffolds have mechanical properties similar to native tissues and are strong enough to withstand *in vivo* dynamic forces as for some tissues these forces are significantly strong, such as cartilage and bone.

### iv) Scaffold architecture

The scaffold architecture is one of the most important aspects to consider in tissue engineering, because the structure of the scaffold is what will allow the cell penetration and survival. There are four characteristics that are considered when characterising the scaffold architecture; pore size, pore shape, porosity and pore interconnectivity. These four characteristics work together to allow adequate transportation of nutrients, gas and wastes essential for cell viability, proliferation and differentiation

### v) Reproducible

The fabrication technique and the biomaterial should be reproducible and cost effective to allow this scaffold to be clinically and commercially viable.

Many if not all of the above mentioned properties that a scaffold should possess are affected by the biomaterial and fabrication method. Therefore, understanding the advantages and disadvantages of each available material and fabrication methods is of critical importance.

## 1.3.2. Scaffold characterisation

Characterising the scaffold is a necessity to successfully engineer a tissue. The characterisations required to fabricate 3D scaffolds that meet the properties mentioned previously are: a) external geometry, b) surface properties, c) pore size and porosity,

d) interface adherence and biocompatibility, e) biodegradation, and f) mechanical properties [55].

### **1.3.2.1. External morphology**

Beginning with the external geometry, as in most cases the scaffold should be mimicking the ECM structure and properties. The key role of ECM is to provide structural support and stability of the tissue. The same applies for the scaffold. Fabricating scaffolds, designing them with micro- and nano- scale architectures, has attracted high attention from tissue engineers, as this preciseness mimics the native ECM geometrical structure. Synthetic materials allow a versatile variety of external geometry characteristics to be produced. Most importantly a scaffold should be highly porous, with interconnected pores, have a high surface density; and high surface-to-volume ratio to promote cell attachment and proliferation [55].

### **1.3.2.2. Surface properties**

Surface properties involve the chemical and topographical characteristics of the scaffold which control the cell adhesion and proliferation [56, 57]. The surface of the scaffold is the site where the cells first interact, and since the proliferation of most cells used in TE is dependent on anchorage the scaffold's surface should allow their attachment. Studies have shown that cell adhesion always follows protein adsorption [58]. Surface chemistry affects the protein adsorption significantly, and there is a large number of functional groups that were characterised for cell adhesion, such as hydroxyl, carboxylic acid and amine groups [59, 60]. They used self-assembling monolayers (SAM) terminated with different functional groups to study the cell interaction. SAM are highly ordered surface coatings that can be coated on specific substrates [57]. Using human fibroblasts the carboxylic acid terminated SAM had similar cell adherence compared to tissue culture plastic (TCP) [59]. Another study

used SAM terminated with multiple functional groups and they found that human fibroblast adhered significantly better on the SAM terminated with amine groups as opposed to hydroxyl groups [57, 60]. The surface properties can be altered using surface chemical gradient, SAM, surface-active bulk additive and surface chemical reaction [57]. The properties that can be altered by surface modification are hydrophobicity/hydrophilicity, the ability to form covalent bonds and the formation of protective barriers. These modifications will then allow the control and improvement of cell adhesion, the bonding of reactive components and the cell response, making the scaffold more biocompatible allowing the cells to recognise it [61]. In most cases, immobilising the surface with biomolecules favours the functionality of the scaffold in TE. For example, the tri-amino acid arginine-glycine-aspartate (RGD) peptide has been used to direct cell attachment on multiple biomaterials (PEG [62], polycaprolactone [63], PLGA [64], polyurethane [65], collagen [63] and fibrin [66]) due to its functionality which is the principal integrin-binding domain within ECM proteins [67]. Additional biomolecules can be fibronectin, collagen and growth factors such as epidermal growth factors (EGF), basic fibroblast growth factors (bFGF) and insulin. Usually these biomolecules can be covalently attached, self-assembled or electrostatically absorbed on the scaffold's surface [68].

### **1.3.2.3. Scaffold architecture: Pore size, shape, porosity and interconnectivity**

While designing a scaffold for TE, characterising its porosity and pore size is important. A highly porous scaffold with interconnected pores will allow uniform cell distribution after seeding, cell ingrowth and enable neovascularisation [69]. While characterising the porosity of the scaffold, the characteristics that need to be examined are pore size and distribution, pore interconnectivity, pore volume, pore shape and pore wall roughness [70]. Many research papers have previously examined how pore

## Chapter 1

size affects tissue regeneration. There is a large degree of variation in the values found to be most effective, but examples include studies which show, that a pore size of 5  $\mu\text{m}$  is optimum for neovascularisation [71], 5-15  $\mu\text{m}$  for fibroblast growth and 20-125  $\mu\text{m}$  for regeneration of adult mammalian skin [72]. Chitosan scaffolds were fabricated with multiple pore sizes and porosities to characterize the effect that they have on fibroblasts [73]. The range of the pore size that these scaffolds exhibited was between 80 – 400  $\mu\text{m}$  and it was found that the scaffolds with  $\sim 190$   $\mu\text{m}$  and  $\sim 87\%$  porous had the highest cell metabolic activity during a 56 days cell culture [73]. These results are contrary to the collagen-glucosaminoglycan scaffolds with pore sizes 5-15  $\mu\text{m}$  that were found optimum for fibroblast growth [72] which indicate that maybe the material used has an effect as well. In addition, poly(l-lactic acid) scaffolds were fabricated with pore sizes ranging from 38 - 150  $\mu\text{m}$  and 90% porous, and when seeded and cultured with fibroblasts it was found that the scaffolds with 106 – 150  $\mu\text{m}$  had the highest metabolic activity but the lowest ECM deposition, which the highest was exhibited from the scaffold with  $< 38$   $\mu\text{m}$  pores [74]. Regarding neovascularisation, a study performed by the author of this thesis and others, demonstrated that the optimum pore size and porosity for angiogenesis and tissue ingrowth was 26.5  $\mu\text{m}$  and 96 % [75, 76]. Concerning pore shape, a study fabricated hydroxyapatite scaffolds with 4 different pore shapes (triangular, square, hexagonal and circular) aiming to investigate their effect on tissue growth. It was found that two geometrical parameters of the pore can affect the kinetics of tissue growth; the pore surface area (related to its perimeter) and the curvature of the pore [77]. For triangular, square and hexagonal shapes the tissue growth began from inside the angles of the pore to form a round central opening, whereas for the circular shaped pores the growth was simultaneous from the perimeter of the pore leading to a faster tissue growth, shown in Figure 1.7 below. Along with

the importance of the pore size and shape the interconnectivity plays a crucial role because cells need to be within 200  $\mu\text{m}$  from blood supply in order to allow gas and nutrient exchange [78]. In addition to this, for oral mucosa tissue engineering the lamina propria and epithelium need to be separated into two distinct layers.

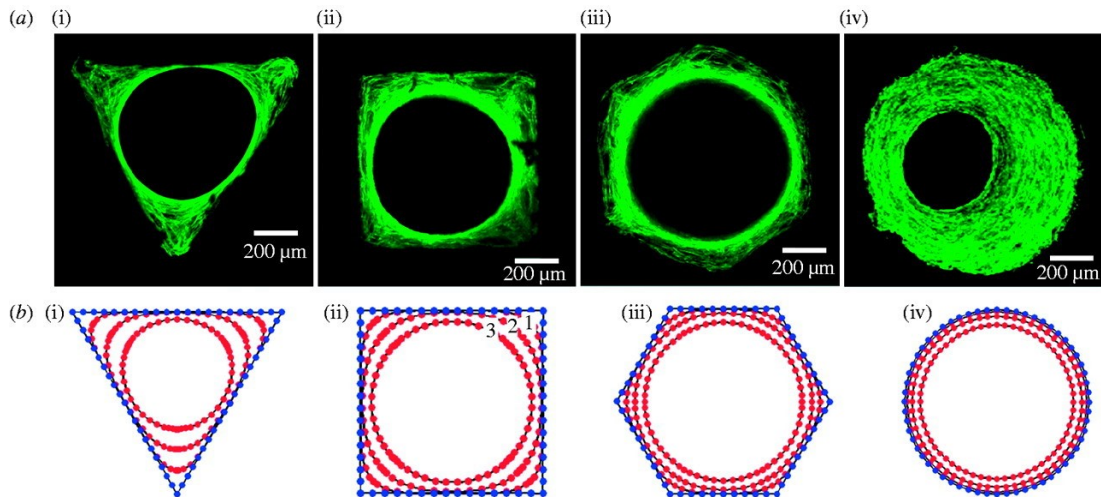


Figure 1.7: (a) Images of tissue development in three-dimensional matrix channels. Actin stress fibres were stained with phalloidin-FITC and visualised using confocal microscopy. (i) Triangular (ii) Square (iii) hexagonal and (iv) circular shape. (b) shows with red dotted lines the tissue development at three time point (1 = early time point and 3 = latest time point). Adapted from Rumpler et al. [77] with permission from Royal Society, copyright 2008.

### 1.3.2.3.1. Mimicking basement membrane matrices

The basement membrane functions by separating the tissue layers, and in oral mucosa the lamina propria from the epithelium. It is structured in such way (low pore size and porosity) that allows gas and nutrient exchange but does not allow cell penetration. Therefore, although the porosity of the scaffold promotes the fibroblast ingrowth, in a recent study a porous surface for the epithelial side resulted into keratinocyte invasion into the scaffold forming epithelial islands within it [30]. To address this issue, they used cell culture inserts to laminate the scaffold with Matrigel™, obtaining a controllable epithelium size and high accuracy in terms of reproducibility. Matrigel™ is a basement membrane protein extract from mouse sarcoma cells consisted of over

## Chapter 1

1000 proteins mainly by laminin, collagen IV, heparin sulphate proteoglycans and entactin, which forms a 3D gel under 37°C that supports cell differentiation, growth and morphogenesis [79, 80]. It has been used before as a BM-like structure for oncogenesis [81], epithelial morphogenesis [82] and intestinal organoids generation [83]. Laminin has also been used as BM-like matrix for 2D and 3D culture system, more specifically laminin-111 which can be isolated from mouse sarcoma cells [84]. The limitations of these natural BM-like matrices are reproducibility (composition and structure variability) and mechanical properties [80]. These limitations decrease the reliability of these natural matrices and renders them unsuitable for clinical use.

Synthetic hydrogels made from poly(acrylic acid) (PAA) [85], poly(ethylene glycol) (PEG) [86] and poly(vinyl alcohol) (PVA) [87] have been fabricated to replicate a BM-like matrix. Hydrogels are defined as hydrophilic, water-swollen polymeric network, crosslinked either through covalent bonding or non-covalent interactions that involve hydrogen bonds, ionic interactions or polymer crystallites [88, 89]. The reasoning behind using synthetic hydrogels is first they closely resemble natural BM-like matrices such as Matrigel in terms of physical properties, but most importantly because biofunctional molecules can be loaded to enhance the epithelial cell attachment as well as proliferation, differentiation and migration [84]. For example, a photocurable PVA hydrogel has been modified with cell adhesion peptides to induce fibroblast proliferation and ECM production [90]. Another study, developed a hydrogel scaffold made from PEG to analyse disease development and drug screening. Puperi et al., developed a system where the PEG hydrogel had localised adhesive ligands and it was shown that cell specific adhesion could be organised within the matrix [91]. Other fabrication techniques have also been developed to

fabricate multilayer scaffolds to facilitate cell co-culture, using additive manufacturing [92] and layering techniques [93].

Despite the advances in cell co-culture, and mimicking the native ECM structure, the BM-like matrices and scaffolds fabricated until now were used to understand cell to cell interaction, disease development or drug screening but not to replace a dysfunctional or damaged tissue. However, a study published by Bye et al. [94], developed two-layer electrospun scaffolds using poly(hydroxybutyrate-co-hydroxyvalerate) (PHBV) and PLA or PCL. The aim of this study was to demonstrate the procedure of fabricating thicker electrospun scaffolds by building the scaffold layer by layer and at the same time to function as BM and separate the cell layers for co-culture [94]. The scaffolds were seeded with human dermal fibroblasts and the cells were restricted within the seeded layer [94].

#### **1.3.2.4. Degradation rate**

Scaffold degradation occurs through degradation mechanisms that can either be physical, chemical or biological, in order for the scaffold to degrade and get replaced by newly formed tissue [95]. The scaffold can undergo bulk or surface erosion, where bulk erosion is when the scaffold erodes from the internal structure reducing its molecular mass and surface erosion is when it breaks down from the surface maintaining its bulk structure [96]. This polymer erosion occurs by the cleavage of hydrolytically or enzymatically sensitive bonds found in the chemical structure of the polymer [97]. Therefore, the biodegradation rate is dependent on the chemical structure, the presence of hydrolytically unstable bonds, its hydrophobicity/hydrophilicity, its crystalline/amorphous structure, the copolymer ratio, the glass transition temperature and the molecular weight [98]. As mentioned

previously, the biodegradation rate of the scaffold should synchronise and match the rate of the tissue growth *in vitro* and *in vivo*.

### 1.3.2.5. Mechanical properties

Williams et al. [99], mentioned that a biomaterial has to perform and exist with the most appropriate response, biological and physical, which depends on the application. In the report the authors stated that biomaterials should be also selected with enough mechanical and physical properties, to withstand mechanical *in vivo* forces such as tensile loading (e.g. oral mucosa), compression (e.g. bone) and fluid flow dynamics (e.g. blood vessels) [99]. These mechanical forces can affect the scaffold's construction integrity, which will eventually affect the cells seeded into it. It was found that having mechanical properties that are similar to the native tissue is important for the scaffold's biostability. The importance of mechanical properties biomimicry arises for two reasons. First the scaffold is strong enough to withstand *in vivo* mechanical forces, and in the case of this study, mechanical forces acting on oral mucosa are tensile load, compression load, friction and hydrodynamic forces, mainly due to mastication, speech, toothbrushing and saliva flow [16]. Second reason is based on findings from multiple studies, that suggest that cells adhere and proliferate better when attached to substrates (scaffolds) with the appropriate mechanical properties [100, 101]. For example, one study investigated the effect that the Young's modulus of polydimethylsiloxane (PDMS) surfaces has on epidermal keratinocytes, and it demonstrated that that the stiffer surface (2.0 MPa) had an increase in cell number, colony size and DNA synthesis compared to the softer surface (0.18 MPa) [100]. Additionally, when human dermal fibroblasts were seeded on collagen gels had a 2 days doubling time on stiffer collagen gels (1.81 MPa) compared 6 days doubling time



on soft collagen gels (0.42 MPa), concluding to that the proliferation of fibroblasts increases with the increase of stiffness (Young's modulus) [101].

### 1.3.3. Oral mucosa scaffold properties

Consequently, a scaffold for oral mucosa regeneration should have a highly interconnected pore structure with high surface-to-volume ratio. The surface of the scaffold should allow cell attachment and proliferation but keep the cell layers distinct from each other. Since oral mucosa is consisted from two cell layers separated by a BM, and it is known that the epithelium does not need a porous scaffold for the epithelial cells to grow into a 3D stratified epithelium, the scaffold should be porous where the lamina propria is situated and have a thin BM-like layer that will allow epithelial cells to adhere on and grow upwards, without cell penetration into the other layer. Therefore, the lamina propria part of the scaffold should be porous with enough pore size (20-30  $\mu\text{m}$ ) for cells to be seeded and grow, and high porosity (>90% porous) to increase the surface-to-volume ratio as well as sufficient gas and nutrient exchange. At the same time the scaffold is required to have a BM-like layer on top of the porous structure for the epithelial cells to grow, while having nanoscale pores (80 - 100 nm) to allow cell communication and nutrient exchange. The degradation rate of the scaffold should be synchronised with the tissue development (at least 30 days before fully degraded [102]) and degrade gradually without a burst in mass loss, which will result in structure support failure.

Knowing that oral mucosa has elastomeric properties and different strength and stiffness dependent on its location in the oral cavity, it is logical that the scaffold should be elastomeric and have tailorable mechanical properties without affecting its biocompatibility, microstructure and degradability. It is also extremely important that

the scaffold can retain its mechanical properties while degrading until the cell produced ECM can support the structure of the tissue.

## **1.3.4. Biomaterials**

All the aforementioned scaffold properties are depended on the biomaterial they are composed of and the fabrication method. In this section the natural and synthetic biomaterials used in OMTE will be reviewed and compared between them.

### **1.3.4.1. Natural biomaterials**

There are multiple natural biomaterials used previously in TE, such as collagen, various proteoglycans, alginate-based substrates and chitosan [103]. All these biomaterials have the advantage of being extremely biocompatible, as well as biodegradable. Additionally, natural biomaterials are bioactive, meaning they can affect their biological surroundings by promoting cell adhesion and growth [103, 104]. The main disadvantage of the natural biomaterials is fabricating scaffolds with homogeneous porous and reproducible structures is difficult [103]. Furthermore, usually these materials have poor mechanical properties, not allowing them to be used in applications where the scaffold will be under high dynamic environment [103].

### **Collagen**

Collagen is the most used natural biomaterial in TE, due to its similar composition to the native ECM, and low immunogenicity and cytotoxicity [105, 106]. Collagen can be used crosslinked and non-crosslinked, and the degree of crosslinking can be controlled in some extent, which allows the material to have slower degradation rates and higher mechanical properties (non-crosslinked: UTS =  $37.7 \pm 4.5$  MPa, Young's modulus =  $1.1 \pm 0.1$  GPa and elongation at break =  $6.8 \pm 1.9$  %; crosslinked: UTS =  $44.1 \pm 4.0$  MPa, Young's modulus =  $1.2 \pm 0.2$  GPa and elongation at break =

6.5 ± 1.4 % [107]) which are both desired in OMTE [15]. However, during collagen crosslinking a disadvantage arises because mainly chemical crosslinking is necessary which involves toxic reagents [108]. It is fair to note that these mechanical properties are achieved from collagen films (non-porous structures), therefore the structure's mechanical properties will be significantly decreased when porosity is introduced (sponge structure: UTS = ~20 KPa) or it is fabricated as hydrogel. This is also true for all materials mentioned in this thesis. Collagen can also be used as a based material for incorporating glycosaminoglycan (GAG) and chitosan. These scaffolds have shown great success in the areas of oral mucosa and skin tissue engineering. GAG are polysaccharide molecules that enhances the ECM's physical properties. Additionally, GAG's form proteoglycans that have the important functionality of binding growth factors and cytokines [109]. Chitosan is also widely used in soft tissue TE because of its excellent biodegradability, biocompatibility and bioactivity. It is derived from the deacetylation of natural chitin and it can be fabricated into a scaffold via covalent/ionic crosslinking with another polymer (usually collagen) [110].

In OMTE, (i) collagen type I, (ii) crosslinked collagen, and (iii) collagen-glycosaminoglycan-chitosan (CGC) were used for engineering an oral mucosa for testing dental biomaterials.

(i) When the collagen type I was seeded with oral keratinocytes and fibroblasts, a stratified squamous epithelium was formed (9-12 layers) but epithelial cells infiltrated into the porous areas of the scaffold which formed epithelial islands. Additionally, few fibroblast cells were found inside the pores of the scaffold. Finally, this scaffold could not be used for the purpose of testing dental biomaterials because the engineered mucosa could not survive more than 2 weeks because of biodegradation [30].

(ii) The cross-linked collagen had an improved biostability compared to the uncrosslinked and it could survive for more than 3 weeks. However, in terms of histological analysis similar results were observed as the scaffold discussed above (collagen type I) with epithelial island formations and low fibroblast infiltration [30].

(iii) The CGC crosslinked sponges demonstrated the best results from this study. It was found to exhibit excellent biocompatibility, biostability and porosity to facilitate a multilayer epithelium development, and fibroblasts were able to infiltrate within the scaffold pores and produce new collagen and other connective tissue components [30].

As mentioned above, natural biomaterials, especially collagen, possess many advantages that made it the most used biomaterial for OMTE. However, collagen is mostly isolated from human or animal tissue which limits their availability, they have batch-to-batch variations, and usually it is expensive [15]. Some of these disadvantages could probably be solved in the future, but until then researchers have also considered using synthetic biomaterials to fabricate scaffolds for OMTE.

### **1.3.4.2. Synthetic biomaterials**

In tissue engineering synthetic scaffolds play a very important role, as these scaffolds can be tailored with specific properties dependent on the native tissue. The ability of their mechanical properties to be designed with biomimicry is the great advantage that they possess over natural scaffolds. Additionally, synthetic scaffolds can be fabricated with various formulations and methods, giving different pore sizes, interconnectivity and degradation rates [55, 103]. As mentioned previously this is again very important in tissue engineering as cells can exchange nutrients and gas efficiently, angiogenesis is promoted, and a controlled degradation rate will allow enough time for cells to

# Chapter 1

produce their own ECM to replace the scaffold construct without losing their structure integrity meanwhile. Needless to say there are also disadvantages in synthetic biomaterials such as, the risk of rejection due to low bioactivity, and their degradation by-products can be toxic or reduce the local pH causing cell and tissue necrosis [111]. Most of the synthetic biomaterials that will be described below were investigated by only one research group, therefore there is a lack of comparing results.

## **Poly(L-lactic acid)**

Poly(L-lactic acid) (PLLA) is a hydrophobic polyester that was characterised numerous times with good biocompatibility and biodegradability [112]. PLLA is a stiff polymer with mechanical properties ranging between 34.5-67.2 MPa UTS, 1.57-4.18 GPa Young's modulus and 2.43-8.57% elongation at break [113].

In OMTE, it was used to co-culture oral fibroblasts and keratinocytes aiming to develop an oral mucosa for testing dental biomaterials. Using electrospinning a PLLA scaffold was fabricated and seeded with oral cells. After 14 days culture the scaffolds were characterised with good biocompatibility and bio-stability, and keratinocytes formed multi-layer epithelium and fibroblasts were found underneath the generated epithelium [30].

## **Poly(ethylene terephthalate)**

Poly(ethylene terephthalate) (PET) is a non-degradable hydrophobic polyester that was found to exhibit good biocompatibility properties [112]. It is usually used as surgical meshes for long-term implants, such as rhinoplasty or ligament reconstruction [114, 115]. PET was characterised with 48-72 MPa UTS, 2.8-4.1 GPa Young's modulus and 30-300% elongation at break [113].

# Chapter 1

Regarding OMTE, PET membranes were purchased from Greiner bio-one, Germany with 3  $\mu\text{m}$  pore size and after 14 days of oral fibroblast/keratinocytes co-culture the samples were characterised using histology and immunohistochemistry. It was found that the PET membranes provided the pore size and porosity for good cell communication, however the membrane lacked from a 3D a matrix development.

## **Polycarbonate**

Polycarbonate (PC) is thermoplastic polymer that exhibits hydrophobic properties and is considered as a biologically inert material [112]. Its mechanical properties range between 60-121 MPa UTS, 2.1-2.4 GPa Young's modulus and 65-150% elongation at break [113].

In OMTE, PC membranes were purchased from Costar, USA with 3  $\mu\text{m}$  pore size, seeded with oral fibroblasts and keratinocytes and characterised the tissue development using histology and immunohistochemistry [30]. As with PET, it was found that the keratinocytes were able to be co-cultured with fibroblasts however the connective tissue layer lacked from ECM development [30].

## **Polystyrene**

Polystyrene (PS) is a biocompatible, non-degradable material that is used vastly for cell culture in 2D (tissue culture plastic) and it can also be fabricated into 3D structure but only for *in vitro* use [112, 116]. Its mechanical properties range between 32-44 MPa UTS, 1.9-2.9 GPa Young's modulus and 1.8-40% elongation at break [113].

Regarding the use of PS in OMTE, electrospinning was used to fabricate PS scaffolds which were therefore seeded and cultured with oral cells for 14 days. It was characterised with good biocompatibility and biostability. It was found that fibroblasts

cells were able to infiltrate into the pores of the scaffold and keratinocytes could grow on the surface of it [30].

### 1.3.4.3. Natural vs synthetic biomaterials

Currently most of the research groups have found that natural scaffolds fit well in engineering oral mucosa equivalents [6, 15]. However, natural scaffolds have the disadvantages of disease transmittance, availability and reproducibility.

Notwithstanding the architecture and biological parameters of the scaffold, the mechanical properties of the scaffold are also of great importance, as Williams et al. reported [99]. They defined biocompatibility as “the ability of a material to perform with an appropriate response in a specific application” [99]. Williams published a leading opinion paper where he discusses the term biocompatibility and how it should be approached when is used as a characteristic of a biomaterial for medical use [117]. A summary of the biocompatibility pathways is shown below in Figure 1.8. It represents the influence of events within the *in vivo* environment by mechanical and molecular signalling in a simple way from a cell biology perspective [117]. Target cells are the cells that the therapy is aimed for, defensive cells are the cells whose functionality is based on repelling and removing harmful external agents (inflammatory cells, platelets) and interfering cells are the cells that may interfere during the tissue generation (osteoclasts in bone and fibroblast infiltration to the epithelium in oral mucosa) [117]. Essentially, according to Williams, a biocompatible biomaterial in tissue engineering is when defensive cells do not induce adverse effects, the target cells interact with the biomaterial and are metabolically active and the interfering cells do not interfere with the tissue generation.

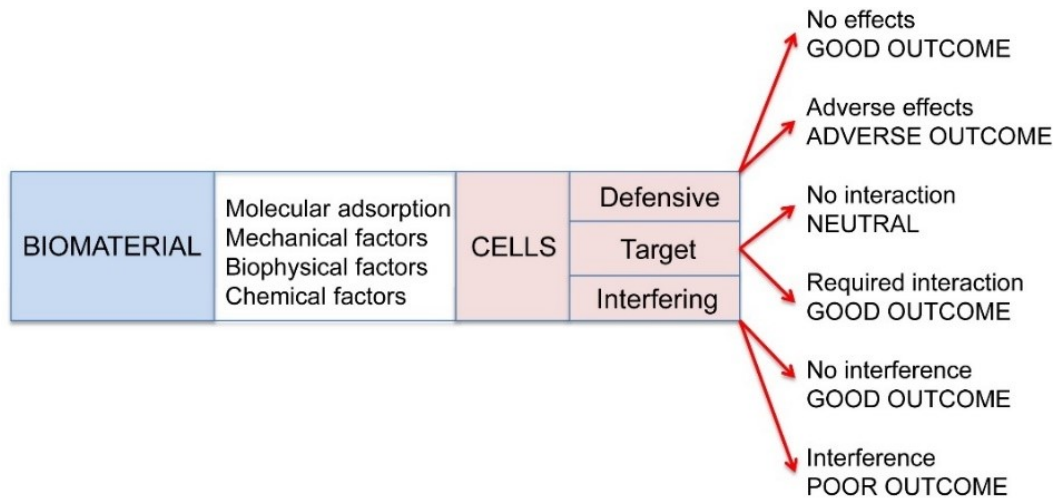


Figure 1.8: Schematic showing the summary of biocompatibility pathways between biomaterial and the defensive, target and interfering cells with their relevant clinical outcomes. Adapted from Williams D. [117] with permission from Elsevier, copyright 2014.

A gap of knowledge was identified from the literature review in using synthetic scaffolds for OMTE, probably due to the great success of using Alloderm or collagen based scaffolds. However, these grafts and materials have limitations in reproducibility (due to batch-to-batch variations), risk of transmitting diseases, processability, and at the moment high cost. In contrast, synthetic materials can be synthesised with specific chemical structures that exhibit biocompatibility, biostability, reproducibility, processability and in some cases produced at a low cost mainly because of the availability of the raw materials (e.g. monomers). For these reasons we believe that there is still room for improvement in developing scaffold for OMTE. Additionally, the synthetic scaffolds that were used do not exhibit elastomeric properties and all undergo plastic deformation when loaded, which is a disadvantage in OMTE, since the native oral mucosa is highly flexible due to its functionality (e.g. resistance to tear). Hence, this thesis will focus on synthesising and fabricating synthetic scaffolds for OMTE using poly(glycerol sebacate) (PGS) based biomaterials.



## 1.4. Poly(glycerol sebacate)

### 1.4.1. Introduction to poly(glycerol sebacate)

PGS is a synthetic elastomer synthesised by polycondensation of glycerol and sebacic acid [118]. This material is biocompatible and biodegradable with sufficient mechanical properties to suit as a scaffold for the initial development of many soft tissues such as cardiac muscle, retinal and nerve tissue engineering [119]. PGS is derived by glycerol and sebacic acid which both form randomly crosslinked coils during the synthesis. The most common synthesis method happens in two steps [120]. The first step results in the synthesis of PGS pre-polymer, a highly viscous material, and during the second step the pre-polymer is polymerised to a crosslinked polymer, shown in Figure 1.9.

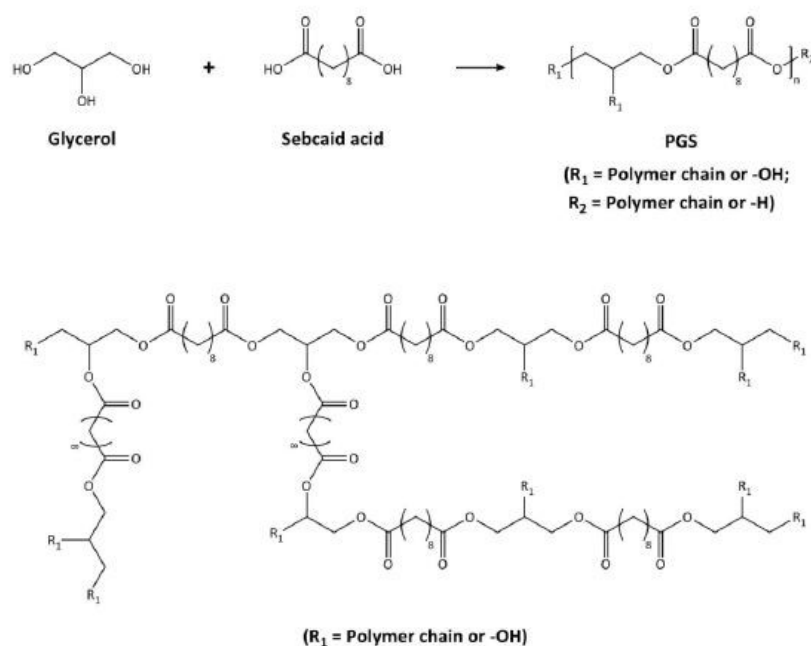


Figure 1.9: The synthesis and chemical structure of PGS. Reprinted from Li et al. [121] with permission from SAGE JOURNALS, copyright 2014..

The reason that this polymer, as well as others, can act as a scaffold for multiple tissues is because its mechanical properties and degradation rate can be tailored

## Chapter 1

according to the need, by controlling temperature, curing time and the reactants molar ratio. PGS has elastomeric tensile strength with non-linear stress-strain behaviour. The mechanical properties can vary between 0.05 – 2.12 MPa Young's modulus, 0.23 – 0.79 MPa tensile strength and 69-448% strain at break [118]. The main advantage of PGS over other synthetic polymers is that it was shown that it exhibits stable mechanical properties after cyclic loading, with minimal loss of tensile strength [122]. This demonstrates good flexibility with mechanical integrity to withstand mechanically dynamic environments. Other popular synthetic materials, such as PLA, PGA, PCL as well as their copolymers, undergo plastic deformation after exposure to mechanical stress, making them unsuitable for many TE applications [123].

Regarding the degradation of PGS, it undergoes linear degradation and it degrades by surface erosion due to hydrolysis of ester groups, into oligomers and monomers that can be resorbed and eliminated through natural pathways [119]. Again, this is an advantage because surface erosion allows the scaffold to retain its geometry as well as retain its mechanical properties relative to the mass loss [124, 125]. When degrading PGS *in vivo* it was noticed that the degradation rate was faster than *in vitro*, exhibiting complete degradation in 60 days, whereas 18% mass loss was observed *in vitro* [120]. When degrading *in vivo* PGS preserves its geometry and maintains its mechanical strength, losing about 8% of mechanical strength every week [120, 126]. After ~70% degradation of the PGS, the Young's modulus was more than 50% from its initial value, which is an important characteristic that other polymeric biomaterials fail to achieve [126]. As mentioned earlier the degradation rate can be tuned by changing the crosslink density, which means the higher the crosslinking the less the water diffusion and hydrolysis [127].

## Chapter 1

When PGS was examined for its biocompatibility it showed good *in vitro* and *in vivo* results, enhanced hemocompatibility and a low inflammatory response [118, 120, 124, 126, 128]. The reason that PGS is biocompatible is due to its monomers, glycerol and sebacic acid, which are basic component of lipids and a derivative of fatty acids respectively [120]. These monomers are considered as nontoxic and have been approved by the United States Food and Drug Administration (FDA) [120]. Compared to other polyesters, PGS showed better or similar biocompatibility [120]. For example the *in vitro* 3T3 fibroblast cell activity was compared between PGS coated dishes and poly(lactic-co-glycolic acid) (PLGA) coated dishes, and it was observed that there was better cell adhesion and growth on the PGS samples [120]. Similar observations were found when using Schwann cells [129] and smooth muscle cells [130]. When *in vivo*, PGS resulted in a lower inflammatory response into rat samples compared to PLGA, lower fibrous capsule formation and did not induce the foreign body giant cell response [120, 129]. These results are partly due to the surface erosion which gradually resorbs inducing less inflammatory response, compared to the rapid mass loss from a PLGA sample [129].

All the aforementioned studies involved PGS characterisation in a 2D structure and with evidence that PGS can outperform popular synthetic polymers research began looking into fabricating PGS scaffolds. It was quickly realised that the performance of PGS scaffolds in terms of biocompatibility, biodegradation and mechanical strength was also heavily dependent on factors such as pore size, porosity [125], hydrophilicity [131], surface and bulk morphology [132]. The issue that arises when attempting to fabricate PGS 3D scaffolds is the harsh curing conditions required during synthesis, which are high temperatures (110-165°C), long curing duration (24-114 hours) and high vacuum pressure [119]. These harsh conditions set limitations on fabricating 3D

scaffolds. As described previously porous scaffolds are essential for tissue generation as they aim to replace ECM-like structures with high surface-to-volume area to allow large tissues to be engineered. As mentioned earlier, fabricating 3D porous scaffolds out of PGS presented a great challenge due to its harsh synthesis and curing conditions.

### **1.4.2. Poly(glycerol sebacate) scaffold preparation techniques**

This limitation is not presented for materials such as PCL, PLA or PLGA, where most if not all scaffold fabrication techniques can be applied. To explain further the effect of the harsh curing conditions, to crosslink PGS high temperature (110-165°C) is required under vacuum environment, and this causes the pre-polymer to liquify which destroys the porous structure that was produced before curing [133].

A summary of the fabrication techniques that were developed to produce PGS in a 3D porous scaffold is shown in the Table 1.3 below. All these methods work but they have great limitations in terms of fabrication cost and the size of the final product is small with low reproducibility. More importantly in many cases the fabrication technique does not allow control of pore size and porosity which affects the cell viability.

Micromoulding is a fabrication technique based on injection moulding technique but to a micro-scale resolution. Aiming to use a scaffold to deliver cells to the retina, Neeley et al. fabricated a porous PGS membrane using micromoulding. The resulting scaffold had good mechanical properties resembling those of retinal tissue and preliminary results showed cell adherence and proliferation [125]. However, this scaffold was very thin (80 µm thickness) and required more than 16 days to fabricate, Figure 1.10. A laser micro-ablation technique allowed the fabrication of porous PGS sheets that exhibited accurate micropatterns and the sheets could be stacked into a

## Chapter 1

multi-layered PGS scaffold [134]. The resulting scaffold had approximately  $\sim 400 \mu\text{m}$  thickness and dependent on the pore structure, the ultimate tensile strength ranged between 40 – 100 kPa. Similar to micromoulding, the inability to produce large 3D porous scaffolds from both techniques limits their applicability in TE, Figure 1.11. A completely different method was utilised to fabricate PGS scaffolds using solid free-form technique. In this case a sacrificial mould was used, made from hydroxyapatite, that is the inverse structure of a 3D printed wax mould, and PGS prepolymer was cast in the mould followed by curing. The resulting scaffold had large pore size ( $\sim 1 \text{ mm}$ ) and low porosity (48%), Figure 1.12. Electrospinning is a more established fabrication technique for PGS, however a blend of natural or synthetic polymers with PGS is necessary to adjust the viscosity of the PGS prepolymer solution to values suitable for electrospinning [131]. The carrier polymers tested for PGS blend solutions are gelatin [135], PVA [136], PCL [131] and polylactic acid (PLLA) [137], Figure 1.13. The PGS-based scaffolds fabricated with electrospinning had fibre diameters ranging between  $0.3 - 8.3 \mu\text{m}$ , with large surface area and fibres could be randomly dispersed or aligned. The issue in fabricating scaffolds with PGS and electrospinning is the inability to crosslink the PGS prepolymer because of the high curing temperature ( $110 - 165 \text{ }^\circ\text{C}$ ) meaning only thin scaffolds can be produced. The last, least complicated technique utilised for PGS scaffold fabrication is porogen leaching and fusion technique [138, 139]. This fabrication technique involves mixing melted PGS prepolymer with a porogen, usually salt, and after PGS thermal crosslinking the porogen is leached using water. Therefore, the pore size depends on the size of the porogen, with an average pore size in the range of  $20 - 300 \mu\text{m}$ , and the porosity depends on the concentration of the porogen, in the range of 75 – 95 %, Figure 1.14. Despite the fact that pore size and porosity can be adjusted, the pore shape and pore

## Chapter 1

interconnectivity adjustment is limited. Furthermore, because the PGS melts while crosslinking, the porogen tends to sink resulting in a dense skin layer formed on the top of the scaffold and subsequently relatively thin scaffolds, 1-5 mm thickness [138, 139].

Sophisticated fabrication techniques were developed and utilised to fabricate pristine PGS scaffolds, but all these scaffolds were characterised with a low throughput and small size scaffolds [119]. Additionally, porous structures and porosities were not easily controlled, not allowing the usage of PGS scaffolds in a vast range of soft TE.

Table 1.3: PGS scaffold fabrication techniques review table.

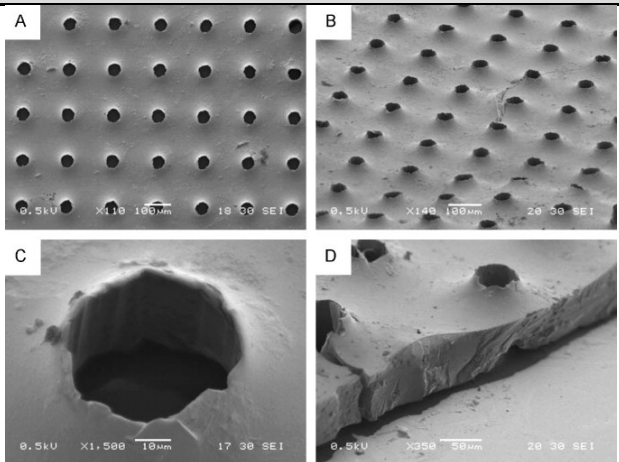
Fabrication technique	Advantages	Disadvantages	Scaffold images	References
Micromoulding	High resolution; Can design complex 2D structures	Fragile scaffolds, Small size; Expensive		[125, 140, 141]

Figure 1.10: SEM images of PGS scaffolds fabricated with micromoulding. (A) Top view, (B) 60° angle view, (C) pore view at 30° angle and (D) edge view at 60° angle. Reprinted from Neeley et al. [125] with permission from Elsevier, copyright 2008.

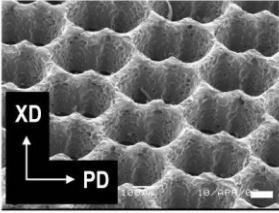
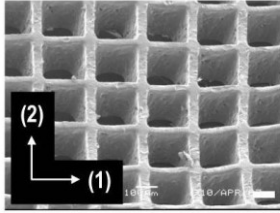
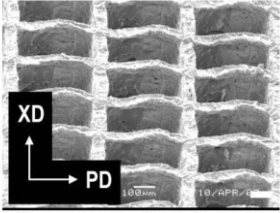
<p>Laser microablation</p>	<p>High resolution; Can design complex 2D structures</p>	<p>Fragile scaffolds, Small scaffold size; Expensive</p>	<div style="display: flex; justify-content: space-around; align-items: center;"> <div style="text-align: center;"> <p><b>a</b></p>  </div> <div style="text-align: center;"> <p><b>b</b></p>  </div> <div style="text-align: center;"> <p><b>c</b></p>  </div> </div>	<p>[134, 142]</p>
--------------------------------	--	--	---	-------------------

Figure 1.11: SEM images of (a) accordion-like, (b) square and (c) rectangular honeycomb PGS scaffolds made using laser microablation. Scale bar is 100  $\mu\text{m}$ . Reprinted with permission from Springer Nature: Engelmayer et al. [134], copyright 2008.



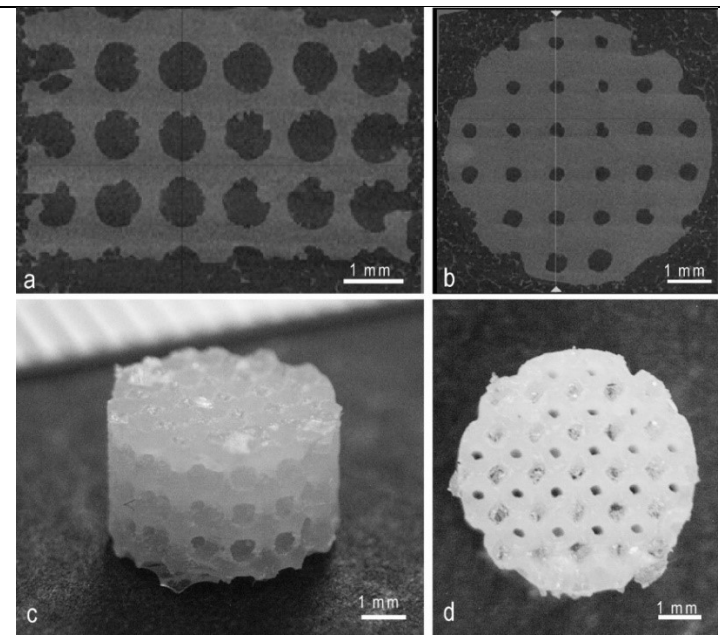
<p>Solid freeform fabrication</p>	<p>Can fabricate complex 3D structures; No need of organic solvent</p>	<p>Sacrificing mould is needed; Low resolution; Expensive</p>		<p>[143]</p>
-----------------------------------	--	---	--	--------------

Figure 1.12: Micro-CT (a,b) and digital (c,d) images of PGS scaffold fabricated using solid freeform fabrication. (a) side view, (b) top view, (c) side view, (d) top view. Reprinted from Kemppainen et al. [143] with permission from John Wiley and Sons, copyright 2010.

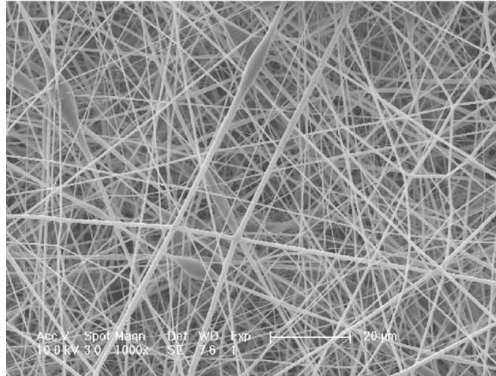
Electrospinning (polymer blend)	High porosity; Low cost	Small pore size; Small scaffold size, Thin scaffolds; Polymer blend is required		[131, 133]
---------------------------------------	-------------------------------	--	---	------------

Figure 1.13: SEM image of PGS/PLLA core/shell nanofibres. Reprinted from Yi et al. [133], with permission from John Wiley and Sons, copyright 2008.

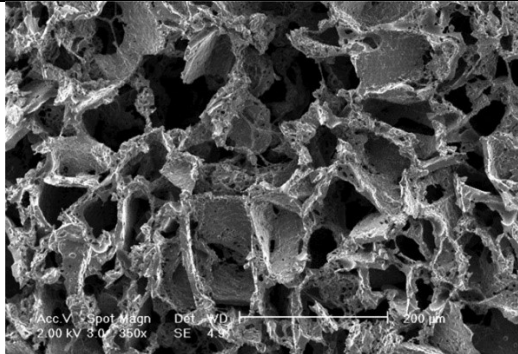
Porogen leaching and fusion	Easy procedure; Can be highly porous; Low cost	Pore interconnectivity; Pore shape is limited; Non- porous skin formed at surfaces		[138, 139]
-----------------------------------	---	--	--	------------

Figure 1.14: SEM image of PGS scaffold fabricated using porogen leaching. Reprinted from Radisic et al. [139], with permission from John Wiley and Sons, copyright 2007.

### 1.4.3. Poly(glycerol sebacate) modifications

All these fabrication limitations are solely because of the harsh curing conditions that PGS requires to crosslink. Therefore PGS-based copolymers, blends and composites, were developed to overcome the fabrication limitations, and to modify the mechanical properties, biocompatibility, degradation and hydrophilic properties of the scaffolds [127, 131, 144].

Nijst et al. [144] addressed these limitations by chemically modifying the PGS synthesis by adding reactive acrylate moieties, making poly(glycerol sebacate) acrylate (PGSA). This new acrylated material was then able to be cured using UV radiation by dissolving it in a photo initiator 2-dimethoxy-2-phenylacetophenone. The curing time was reduced significantly to a few minutes compared to 48 hours and it also overcame the thermal curing limitation, allowing an expansion in its applications. Additionally, by controlling the acrylate moieties in the PGSA, the mechanical properties could also be tuned [144].

Poly(glycerol sebacate) methacrylate (PGSM) was also synthesised which could be cured using UV light. The synthesis procedure was similar to PGSA but methacrylate groups were used to functionalise the PGS and render it photocurable. This material was mostly studied as a film showing human dermal fibroblasts were metabolically active and no adverse effects were found within the 7 days culture [145]. As proof of concept a 3D scaffold was also fabricated using a technique called 2-photon polymerisation. The mechanical properties and degradation rates could be controlled by changing the molecular weight and degree of methacrylation [145].

A polymer blend, PGS/PLLA, was also developed to enhance the fabrication technique of PGS based scaffold, where PLLA acted as a structure supportive polymer

[146]. PLLA acted as a structure supporting polymer because of its high melting point (173 -178°C) which allowed the scaffold to maintain its structure during the harsh curing conditions of PGS, after giving its porous structure using freeze-drying. These results demonstrated the ability to fabricate large porous scaffolds with good pore interconnectivity, but fast degradation rate [146].

#### 1.4.4. Poly(glycerol sebacate urethane)

Another approach to extend the capabilities of the PGS material was successfully attempted by Pereira et al. [147]. In their study they developed a new material, poly(glycerol sebacate urethane) (PGSU). Incorporating urethane linkages is a simple processing method to fabricate elastomers with a wide range of mechanical properties demonstrating an advantage over other techniques. PGSU was synthesised by introducing isocyanate that reacted with the hydroxyl groups to form a cross-linked PGSU. This method had the advantage of using mild temperature (55°C) to crosslink. The PGSU was then shown to be biocompatible with tuneable biodegradation rate dependent on the degree of crosslinking, shown in Figure 1.15. Additionally, PGSU exhibits the ability of producing materials with various mechanical properties by altering the reactants ratio, summarised in Figure 1.16.

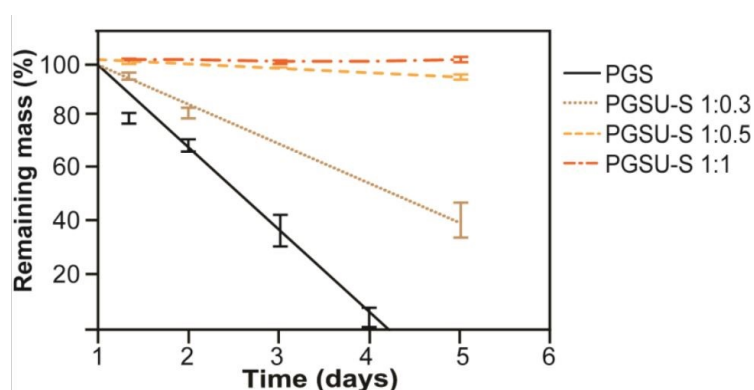


Figure 1.15: *In vitro* enzymatic degradation of PGSU films synthesised using different reactants ratio and cured PGS. Reprinted from Pereira et al. [147], with permission from John Wiley and Sons, copyright 2012.

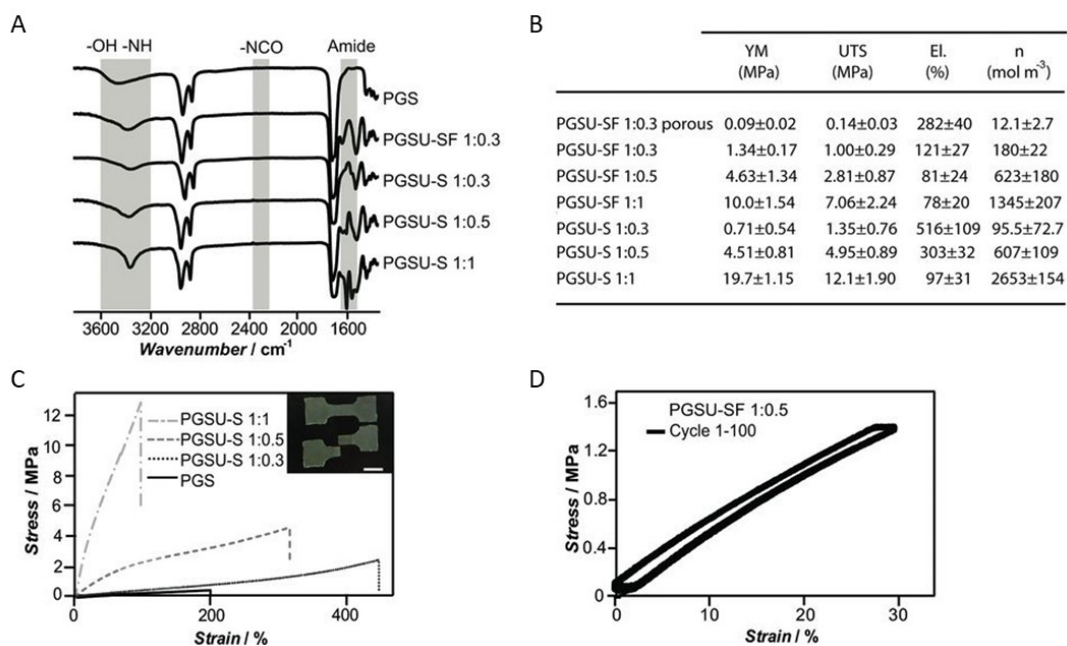


Figure 1.16: (A) FTIR spectroscopy analysis of PGS and PGSU, (B) summary of the mechanical properties of PGSU, (C) representative stress-strain curves of PGSU and cured PGS, (D) stress-strain curve of PGSU during 100 cyclic loading cycles. PGSU-SF = solvent free synthesis, PGSU-S = with solvent synthesis, YM = Young's modulus, UTS = ultimate tensile strength, EL = elongation at break. Reprinted from Pereira et al. [147], with permission from John Wiley and Sons, copyright 2012.

In the following figures, Figure 1.17 and Figure 1.18, the ultimate tensile strength (UTS) and Young's modulus measured in Pereira's work compared to the minimum and maximum UTS and Young's modulus of oral mucosa, are plotted. In both cases the UTS and Young's modulus increase while the isocyanate increases. This occurs because of the higher crosslinking density [147]. Additionally, the mechanical properties obtained from his study lie between the maximum and minimum values of the mechanical properties of oral mucosa, demonstrating that PGSU is a polymeric material that has the potential to replicate the mechanical properties of oral mucosa. Furthermore, biomaterials are often manipulated prior to transplantation and thus they should maintain their structure integrity. Therefore, taking into consideration that aliphatic polyurethanes undergo permanent deformation once exposed to tensile

forces, Pereira et al., examined PGSU and showed minimal creep deformation and minimal loss of tensile strength after 100 tensile cycles, Figure 1.16 (D) [147].

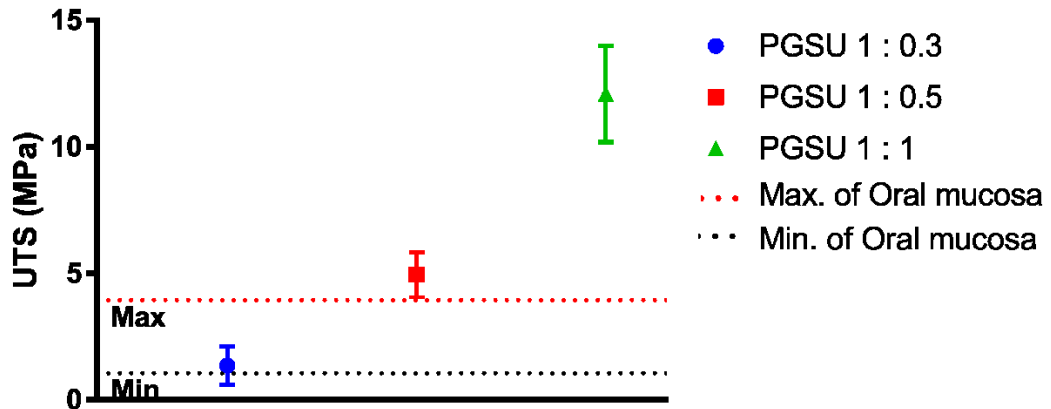


Figure 1.17: Ultimate Tensile strength of PGSU obtained from literature. Horizontal lines indicate the maximum and minimum UTS of oral mucosa dependent on the location. Data used in this figure were obtained from [16, 147] and plotted by the author.

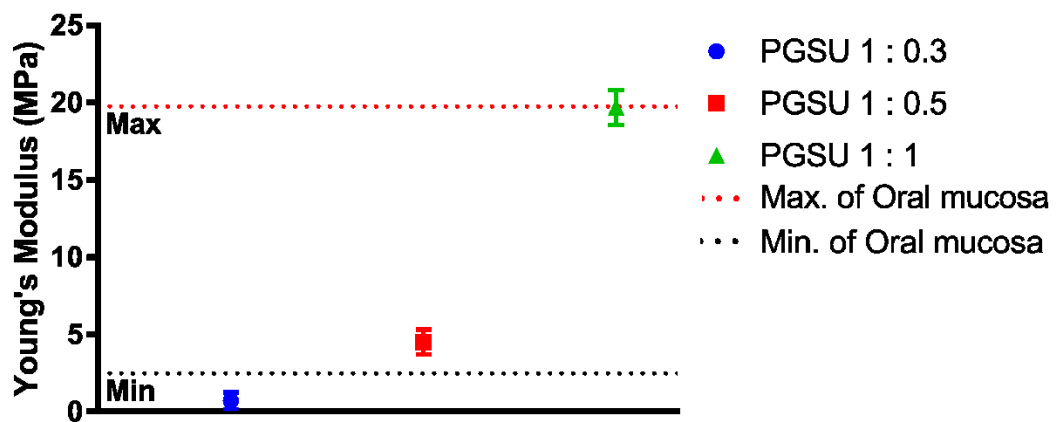


Figure 1.18: Young's modulus of PGSU obtained from literature. Horizontal lines indicate the maximum and minimum Young's Modulus of oral mucosa dependent on the location. Data used in this figure were obtained from [16, 147] and plotted by the author.

The assessment of biodegradation and cytocompatibility *in vitro* was also evaluated (Figure 1.15). Using cholesterol esterase, the PGSU films demonstrated a degradation profile dependent on the degree of crosslinking. Specifically, cured PGS had lower than 20% remaining mass after 4 days, whereas PGSU 1:0.3, 1:0.5, and 1:1 had

## Chapter 1

approximately 50%, 90% and 95% remaining mass respectively. This indicates that ester groups found on the polymer backbone are sensitive to enzymatic degradation, but by incorporating urethane linkages the ester bonds are hindered resulting in significantly slower degradation rate [147]. For their *in vitro* cytocompatibility test they seeded human mesenchymal stem cells on PGSU films and assessed their metabolism using 3-(4,5-dimethylthiazol-2-yl)-2,5-diphenyltetrazolium bromide (MTT) assay, having cells cultured on TCP as a positive control. On day 1 fewer cells were found on the PGSU films but towards day 8 the cells proliferated giving no statistical significance from cells on TCP.

Considering the success of the cytocompatibility results they then moved *in vivo* examining acute and chronic inflammatory response, Figure 1.19 (A, B). PGSU films were transplanted subcutaneous in a rat animal model and compared with PLGA which is a biodegradable material that has been approved by FDA for internal use. During the 40-week period no adverse reaction or any complications were observed. Specifically, at time points week 1 and 4, the PLGA showed a significantly higher foreign body response compared to the PGSU films [147].

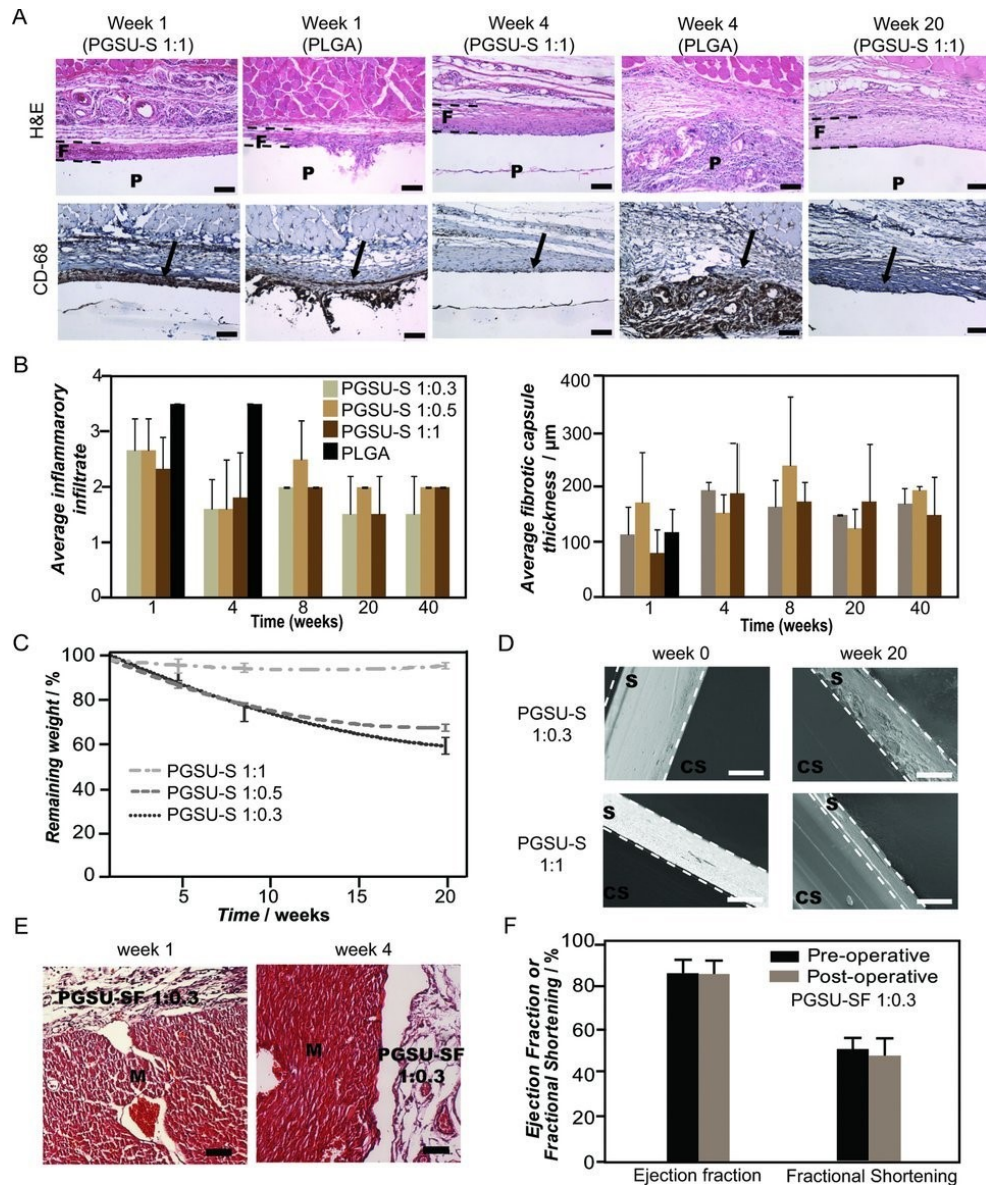


Figure 1.19: *In vivo* subcutaneous and cardiac biocompatibility and biodegradation of PGUSU films. (A) Histological images and anti-CD68 stained subcutaneous tissue, comparison between PGUSU and PLGA. (B) characterisation of foreign body response during *in vivo* study (0 mean no infiltration and 4 severe infiltration). (C) *in vivo* biodegradation of PGUSU at different reactant ratios, (D) Cross section SEM images during degradation (scale bar = 50 µm). (E) H&E stained sections during myocardium implantation (M = myocardium). (F) Cardiac function before and after PGUSU implantation. Reprinted from Pereira et al. [147], with permission from John Wiley and Sons, copyright 2012.

In the previous work from our group, Frydrych et al. [148], developed 3D PGUSU scaffolds using freeze-drying, synthesised with three different hexamethylene diisocyanate (HDI) contents. Using this technique, a PGUSU prepolymer solution was



crystallised (frozen) and the solvent was sublimed directly from solid phase into vapour phase by reducing the chamber pressure, leaving a porous PGSU prepolymer scaffold which was cured to obtain PGSU scaffolds [148, 149]. Frydrych et al. investigated the effect the crosslinker concentration had on the properties of the scaffolds, and a significant increase in mechanical strength (the Young's modulus, UTS and elongation at break ranged between 30-40 kPa, 18-22 kPa and 49-82% respectively) was found. The crosslinker concentration also affected the degradation rate (30-62% mass loss over 112 days) and the scaffolds exhibited porosities between 77-88% and pore sizes 55-74  $\mu\text{m}$  [148].

### 1.5. Scaffold fabrication

#### 1.5.1. Freeze-drying

During scaffold fabrication the porous scaffold is aimed to mimic the native structure of ECM. Using freeze-drying well-defined porous structures have been reported [118, 150, 151].

Freeze-drying takes place in three stages, freezing, primary drying and secondary drying shown in Figure 1.20. For the first two stages it is extremely important to understand the phase that a solvent is at a certain temperature and pressure. For ease of understanding water will be used as an example during the description of each freeze drying stage, and its phase diagram is shown in Figure 1.21. The first stage is freezing the sample, where the sample's temperature is reduced below its melting point ( $T_m$ ) which is depended on the solvent. In the case of water, its  $T_m$  is  $0^\circ\text{C}$  at atmospheric pressure (101 kPa). This stage is critical for the resultant structure of the scaffold. The pores in the scaffold are dependent on the freezing process, as the ice crystals are formed during freezing, and they act as a porogen so when ice crystal are

# Chapter 1

removed they leave pores in the scaffold's structure that reflects the ice crystal's structure. With this said, the method of freezing (freezing rate) is what determines the crystalline structure therefore the pore structure/size. The basic principle behind the freezing stage is: fast freezing rate produces smaller ice crystals and slow freezing rate produces larger ice crystals. Additionally, the temperature gradient across the sample is what determines the homogeneity of the pore structure. Being able to control the freezing process of the sample allows a tightly controlled pore size of the scaffold [149].

During the primary drying stage, the now frozen sample is kept below its critical temperature allowing it to stay frozen and vacuum pressure is applied. When the pressure is reduced below the triple point of the solvent the process called sublimation occurs. Considering water, sublimation will occur when the pressure is below 0.61 kPa and the temperature is below 0°C, when this is true the ice crystals sublime to a vapour skipping the liquid phase [149].

As a last step, secondary drying is done to remove any water which is chemically bound to the lattice, also called desorption process. The desorption process occurs by raising the temperature of the sample and reducing the pressure to the minimum [149].

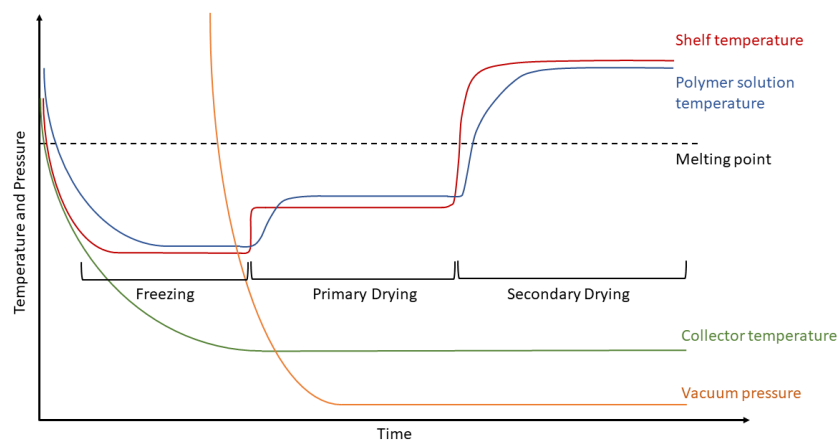


Figure 1.20: Normal freeze drying cycle during scaffold fabrication. The schematic is not scaled.

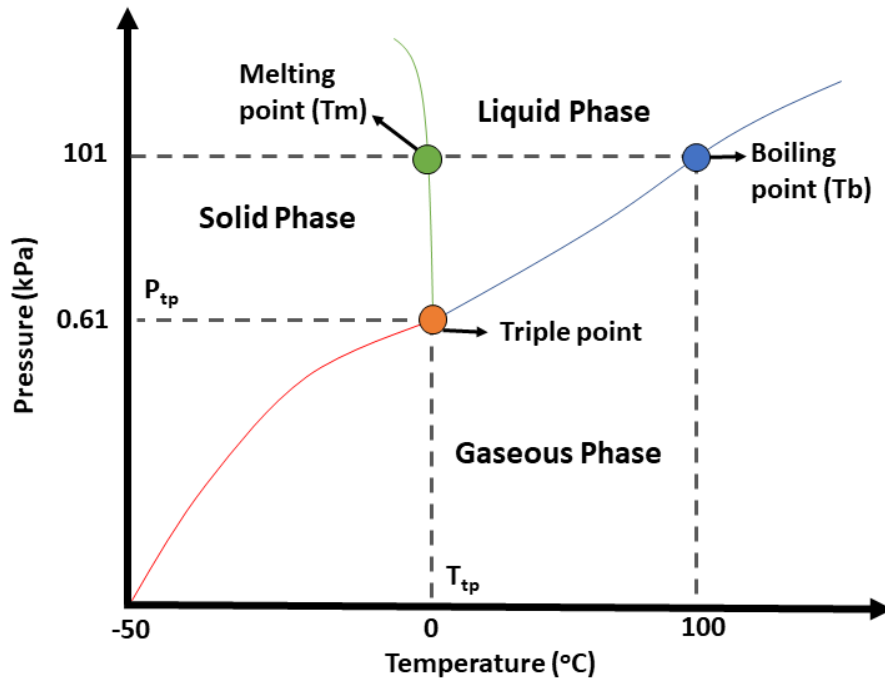


Figure 1.21: Three-phase diagram of water derived from the data provided from National Institute of Standards and Technology (NIST, <https://webbook.nist.gov/cgi/cbook.cgi?ID=C7732185&Units=SI&Mask=4#Thermo-Phase>).  $T_{tp}$ : Triple point temperature,  $P_{tp}$ : Triple point pressure.

Faraj et al. [42], attempted to fabricate porous collagen scaffolds examining the freezing stage of the process. Collagen solutions frozen at  $-20\text{ }^{\circ}\text{C}$  freezer resulted in much larger pores (top side:  $100 \pm 8\text{ }\mu\text{m}$ , cross-section:  $89 \pm 24\text{ }\mu\text{m}$ , bottom side:  $123 \pm 21\text{ }\mu\text{m}$ ) compared to fast freezing at  $-80\text{ }^{\circ}\text{C}$  (top side:  $57 \pm 21\text{ }\mu\text{m}$ , cross-section:  $42 \pm 6\text{ }\mu\text{m}$ , bottom side:  $29 \pm 3\text{ }\mu\text{m}$ ) using dry ice and ethanol. Furthermore, using liquid nitrogen a very rapid freezing at  $-196\text{ }^{\circ}\text{C}$  was established resulting in the smallest pores (top side:  $31 \pm 2\text{ }\mu\text{m}$ , cross-section:  $24 \pm 4\text{ }\mu\text{m}$ , bottom side:  $5 \pm 1\text{ }\mu\text{m}$ ). Therefore, as mentioned previously the higher the freezing rate, the smaller the pore size.

When freeze drying was used for fabricating PGSU scaffolds the study did not attempt to characterise the freeze drying cycle effect on the scaffold's microstructure [148].

## 1.5.2. Airbrushing

Airbrushing (also referred to as air jet spinning, blow spinning and solution spraying) is a fabrication technique that has been recently developed to fabricate nanofibers by spraying a polymer solution through a small nozzle (usually less than 350  $\mu\text{m}$ ) using an air pump or compressed air [152-154]. It works by ejecting air through the nozzle which overcomes the surface tension of the polymer solution that results into stretching the solution into nanoscale fibres [155]. Additionally, while the polymer solution is sprayed it leads into vaporising the solvent from the produced nanofibers. This fabrication technique has been found to be 10 folds faster and 100 fold less expensive to set-up compared to electrospinning (due to not needing a high potential voltage) [152].

A few materials have been fabricated using this relatively new fabrication technique including PCL [152], PLA [156], hydroxyapatite/PLA [153] and hydroxyapatite/poly(vinyl acetate [154] composites. From these fibrous scaffolds, the most interesting was the PCL. After air brushing PCL they used 100% ethanol to separate the PCL fibres and then compressed them into a 10 mm thick fibrous scaffold [152]. After loading these scaffolds with magnesium (Mg) particles they found that Mg ions were released at a controlled rate for up to 2 months, the scaffold encouraged human osteoblasts to attach, spread and migrate throughout the scaffold [152].

## 1.6. Summary of literature review

Due to the limitation of donor oral tissue, treating wounds and defects caused from trauma, chronic infection and oral cancer in the oral cavity, remains challenging. OMTE is a science that has the potential to address this limitation by developing autologous 3D oral mucosa grafts to use for the treatment of oral mucosa wounds.

## Chapter 1

The most successful attempt to develop an oral mucosa equivalent was demonstrated using EVPOME. It was shown clinically that using Aloderm to culture oral keratinocytes, had superior results than using an autograft [157]. It was demonstrated that EVPOME was able to accelerate oral mucosa healing and matched the surrounding tissue properties and colour [1, 157]. The major disadvantages of Aloderm are batch to batch variation, limited ability to be tailored for specific applications and extensive processing to ensure that no disease transmission and all cellular components are removed. Synthetic scaffolds however do not possess any of the above disadvantages. Synthetic scaffolds can be synthesised with high precision and fabrication techniques can be optimised and established to increase the reproducibility of the scaffold's physical properties.

One important aspect of OMTE is the scaffold used and the scaffold's properties must be as biomimetic as possible. Oral mucosa has multiple biomechanical properties, which depend on its location within the oral cavity. Therefore, the scaffold should have tuneable mechanical properties. Additionally, since oral mucosa is constantly under *in vivo* dynamic forces the scaffold should also be able to sustain those forces but at the same time it should be able to recover. With this said, PGSU is a promising material to investigate for OMTE, as its mechanical properties can be tailored, and it does not undergo plastic deformation after loading. This material has not been widely investigated for its TE potentials, however preliminary results from literature have shown that it is biocompatible, with *in vivo* results to be, in some aspects, better than existing FDA approved materials such as PLGA.

Freeze drying is a fabrication technique that allows high control of pore size and pore structure and ensures high pore interconnectivity. Additionally, freeze drying can be used to fabricate large 3D scaffolds, which some other popular fabrication

techniques cannot (such as electrospinning). PGSU scaffolds have been fabricated before using freeze drying but were never processed and optimised for its biological properties. For example, the pore size was never adjusted for optimum fibroblast growth (20-30  $\mu\text{m}$ ), or it was never attempted to fabricate multiple layer structures that could exhibit a BM-like layer to mimic oral mucosa.

In the following thesis we fabricated porous PGSU scaffolds using freeze drying. The scaffolds were characterised for their microstructure, mechanical properties and cytocompatibility. The methods, results and discussion will be reported in the following chapters.

## **1.7. Aims and Objectives**

The overall aim of this project is to develop a PGS based scaffold to be used in oral mucosa tissue engineering. The scaffold's microstructure, mechanical properties, cell adherence, biocompatibility and biodegradation will be evaluated to determine the suitability for use in the oral cavity.

### **Hypotheses**

The hypotheses of this thesis are:

- i. Pore size, mechanical properties and degradation rate can be controlled in PGSU scaffolds by adjusting the polymer concentration during synthesis and fabrication.
- ii. Differences in PGSU scaffold microstructure can affect the biological response of cells by influencing protein production and cell behaviour.
- iii. PGSU scaffolds can be fabricated with a BM-like layer to facilitate cell co-culture and restrict cell infiltration.

The objectives of this thesis are outlined below:

# Chapter 1

1. To develop PGSU scaffolds using freeze-drying and to characterise their physical properties and the effect that the freeze drying and sterilisation techniques have on mechanical properties and microstructure.
2. To optimise the microstructure of the PGSU scaffolds and investigate how the mechanical properties, degradation rate, biocompatibility and collagen production are affected by the polymer concentration in the freeze drying solution.
3. To fabricate PGSU scaffolds with multiple pore architecture (orientation, pore size, porosity and multi-layer) to mimic different native soft tissue structures.
4. To develop a 2-layer scaffold resembling a basement membrane (BM) and lamina propria to determine the scaffold's ability to support oral cell co-culture and the ability to distinguish tissue layers.

The following thesis includes three experimental chapters that demonstrate the systematic approach in fabricating a PGSU scaffold for OMTE. The first experimental chapter (Chapter 2) shows the study of PGS and PGSU synthesis as well as PGSU scaffold fabrication using freeze-drying. The aim of this chapter was to understand the advantages and disadvantages of the scaffold and set a starting point to improve it in order to reach our final objective which is engineering an oral mucosa tissue. The scaffold was then tested for its microstructure, mechanical properties, enzymatic degradation, permeability as well as the sterilisation effect on its mechanical properties, permeability and a 9-day *in vitro* cell culture to demonstrate that cells can adhere and be metabolically active on the scaffold's substrate.

The second experimental chapter (Chapter 3) was built on the results from Chapter 2 and shows that the scaffold can exhibit multiple microstructures, mechanical properties, degradability and permeability by changing the polymer concentration

## Chapter 1

before freeze drying. The aim of this chapter was to improve the scaffold in terms of its physical properties and perform longer *in vitro* cell culture experiments before using human oral cells and co-cultures.

The final experimental chapter (Chapter 4) involves fabricating complex microstructure scaffolds by combining mould technology, airbrushing and freeze drying fabrication methods. From the knowledge obtained from the previous two chapters we developed multi-layered scaffolds that were distinguished by their pore size/porosity, and mono-layer scaffolds that had unidirectional (anisotropic) pore structures. The aim of this chapter was to demonstrate the ability of fabricating PGSU scaffolds that can mimic native ECM structures. A 2-layer scaffold that exhibited a thin non-porous layer which acted as a BM was then used to co-culture human oral cells and the collagen production and epithelium development was quantified as well as the ability of the non-porous layer to separate the cell types during co-culture.

The complete characterisation of the PGSU scaffolds is expected to demonstrate the potential of these scaffolds in OMTE and soft TE.



# Chapter 2 Poly(glycerol sebacate urethane) synthesis, scaffold fabrication and effect of sterilisation method

## Aim

To develop a fabrication technique for PGSU scaffolds with controlled properties and to test the biocompatibility and ability to sterilise these PGSU scaffolds.

## 2.1. Introduction

As discussed in Chapter 1, there are multiple biomaterials which have been successfully used in TE. PGS was shown to have the same advantages as many other synthetic materials, such as biocompatible, biodegradable, tailorable mechanical properties and degradation rate, but it also demonstrated stable mechanical properties prior to and post degradation. After cyclic loading PGS can recover its initial shape and mechanical integrity with minimal loss [122]. These properties are of great importance in TE as most if not all tissues are constantly under some sort of load and unload, therefore the scaffold should be mechanically stable during degradation and should recover its mechanical strength after loading.

PGSU, developed by Pereira et al. [147] and the freeze drying fabrication technique utilised by Frydrych et al. [148] solve the issues of low throughput, low reproducibility and inability to control pore size and porosity associated with PGS fabrication techniques. However, PGSU as a scaffold has not been characterised for its *in vitro* biocompatibility before this thesis.

When approaching a novel study of a newly developed scaffold that is designed to support cell growth *in vitro*, it is important to know how to sterilise it and how the sterilisation method affects its properties. In the past other research groups have used

70% ethanol, paracetic acid (PAA) and autoclaving to sterilise PGS scaffolds and films [126, 158]. These methods are the most common amongst most polymeric biomaterials in *in vitro* development because more clinically relevant sterilisation methods such as ethylene oxide and gamma irradiation are difficult to access and have been shown to be unsuccessful in maintaining the structural and biochemical properties of the scaffolds [159]. Additionally, ethanol and PAA have the advantage of working at low temperature, low cost and no complex equipment is needed for fast sterilisation [159].

This chapter will present the study performed on PGSU scaffolds fabricated using freeze drying, looking at the effect that the fabrication technique and the sterilisation method has on the scaffold's physical properties and biocompatibility. To assess the effect of pre-freezing conditions three different freezing temperatures were used (0 °C, -20 °C and -50 °C) and three sterilisation methods were used (paracetic acid, ethanol and autoclave) to sterilise PGSU samples and the scaffolds were tested for their chemical structure, microstructure, tensile strength, water permeability, and cell metabolic activity.

## 2.2. Materials and Methods

### 2.2.1. Materials

Sebacic acid (99%), glycerol (>99%), 1,4-dioxane (anhydrous, 99.8%), hexamethylene diisocyanate (HDI, 99%), Tin(II) 2-ethylexanoate, lipase enzyme from porcine pancreas (54 U mg<sup>-1</sup>), Dulbecco's modified eagle's medium (DMEM), penicillin-streptomycin (P/S), L-glutamine (200 mM), fetal calf serum (FCS), MEM non-essential amino acid solution (NEAA), HEPES buffer solution (1M),

trypsin/ethylenediaminetetraacetic solution (trypsin/EDTA), thiazol blue tetrazolium bromide (MTT) and resazurin sodium salt were purchased from Sigma-Aldrich.

### 2.2.2. Methods

#### 2.2.2.1. Pre-PGS synthesis

This method was obtained from previously reported methods [160]. Pre-PGS was synthesised at 1:1 M ratio between sebacic acid and glycerol. The synthesis setup is shown in Figure 2.1. Both were mixed in a three-neck flask and attached to a Dean-Stark trap with a condenser and nitrogen flow. The mixture was allowed to react at 120 °C under stirring and low nitrogen flow for 72 hours. Highly viscous pre-PGS was then formed and stored in a container at room temperature.

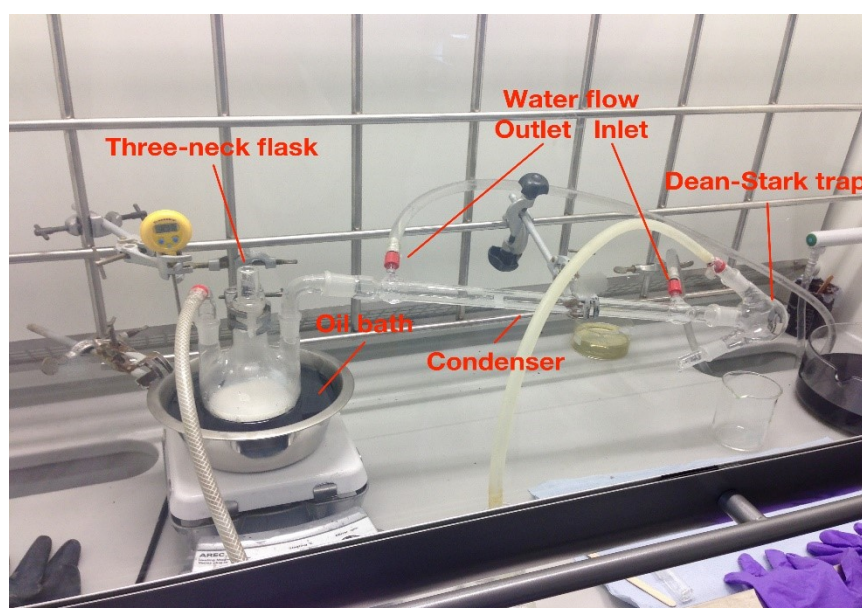


Figure 2.1: Pre-PGS synthesis setup.

#### 2.2.2.2. Gel permeation chromatography of pre-PGS

Gel permeation chromatography (GPC) was used to quantify the average molecular weight distribution of pre-PGS, more specifically for the number average molecular weight,  $\bar{M}_n$ , the weight average molecular weight,  $\bar{M}_w$ , and the polydispersity index (PDI). This works by injecting a small volume of polymer

solution into a set of columns containing a crosslinked gel. While the solution goes through the gel the smaller chains are absorbed and the longer chains pass through it faster. The smaller chains are then released giving a distribution curve for the sample [161, 162]. For this experiment tetrahydrofuran (THF) was used as eluent at a flow rate of  $1.0 \text{ ml min}^{-1}$  with 1 x PLGel 10  $\mu\text{m}$  Guard and 3 x PLGel 10  $\mu\text{m}$  Mixed B as columns. A Gilson 307 pump and an Erma ERC-7512 refractive index detector were used for the GPC measurements, and polystyrene samples were used for calibration.

### 2.2.2.3. PGSU-film and PGSU-2.5% fabrication

For the purpose of the following experiments porous PGSU scaffolds and non-porous film were fabricated. Pre-PGS was firstly dissolved into 1,4-dioxane at the required concentrations (2.5 w/v%) and pre heated to  $55 \text{ }^\circ\text{C}$  with 0.05% w/v of Tin(II) 2-ethylhexanoate. Once heated, HDI was added at a 0.6 molar ratio (glycerol:HDI) and left at  $55 \text{ }^\circ\text{C}$  for 5 hours under constant stirring. For ease of documentation, the nomenclature of the samples is PGSU-X where X refers to the polymer concentration (w/v%), e.g. 2.5% or PGSU-film.

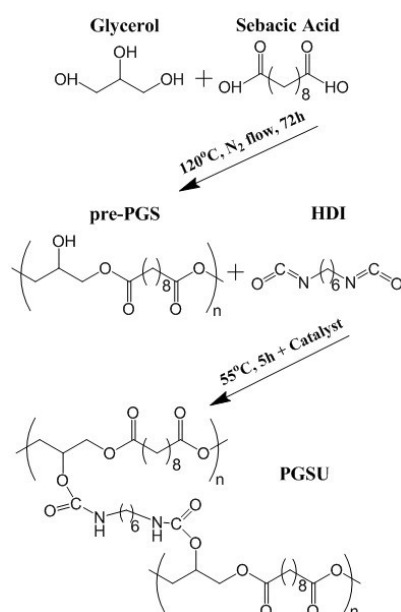


Figure 2.2: Synthesis of pre-PGS and PGSU polymer.

## Chapter 2

To produce a PGSU-film the solution was cast in a PTFE tray and left in the fume hood to allow the 1,4-dioxane to evaporate. To produce a PGSU-2.5% scaffold the solution was frozen and 1,4-dioxane was removed using freeze drying (FreeZone Triad Freeze Dry System, Labconco Co., USA). According to the National Institute of Standards and Technology (NIST) the melting point of 1,4-dioxane is 11.4 °C (NIST, <https://webbook.nist.gov/cgi/cbook.cgi?ID=C123911&Mask=4#Thermo-Phase>), therefore to freeze the solution and ensure a complete freeze it was decided to have 0 °C as the highest freezing temperature and the lowest freezing temperature -50 °C (lowest temperature setting possible from the FreeZone Triad Freeze Dry System) as well as a temperature in between the highest and lowest to understand the effect of the pre-freezing temperature on the scaffold's properties. The porous scaffold solution was cast into a PTFE baking tray and frozen at 0 °C, -20 °C or -50 °C overnight. On the next day the baking tray with the scaffold was placed in the freeze drier for lyophilisation. The freeze drier was set to -10 °C at 1 °C cooling or heating rate and left for 24 hours under vacuum pressure (0.1 mbar). Two hours before removing the scaffold from the freeze drier the temperature was raised to 20 °C to avoid drawing moisture in the scaffold upon exiting the freeze drier. The freeze drying cycle is shown at Figure 2.3 where during the pre-freeze stage the PGSU/1,4-dioxane solution temperature is reduced below its melting point to freeze and then during the primary drying stage the temperature and pressure is kept below the triple point of 1,4-dioxane to allow lyophilisation, shown in Figure 2.4. Finally, the scaffold and film were placed in the vacuum oven for 48 hours at 40 °C for further curing and drying. A schematic of the synthesis and fabrication procedure is shown in Figure 2.5.

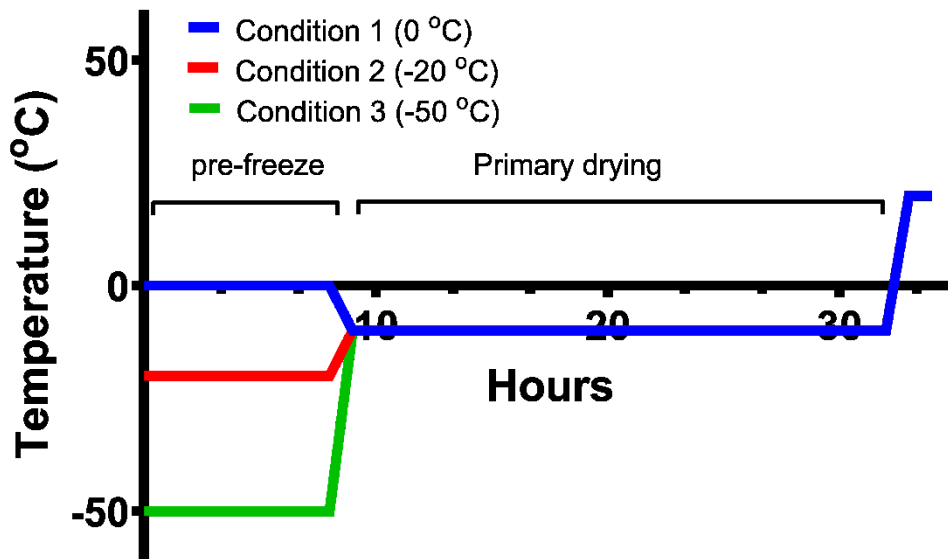


Figure 2.3: Freeze drying cycle for PGSU-2.5% scaffolds. The 1,4-dioxane/polymer solution was frozen at 3 different temperatures, 0 °C, -20 °C or -50 °C, and lyophilised the same way.

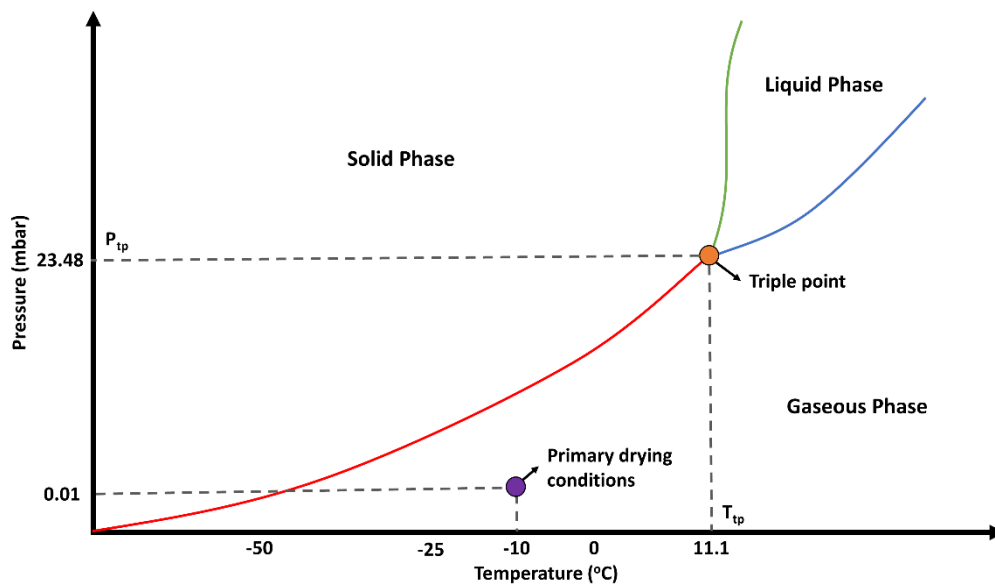


Figure 2.4: Three-phase diagram of 1,4-dioxane derived from the data provided from National Institute of Standards and Technology (NIST, <https://webbook.nist.gov/cgi/cbook.cgi?ID=C123911&Mask=4#Thermo-Phase>).  $T_{tp}$ : Triple point temperature,  $P_{tp}$ : Triple point pressure. The purple circle shows the temperature and pressure of the 1,4-dioxane during primary drying in the freeze drier.

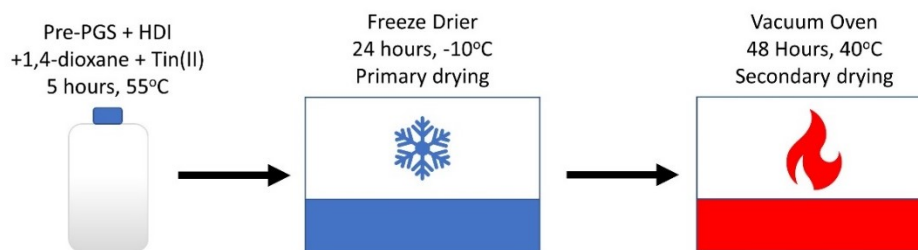


Figure 2.5: Schematic of synthesis and fabrication method for PGSU-2.5% scaffolds.

All scaffolds were washed with ethanol to remove any unreacted substances from the construct. The washing was done by submerging the scaffold in 100%, 70% and 50% Ethanol for 2 hours each, and then immersed in distilled water overnight. Shaking was also applied to the scaffolds during washing.

#### 2.2.2.4. Scaffold sterilisation

Three different sterilisation methods were assessed. The first was submerging the scaffolds into 70% ethanol overnight while shaking. Then under sterile conditions the scaffolds were washed three times using sterile PBS and left in PBS overnight under shaking. The same procedure was followed for the second sterilisation method but instead of ethanol, 0.1 % (v/v %) paracetic acid (PAA) was used. Last sterilisation method was done by autoclaving at 121 °C for 15 minutes. For comparison reasons a PGSU film was also sterilised using the same three methods.

#### 2.2.2.5. Porous scaffold characterisation

##### 2.2.2.5.1. Fourier transform infrared spectroscopy

Fourier transform infrared spectroscopy (FT-IR) was performed using Perkin Elmer Spectrum One NTS analyser. Attenuated total reflection (ATR) was used at mid-infrared region of 4000-550  $\text{cm}^{-1}$  and recording resolution of 4  $\text{cm}^{-1}$  at room temperature. The test was repeated three times with technical triplicates using pre-PGS, PGSU scaffold before ethanol extraction and PGSU scaffold after ethanol

extraction. The samples were collected from the centre and sides of the fabricated scaffolds. A small amount of pre-PGS, cured PGS and small solid pieces of PGSU were placed on the test area for scan. The number of scans was set to 20 and an average spectrum was plot.

### 2.2.2.5.2. Scanning electron microscopy

To examine the microstructure of the porous scaffolds scanning electron microscopy (SEM) was utilised using the FEI™ Inspect F50. The porous samples were attached on an aluminium stub and gold coated using High Resolution Polatron Spetter Coater at 15 kV for 1.5 minutes. To measure the average pore size ImageJ software was used. Firstly, the scale of the image was set into the software and then using the free hand selection tool, the pore's periphery was selected and the area was measured using an in-built function provided by the software, as shown in Figure 2.6. The pore diameter was calculated using:

$$A = \pi r^2 \quad \text{Eq. (1)}$$

with  $A$  = pore area and  $r$  = pore radius. Therefore, when pore size is mentioned it implies the pore diameter. The images were taken from the top view, cross section, bottom view and top to bottom of the produced scaffolds. Only fully defined pores were used to determine the average pore size, with 50 pores measured per image.

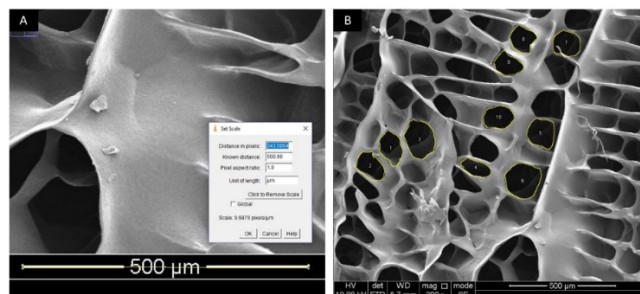


Figure 2.6: Example of pore size measurements using ImageJ. A) Shows an example of how the scale of the SEM image is set into the software and (B) is a representation of how the pores were selected using the freehand tool.



### 2.2.2.5.3. Porosity measurement

The porosity of the scaffolds was measured using the gravimetric method [163]. Circular disks were cut with diameter 10 mm and thickness ~5 mm for the scaffold and ~2 mm for the film. The densities of porous scaffold ( $\rho_s$ ) and film ( $\rho_f$ ) were calculated by dividing the mass with the volume of the sample, measured using a four-decimal point balance and a three-decimal point caliper respectively. Five specimens were used from each batch of scaffold. Knowing the density of the sample the equation below was then used to calculate the porosity Eq. (2),

$$P = \left(1 - \frac{\rho_s}{\rho_f}\right) \times 100 \quad \text{Eq. (2)}$$

### 2.2.2.5.4. Mechanical testing

PGSU porous scaffolds were tested for their tensile strength following the BS EN ISO 1798:2008 standard using a Hounsfield H100KS testing machine (Tinius Oles, USA). The samples were prepared in dog-bone shape (using test sample cutter with gauge length = 25 mm, width = 3.25 mm) and tested at a 500 mm/min rate of travel using a 10 N load cell until failure. Sufficient test pieces were used to provide 5 breaks within the gauge length.

### 2.2.2.5.5. *In vitro* enzymatic degradation testing

*In vitro* degradation was performed on the PGSU-2.5% scaffolds and films using lipase enzyme at an activity of 40 U/ml. Lipase can catalyse the hydrolysis of ester bonds in polyester materials in aqueous solutions, hence it is one of the most common enzymes used when examining the *in vitro* degradation characteristics of polyester materials [148, 164]. Furthermore, lipase is one of the two dominating enzymes (lingual lipase) found in the human saliva [165]. However, pancreatic lipase was used in this thesis due to a lack of commercially available lingual lipase. The enzyme

activity was chosen to mimic the *in vivo* lipase activity of the gastric juice (40 U/ml) which is attributed to the lingual lipase secreted by the Von Ebner secretory glands located in the back of the tongue [166]. Prior to the experiment all samples were sterilised with 70% ethanol overnight, and then dried in a vacuum oven overnight at 40 °C. The samples were fully submerged in triplicates into PBS/lipase solutions for a total of 28 days and placed in a shaker incubator at 37 °C and 100 rpm, changing the enzyme solution every day because the half-life of lipase is approximately 10.2 hours [167]. Every 7 days the samples were washed thoroughly with distilled water to remove any polymer by-products and lipase that can affect the mass of the sample and dried in a vacuum oven at 25 °C overnight to allow the measure of the sample's dry mass. The samples were then weighed, recorded, and then placed back into the enzyme solution. Samples were also degraded in phosphate buffered solution (PBS) without enzymes as a control.

### 2.2.2.5.6. Water contact angle

The water contact angle of PGS-film, PGSU-film and PGSU-2.5% scaffold was measured at room temperature using distilled water. The sample was placed on a levelled surface and a 10 µl water droplet was deposited on the top surface of the sample. Images were taken after 10 and 60 seconds to measure the contact angle ( $\theta$ ). ImageJ was used to measure the  $\theta$  and the angle was calculated using the sphere approximation. The software works by manually choosing the baseline of the droplet, and then another 5 points around the periphery of the droplet. It then draws a tangent line from the periphery of the droplet to the baseline and calculates the angle between them. This experiment was done at n=3 and when  $\theta$  was less than 90° the surface was considered hydrophilic while when higher than 90° is was considered as hydrophobic [168].

### 2.2.2.5.7. Permeability testing

The term permeability is intended to show how much of fluid can permeate through the scaffold's walls with respect to pressure, and this was calculated using the Darcy's Law found below (Eq. 4). The setup of the experiment is called constant head method and it was inspired by Pennella et al [169]. As shown in Figure 2.7, the constant head reservoir was set to a constant height and the water was collected into a container that was sitting on a balance to measure the weight and use it to calculate the flow rate (Q). The scaffold was fixed inside a silicon sleeve (water could only go through the scaffold) and mounted onto tygon tubing and was hanged vertically. The fluid level of the constant head reservoir was kept constant using a peristaltic pump that was adjusted to the necessary flow rate to fulfil the fluid loss. The level of the water was kept constant to keep the hydrostatic pressure constant.

Prior to the beginning of the experiment the scaffold was submerged into ethanol to push any air bubbles out of the scaffold construct. The whole system was filled up with distilled water, making sure that all air has left the system. The scaffold was then mounted in place and the experiment was ready to begin. Each scaffold was tested for 10 minutes taking a recording of the flow rate every minute. Thus the volume of water collected divided by the time gives the Q. Knowing the constant head height, scaffold thickness (L), scaffold cross section area and Q the hydraulic conductivity of the scaffold can be calculated using Eq. (3) below:

$$K = \frac{QL}{AH} \quad \text{Eq. (3)}$$

And by substituting the results of Eq. (3) into Eq. (4) the permeability (k) can be calculated using Darcy's law.

$$k = K \frac{\mu}{\rho g} \quad \text{Eq. (4)}$$

With:  $k$  = permeability ( $m^2$ ),  $\mu$  = dynamic viscosity ( $kg/ms$ ),  $\rho$  = water density ( $kg/m^3$ ) and  $g$  = gravity ( $m/s^2$ ).

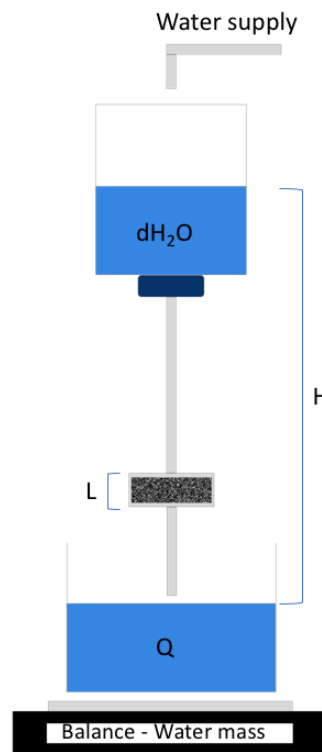


Figure 2.7: Schematic of permeability test setup using the constant head method. dH<sub>2</sub>O is distilled water, H is constant head length, L is scaffold thickness and Q is flow rate. The schematic is not scaled.

### 2.2.2.6. Validation of cytocompatibility and sterilisation method

#### 2.2.2.6.1. L929 cell culture

L929 cells (immortalised dermal mouse fibroblast cell line) were cultured using DMEM 10% Serum media (10% (v/v) FCS, 2 mM L-Glutamine, 1% NEAA, 100 IU/ml penicillin, 100  $\mu$ g/ml streptomycin and 10 mM HEPES). These cells have been suggested by ISO 10993-5:2009 as the standard cells to use for *in vitro* cytotoxicity testing.

Prior to the experiment two confluent T75 flasks were washed with PBS and 5mL of 0.1% trypsin/EDTA was added to each flask and incubated for 2-3 minutes. The flasks were then examined under an inverted light microscope to ensure that the cells

were detached from the tissue culture plastic of the flask. Then 5 ml of warm media was added in each flask to neutralise trypsin and then the cell suspension was moved into a universal and centrifuged at 1000 rpm for 5 minutes. The supernatant was carefully removed, and the remaining cell pellet was resuspended in 10 ml of media. Using a haemocytometer, 10  $\mu$ l of the cell suspension was added on each side and the cells were counted under a light microscope. The required cell number was then calculated and moved into a new universal. Media was then added to make up the desired volume.

### **2.2.2.6.2. Sample preparation and cell seeding**

The samples were prepared by punching small 15 mm diameter circular porous scaffolds and films, 12 samples each. Nine of each, scaffold and film samples, were then sterilised using the three sterilisation methods mentioned earlier, hence three samples each method. The three remaining samples were autoclaved and served as the negative control. Afterwards, the scaffolds and films were placed into two 24 well plates and passively seeded, by overlaying them with 200  $\mu$ l cell/media suspension ( $3.0 \times 10^4$  cells/sample). The cells were allowed to attach on the samples for 1 hour and then media was added to make up to 1 ml. Positive and negative controls were also used for comparison purposes, with positive control to be cells seeded on tissue culture plastic (TCP) and negative control scaffold or film with only media. Each assay was repeated three times ( $n=3$ ) in technical triplicates.

### **2.2.2.6.3. Cell metabolic activity assays**

To validate the scaffold's cytocompatibility and how to sterilise them prior to cell seeding, MTT (3-(4,5-dimethylthiazol-2-yl)-2,5-diphenyltetrazolium bromide) and resazurin assays were used. Both assays measure some aspect of general cell metabolism of viable cells. MTT assay measures the metabolic activity of viable cells

by converting MTT into a purple formazan product [170]. Resazurin metabolic assay acts the same way as AlamarBlue® [171]. The resazurin reduction test works by changing its original blue colour (resazurin) to a pink fluorescent dye (resorufin) in the medium by cell activity (likely to be by oxygen consumption through cell metabolism)[170, 171]. The advantage of resazurin assay over MTT assay is that it does not kill the cells; therefore, readings of cell metabolic activity can be taken at multiple time intervals.

### **2.2.2.6.3.1. MTT assay**

The cell-seeded scaffolds were cultured for 48 hours in an incubator. MTT solution was then prepared at 0.5 mg/ml. After 48 hours, the media was removed from each well and washed three times with sterile PBS. Each well was then submerged into 1 ml of MTT solution and left for 1 hour, wrapped in aluminium foil inside the incubator. The MTT solution was then removed, replaced with 300 µl acidified isopropanol and left for 10 minutes on a shaker. Duplicates of 150 µl were then transferred to a 96 well plate from all the samples and the optical density (OD) was measured in an absorbance spectrometer reader at wavelength 570 nm.

### **2.2.2.6.3.2. Resazurin reduction assay**

This experiment was run for 9 days performing a resazurin assay every 3 days. To prepare the resazurin stock solution at 0.25 w/v%, 0.0251g of resazurin sodium salt was weighed into a container. Then 100 ml of deionized water was added and the container was wrapped in aluminum foil to protect from light. The solution was then filtered using sterile syringe and sterile syringe filter (0.20 µm) inside the cell culture cabinet. The resulting sterile resazurin solution was then stored in the fridge until further use.

## Chapter 2

On the day of the reading, resazurin working solution was prepared by mixing resazurin stock solution with media at 10 v/v%. For each repeat of the experiment we needed 60 ml of working solution therefore 6 ml of resazurin solution plus 54 ml of media. The media was removed from the well and the seeded samples were washed with PBS. Then the samples were moved to a new well plate, to allow us to measure the cell activity on the samples and not on the well plate, and resazurin assay was performed at both well plates (well plate 1 = cells on tissue culture plastic (TCP), well plate 2 = cells on scaffold or film). The working solution was added at 1 ml per well. The well plate was then wrapped in aluminum foil and left in the incubator for 2 hours. Two hours later the now reduced working solution was transferred into a 96 well plate at 200  $\mu$ l in triplicates. The plate was read using the BioTek ELx800™ absorbance reader at 570 nm. To prepare the samples for the next three days they were washed 5 times with PBS ensuring that all the working solution has been washed off and then placed back in the original well plate with 1ml of media. The same procedure was repeated on Day 6 and Day 9.

The results were normalized against the positive control (cells on TCP). To normalize the results, the absorbance of positive control was assumed to be 100% of cell activity, and the ratio of between the positive control and the absorbance obtained from the cells seeded on the samples was plotted.

Additionally, the seeding efficiency was quantified during the day 3 resazurin assay results. The results obtained from the well plate 1 (cells on TCP) and well plate 2 (cells on scaffold or film) were assumed to be 100% of cells. Therefore, the seeding efficiency could be estimated by calculating the ratio of the metabolic activity from the cell seeded scaffold or film to the 100% of cells.

### 2.2.2.7. Statistical analysis

The statistical analysis was performed using one-way and two-way ANOVA with post hoc Tukey with null hypothesis set that there is no interaction between sample groups, using Graphpad Prism 7.03. All measurements were reported as mean  $\pm$  standard deviation (SD), and considered significant when  $p \leq 0.05$ .

## 2.3. Results

### 2.3.1. Pre-PGS and PGS characterisation

Visually pre-PGS was found to have a yellowish colour, shown in Figure 2.8 (A); and when cured, the PGS film was transparent, shown in Figure 2.8 (B).

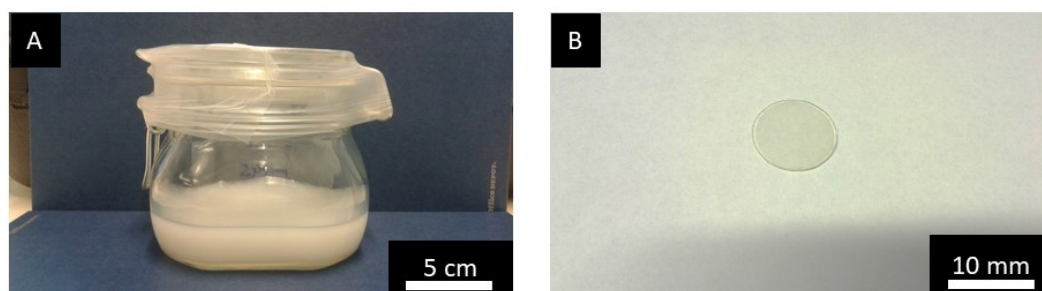


Figure 2.8: Macroscopic images of (A) pre-PGS and (B) cured PGS film.

For this project one batch of pre-PGS was synthesised, and GPC was used to quantify the average molecular weight distribution and the results are shown in Table 2.1. The PDI was equal to 3.32 showing a uniform molecular weight distribution.

Table 2.1: Gel permeation chromatography results from pre-PGS.  $\bar{M}_n$ ,  $\bar{M}_w$  and PDI are number average molecular weight, weight average molecular weight and polydispersity index respectively.

	$\bar{M}_n$ (g/mol)	$\bar{M}_w$ (g/mol)	PDI
Pre-PGS	2246	7459	3.32



ATR-FTIR was used to examine the chemical structure of the pre-PGS and cured PGS films shown in Figure 2.9. The pre-PGS spectrum presented a broad absorption peak at  $3451\text{ cm}^{-1}$  due to hydroxyl groups as well as two sharp peaks at  $2928\text{ cm}^{-1}$  and  $2852\text{ cm}^{-1}$  which belong to alkane groups stretch vibrations [172, 173]. The ester bonds formation is shown from the sharp peak at  $1732\text{ cm}^{-1}$  and the rest of the peaks between  $1384\text{--}1049\text{ cm}^{-1}$  are due to the stretch vibration bands of carboxyl bonds. After the pre-PGS curing process the hydroxyl group broad peak reduced and slightly shifted from  $3451\text{ cm}^{-1}$  to  $3455\text{ cm}^{-1}$ . A slight increase in intensity from the ester bonds at  $2929\text{ cm}^{-1}$  and  $2853\text{ cm}^{-1}$  in combination with a decreased intensity from the carboxyl groups between  $1378\text{ cm}^{-1}$  and  $1047\text{ cm}^{-1}$ , indicate an increase in crosslink density of PGS [119, 172, 173].

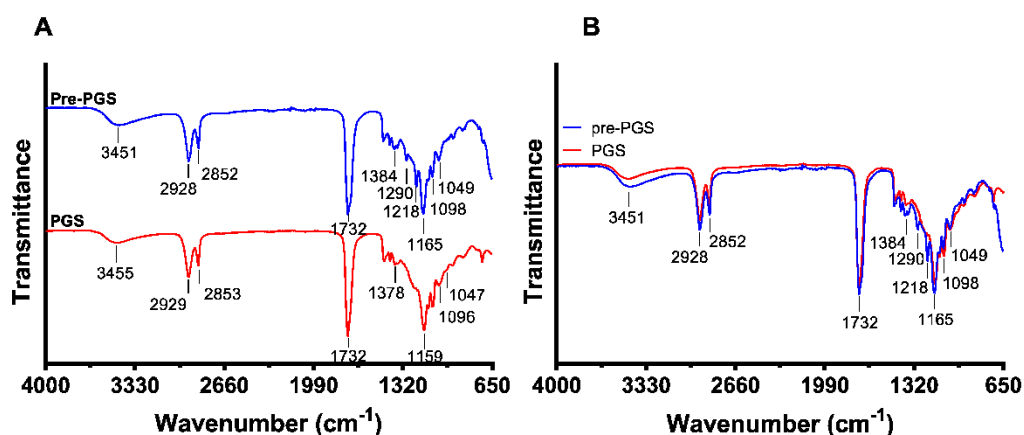


Figure 2.9: FTIR spectra of pre-PGS and cured PGS. (A) vertically shifted and (B) overlapped spectra.  $n=3$

### 2.3.2. PGSU-2.5% scaffold characterisation

After characterising the PGS, HDI was mixed with pre-PGS and PGSU was synthesised. The PGSU-films had a transparent colour whereas the porous scaffold had a white colour with good mechanical properties, easy to handle, shape recovery properties and low adhering properties, shown in Figure 2.10.

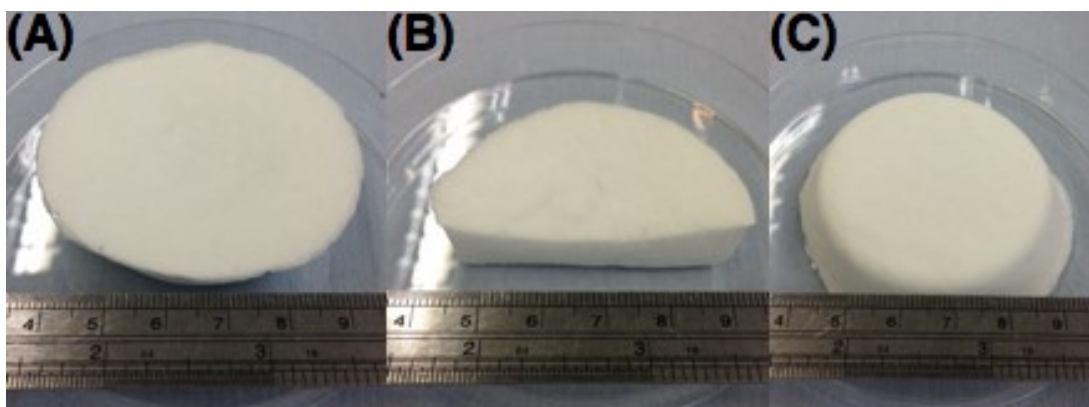


Figure 2.10: Macroscopic images of PGSU-2.5% scaffolds. (A) Top, (B) cross section and (C) bottom.

The PGSU-2.5% characterisation began with FTIR to confirm the synthesis and chemical structure of the scaffold. FTIR was repeated three times each repeat with a different PGSU-2.5% batch. The results obtained are shown below Figure 2.11. The ATR-FTIR spectra below are for pre-PGS, PGSU-2.5% washed with ethanol, PGSU-2.5% not washed with ethanol, and HDI for comparison. Briefly a shift of  $\text{-OH}$  group from  $3450\text{ cm}^{-1}$  to  $3350\text{ cm}^{-1}$  ( $\text{-NH}$ ) is observed between pre-PGS and PGSU-2.5% samples indicating that the free hydroxyl groups reacted with the isocyanate groups. Primary and secondary amides are also found for the PGSU-2.5% samples at  $1620\text{ cm}^{-1}$  and  $1578\text{ cm}^{-1}$  indicating the formation of urethane linkages. To demonstrate the peak of the isocyanate, pure HDI was tested using the same method applied for the other samples. All three spectra lack an  $\text{NCO}$  ( $2250\text{ cm}^{-1}$ ) peak implying a complete reaction between the hydroxyl and isocyanate groups.

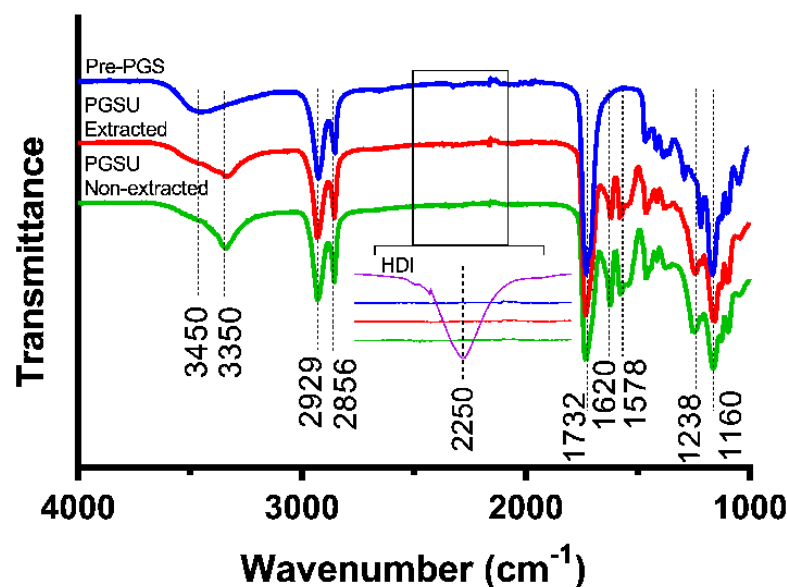


Figure 2.11: ATR-FTIR spectra of pre-PGS and PGSU-2.5% scaffolds. Scaffolds were examined before prior ethanol extraction and post ethanol extraction and compared between them and against pre-PGS that served as a control. FTIR was also carried out for the HDI.  $n=3$ .

The SEM images in Figure 2.12 represent the porous PGSU-2.5% scaffold fabricated using freeze-drying. The scaffolds exhibited a random structure with pores which are not fully defined. Additionally, the pore structure and size are different between sections (top, cross and bottom sections). The pore structure at the top section (see Figure 2.12 (A1-2)) are relatively defined and circular, whereas at the cross section the pore structure is not defined (Figure 2.12 (B1-2)). The pore structure at the bottom section is more uniform and open pore with a flake-like structure (Figure 2.12 (C1-2)). The scaffold was also imaged from top to bottom looking into its cross section, Figure 2.13, and it appears that the microstructure of the scaffold is denser at its top and becomes less dense while moving towards the bottom section of the scaffold. Meaning that there is a porosity gradient moving upwards (porosity increases as a function of scaffold depth).

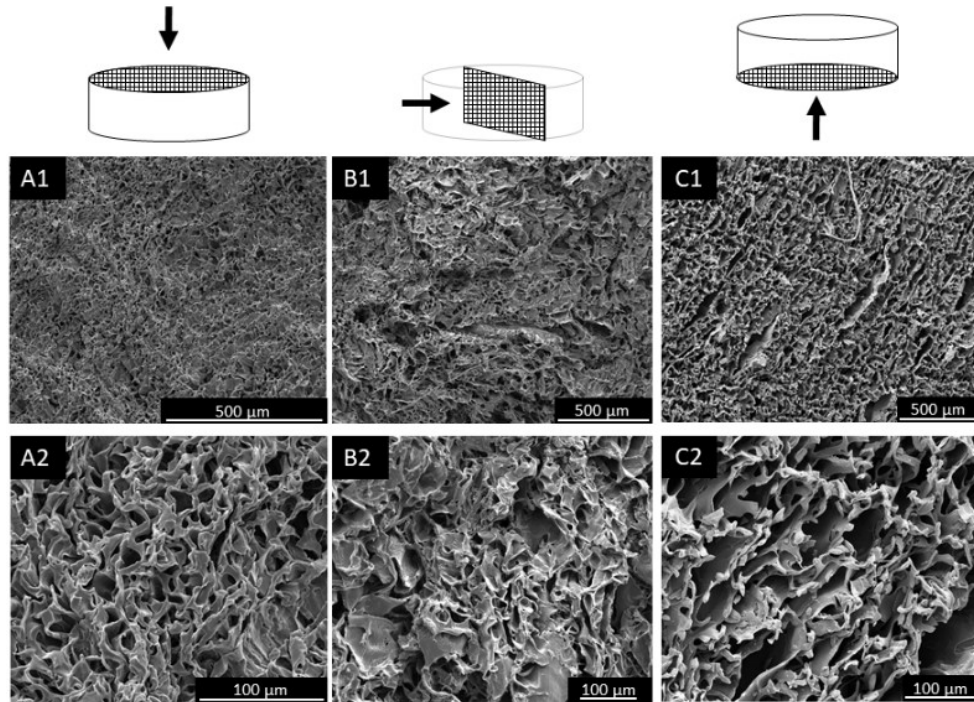


Figure 2.12: SEM images of PGSU-2.5% scaffolds taken from A1-2) top, B1-2) cross and C1-2) bottom section.

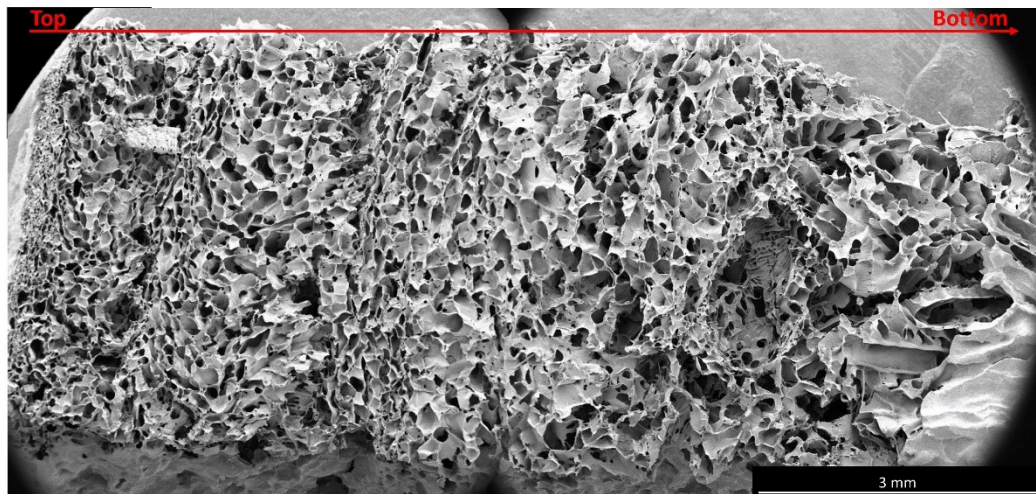


Figure 2.13: PGSU-2.5% scaffold cross section from top to bottom.

The pore size and porosity of the PGSU-2.5% scaffolds were measured and are summarised in Figure 2.14 and Table 2.2. The pore size changes significantly between sections, with the smaller pore size to be found on its top section,  $12.7 \pm 0.7 \mu\text{m}$ , then a 2-fold increase for the cross section,  $24.6 \pm 7.4 \mu\text{m}$  and the largest pore size was found at the bottom section,  $45.4 \pm 2.3 \mu\text{m}$ . A very high porosity was also

demonstrated,  $96.9 \pm 0.71$  %. The higher variability of pore size in the cross section ( $\pm 7.4 \mu\text{m}$ ) is due to the difference of the pore structure over depth, shown in Figure 2.13.

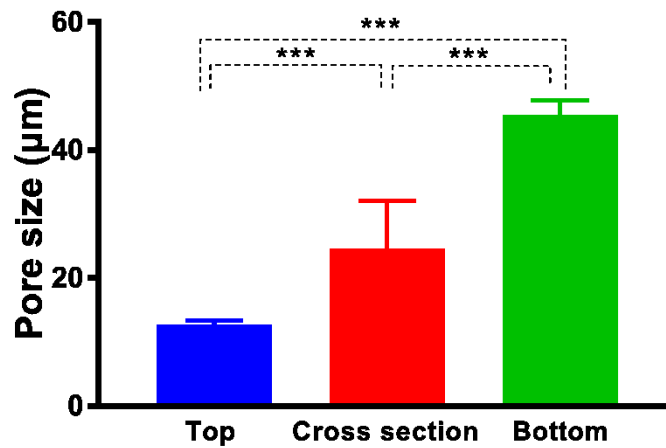


Figure 2.14: Pore size of PGSU-2.5% scaffolds. Results are shown as mean  $\pm$  standard deviation. (n=50 and \*\*\* when  $p < 0.001$ )

Table 2.2: Pore size and porosity of PGSU-2.5% scaffolds. Results are shown as mean  $\pm$  standard deviation. (n=50 for pore size and n=3 for porosity, \*\*\* when  $p < 0.001$ )

PGSU-2.5% scaffold		
	Pore size ( $\mu\text{m}$ ) $\pm$ SD	Porosity (%) $\pm$ SD
Top section	$12.7 \pm 0.7$ ***	$96.9 \pm 0.7$
Cross section	$24.6 \pm 7.4$ ***	
Bottom section	$45.4 \pm 2.3$ ***	

PGSU-2.5% scaffolds were also mechanically tested for their tensile strength. Figure 2.15 shows the representative tensile strength – strain curve obtained from the scaffold. The Young's modulus was  $0.03 \pm 0.01$  MPa, the UTS was  $0.01 \pm 0.01$  MPa

and elongation at break was  $61.0 \pm 8.2$  %. A more detailed figure is shown below at Figure 2.20.

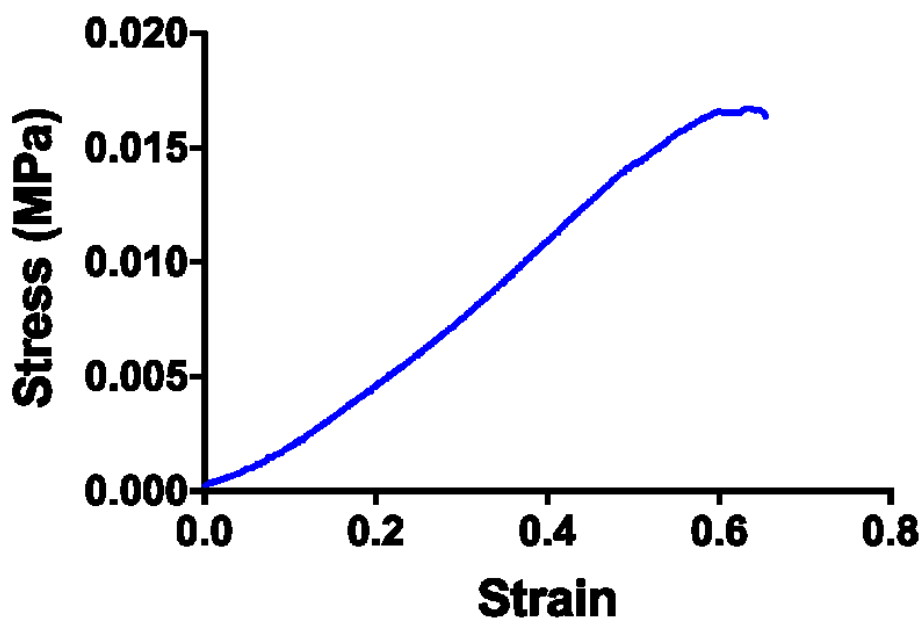


Figure 2.15: Representative tensile strength - strain curve of PGSU-2.5% scaffolds.

To determine the degradation rate, PGSU-2.5% scaffolds were degraded *in vitro* using lipase and PBS, for comparison PGSU-films were also degraded, and the results are shown in Figure 2.16. Both the film and the scaffold samples had a very low mass loss in PBS, approximately  $\sim 4$  % after 28 days. However, a higher mass loss was observed when lipase was used, and a significant difference was found between the PGSU-2.5% and PGSU-film. Both samples degraded linearly, reaching their highest mass loss at day 28, with PGSU-2.5% degraded  $71.9 \pm 5.4$  % and the PGSU-film degraded  $24.5 \pm 1.9$  %.

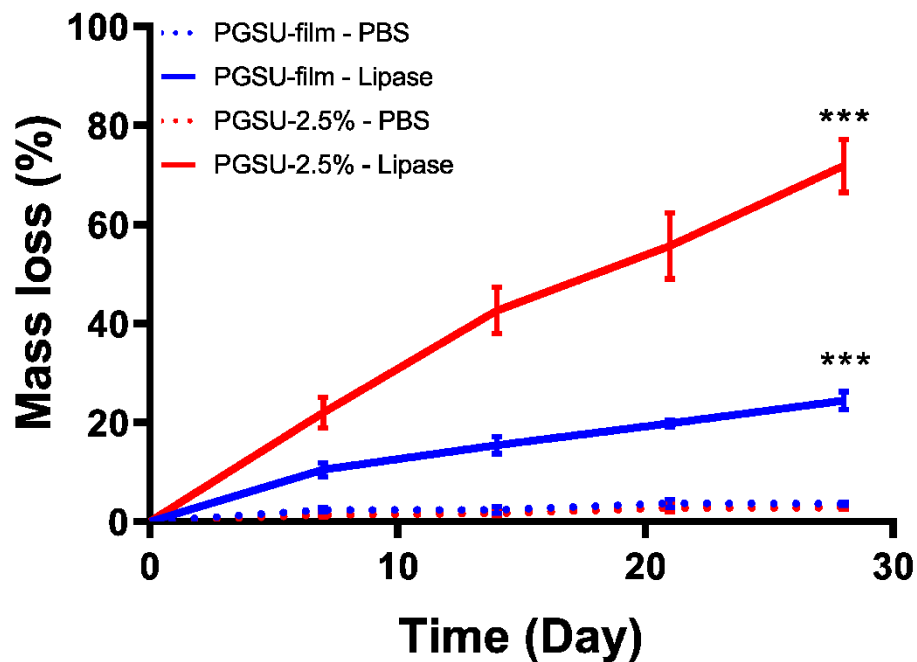


Figure 2.16: PGSU film and scaffold enzymatic degradation over 28 days period. Results are shown as mean  $\pm$  standard deviation. (n=3, \*\*\* when  $p < 0.001$  compared with PBS and PGSU-film)

### 2.3.3. PGSU-2.5% fabrication characterisation – freezing temperature

PGSU-2.5% scaffolds were fabricated at different freezing conditions to determine the effect on the microstructure. SEM was used to image the microstructure of the scaffolds freeze dried at 0 °C and -50 °C shown in Figure 2.17 and Figure 2.18 respectively.

Similar to previous results, there is a gradient in pore size (increasing from top to bottom) and shape, however the scaffolds fabricated at 0 °C have a fairly uniform and circular pore structure. The SEM images from the PGSU scaffolds frozen at -50 °C have a completely different pore structure compared to the 0 °C and large voids were formed within the scaffold's architecture.

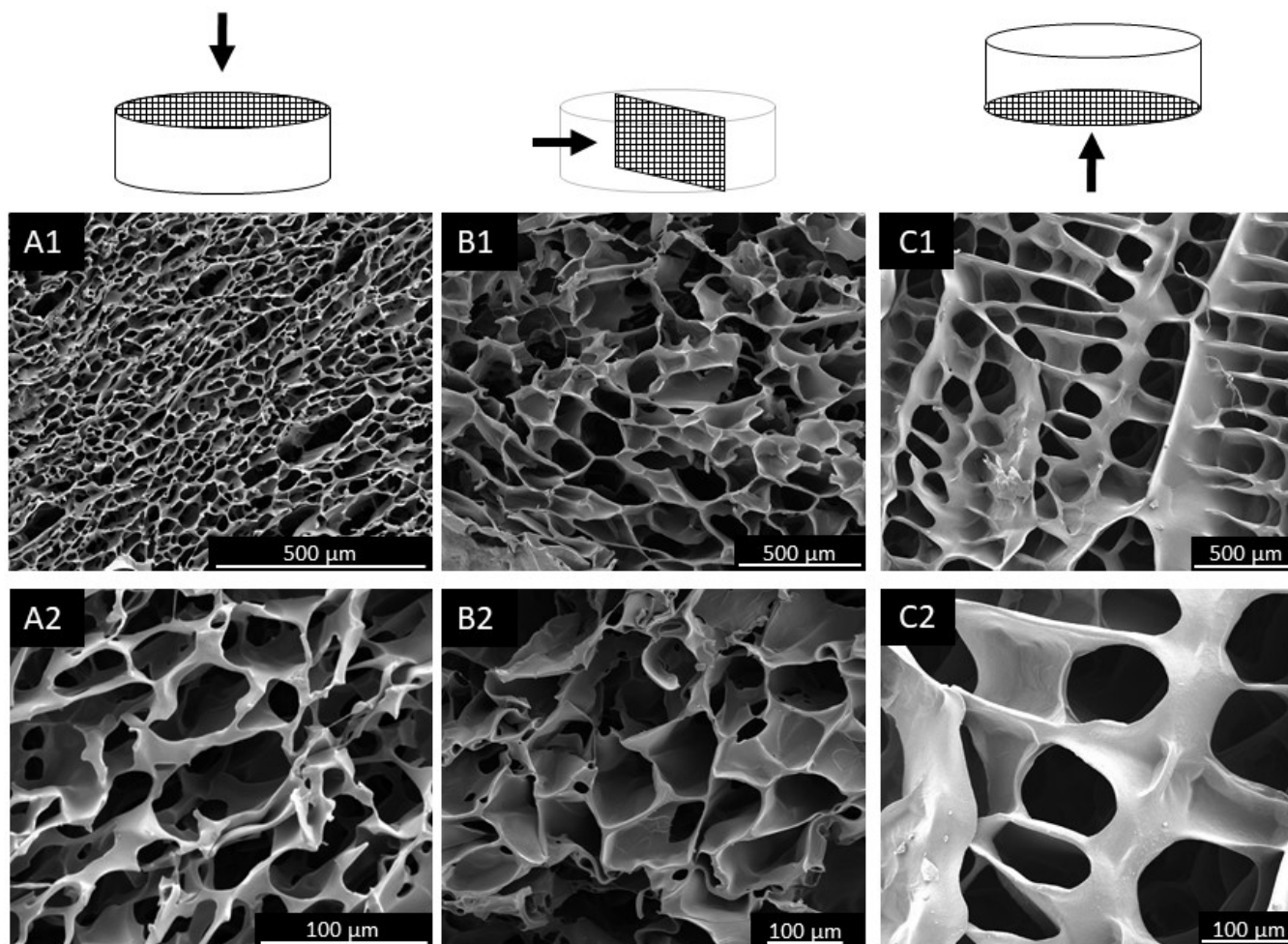


Figure 2.17: SEM images of PGSU-2.5% scaffolds frozen at 0 °C taken from A1-2) top, B1-2) cross and C1-2) bottom section.



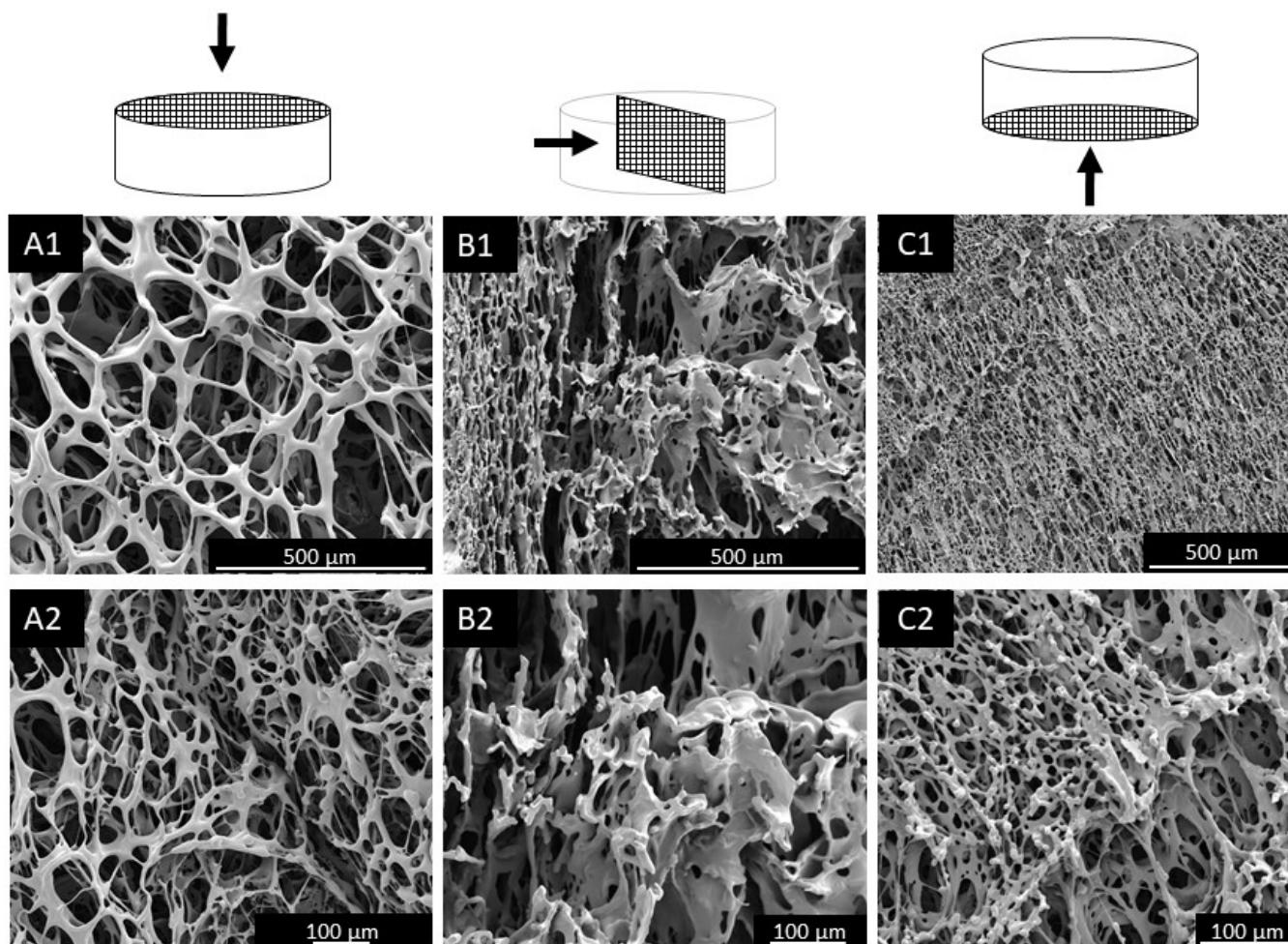


Figure 2.18: SEM images of PGSU-2.5% scaffolds frozen at -50 °C taken from A1-2) top, B1-2) cross and C1-2) bottom section

When the pore size was calculated, Figure 2.19, there was a significant difference found when changing the freezing temperature during the first stage of freeze drying. However, when comparing the pore sizes from -20 °C and -50 °C there was no significant difference observed. Additionally, within each freezing condition group the pore size changes significantly between scaffold sections.

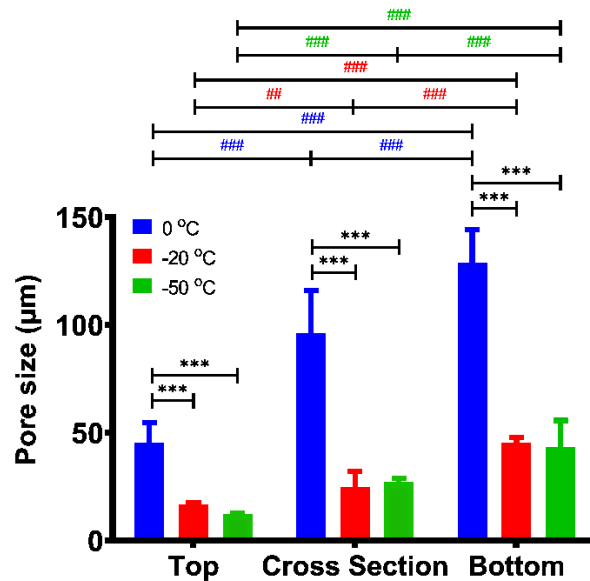


Figure 2.19: Pore sizes of PGSU-2.5% scaffolds frozen at different temperature, 0 °C, -20 °C and -50 °C. Results are shown as mean  $\pm$  standard deviation. n=50, \*\*\* when  $p < 0.001$  between groups and ### when  $p < 0.001$  within groups (colours are used for # to distinguish the groups).

The calculated porosity of the scaffolds is not affected by the freezing condition, as there was no significant difference between them, see Table 2.3.

Table 2.3: Porosity of PGSU-2.5% scaffolds frozen at different temperatures. Results are shown as mean  $\pm$  standard deviation. n=3.

Freezing condition	Porosity (%) $\pm$ SD
0 °C	96.61 $\pm$ 0.29
-20 °C	96.89 $\pm$ 0.71
-50 °C	95.43 $\pm$ 0.56

## Chapter 2

The mechanical properties of the scaffolds are shown in Figure 2.20. The Young's modulus, Figure 2.20 (B), ranges between  $0.029 \pm 0.009$  to  $0.319 \pm 0.297$  MPa, but no significant difference was found. Similarly, the elongation at break, Figure 2.20 (D), did not change significantly. However, it was found that the UTS from the scaffolds frozen at  $-20$  °C is significantly lower than the scaffolds frozen at higher and lower temperatures, ranging between  $0.02 \pm 0.01$  to  $0.93 \pm 0.02$  MPa, shown at Figure 2.20 (C).

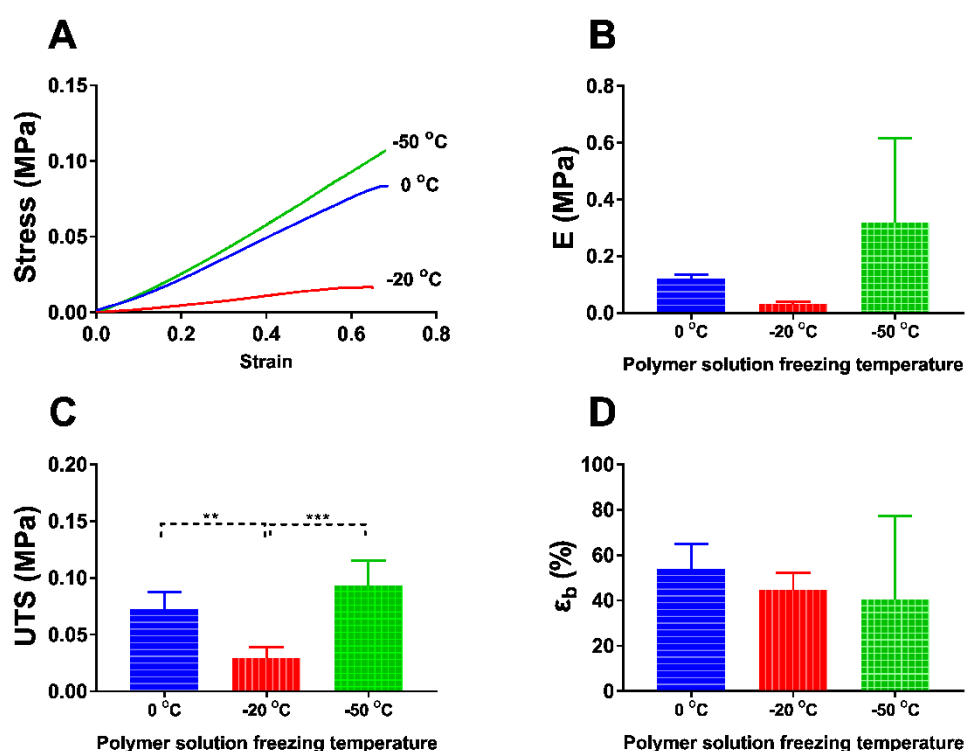


Figure 2.20: Mechanical properties of PGSU-2.5% scaffolds frozen at different temperatures, 0 °C, -20 °C and -50 °C. Results are shown as mean  $\pm$  standard deviation. (n=5, \*\* when  $p < 0.01$ , \*\*\* when  $p < 0.001$ )

Figure 2.21 shows the results of the water contact angle measurements from the PGS-film, PGSU-film and PGSU-2.5% scaffolds. A significant increase in the water contact angle was found between PGS and PGSU (both film and scaffold) probably due to the urethane linkages formed during crosslinking. The PGSU-film and PGSU-2.5% exhibited a hydrophobic surface ( $\theta = 103.2 \pm 4.4^\circ$  and  $\theta = 106.7 \pm 4.5^\circ$  respectively)

## Chapter 2

at 10 seconds but at 60 seconds the water contact angle reduced significantly ( $\theta = 59.1 \pm 2.9^\circ$  and  $\theta =$  could not be measured; respectively), while cured PGS-film had a hydrophilic surface ( $\theta = 46.5 \pm 3.3^\circ$ ) for both time points. The droplet was fully absorbed from the PGSU-2.5% scaffolds (Figure 2.21 (C2)) and it could not be measured.

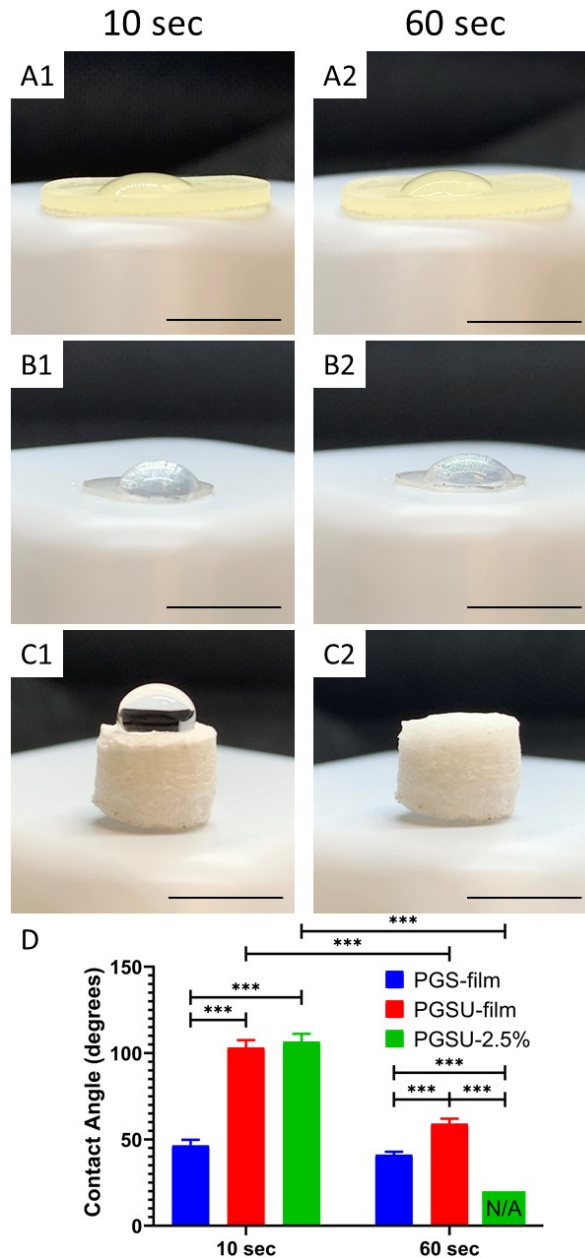


Figure 2.21: Water contact angle of cured PGS film, PGSU-film and PGSU-2.5% scaffold over a period of 60 seconds. A1-2) Cured PGS-film, B1-2) PGSU-film, C1-2) PGSU-2.5% scaffold and D) measured water contact

angle. The water contact angle of PGSU-2/5% scaffold was  $0^\circ$  at 60 seconds. Results are shown as mean  $\pm$  standard deviation. (n=3, \*\*\* when  $p < 0.001$ )

Figure 2.22 shows the permeability results from PGSU-2.5% scaffolds fabricated at different freezing temperatures. Despite the significant difference in pore size and pore structure the permeability of the scaffold was not affected, and it ranged between  $2.7 \times 10^{-3} - 2.8 \times 10^{-3} \text{ m}^2$ .

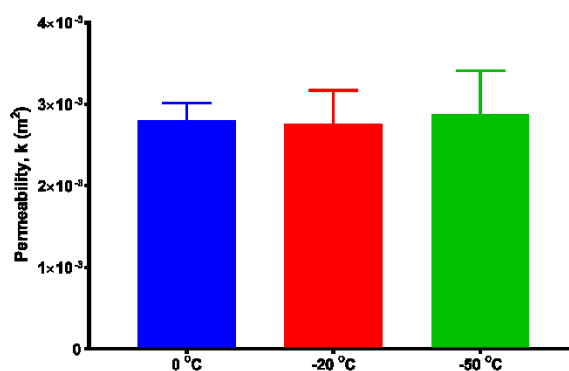


Figure 2.22: Permeability results measured from PGSU-2.5% scaffolds frozen at different temperature, 0 °C, -20 °C and -50 °C. Results are shown as mean  $\pm$  standard deviation. n=3.

### 2.3.4. PGSU scaffold - sterilisation effect

#### 2.3.4.1. Physical properties

FTIR was used to determine if the sterilisation method affected the chemical structure of the PGSU scaffolds, shown in Figure 2.23. It was found that the sterilisation method did not have a significant effect on the chemical structure, despite the fact that in the case of autoclaving the scaffold was exposed to high temperature (120 °C) and pressure.

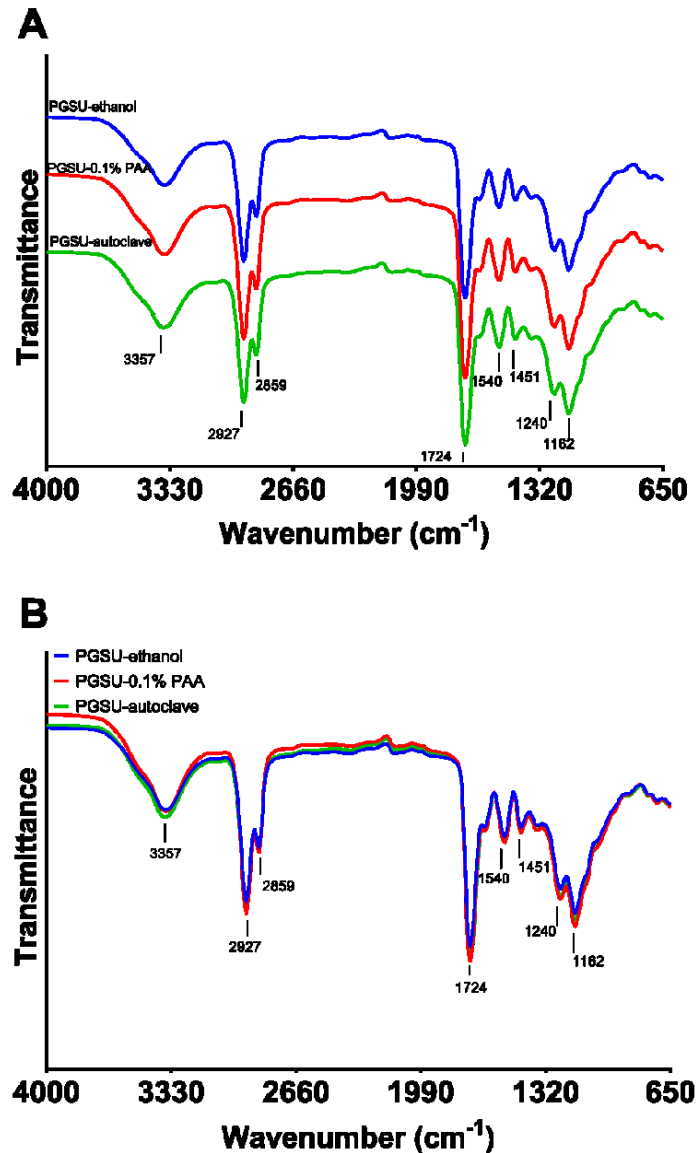


Figure 2.23: FTIR spectra of PGSU-2.5% compared against their sterilisation method.

To assess the effect of the sterilisation on the scaffold's mechanical properties they were tested for their UTS, Young's modulus and elongation at break, shown in Figure 2.24. The highest Young's modulus was acquired by the samples sterilised with 0.1 % PAA ( $0.042 \pm 0.014$  MPa), whereas the samples sterilised with 70% ethanol had higher UTS and elongation at break ( $0.506 \pm 0.127$  MPa and  $1.373 \pm 0.546$  %, respectively). However, no statistical significance was found between the groups.

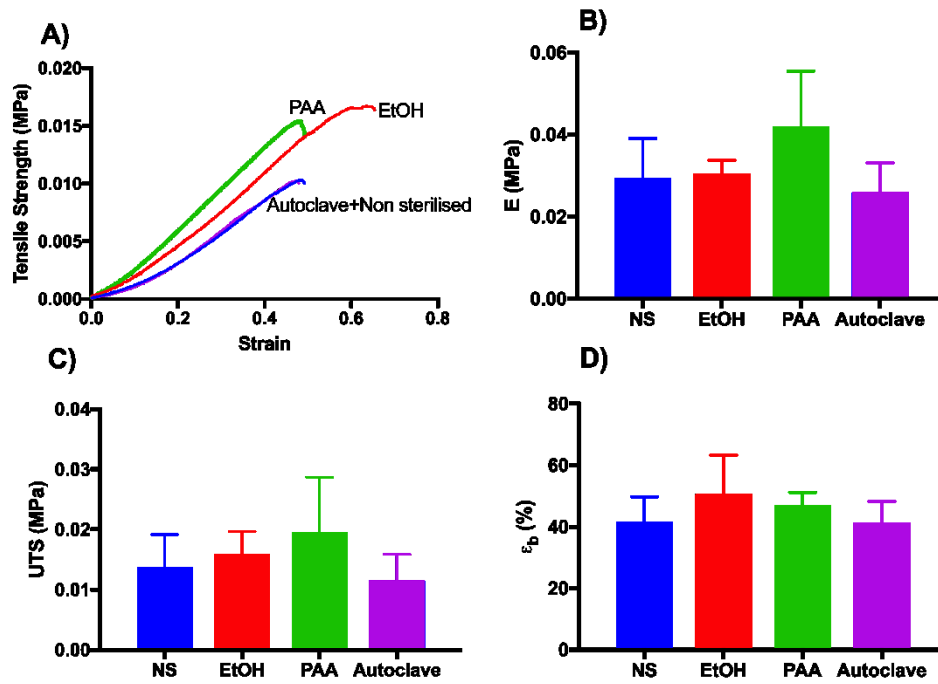


Figure 2.24: Mechanical properties obtained from the porous PGSU-2.5% scaffolds compared against their sterilisation method. A) Representative tensile strength - strain curves, B) Young's modulus, C) ultimate tensile strength and D) elongation at break. NS = non sterilised, EtOH = 70% ethanol, PAA = 0.1% paracetic acid. Results are shown as mean  $\pm$  standard deviation. n=5.

The permeability of the scaffolds was also characterised and the results are shown in Figure 2.25. Similar to before no significant difference was observed between sample groups indicating the sterilisation method had no effect on the scaffold's permeability.

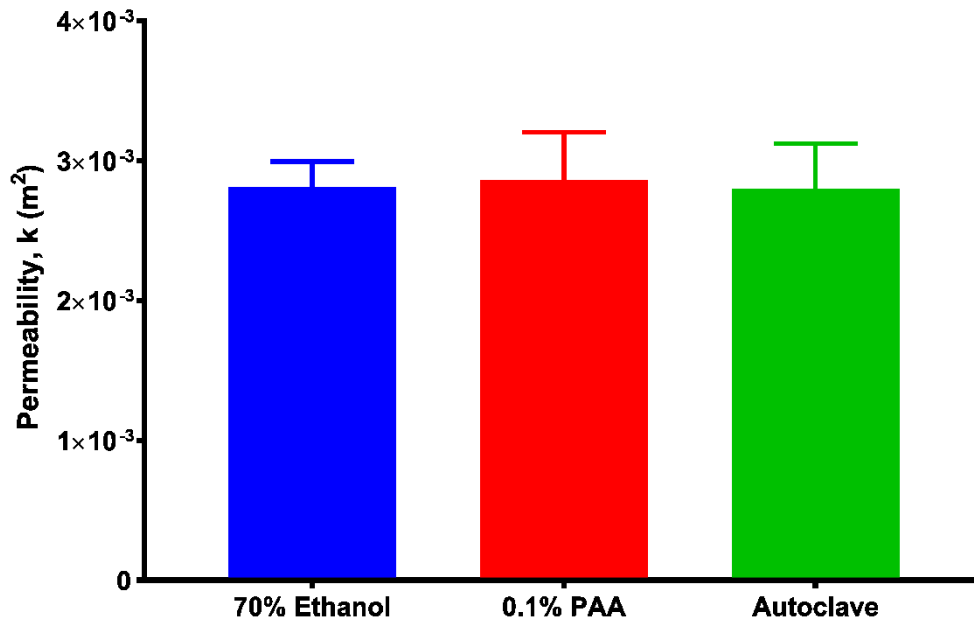


Figure 2.25: Permeability of PGSU-2.5% compared against their sterilisation method. Results are shown as mean  $\pm$  standard deviation.  $n=3$ .

#### 2.3.4.2. Cell metabolic activity

To examine the effects of the scaffold and its sterilisation on cellular activity, MTT and resazurin reduction assays were used.

##### 2.3.4.2.1. MTT assay

Results obtained from MTT assay of the scaffolds and films are shown below in Figure 2.26. The results are normalised against the TCP, presented as a percentage considering the TCP as 100%. The MTT assay performed on the scaffold samples sterilised with all three methods showed a statistically significant low optical density compared to the positive control, ranging between 10-20% ( $p < 0.001$ ). Additionally, the cell activity measured from the PGSU-2.5% sterilised with 70% ethanol is significantly higher than the 0.1% PAA. The results obtained from the film have higher optical density than the scaffold with no significant difference between the TCP and the sterilisation methods.



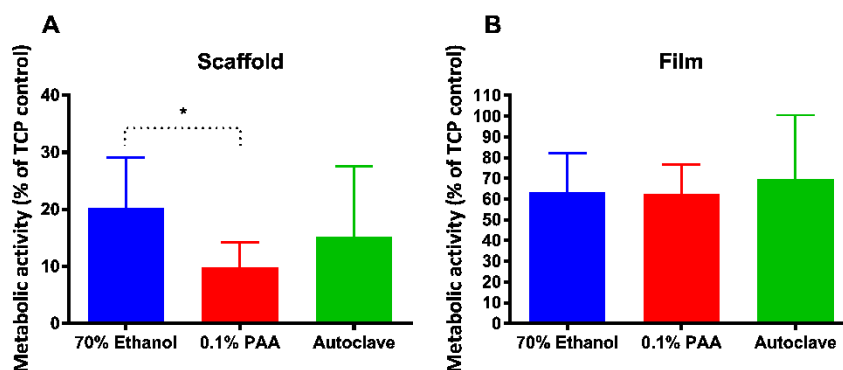


Figure 2.26: MTT assay of (A) PGSU-2.5% scaffolds (B) and films normalised against the TCP. Results are shown as mean  $\pm$  standard deviation.  $n=3$ , \* when  $p < 0.05$ .

#### 2.3.4.2.2. Resazurin reduction assay

This experiment was done in such a way so that cell activity would be detected on the porous scaffold and film over time. For comparison reasons the reduction of the resazurin from the cells found on the well plate was also recorded and considered as the positive control. The seeding efficiency was also calculated using the day 3 results by normalising the absorbance of scaffold/film against the absorbance found on the well plates.

Starting with the results obtained from the cell-seeded PGSU-film (Figure 2.27 (A)) no significant difference was observed between sterilisation methods during all time intervals, but the samples sterilised with 70% ethanol had the highest cell activity. However, the cell activity measured from the cells on the films was significantly lower than the TCP at all three time points. In the case of cell activity from cells cultured on the PGSU-2.5% scaffolds (Figure 2.27 (B)) a positive trend was recorded throughout the experiment with the 0.1% PAA having higher values in most cases compared to the other two sterilisation groups. However, no significant difference was found between the sterilisation methods. There was significant difference when comparing

the results of PGSU-2.5% on day 3 with the TCP control, and on day 6 only the cell activity from the autoclaved samples were significantly different than the TCP.

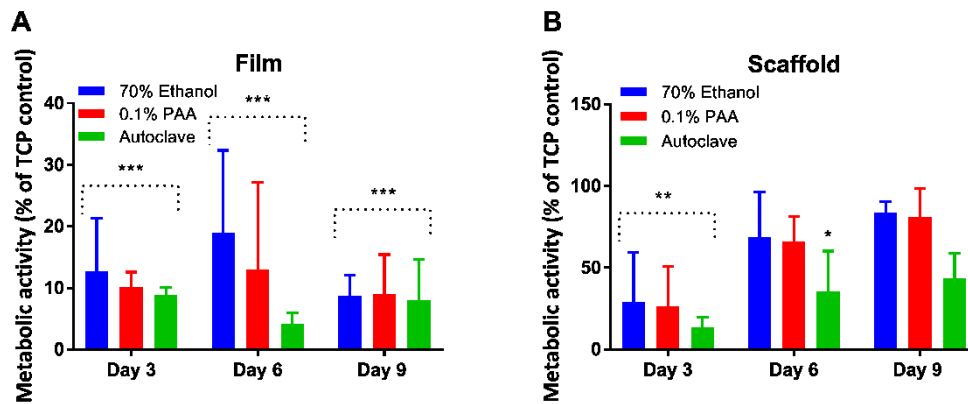


Figure 2.27: Normalised absorbance from the resazurin assays of PGSU-film and PGSU-2.5%. A) Metabolic activity of cells seeded on the PGSU-film. B) Metabolic activity from cells seeded on the PGSU-scaffold. Results are shown as mean  $\pm$  standard deviation.  $n=3$ , \*\* when  $p < 0.01$ , \*\*\* when  $p < 0.001$ .

Finally, Figure 2.28, shows the seeding efficiency calculated on day 3 by normalising the cell activity of the scaffold or film against their corresponding the cell activity measured from cells that left on the seeding well plate. In all cases the seeding efficiency on the scaffolds was significantly higher than the films. But no significant difference was found between sterilisation methods.

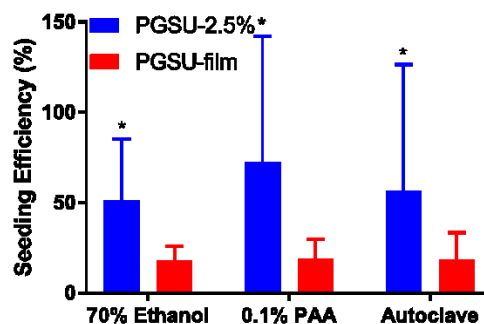


Figure 2.28: Seeding efficiency achieved from seeding PGSU-2.5% scaffold and films. The asterisks signify the significant difference between PGSU-2.5% scaffold and film. Results are shown as mean  $\pm$  standard deviation,  $n=3$ , \* when  $p < 0.05$ .

### 2.4. Discussion

The study presented in this chapter began with synthesising PGS. To assess the synthesis procedure, that was according to studies published by [118, 146, 148], ATR-FTIR was used. The sharp peak at  $1732\text{ cm}^{-1}$  confirms the formation of ester bonds. Additionally, the absorption peak at  $3451\text{ cm}^{-1}$  indicates the presence of hydroxyl groups which were then used for PGSU synthesis.

The PGSU was synthesised successfully and the porous structure formed using freeze-drying resulted in a large (50 mm diameter x 15 mm thickness), easy to handle soft PGSU porous scaffold. The scaffold could be removed from the baking tray effectively without damaging its structure, Figure 2.10. The size of the scaffold fabricated is considerably thicker than other PGS scaffolds described in Chapter 1, which depending on the fabrication method ranged between 1.50 – 5 mm thick. This is a great advantage over other PGS fabrication techniques, as being able to have a high throughput immediately reduces the cost of the fabrication and allows the scaffold to be examined and developed for larger tissue grafts. Additionally, using freeze drying allows the thickness of the scaffold to be adjusted by altering the volume of the polymer solution, therefore even larger scaffolds could be fabricated using this technique if required.

The synthesis procedure of PGSU was reported previously by [118, 147, 148, 160] and accordingly this study followed similar procedures. To determine the reaction efficiency and chemical structure of the material synthesised we used ATR-FTIR, Figure 2.11. As expected, the free hydroxyl groups from pre-PGS reacted with the isocyanate group to form a urethane group. Primary and secondary amides are also found from the PGSU spectra signifying the formation of urethane linkages. According to the safety data sheet of the HDI manufacturer (Sigma-Aldrich) it has

## Chapter 2

been shown that HDI is highly toxic when inhaled (acute toxicity: category 1) as well as it can cause skin corrosion when in contact with skin (skin corrosion/sensitisation: category 1C). However, when used to synthesise a polymer such as PU, or crosslink collagen, no significant adverse effect in terms of cytotoxicity was found [174, 175]. Due to HDI's hazardous properties the PGSU scaffolds that were not washed with ethanol were characterised to investigate if any HDI has been left unreacted and remained in the structure (Figure 2.11). A peak between 2270-2250  $\text{cm}^{-1}$  would be indicative of an isocyanate group if it was present, however this peak was not present in any of the samples. In all repeats similar spectra were obtained confirming the successful synthesis of PGSU using the synthesis method established by Pereira et al. and replicated in this work [147].

To observe the scaffold's microstructure SEM imaging was used (Figure 2.12). An open-pore interconnected porous structure was shown during all repeats. Microstructure like this is commonly found when freeze-drying is used with 1,4-dioxane as the solvent [160, 164]. From these results the scaffold's pore size increases while moving from the top to the bottom. The reason for this association between pore size and scaffold depth is related to the pre-freezing stage of the freeze-drying cycle, more specifically the freezing rate within the polymer solution. To explain this in a simple way, having the top surface of the polymer solution directly exposed to cold air coming from the freezer ( $-20\text{ }^{\circ}\text{C}$ ) the freezing rate is higher than the polymer solution that is in contact with the Teflon baking tray. Additionally, due to the low thermal conductivity of Teflon ( $0.25\text{ W/m K}$ ) the freezing rate is reduced even more. Since the ice crystal size is affected by the freezing rate the pore size gradient is formed. Nevertheless, the pore size gradient could be advantageous in cases where the tissue being developed consists of multiple tissue layers. Different cell types, cell

## Chapter 2

behaviour, pore size and structure are required for optimum results in terms of cell growth and neovascularisation [71, 72]. The disadvantage of pore size gradient could be when the scaffold is used for homogeneous tissues where a uniform pore size scaffold is necessary these scaffolds may not encourage uniform tissue regeneration.

According to literature the optimum pore size for fibroblast growth varies significantly. One study has found that 5-15 $\mu\text{m}$  pore size is optimum for fibroblast growth [72], while another study has found that scaffolds made from poly(lactic-co-glycolic acid)/polybutylene terephthalate copolymer has the highest fibroblast growth when pore sizes were  $160 \pm 56 \mu\text{m}$  [176]. Additionally, a more recent study, found that poly(2-hydroxyethylmethacrylate) scaffolds with 40  $\mu\text{m}$  pore size were able to form dermal and epidermal layers of skin [177]. Combining the knowledge from the above three studies concludes to that the cell growth is not only depended on the pore size, but also from the biomaterial and pore structure. The pore sizes of the PGSU-2.5% scaffolds fabricated in this study varied between  $24.6 \pm 7.4 - 96.2 \pm 19.8 \mu\text{m}$  (cross section pore size) depending on the freezing temperature during the fabrication process. This means that the PGSU scaffolds used in this study fall within the range of the optimum pore sizes reported in literature for fibroblast growth, however PGSU scaffolds using freeze drying were never examined for their cytocompatibility, and this was one of the objectives of the next chapter.

The aim of this thesis was to develop a PGSU scaffold for OMTE, which the scaffold structure should exhibit a uniform pore size distribution layer with a thin surface layer that acts as a basement membrane to separate the cell types, fibroblasts and epithelial cells. However, we found that pore size distribution was not uniform for the PGSU-2.5% scaffolds and the freezing temperature did not improve the uniformity. Pore size homogeneity can be achieved by two different ways, and both

## Chapter 2

will be characterized in the following chapters. The first is change the polymer concentration, and the second is change the mould material to a high thermal conductive material, for example stainless steel. The thermal conductivity of the mould used in this chapter, Teflon, is 0.25 W/m K which is very small compared to stainless steel (16 W/m K). A study done by Davidenko et al. [178] produced 5 different moulds made from different materials aiming to fabricate anisotropic pore architecture. Of interest from this work is that the mould they made by a high thermal conductive 316L stainless steel (diameter 45 mm and height 13 mm) was able to successfully produce a collagen porous scaffold, fabricated using freeze-drying, with a consistent pore size throughout its depth.

The porosity of the scaffolds in this study was very high, average porosity  $96.89 \pm 0.71$  % (Table 2.2) and due to the high porosity, the water permeability was also very high (Figure 2.25). The combination of these two characteristics of the PGSU-2.5% scaffold aid in pore interconnectivity and subsequently in seeding efficiency, cell distribution and adequate nutrient and gas exchange between cells. As with pore size, the optimum porosity for tissue engineering is again debated in the literature and it is heavily depended on application, cell type and biomaterial. For example, for chondrogenesis a PCL scaffold should have 95% porosity [179] while a chitosan scaffold should have 80% porosity [180]. Regarding fibroblast proliferation, a silk fibroin scaffold with 86% porosity had lower cell proliferation than the same scaffold with 91% porosity [181].

The permeability of the scaffold is also important (Figure 2.22). This property is rapidly gaining interest in the literature because a direct link was found between permeability and nutrient diffusion and it also serves as a measure of interconnectivity [169]. What was found from this study was that all scaffolds were highly permeable,

## Chapter 2

but the permeability did not change between samples, even though the pore size and structure was different. Therefore, since the permeability was not affected by pore size and pore structure, it can be concluded that the porosity plays a more important role on the permeability of the scaffold. Comparing the permeability results from the PGSU-2.5% scaffold with the literature is difficult because there is no standard method for measuring permeability [169]. In this study we used the constant head method and calculated the permeability using Darcy's law. One study fabricated collagen/hydroxyapatite scaffolds using freeze drying with the highest porosity equal to ~87.5% and measured the permeability of their scaffolds with the same method as in this study. The permeability reported from their scaffolds was between  $0.17 \times 10^{-8}$  -  $7.0 \times 10^{-8} \text{ m}^2$ , and compared to the scaffolds from this study ( $\sim 2.8 \times 10^{-3} \text{ m}^2$ ) they are five orders of magnitude less permeable, probably because of the ~10% higher porosity found from the PGSU-2.5% scaffolds, as well as the hydrophobic property of the scaffold ( $2.68 \pm 0.93$  % swelling ratio in PBS solution after 24h [148]) compared to a high hydrophilic collagen scaffold (>200 % swelling ratio in PBS solution at 5 min) [182, 183]. The results presented in this chapter demonstrate we have developed a scaffold with high pore interconnectivity that will allow nutrient diffusion, which is necessary for cell and tissue viability before a sufficient blood supply is established.

The PGSU-2.5% scaffolds were also characterized for their mechanical strength using tensile testing, Figure 2.15. The purpose of this was to understand the mechanical behavior of the scaffold and determine the maximum load it can withstand as well as how much it can be stretched before breaking. The scaffold appears to have weak UTS ( $0.013 \pm 0.005 \text{ MPa}$ ) compared to the oral mucosa ( $1.29 \pm 0.19 \text{ MPa}$ ), which could be a problem as high forces will be applied to it once implanted and the scaffold will not be able to support the cells. The reason for the weak mechanical

properties is its high porosity and non-uniform pore structure. The material itself when it was characterised by Pereira et al. [147] as a 2D film had mechanical properties higher than oral mucosa ( $1.35 \pm 0.76 - 12.1 \pm 1.9$  MPa), however in their case they were using PGSU-film. When the PGSU was fabricated into a highly porous structure it immediately lost its mechanical strength. This could be solved by three ways; the first one is by altering the molar ratio of the reactants; the second is to change the microstructure of the scaffold; and third is change the polymer concentration. The latter two will be investigated in this thesis (Chapter 3).

*In vitro* enzymatic degradation was also examined for PGSU-2.5% and PGSU-films to determine the degradation kinetics. The enzyme used, lipase, is known to play an important role in degrading polyesters when *in vivo* acting as a catalyst for hydrolysis. It was found that the PGSU-2.5% degraded ( $71.85 \pm 5.4$  %) significantly faster than the PGSU-film ( $24.5 \pm 1.9$  %). From previous work on PGSU it was shown that this polymer degrades through hydrolysis by surface erosion [147]. Knowing this we can justify that the faster degradation rate of the scaffold was because it is a scaffold, it has a higher surface area compared to the film, meaning higher exposure to lipase and hydrolysis. Pereira et al., characterised the *in vivo* degradation rate of PGSU films, lower and higher reactant ratio than this study (Figure 1.19 (C)), and found that the PGSU films degraded slower than *in vitro* (Figure 1.15) [147]. This does not agree with PGS. PGS was found to completely degrade in 60 days when *in vivo* whereas it degraded 18% *in vitro* [126]. This contradiction is probably because of the urethane linkages found within PGSU, that protect the ester bonds from degrading as fast as PGS does. Therefore, from Pereira et al., work we can assume that PGSU-2.5% and PGSU-film will degrade slower *in vivo*, however this should be examined in future work.



## Chapter 2

We attempted to investigate the freezing temperature effect on the scaffold's microstructure. The aim of this was to understand how the scaffold's microstructure relates to its mechanical properties and permeability. Knowing that the melting point of 1,4-dioxane is 11.4 °C we chose three temperatures that were below the melting point, 0 °C, -20 °C and -50 °C. The scaffolds fabricated at -20 °C are the ones that were discussed above. When the polymer solution was frozen at higher temperature, 0 °C, in other words lower freezing rate, we found that the pore structure had a more defined circular structure and was more uniformly distributed (Figure 2.17). But in the case of lower temperature, -50 °C, or higher freezing rate, a less defined structure was observed with large voids and thin walls separating each pore (Figure 2.18). The size of the pores also significantly decreases as freezing rate increase, which was expected. Therefore, we determined that the slower the polymer solution is frozen a more defined and uniform pore structure is achieved, and significantly higher pore size. However, the pore size gradient is evident from these scaffolds as well, meaning that altering the freezing rate cannot eliminate the gradient in pore size but only change its size and make it more defined when it is frozen at a slower rate.

The mechanical properties increased significantly when the freezing rate was both higher and lower, Figure 2.20. This is probably due to the microstructure of the scaffolds, and since the porosity remained the same it is most likely due to differences in the pore size and structure. Beginning with the lower freezing rate, or highest temperature, 0 °C, the scaffold had the highest pore size and circular uniform pore structure which most probably helped in increasing the UTS by distributing the mechanical load evenly throughout its structure. For the highest freezing rate, or lowest temperature, -50 °C, the scaffold did not show any significant difference in pore size, but the pore structure was more defined compared to the -20 °C scaffolds, leading

## Chapter 2

to a higher UTS. Therefore, the pore structure has a significant effect on how the scaffold behaves under mechanical load by increasing its UTS but keeping its resistance to deformation (Young's modulus) and elongation at break similar.

The next step of this chapter was to determine the best and easiest method to sterilise the scaffold for laboratory cell culture use. We chose the three most used sterilisation methods for preliminary laboratory use, 70% ethanol, 0.1% PAA and autoclave, and a preliminary study was performed to understand the effect that each sterilisation method had on the scaffold's chemical structure, mechanical properties, permeability, cell metabolic activity and cell seeding. FTIR was used to characterise the chemical structure of the scaffolds after sterilizing (Figure 2.23) and no difference was found between the spectra, meaning that the chemical structure remained the same after sterilisation.

The effect the sterilisation method had on the scaffold's mechanical properties was also investigated. It was found that the sterilisation method did not significantly affect the tensile strength of the scaffolds. The only consistency found was that the autoclaved samples had the lowest UTS, Young's modulus and elongation at break which indicated that the high temperature during autoclaving (120°C) might have a negative effect on the mechanical properties. However, no significant difference was found. These results are advantageous, as the scaffold should not have its mechanical properties changed when sterilized if it is going to be used commercially. With this said we have not tested any other clinically acceptable sterilisation methods (ethylene oxide, gamma irradiation) as we did not have access to these, but it is planned for future work. There are a few studies that looked into how their scaffolds change when sterilised and most of them looked into the mechanical properties. For example when PLGA was sterilized using PAA its mechanical strength decreased, the same occurred

## Chapter 2

when ethanol was used, believed to be due to scaffold structural change [184]. Additionally, when PLA scaffold was autoclaved its mechanical strength increased due to recrystallisation of the polymer [185].

When comparing the permeability of the scaffolds sterilised with different methods there was not significant difference found, meaning that after sterilizing the scaffold it will still be highly permeable and allow good nutrient diffusion essential for the cell survivability.

To examine the cytocompatibility of PGSU-2.5% scaffolds and PGSU-films we used MTT and resazurin assays. MTT assay was the first assay used performed 48 hours post seeding the samples. It was noticed that the optical density from PGSU-2.5% scaffolds was very low compared to the PGSU-film and TCP. Examining visually the scaffolds after the MTT assay it was realised that the scaffolds converted the MTT into dark purple formazan, expected from MTT assay, however the stain could not be eluted from the scaffold and read, hence a low optical density was measured. This issue was not present for the PGSU-film and TCP resulting in a non-accurate comparison for cell activity assay.

We then moved into using resazurin assay that eliminated the procedure of eluting off the substance produced by the assay to measure its optical density. It also had the advantage of not killing the cells after the assay, therefore we were able to measure the cell activity through nine days culture at multiple time points. When examining PGSU-2.5% scaffold for their cell activity a positive trend was formed during the nine days of culture. This indicated that cells adhered and were metabolically active on the samples as the amount of cell metabolism increased over time, most likely as a result of cell proliferation, however proliferation was not measured in this study. It was

## Chapter 2

found that only the scaffolds sterilised with 70% ethanol and 0.1% PAA had a significantly higher metabolic activity between days 3 and 9 compared to autoclaved samples. This means that sterilising PGSU scaffolds with autoclave has a small negative effect on both mechanical properties and cytocompatibility. To allow us to further establish which sterilisation method we should use for the rest of the project, we examined the seeding efficiency. As shown in Figure 2.28 the seeding efficiency was significantly higher for the PGSU-2.5% scaffolds compared to the PGSU-film, and this is because the scaffold has higher surface area and pores which allows the cells to penetrate its structure. When looking at the effect of the sterilisation method, the PGSU-2.5% scaffolds showed no significant difference between sterilisation methods, but it was found that the standard deviation was higher for 0.1% PAA and autoclaved samples compared to those sterilised in 70% ethanol. For this reason, 70% ethanol was used for subsequent experiments. The non-reproducible seeding efficiency was directly reflected to the cell activity assays, both MTT and resazurin, thus the high error bars found in those assays. With this said, the seeding method must be modified, and a robust, repeatable protocol should be established. The resazurin assay demonstrated an advantage over the MTT assay allowing us to examine the cell metabolism over time, overcoming the issues occurred while using MTT assay.

### 2.5. Conclusion

This experimental chapter focused on understanding the synthesis and fabrication of the PGSU scaffold as well as to determine how the scaffold should be treated and prepared for cell culture. The results from this study demonstrate that:

1. PGSU was successfully synthesised and crosslinked

## Chapter 2

2. PGSU-2.5% scaffolds were successfully fabricated with high porosity and water permeability
3. The pore size, pore structure and mechanical properties of the scaffolds was significantly different when the pre-freeze temperature was changed
4. Pore size gradient was evident for all the PGSU scaffolds that were fabricated
5. The permeability of the scaffolds was not affected by pore size/structure but was determined solely by the porosity of the scaffolds
6. The mechanical properties of the scaffolds were significantly lower than oral mucosa's biomechanical properties
7. The sterilisation method did not affect the chemical structure and mechanical properties of the scaffold, and no contamination was observed during the 9 days *in vitro* cell culture
8. The seeding efficiency was more consistent when the scaffolds were sterilised with 70% ethanol

The findings of this chapter demonstrate that the PGSU scaffold should be improved in terms of its mechanical properties to be able to mimic at least the buccal mucosa in order to ensure that it can withstand *in vivo* mechanical forces. Furthermore, the pore size gradient should be reduced which can help in improving mechanical properties (by distributing the mechanical load homogeneously), but also to mimic the lamina propria of the oral mucosa. Regarding the *in vitro* cell culture aspect of this chapter, it was determined that the seeding technique requires significant optimisation to increase the seeding efficiency. From the three sterilisation methods used, it was decided to proceed with using 70% ethanol because it did not affect the physical properties of the scaffold (chemical structure, mechanical properties, permeability)

and it had the least seeding efficiency error compared to the other two sterilisation techniques.

# **Chapter 3 Biocompatible poly(glycerol sebacate urethane) scaffolds with controllable porous structures and mechanical properties**

## **Aim**

To fabricate PGSU scaffolds with controlled microstructure, mechanical properties and degradation rate and to investigate their effect in tissue development.

## **3.1. Introduction**

The successful synthesis and scaffold fabrication of PGSU described in Chapter 2 allowed us to characterise its physical and biological properties and helped us to understand what needs to be optimised and how to further examine these scaffolds. Following the results of Chapter 2 we wanted to improve the microstructure of the scaffold and mechanical properties as well as the cell seeding technique. The aims of this chapter were to achieve a homogeneous architecture with good reproducibility, and to significantly increase the mechanical properties, to make them closer to native oral mucosa, compared to those reported in the previous chapter.

One method to vary a scaffold's properties is to alter porosity without changing the chemical structure of the polymer. Porosity is essential to a scaffold, as it is necessary for cell seeding and vascular/cell ingrowth [186]. For example, PU scaffolds were fabricated with two different porosities, 73% and 86%, and were subcutaneously implanted on the back of 24 Wistar albino rats and examined for tissue ingrowth after 24 weeks. Significantly higher tissue ingrowth was found for the 86% porosity scaffolds [187]. A higher degree of porosity decreases stiffness and strength, but

allows for bodily fluids to perfuse the structure more easily, and may allow for more rapid ingrowth of host tissue [188].

The freeze-drying scaffold fabrication technique enables control of pore size and porosity based on freezing procedure and polymer concentration [149]. In this study freeze-drying was used to fabricate PGSU scaffolds with different pore sizes and porosities by changing the polymer concentration. We aimed to determine the effect of polymer concentration on the mechanical properties and degradation of the scaffold as well as the biological response to the scaffolds *in vitro* (measuring cell viability and matrix production). SEM was used to determine the scaffold's microstructure, the mechanical properties were investigated in a range of mechanical tests (tensile testing, cyclic loading etc) and the degradation rate was measured *in vitro* using enzymes. The *in vitro* cell activity was studied using resazurin assay over 15 days of culture. The new knowledge gained from this study will inform the development of PGSU scaffolds for a range of TE applications.

### **3.2. Materials and Methods**

#### **3.2.1. Materials**

The materials for this chapter are the same as in Chapter 2 with the addition of:

Direct red 80 was purchased from Sigma-Aldrich and Rat tail high concentration collagen type I was purchased from Corning®. The aluminium plate 6082 T651 was purchased from Aluminium Warehouse.

#### **3.2.2. Methods**

##### **3.2.2.1. Pre-PGS synthesis**

Pre-PGS was synthesised as in Chapter 2: Section 2.2.2.1.



### 3.2.2.2. PGSU-5, 10, 15% scaffolds

#### 3.2.2.2.1. Aluminium tray mould

An inhouse aluminium grade 6082T6 tray was manufactured to feature 6 symmetrical wells as shown in Figure 3.1. This mould will be referred as “Mould-random” in the following sections.



Figure 3.1. Aluminium tray mould with 6 wells for random orientation (mould-random) scaffold fabrication. Scale bar is 5 cm.

#### 3.2.2.2.2. Random orientation PGSU scaffolds

Porous PGSU scaffolds were synthesised by dissolving pre-PGS into 1,4-dioxane at the required concentrations (5, 10 and 15 w/v%) and pre heated to 55 °C with 0.05% w/v of Tin(II) 2-ethylexanoate. Once heated, HDI was added at a 0.6 molar ratio (glycerol:HDI) and left at 55 °C for 5 hours under constant stirring. For ease of documentation, the nomenclature of the samples is PGSU-X where X refers to the polymer concentration (w/v%), 5%, 10%, 15%.

## Chapter 3

The PGSU solution was cast into mould-random and placed into a freeze dryer (FreeZone Triad Dry System, Labconco Co., USA) set at  $-50\text{ }^{\circ}\text{C}$  and left for 3 h for the solution to completely freeze. The lyophilisation process then started with the shelf temperature heated at a rate of  $1\text{ }^{\circ}\text{C}/\text{min}$  to  $0\text{ }^{\circ}\text{C}$  and left for 16 h under vacuum pressure (0.1 mbar). For the secondary drying stage, the temperature was increased at a rate of  $1\text{ }^{\circ}\text{C}/\text{min}$  to  $40\text{ }^{\circ}\text{C}$  for another 24 h. The reason the freeze-drying cycle changed was to increase the freezing rate which was hypothesised that it will increase the uniformity of the scaffold microstructure, and the lyophilisation (primary drying) temperature was increased to  $0\text{ }^{\circ}\text{C}$  from  $-10\text{ }^{\circ}\text{C}$  because the 1,4 dioxane could still be below its triple point (shown in Figure 3.3) but the sublimation rate could be increased. The freeze drying cycle is shown in Figure 3.4.

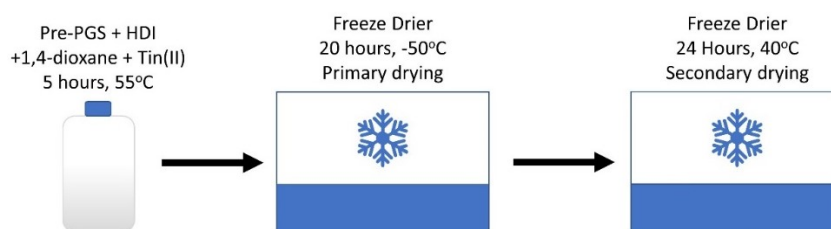


Figure 3.2. Synthesis and fabrication method schematic for PGSU scaffolds.

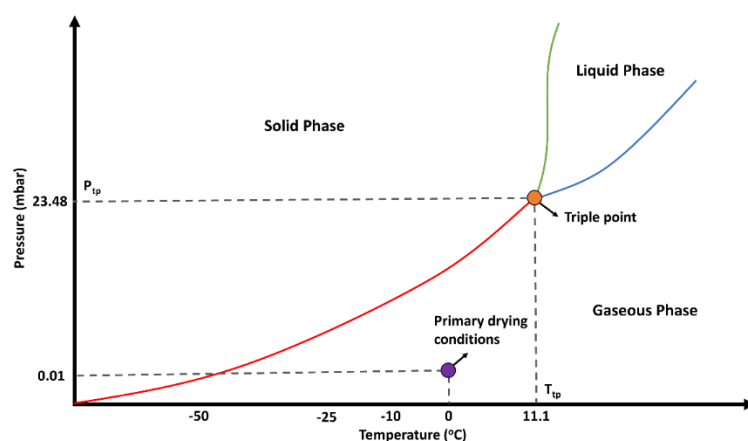


Figure 3.3: Three-phase diagram of 1,4-dioxane derived from the data provided from National Institute of Standards and Technology (NIST, <https://webbook.nist.gov/cgi/cbook.cgi?ID=C123911&Mask=4#Thermo>

Phase). Ttp: Triple point temperature, Ptp: Triple point pressure. The purple circle shows the temperature and pressure of the 1,4-dioxane during primary drying in the freeze drier.

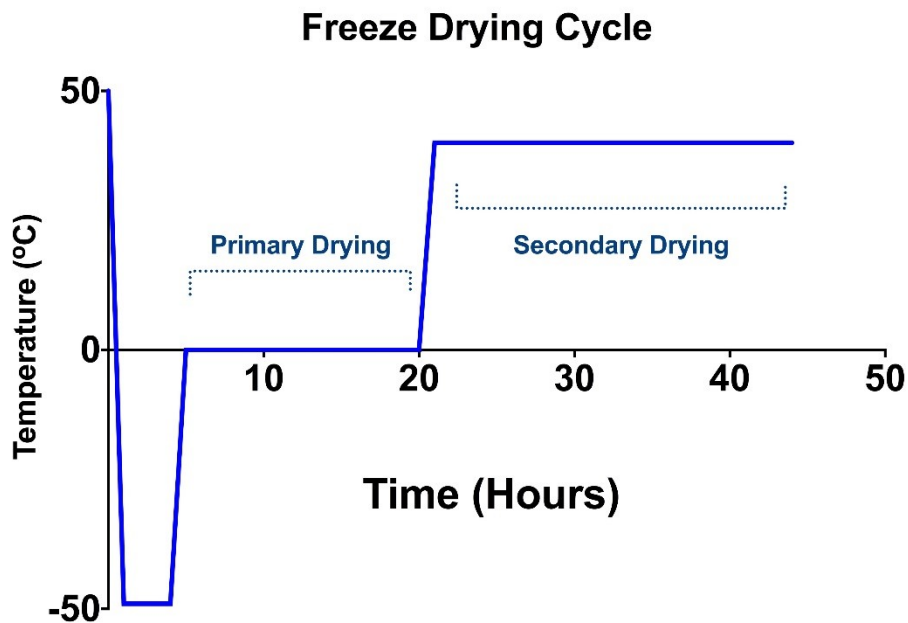


Figure 3.4. Freeze drying cycle during the PGSU porous scaffolds fabrication procedure.

All scaffolds were washed with ethanol to remove any unreacted substances from its construct. The washing was done by submerging the scaffold in 100%, 70% and 50% Ethanol for 2 hours each, and then immersed in distilled water overnight. Shaking was also applied to the scaffolds during washing.

### 3.2.2.3. Porous scaffold characterisation

The scaffold was characterised as in Chapter 2: Section 2.2.2.5 with the addition of cyclic loading and suture retention strength described below.

The cyclic loading was performed using the same sample dimensions as in Section 2.2.2.5.4 ( $n = 3$ ) in which the samples were tensile loaded to 30% strain for 100 cycles at 100 mm/min rate of travel using a 10 N load cell. The first and last cycle were recorded and plotted as strain-stress curves.

The suture retention strength was done according to BS EN ISO 7198:2017 standard. The sample was cut normal to the long axis and a suture was inserted 2 mm from the end of the sample and a half loop was formed. The suture was then pulled, using a 10 N load cell, at 200 mm/min and the force required to pull the suture through was recorded and plotted in grams. Five specimens were tested for each condition.

### **3.2.2.4. Microstructure effect on cell viability**

L929 mouse fibroblasts cells were cultured as in Chapter 2: Section 2.2.2.6.1.

#### **3.2.2.4.1. Sample preparation and cell seeding**

All the cell experiments were repeated three times in triplicates. PGSU scaffolds were prepared with diameter = 10 mm, thickness = 2 mm in triplicates for each concentration. The samples were sterilised overnight with 70% ethanol and then under sterile environment washed thoroughly with PBS. To optimise the seeding efficiency from the previous chapter, the samples were placed in a 12 well-plate and fixed within a 10 mm inner diameter surgical stainless steel ring. The samples were passively seeded, by overlaying them with 200  $\mu$ l of cell/media suspension ( $0.5, 1.0, 2.0 \times 10^6$  cells/sample which amounts to  $\sim 3000, 6000, 12000$  cells/ $\text{mm}^3$ ) and topped up to 2 ml after 2 h incubation. The next day the seeded scaffolds were moved to a fresh well-plate to ensure that any cell activity measured during the experiments was due to the cells on the scaffold. All the cell cultures were carried out for 15 days. Cells seeded on TCP acted as positive control, and acellular scaffolds as negative control.

#### **3.2.2.4.2. Resazurin reduction assay**

The cell metabolic activity was measured every 3 days using resazurin metabolic activity assay. The resazurin stock and working solutions were prepared as mentioned previously (Section 2.2.2.6.3.2). The samples were washed 3 times with PBS, and 2

ml of working solution was added to each sample and left in the incubator for 3 h, wrapped in aluminium foil. Then, 200 µl of reacted resazurin working solution were transferred into a 96 well-plate in sextuplicate, and the plate was read using the BioTek ELx800™ absorbance reader at 570 nm. The samples were then washed three times and fresh media was added.

### **3.2.2.5. Histology**

After 15 days culture the samples were fixed in 3.7% formaldehyde. The samples were paraffin-embedded and sectioned (6 µm). The sections were dewaxed, rehydrated and stained with haematoxylin and eosin (H&E).

### **3.2.2.6. Sirius red staining**

Sirius red is used to stain collagen for histochemistry and to assess the amount of collagen found in the samples. Sirius red is an anionic dye, which can bind on the positively charged guanidine group of arginine found on the collagen molecule, more specifically collagen types I and III [189].

The collagen production was quantified using Sirius red stain (0.1% (w/v) Direct Red 80 in saturated picric acid). The stain was added (2 ml per sample) and left for 16 h to bind on the collagen. The excess stain was then removed by washing the samples distilled water for 15 times. The samples were then dried in a vacuum oven at 25 °C, weighed and the stain was eluted using 2 ml of 0.2 M NaOH:methanol 1:1 for 15 min on a rocking shaker. The absorbance was then measured at 490 nm in an absorbance plate reader (Bio-Tek ELx800).

To create a Sirius red standard curve the same procedure above was done on known amounts of rat tail collagen type I. Briefly, the collagen, which was dissolved in acetic acid, was pipetted in a series of dilutions starting from 0.1 mg/ml to 0.001

mg/ml in cold distilled water. The solutions were then frozen and freeze dried to remove all the solvents (acetic acid and water). Sirius red was then carried out as above and the results were plotted as absorbance against collagen mass.

### 3.2.2.7. Statistical analysis

The statistical analysis was performed as in Chapter 2: Section 2.2.2.7.

## 3.3. Results

### 3.3.1. Characterisation of PGSU scaffold

#### 3.3.1.1. ATR-FTIR of PGSU scaffolds

ATR-FTIR was carried out to confirm the synthesis and chemical structure of PGSU, with the spectra shown in Figure 3.5. The pre-PGS is characterised by the -OH stretch at  $3450\text{ cm}^{-1}$ , sharp peaks at  $2929\text{ cm}^{-1}$  and  $2856\text{ cm}^{-1}$  which belong to the stretch vibration of C-H, finally carbonyl (C=O) and ether (C-O) stretching vibrations are observed at  $1732\text{ cm}^{-1}$  and  $1160\text{ cm}^{-1}$ , respectively [172]. The PGSU samples exhibit amine (-NH) stretch vibration at  $3350\text{ cm}^{-1}$  and bending vibration of amide I, II and III bands at  $1620\text{ cm}^{-1}$ ,  $1578\text{ cm}^{-1}$  and  $1238\text{ cm}^{-1}$ , respectively, which are all absent in pre-PGS proving the formation of urethane linkage [147, 148]. Additionally, HDI was examined using FTIR and compared with the spectra obtained from the PGSU scaffolds and it was found that the scaffolds were lacking from an NCO peak at the  $2250\text{ cm}^{-1}$  indicating complete reaction of pre-PGS and HDI.

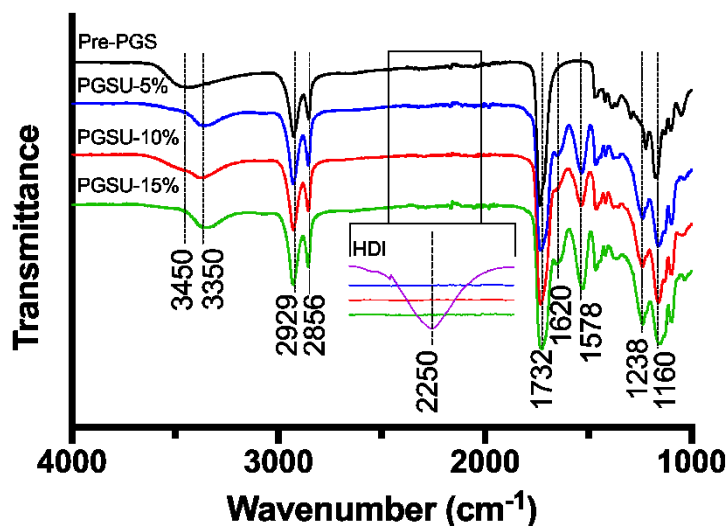


Figure 3.5: ATR-FTIR spectra of pre-PGS and the PGSU scaffolds. All three polymer concentrations were examined and compared against pre-PGS that served as a control. FTIR was also carried out for the HDI.  $n=3$ .

### 3.3.1.2. Microstructure of the PGSU scaffolds

Unlike the previous chapter a different mould was used, referred to as mould-random, and the  $-50\text{ }^{\circ}\text{C}$  freeze drying cycle was used to fabricate PGSU porous scaffolds. The scaffolds were imaged using SEM and they presented a more uniform open pore interconnected structure. Figure 3.6 shows the measured pore size and porosity from each scaffold respectively. The top section of PGSU-5% and PGSU-10% (Figure 3.7 (A1-2), (B1-2) respectively) presented a circular pore structure and there was no significant difference in pore size. However, the pore structure and pore size were significantly different for the PGSU-15% (Figure 3.7 (C1-2)), where the pore size decreased by almost half (from  $12.3 \pm 1.9\ \mu\text{m}$  to  $6.4 \pm 1.6\ \mu\text{m}$ ). The cross sectional area of all scaffolds had the same uniform pore structure, with elongated pores stacked on each other, but the pore size significantly decreased from  $28.2 \pm 5.3\ \mu\text{m}$  to  $16.1 \pm 2.6\ \mu\text{m}$ , as polymer concentration increased. The bottom section of the scaffolds had less pores when the polymer concentration was increased to the higher concentration, resulting in the PGSU-15% having an almost non-porous bottom surface, however,

when there were pores they were larger than in the PGSU-10%. Pore size gradient was found for all three scaffolds. The less gradient was observed from PGSU-10% as there was no significant difference when comparing its top with bottom sections. Additionally, it was observed that for PGSU-5% and PGSU-10% scaffolds their cross-section had the largest pores compared to their top and bottom sections. The porosity was also affected by the polymer concentration. It was found that PGSU-5% (lowest polymer concentration) was the most porous ( $96.4 \pm 0.3\%$ ), PGSU-15% the least porous ( $88.9 \pm 0.4\%$ ), and PGSU-10% was in between ( $92.3 \pm 0.7\%$ ).

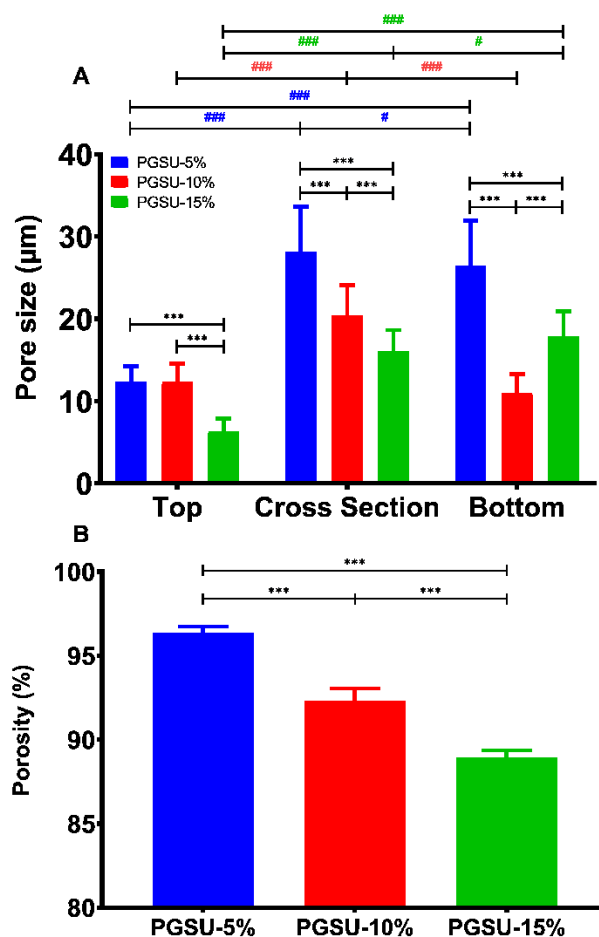


Figure 3.6: Measured (A) pore size ( $n=50$ ) and (B) porosity ( $n=5$ ) of the PGSU scaffolds from three different sections. Results are shown as mean  $\pm$  standard deviation, (A)  $n=5$ , \*\*\* when  $p < 0.001$  between groups and ### when  $p < 0.001$  within groups (colours are used for # to distinguish the groups); (B)  $n=5$ , \*\*\* when  $p < 0.001$ .



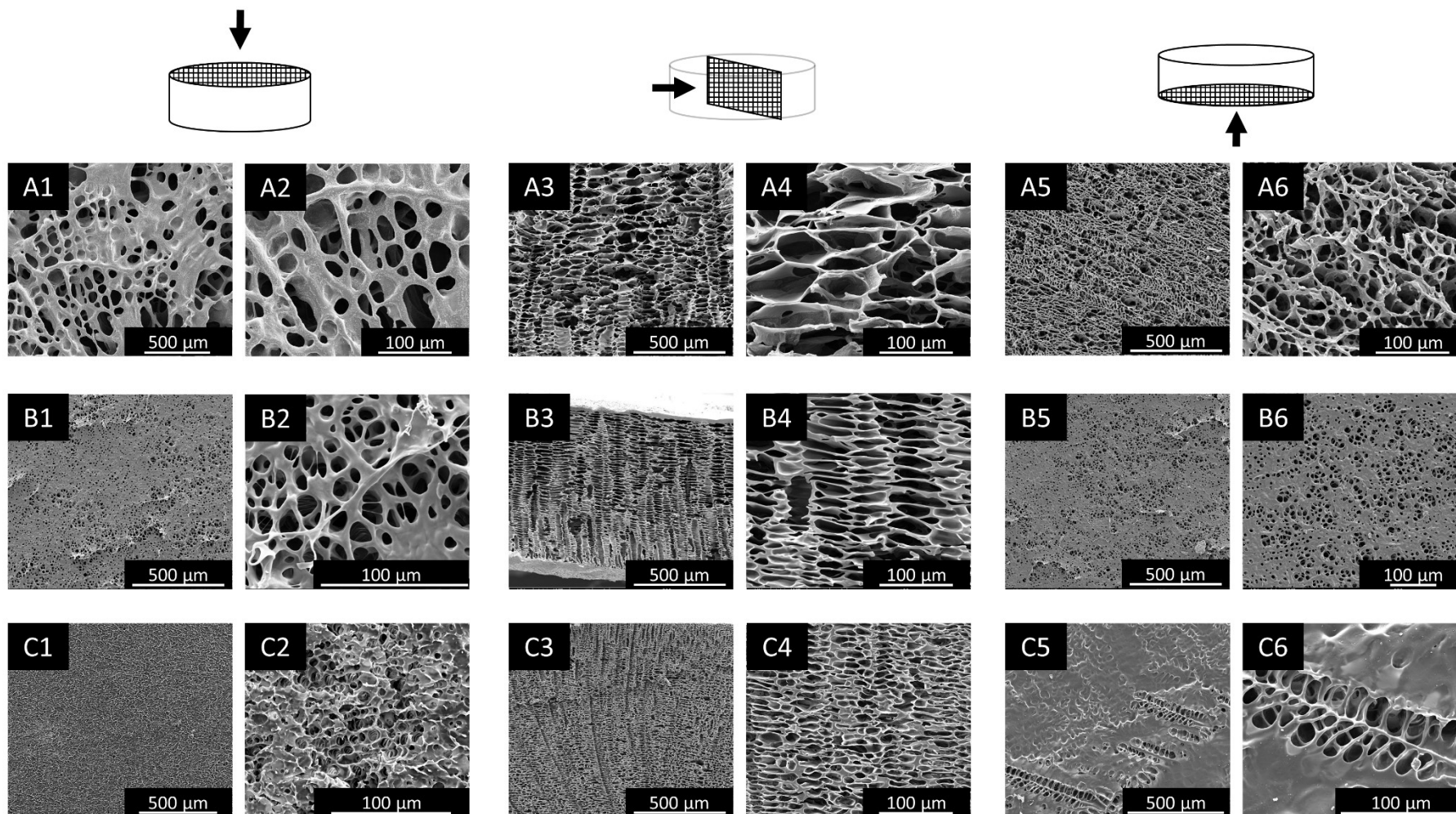


Figure 3.7: SEM images of porous (A1-6) PGSU-5%, (B1-6) PGSU-10% and (C1-6) PGSU-15% scaffolds.

### 3.3.1.3. Mechanical Properties

The scaffolds were subjected to tensile testing to examine their mechanical behaviour. Figure 3.8 (A) shows the stress-strain curves of PGSU scaffolds fabricated with different polymer concentrations, and Figure 3.8 (B-D) show a summary of the results. When the polymer concentration increased, so did the Young's modulus, UTS and elongation at break with the highest values obtained from PGSU-15% equal to  $0.65 \pm 0.18$  MPa,  $0.86 \pm 0.21$  MPa and  $122 \pm 19$  %, respectively. The polymer concentration significantly affected UTS, when comparing PGSU-5% to PGSU-10% the UTS increased by ~9-fold and comparing PGSU-10% to PGSU-15% UTS increased ~2-fold. Similar increases were found for the Young's modulus as well, which increased ~9-fold between PGSU-5% and PGSU-10%, ~12-fold for PGSU-5% against PGSU-15% and ~1.5-fold when comparing PGSU-10% with PGSU-15% (Figure 3.8 (B)). The elongation at break was only statistically higher when comparing the values of PGSU-5% and PGSU-15% (~1.3-fold higher) (Figure 3.8 (D)). A negligible loss of tensile strength was observed for all three scaffolds after 100 tensile cycles, signifying the ability of the scaffold to recover its strength and shape after deformation. The last mechanical property that was examined was the suture retention strength of the scaffolds, shown in Figure 3.8 (F). As expected the suture retention was significantly increased while the polymer concentration increased, with the highest force of  $247.5 \pm 37.5$  g obtained from the PGSU-15%, which is well above the surgical requirement (183 g, shown as dotted line [190]).

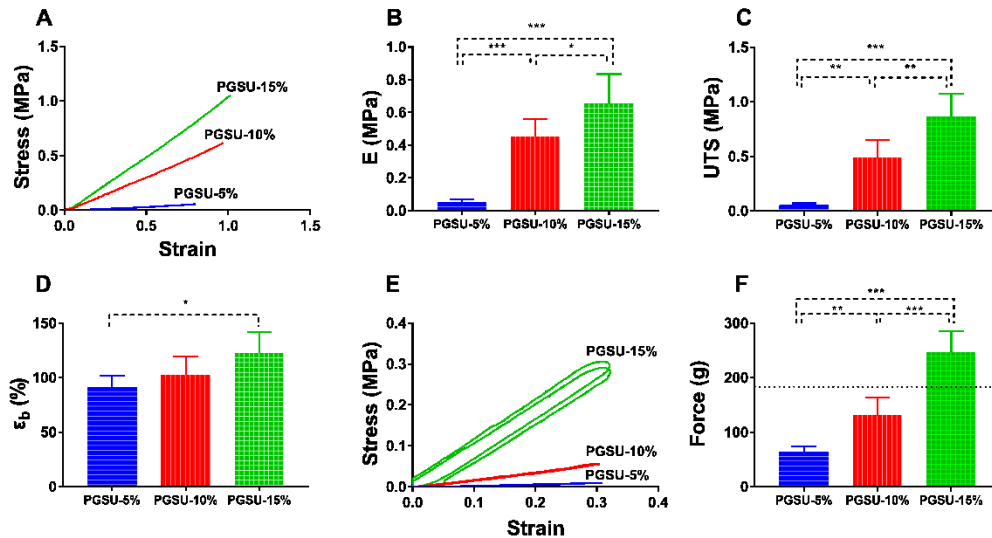


Figure 3.8: (A) Representative stress-strain curve, (B) Young's modulus, (C) ultimate tensile strength, (D) elongation at break, (E) cyclic loading, and (F) suture retention strength of the PGSU scaffolds. Results are shown as mean  $\pm$  standard deviation,  $n=5$ , \* when  $p < 0.05$ .

### 3.3.1.4. *In vitro* enzymatic degradation

Figure 3.9 shows the mass loss of scaffolds over time degraded in lipase solution, with enzyme-free PBS as a control. When the concentration of polymer was increased, the degradation rate decreased. In lipase, PGSU-5% degraded  $52.3 \pm 3.8\%$ , a slightly slower degradation rate was observed for PGSU-10% with mass loss equal to  $39.3 \pm 3.9\%$  and consequently, the highest concentration, PGSU-15%, exhibited an even smaller mass loss of  $19.1 \pm 1.0\%$ . For the scaffolds degrading in the PBS without the enzyme there was only minimal losses observed (PGSU-5% =  $1.99 \pm 0.55\%$ , PGSU-10% =  $0.47 \pm 0.23\%$ , PGSU-15% =  $0.22 \pm 0.19\%$ ) from all three scaffolds with no significant difference between the groups.

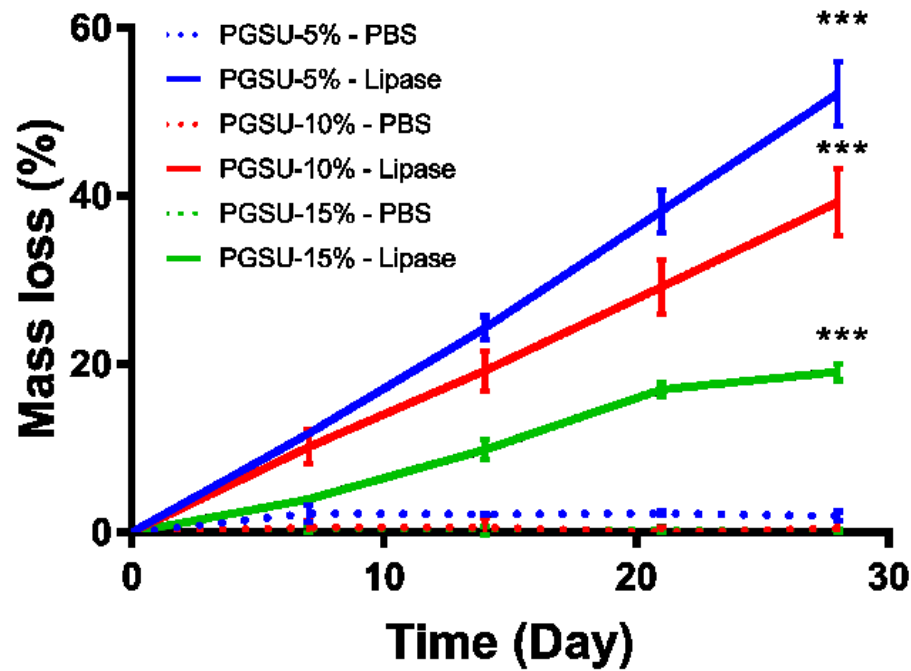


Figure 3.9: In-vitro enzymatic degradation of PGSU5%, 10% and 15% scaffolds. Samples were degraded in PBS as a control. Results are shown as mean  $\pm$  standard deviation, n=3, \*\*\* when  $p < 0.001$ .

### 3.3.1.5. Scaffold permeability

The permeability of the scaffolds (Figure 3.10) was also significantly affected by the polymer concentration. The PGSU-5% scaffolds had the highest water permeability ( $3.8 \times 10^{-3} \text{ m}^2$ ), in PGSU-10% scaffolds the permeability reduced by almost half ( $1.9 \times 10^{-3} \text{ m}^2$ ), while for PGSU-15% scaffolds the permeability was reduced by an order of magnitude ( $2.2 \times 10^{-4} \text{ m}^2$ ).

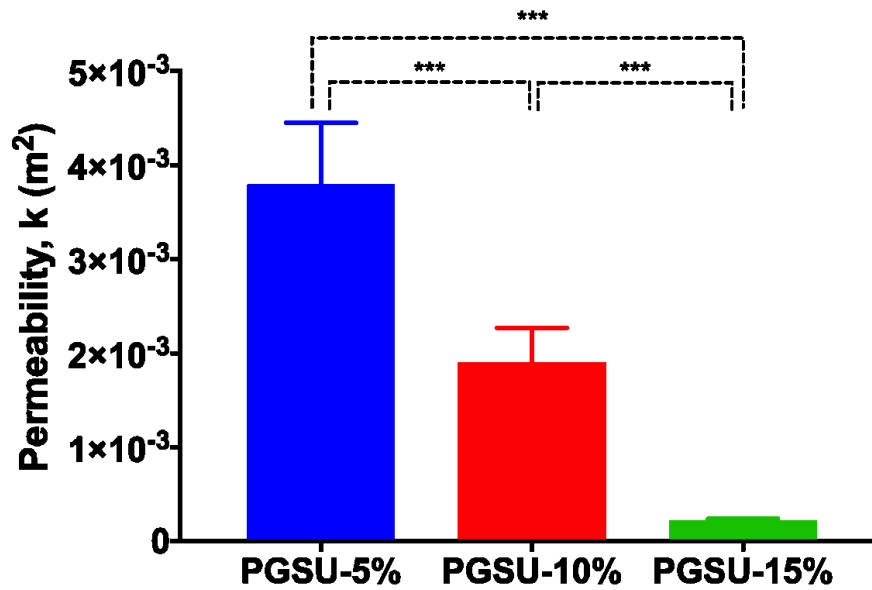


Figure 3.10: Scaffold water permeability using the constant head method and Darcy's law. Results are shown as mean  $\pm$  standard deviation,  $n=3$ , \*\*\* when  $p < 0.001$ .

### 3.3.2. Long term cell culture

The cell culture study began with an investigation into a suitable cell seeding density (L929 mouse fibroblasts) using resazurin assay at day 1 (Figure 3.11). It was found that seeding the scaffolds (10 mm diameter, 2 mm thickness) with  $0.5 \times 10^6$  cells had a significant variation between cell activity on the PGSU scaffolds, with PGSU-10% having the lowest cell metabolic activity. However, the other two seeding densities,  $1.0$  and  $2.0 \times 10^6$  cells, did not show any significant difference between them, leading to the assumption that the scaffolds had the same number of cells attached.

The seeding efficiency was also examined by normalising the day 3 resazurin assay results (seeded with  $1.0 \times 10^6$  cells) with the TCP (positive control) (Figure 3.12). There was significant difference found between the cell metabolic activity on the scaffolds compared to the TCP, but no significant difference was found between scaffolds, indicating that the seeding technique is efficient enough to at least compare between scaffolds.

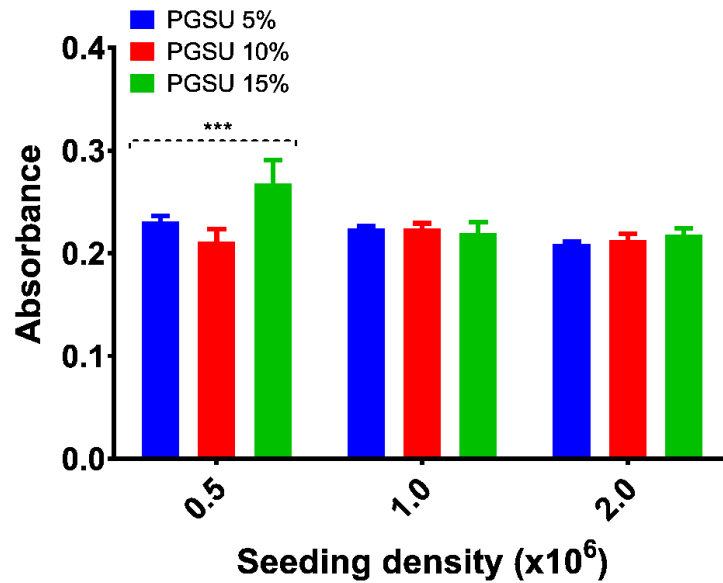


Figure 3.11: Resazurin assay of multiple cell seeding densities at day 1. Results are shown as mean  $\pm$  standard deviation,  $n=3$ , \* when  $p < 0.001$ .

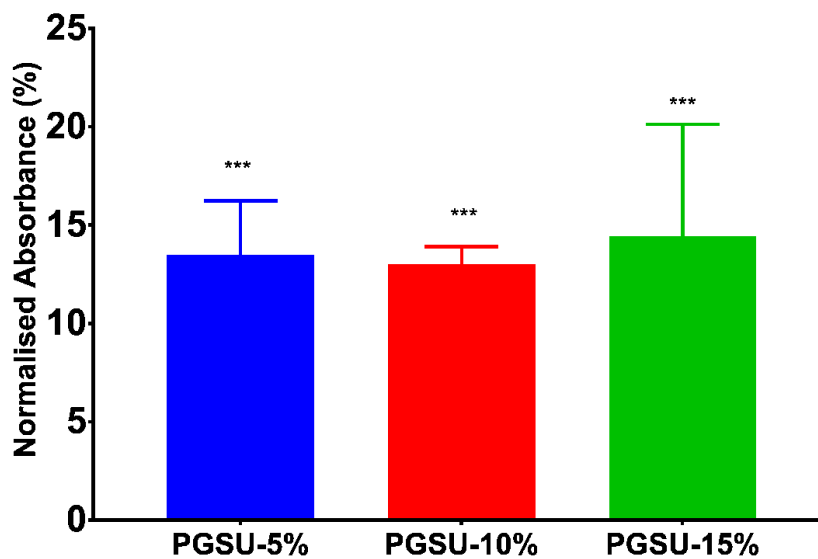


Figure 3.12: Seeding efficiency experiment calculated by the cell metabolic activity found on the scaffolds normalised against the TCP (positive control) on day 3 using resazurin assay. The statistical significance is shown against the TCP. Results are shown as mean  $\pm$  standard deviation,  $n=3$ , \*\*\* when  $p < 0.001$ .

### 3.3.2.1. Cell activity

Scaffolds in TE must provide the cells with a viable environment to let them adhere and proliferate. To test this, we seeded the scaffolds with L929 mouse dermal

fibroblast cells ( $1.0 \times 10^6$  cells), which are the cells suggested by BS EN ISO 10993-5:2009 for biological evaluation of medical devices and the results are shown in Figure 3.13. In the range of 15 days culture the cell activity significantly increased every 3 days reaching ~4-fold increase in cell activity, but no significant difference was found between polymer concentration groups. Between days 12 and 15 there was no significant increase in cell metabolic activity which suggests that high cell confluency was reached around day 12.

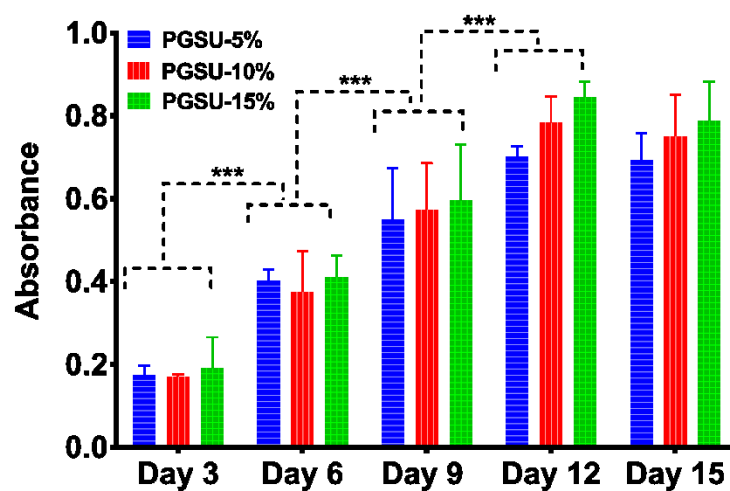


Figure 3.13: Cell activity of L929 cells seeded on PGSU-5%, 10% and 15% scaffolds measured by resazurin assay. (n=3, \*\*\* when  $p < 0.001$ )

The samples were fixed and sectioned at the end of the 15 days culture and histological analysis was performed, their cross section is shown in Figure 3.14. Cells were attached onto all three types of scaffold, with a dense cell layer on the seeding surface. When comparing the cell penetration inside the scaffolds, the cells penetrated deeper into the PGSU-5%, and less penetration was found in the scaffold with the higher polymer concentrations.

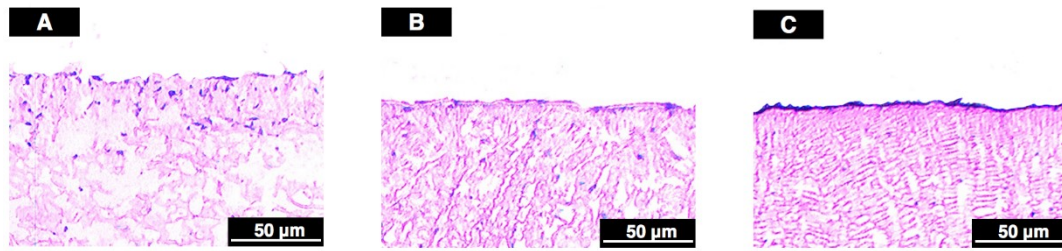


Figure 3.14: Histological analysis (H&E staining) of the cell seeded PGSU scaffolds for all three concentrations (A) PGSU-5%, (B) PGSU-10% and (C) PGSU-15% after 15 days L929 culture.

### 3.3.2.2. Collagen content

To produce a Sirius red standard curve an assay was run on known amounts of collagen type I isolated from rat tail. The results are shown below in Figure 3.15. The gradient of the curve was almost equal to 1 which shows that the equation produced will give accurate results when converting absorbance into collagen mass, with limit of detection (LOD) = 0.000413 mg and limit of quantitation (LOQ) = 0.001251, shown in Figure 3.15 insert (bottom right corner).

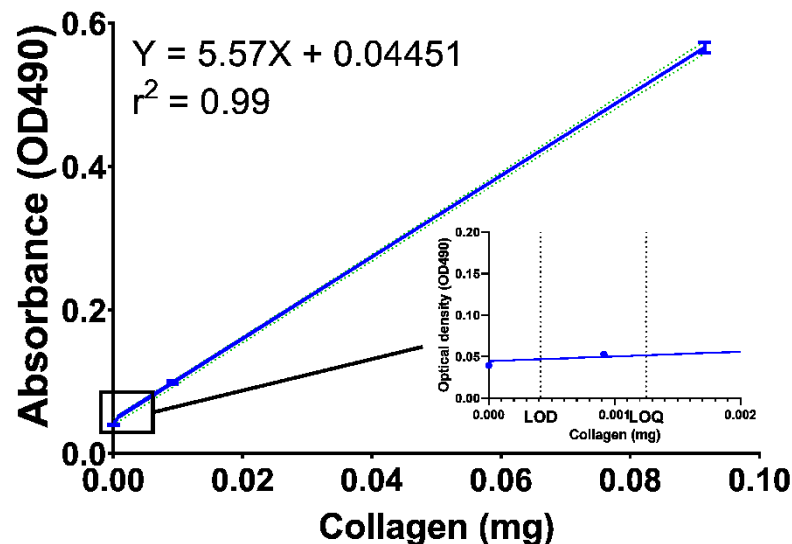


Figure 3.15: Standard curve of Sirius red on known amounts of collagen type I isolated from rat tail. A magnification of the standard curve is also shown to indicate with a vertical dotted line where the limit of detection (LOD) and limit of quantitation (LOQ) are. (n=3)



Figure 3.16 shows the results of the collagen content measured by Sirius red on cell seeded scaffolds cultured for 15 days. The results are presented as collagen / dry sample (w/w%), and their summary is shown in Table 3.1. The PGSU-5% showed a significantly higher collagen content,  $7.5 \pm 2.6\%$ , compared to the PGSU-10%,  $1.7 \pm 0.6\%$ , and PGSU-15%,  $0.4 \pm 0.3\%$ . Macroscopic images of the stained PGSU samples were also taken and are shown in Figure 3.17, which demonstrated the difference in colour intensity prior to eluting the stain. Additionally, there was contraction observed for the PGSU-5%, assumed to be cell driven, due to the higher collagen content and weaker mechanical properties. SEM images were also taken looking at the cross sectional area of the samples after the 15 days cell culture (Figure 3.16 (B-D)). The SEM images demonstrated that a previously highly porous PGSU-5% scaffold had an enclosed pore structure due to the collagen deposition, and the amount of collagen seen decreased with an increase polymer concentration.

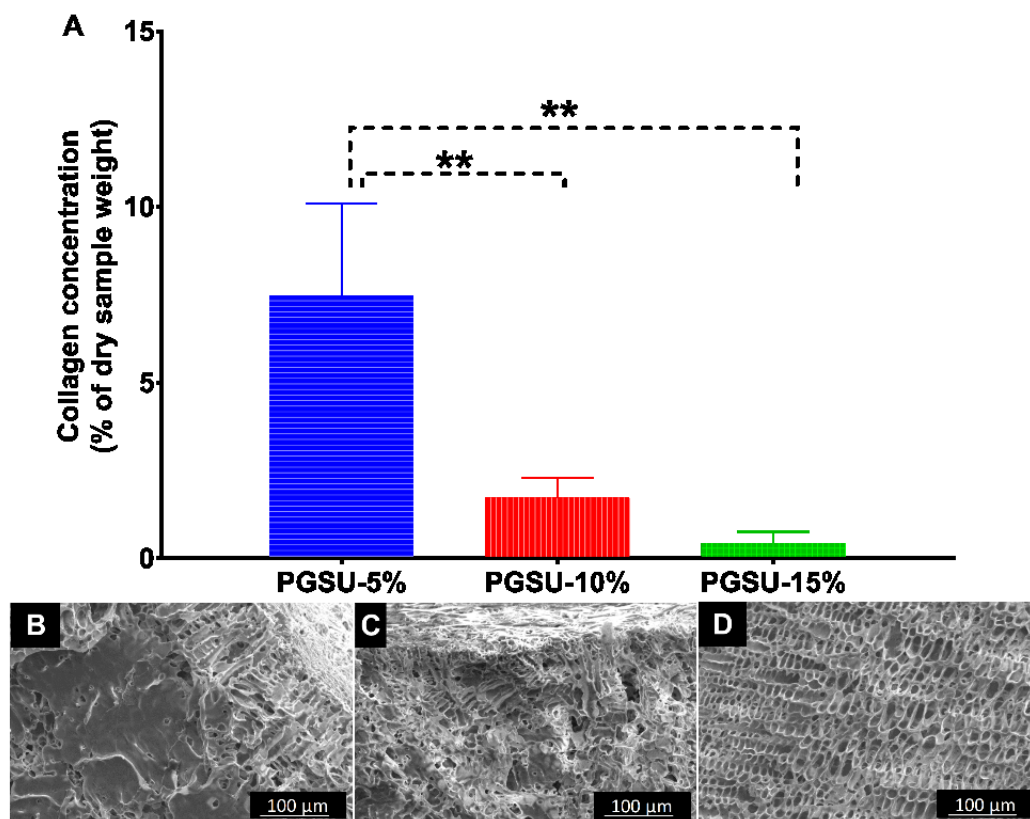


Figure 3.16: (A) Collagen content as a percentage of the dry sample's mass deposited by L929 cells after 15 days of culture. SEM images of (B) PGSU-5%, (C) PGSU-10% and (D) PGSU-15% from the cross section area of the scaffolds after culture. Results are shown as mean  $\pm$  standard deviation, n=3, \*\* when  $p < 0.01$ .

Table 3.1: Collagen content and dry sample mass measured on each sample group. The ratio was then calculated and demonstrated as collagen concentration per dry sample mass. Results are shown as mean  $\pm$  standard deviation, n=3, \*\* when  $p < 0.01$ .

	<b>Collagen content (mg)</b>	<b>Dry sample mass (mg)</b>	<b>Collagen concentration (% of dry sample weight)</b>
<b>PGSU-5%</b>	0.16 $\pm$ 0.08	1.81 $\pm$ 0.13	7.48 $\pm$ 2.13**
<b>PGSU-10%</b>	0.10 $\pm$ 0.08	3.42 $\pm$ 0.18	1.72 $\pm$ 0.48
<b>PGSU-15%</b>	0.03 $\pm$ 0.02	4.56 $\pm$ 0.73	0.44 $\pm$ 0.26

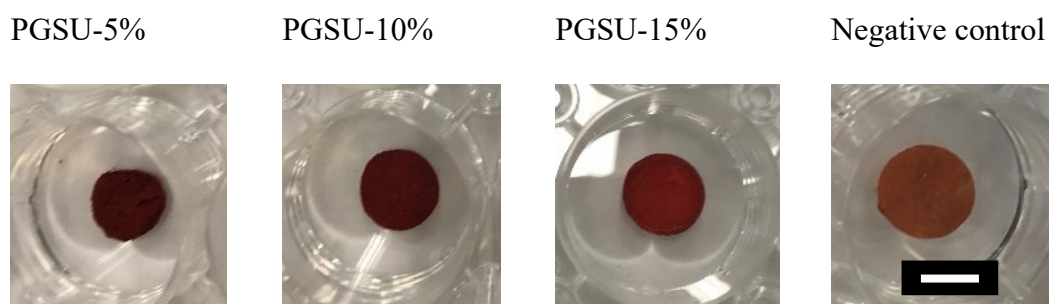


Figure 3.17: Representative images showing the scaffolds after picosirius red staining, which stains collagen with red dye. A shrinkage is observed for the PGSU-5%, due to its weaker mechanical properties and higher collagen content. Negative control were acellular scaffolds. Scale bar is 10 mm.

### 3.4. Discussion

Following the results from Chapter 2 the objective of this chapter was to optimise the microstructure and enhance the mechanical properties of the scaffolds. The microstructure of the scaffold had to be uniform with defined pore structure, while keeping the porosity high (>90%). The mechanical properties, more specifically the

## Chapter 3

UTS and Young's modulus, needed to be enhanced since they were considerably weaker than the biomechanical properties of oral mucosa. Since the fabrication technique was freeze drying, we determined a simple method to alter both simultaneously and we performed a thorough characterisation of these scaffolds in this chapter. Therefore, to perform this study, we synthesised and fabricated porous PGSU scaffolds with various uniform microstructures and enhanced physical properties as both have been shown to affect the cell biocompatibility and tissue regeneration [187, 191].

When changing the PGSU synthesis procedure, by either changing the reactant ratio or the polymer concentration, the chemical structure of the material might change as well. This was well demonstrated by [147] and [118, 148], which found that by changing (increasing) the reactants ratio there were more urethane groups present. In this study we did not change the reactant ratio (1:0.6) but we increased the concentration of pre-PGS during polymer synthesis. Using ATR FT-IR (Figure 3.5) we found that the results closely resembled the results of Chapter 2, Pereira et al. [147] and Frydrych et al. [148]. Additionally, the absence of the characteristic HDI peak ( $2250\text{ cm}^{-1}$ ) from the PGSU spectrum, demonstrates a complete reaction of the isocyanate groups with the hydroxyl groups. As mentioned in the previous chapter it is essential to completely remove the HDI from the scaffold construct because of its highly toxic properties. Hence the reason for the thorough ethanol washing that was done to all PGSU scaffolds in this study. In an encyclopaedia of industrial chemistry it was reported that one of the best ways to purify from HDI is using 50% ethanol due to its solubility in this solvent [192].

During freeze drying the pores in the scaffold are dependent on the freezing process, as the ice crystals formed during freezing leave a pore in the scaffold after it

## Chapter 3

has dried. Therefore, controlling the way of freezing leads to controlling the crystalline structure and subsequently the pore size and structure [149]. In this chapter, unlike the scaffolds fabricated in Chapter 2 we designed a new mould made from aluminium and from the results of Chapter 2 we used an optimised freeze drying cycle. The modification in the scaffold fabrication was to increase the freezing rate. The control of freezing rate and thermal gradient is also called ice templating. During the freezing stage, the nucleation is considered as the moment that defines the ice structure formation, which renders it important in scaffold fabrication using freeze drying [193]. However, the final pore structure is also affected by the ice crystal growth, which is influenced by the freezing system. A major contribution in the freezing system was found to be the mould (its design and material) [194]. The role of the mould during ice templating is to control the heat flow. It was shown before that having a symmetrical mould in terms of geometry and thermal conductivity, less gradient in heat flow is formed therefore more uniform pore structures can be obtained [194]. In this chapter we improved both freezing system and freeze drying cycle. Using aluminium over Teflon the thermal conductivity of the mould was  $\sim 820$  times higher and the pre-freeze stage happened in the freeze drier at  $-50\text{ }^{\circ}\text{C}$  compared to freezer at  $-20\text{ }^{\circ}\text{C}$ . This fast freezing allowed a more uniform microstructure to be formed.

By keeping the fabrication technique the same but altering the polymer concentration allowed us to develop scaffolds with different pore size and porosity. We found that the freeze dried scaffolds using the same freeze drying cycle but different polymer concentrations, exhibited different pore sizes ranging between  $16.1 \pm 2.6\text{ }\mu\text{m}$  to  $28.2 \pm 5.3\text{ }\mu\text{m}$ . These results demonstrate that altering the polymer concentration is an alternative way to control pore size as well as the porosity of the scaffold during freeze drying, in line with the literature [42, 186].

## Chapter 3

The porosity decreased significantly when polymer concentration increased, which is higher than previously reported PGSU scaffolds ( $87.9 \pm 1.3\%$ ) that used polymer concentration of 2.6% (less polymer concentration than the PGSU-5%) [148]. This could be due to two reasons. First, in Frydrych et al. different methods were used to measure the densities of the scaffold and film (combination of helium pycnometer and gravimetric method). Second reason is, because of the difference in freeze drying cycle as well as mould. It is known from previous studies that the mould can affect the final porous structure [193, 195]. Our findings are that in all cases the scaffolds demonstrated a highly porous structure with evenly distributed pores. A highly porous scaffold with interconnected pores, will allow uniform cell distribution after seeding, cell ingrowth and enable neovascularisation [69]. The high porosity is also advantageous as it is required to allow adequate gas and nutrient exchange. This was tested by measuring water permeability through the scaffold. We found that all scaffolds exhibited high permeability and that permeability was significantly affected by the polymer concentration. Comparing the permeability of this study's PGSU scaffolds with other freeze dried scaffolds made from collagen/hydroxyapatite hybrid the PGSU scaffolds had at least 4 orders of magnitude higher permeability (PGSU scaffolds permeability:  $3.8 \times 10^{-3} - 2.2 \times 10^{-4} \text{ m}^2$  compared to  $7.0 \times 10^{-8} \text{ m}^2$ ) [182].

The next objective was to enhance the mechanical properties of the scaffolds without sacrificing its microstructure and porosity. It is well known that tissue engineering scaffold needs to have mechanical strength sufficient to withstand physiological *in vivo* forces and maintain its integrity until it is replaced by the newly formed tissue. The material itself plays an important role on the mechanical properties of the scaffold but the microstructure does as well. With this in mind there should be a good balance between pore size, porosity and mechanical properties, to facilitate cell

## Chapter 3

infiltration, angiogenesis and mechanical stability [163]. Native soft tissues exhibit elastic behaviour strongly influenced by their ECM structural arrangement. For example soft tissues such as skin and aorta have UTS between 1-20 MPa and 0.3-0.8 MPa respectively, and their elongation at break is 30-70% and 50-100%, while tendon and ligaments exhibit UTS ranging 50-100 MPa and elongation at break 10-15% [196, 197]. The PGSU scaffolds fabricated for this work were highly flexible and there was no yielding found before failure despite the high porosity, their UTS ranged between 0.05 – 0.86 MPa, Young's modulus ranged between 0.05 – 0.65 MPa and elongation at break ranged between 91.42 – 122.60 %. Therefore, the UTS is close to skin and within the range of aorta, while the elongation at break is within the range of all above mentioned tissues. Regardless of the changes made to scaffold preparation the mechanical properties of the oral mucosa (UTS: 1.06 – 2.83 MPa, Young's modulus: 2.48 – 19.75 MPa [16]) are still above the range of mechanical strengths obtained from this chapter's scaffolds. Despite this, it has previously been shown that softer and less strong materials have been used successfully in OMTE which indicates that the PGSU scaffolds still have the potential to be used successfully for this application [15].

Mimicking the target tissue's mechanical properties has been proven to be beneficial in studies where the response of individual cell types was examined on substrates with different mechanical properties. As discussed in Section 1.3.3, it was found that epidermal keratinocytes proliferated better on stiffer surfaces (2.0 MPa) compared to softer surfaces (0.18 MPa) [100]. Similarly, human dermal fibroblasts cell number doubled in 2 days on stiffer collagen gels (1.81 MPa) as opposed to soft collagen gels (0.42 MPa) [101]. On the PGSU scaffolds in this study, the L929 mouse fibroblast cells demonstrated a ~4.5 folds higher metabolic activity over 15 days culture and this was true for all three scaffolds used in this chapter. The scaffolds also

## Chapter 3

supported the deposition of collagen but in this case the PGSU-5% had ~4 folds higher collagen compared to PGSU-10% which indicates the scaffold's properties are able to support the desired cell behaviour *in vitro* despite the low mechanical properties of the scaffolds compared to oral mucosa. While not tested here it may be that the deposited collagen is able to increase the scaffold's mechanical strength prior to implantation, bringing it closer to native tissue.

In terms of mechanical properties, an advantage of PGSU over most other synthetic and natural biomaterials is its ability to recover its initial structure and strength after loading is applied. This was confirmed from the cyclic loading experiment, where all scaffolds showed a negligible loss of mechanical strength after 100 cycles at 30% strain, indicating that these scaffolds can maintain their mechanical strength after deformation making them suitable for load-bearing applications, where both strength and elasticity is required. Other polymeric materials, such as, PLGA, PCL and PEG, lack this property which and have been reported to undergo plastic deformation after tensile testing, making them incompatible for use in soft TE [198]. Additionally, biomaterials are usually manipulated before transplantation during which they should maintain their structure and mechanical integrity [147].

When a scaffold is implanted, in most cases it is sutured at the implantation site, thus the suture retention strength of the scaffold needs to be characterised. It was reported that the suture retention surgical requirement is 1.8 N (or 183 g, shown with dotted line Figure 3.8 (F)) [190]. The PGSU-15% scaffold had a higher suture retention strength than the surgical requirement meaning that it can be securely sutured at the implantation site without structure failure. While sutures are the most commonly used method to secure biomaterials in place, other methods are available which may be compatible with the weaker PGSU scaffolds, for example fibrin glue.

The degradation mechanism of PGSU is based on surface erosion [147, 148]. Lipase can catalyse the hydrolysis of ester bonds in polyester materials, hence it is one of the most common enzymes used when examining the *in vitro* degradation characteristics of polyester materials [118, 146, 199]. Degrading the PGSU samples *in vitro* with lipase shows a linear degradation rate which is dependent on the polymer concentration. The polymer concentration affects the degradation kinetics by reducing the surface area exposed to the enzyme, and since PGSU degrades by surface erosion, the degradation rate is decreased. Previous work has shown that the surface to volume ratio has a significant effect on the degradation rate of the scaffold, which is in agreement with the results of this study [200]. Additionally, the permeability of the scaffolds was significantly lower when the polymer concentration was higher, which means that it was more difficult for the lipase solution to penetrate the inner part of the scaffold to cleave the ester bonds, therefore reducing its efficiency. The linear degradation observed from these scaffolds is also found from PGS scaffolds, which have previously been shown to retain their mechanical properties during degradation, losing mechanical strength at a lower rate than mass loss [120, 126]. As PGSU is based on PGS and they both exhibit linear degradation, it can be assumed that the PGSU scaffolds could also retain their mechanical strength in a similar manner. In order to estimate the *in vivo* degradation rate of the PGSU scaffolds we can use and combine the *in vitro* and *in vivo* degradation results from the original PGSU study [147]. It was reported that the PGSU film (1:0.5 crosslinker ratio) degraded ~10% in 5 days *in vitro* (Figure 1.15) while it degraded ~34% in 20 weeks *in vivo* (Figure 1.19 (C)). In the present study, PGSU-film (1:0.6 reactant ratio) degraded ~10% in 5 days *in vitro*, which is similar to the results from Pereira [147]. Comparing the PGSU-film (Figure 2.16) and PGSU-5% (Figure 3.9), the PGSU-5% degraded 1.5 times faster in 5 days



(~15% mass loss). Therefore, if we assume that the degradation rate is linear and the ratio between PGSU-film and PGSU-5% remains true over time, it is expected that the PGSU-5% scaffold should degrade approximately ~51% in 20 weeks *in vivo*.

Pereira et al. examined PGSU films *in vitro* for their cell biocompatibility using MTT assay concluding to no adverse effect on cell activity [147], however they did not examine the biocompatibility of 3D PGSU scaffolds. PGSU porous scaffolds could affect the cell biocompatibility differently, since the scaffold has significantly higher surface area allowing cells to infiltrate its structure which may lead to isolating the cells from cell culture media which may lead to cell death. The *in vitro* cell biocompatibility results from this study showed an increase in cell activity over time and did not indicate any adverse effect on cell metabolic activity. These results show that the scaffolds provided a surface for the cells to adhere and proliferate despite the hydrophobic nature of PGSU ( $2.68 \pm 0.93$  % swelling ratio in PBS solution after 24h [148]). This is maybe due to the carboxyl group found in PGSU, shown in the FTIR results Figure 3.5. Multiple studies have examined how and why cells adhere on surfaces and they found that surface with carboxylic acid (COOH) has superior cell adherence and spreading compared to other more hydrophilic surfaces that exhibit functional groups such as hydroxyl groups (OH) [58, 60]. This occurs because of protein adsorption on the materials surface prior to cell adhesion. However, strong adsorption of some proteins might be disadvantageous when the surface is meant for cell attachment and growth [58]. For example, albumin (major component of serum) adsorbs strongly on hydrophobic surfaces, and larger proteins, such as fibronectin, cannot displace it to facilitate cell attachment [58]. Faucheux et al., characterised the ability of fibroblast cells to attach and spread on COOH and they concluded that more fibroblasts attached on surfaces with COOH functional groups compared to PEG and

## Chapter 3

surfaces with OH groups [60]. In terms of spreading the cells were fully spread within 2 h on COOH, and the fibroblasts were also producing fibronectin which is known to help in regulating cell attachment, growth and function [60, 201].

Plenty of studies have shown that the cell metabolic activity is influenced significantly by pore size and porosity [163]. In the case of this study, there was no effect found on cell metabolic activity when pore size and porosity were different. However, the cell penetration and cell distribution were affected. When the scaffolds were histologically analysed it was observed that the cells could penetrate less when the pore size was decreased. These findings are thought to be due to the hydrophobic nature of PGSU and small pore size of the scaffold meaning seeding cells into these scaffolds passively is extremely inefficient. The average size of human fibroblasts is 10-15  $\mu\text{m}$  [202]. The PGSU-15% had a significantly smaller pore size (6.4  $\mu\text{m}$ ) on the top surface which would not allow the cells to penetrate, rather providing a surface for them to attach, adhere and proliferate through the mechanism mentioned above. The PGSU-15% scaffold also had a significantly lower permeability ( $2.2 \times 10^{-4} \text{ m}^2$ ) which could also be responsible for the lower cell penetration. It is believed that the reason this smaller pore size surface is formed is because during the pre-freezing stage the 1,4-dioxane freezes first at the bottom and then the top surface at a high freezing rate resulting in small pores. This theory will be examined further in the next chapter. The top surface of the scaffold could be removed in future studies to enhance the cell penetration and distribution by slicing it off.

Natural ECM is largely composed of collagen, therefore it is important to examine if the cells produced new collagen. The tissues we aim to replace are predominantly collagen therefore as scaffold degrades new collagen should be produced to replace the structural support previously provided by the scaffold. Additionally, previous

research studies have shown that cell produced collagen, aids to retain or even increase the mechanical properties of the scaffold, thus the scaffold maintains its structure integrity allowing enough time for the ECM to completely replace it as it degrades [203, 204]. The PGSU-5% supported the deposition of a significantly higher collagen amount ( $7.5 \pm 2.6\%$  of dry sample weight) compared to the other two scaffolds, which can be explained by better cell penetration, distribution and a higher surface area [205]. For comparison reasons, the collagen in bone tissue accounts for 25-30% of the dry weight of bone, in cartilage 10-20% and in ligaments 70-80%, aorta 25-35% and skin 60-80% [197, 206]. In this study we demonstrated that PGSU-5% encouraged collagen production reaching collagen amount close to cartilage tissue in 15 days static cell culture. This occurred because of the combination of chemical structure, pore size, porosity and permeability of the PGSU-5% scaffold. PGSU-5% degraded approximately 23% on day 14 which is faster degradation compared to collagen production ( $7.5 \pm 2.6\%$ ). This might be beneficial in terms of accelerating the collagen production because the surface area increases while the scaffold degrades which might lead to higher collagen production rate. Wang et al. demonstrated that cell orientation determines the alignment of cell produced collagen matrix [207]. With this said, the PGSU-5% microstructure had a random orientation meaning the subsequent collagen produced by the cells also had random orientation. Longer cell culture should be examined to determine if the collagen amount further increases over time. Despite the potential increase in mechanical strength due to collagen production, another advantage of having collagen presence is that the scaffold becomes more biocompatible and hydrophilic supporting the development of new natural tissue.

### 3.5. Conclusions

The aim of this chapter was to improve the uniformity of the PGSU microstructure and to enhance the mechanical properties of the scaffold to make them closer to oral mucosa. In conclusion in this chapter we:

1. Improved the freeze drying protocol by changing the freeze drying cycle and freeze drying system to fabricate uniform scaffold microstructures.
2. Controlled the pore size, structure and porosity of the scaffold by changing the polymer concentration. Scaffolds made with higher polymer concentrations had smaller pore sizes and lower porosity.
3. Enhanced the mechanical properties of the scaffolds to make them closer to the oral mucosa's biomechanical properties and demonstrated the shape and strength recovery of the scaffolds using cyclic loading.
4. Found that the permeability of the scaffolds was dependent on the porosity of the scaffolds.
5. Demonstrated that the cell metabolic activity was not different between scaffold microstructures but significantly increased over time.
6. Used histology to examine the cell distribution and found that the cells could not penetrate the surface of the scaffolds with smaller pore sizes (PGSU-15%).
7. Examined the cell collagen production of the scaffolds and found that the scaffold with the highest porosity had a significantly higher collagen production.

The results of this chapter have shown that the PGSU scaffold physical properties have significant effect on the biological properties of the scaffold. It was realised that PGSU-5% had the best microstructure to allow adequate cell metabolic activity and promote collagen production. The issues observed during this chapter was the

## Chapter 3

PGSU-5% had lower mechanical properties compared to oral mucosa and the cells were minimally infiltrating within the scaffold's structure probably because of the cell seeding technique. Therefore, for the next chapter it was decided to proceed with using PGSU-5% for oral mucosa tissue engineering, but to attempt to improve the cell seeding technique and imitate the 2-layer structure of the native oral mucosa (lamina propria + basement membrane). Furthermore, some initial, proof-of-concept results will be included in the next chapter to demonstrate the ability of freeze-drying to fabricate more complex microstructure scaffolds.

# Chapter 4 Hierarchical multilayer poly(glycerol sebacate urethane) scaffolds to replicate native tissues

## Aim

To develop novel methods to fabricate isotropic, anisotropic and multilayer scaffolds with hierarchical microstructure to be used in oral mucosa and soft tissue engineering.

## 4.1. Introduction

In the last two chapters we demonstrated that PGSU scaffolds can be fabricated with multiple pore sizes and porosities as well as sterilised with conventional laboratory methods without a major effect on its properties. It exhibits chemical structure that is advantageous for cell attachment and spreading and provides a biocompatible environment for the cells to be metabolically active and the PGSU-5% produced significant amounts of collagen while it degraded linearly in lipase. The scaffolds fabricated in Chapter 3 display good mechanical properties with almost full and fast recovery of its tensile strength. From these results we can therefore complicate the scaffold porous structure to mimic the native ECM of oral mucosa and other soft tissues.

As mentioned in Chapter 1, oral mucosa consists of an epithelium that overlies the lamina propria, which are attached at the basement membrane [8]. On the one hand, to grow an epithelium in 3D it requires a surface for the epithelial cells to attach and go through various degrees of differentiation to build a stratified squamous epithelium. On the other hand, the fibroblast cells require a scaffold to be seeded in and then develop the lamina propria [30]. Meanwhile, a BM is found between them to keep the cells separate and prevent cell infiltration into the other layer, while allowing cell

communication and gas/nutrient exchange. Therefore, a scaffold should be designed to provide a surface for epithelial cells, a scaffold for fibroblasts and a thin BM-like layer to separate them until fibroblasts generate the natural ECM and BM.

A major part in the field of TE is the scaffold which temporarily provides the cells with a 3D structure until they produce their own ECM and replace it. Until then this scaffold should be able to sustain cell growth and collagen production as well as provide guidance to the newly developed tissue. A logical way to provide guidance is to produce a scaffold that mimics the native ECM which allows the cells to grow in a specific direction. Knowing that every tissue has its own specific 3D ECM structure it is important to be able to produce scaffolds that follow that structure in a reproducible and inexpensive manner. According to the literature controlling the freezing of the polymer solution during freeze drying can control the architecture of a scaffold's microstructure and pore direction [178, 191, 193]. The advantage of having oriented pore architecture is that it can mimic natural *in vivo* ECM of tissues which require alignment, for example tendons and nerves. Several research groups approached this topic by fabricating scaffolds with anisotropic pore architecture by combining freeze drying technique and moulding technology [178, 193]. Successful attempts to fabricate unidirectional scaffolds using freeze drying were reported in [178, 193, 208-211] using various biomaterials, such as collagen, gelatin, poly(vinyl alcohol) and PLGA. A general conclusion from most of these studies was that the scaffolds fabricated were unidirectional (anisotropic), had optimised mechanical properties in the direction of the pores and ECM production from the cells was aligned with the pores.

Multilayer scaffolds were also fabricated to further mimic the native tissue multilayer structure using various methods. For example, micromoulding methods

## Chapter 4

were used to fabricate 2-layer PGS porous scaffold with 100 – 150  $\mu\text{m}$  pore size for the purpose of cardiac tissue engineering. Neal et al. seeded these scaffolds with rat heart cells and cultured them *in vitro* for a week and they found that the multilayer structure promoted the cell growth and enhanced the mechanical properties by allowing contraction [212]. However, as mentioned in the literature review (Chapter 1) the micromoulding fabrication technique can only produce thin scaffolds, approximately 150  $\mu\text{m}$ , which limits their application. Another group used freeze drying to develop a natural triple layered vascular graft made out of collagen type I, fibrils and elastin fibres for vascular tissue engineering. Three tubular moulds that had different sizes were used to build the scaffold layer by layer. The scaffolds were tested for their mechanical properties and exhibited suitable properties for vascular tissue engineering [213].

Until now we demonstrated the fabrication techniques to develop one-layer scaffolds with uniform pore structures that were depended on the polymer concentration. However, there is a gap in our knowledge and techniques to fabricate more complex, hierarchical multilayer scaffolds to mimic multilayer ECM native structures. To address this, we will utilise freeze drying, moulding and airbrushing techniques and their combinations to develop one-, two- and three-layer scaffolds that exhibit different porosities and pore sizes as well as one-layer scaffolds that have unidirectional pore structure.

In this chapter we will fabricate PGSU scaffolds that mimic the 3-D architecture of the native ECM of oral mucosa. For these scaffolds a combination of two fabrication techniques was applied to create a thin layer that mimics the basement membrane



found in tissues such as skin and oral mucosa. A step-by-step process will be used to examine firstly the ability of oral keratinocytes to adhere and survive on the PGSU-film, then solve the seeding issue we had during chapters 2 and 3, and last apply cell co-culture on the scaffolds and examine them using histology and immunohistochemistry. Additionally, a proof-of-concept study was done to fabricate unidirectional, and multilayer PGSU scaffolds using freeze-drying that could potentially be used in soft TE.

### **4.2. Materials and Methods**

#### **4.2.1. Materials**

The materials for this chapter are the same as in Chapters 2 and 3 with the addition of: Nutrient mixture F12 (Ham's F12) was purchased from Biosera. Adenine, Insulin, hydrocortisone, epidermal growth factor, cholera toxin, 3,3,5-Tri-iodothyronine/Apo-Transferrin, amphotericin B and collagenase A (extracted from *Chlostridium histolyticum*) were purchased from Sigma Aldrich. Vectastain Elite ABC kit and 3'-diaminobenzidine tetrahydrochloride (DAB) were purchased from Vector Labs. AE1/AE3 primary antibodies were purchased from Dako. Polytetrafluoroethylene (PTFE) virgin rod was purchased from Plastock.

#### **4.2.2. Methods**

##### **4.2.2.1. Pre-PGS synthesis**

Pre-PGS was synthesised as in Chapter 2: Section 2.2.2.1.

##### **4.2.2.2. PGSU-5, 10, 15% scaffolds**

PGSU was synthesised as in Chapter 3: Section 3.2.2.2 and the scaffold fabrication using the following methods.

### 4.2.2.2.1. Aluminium tray with PTFE mould

To control the orientation of the porous microstructure of the scaffolds two inhouse moulds were designed that allowed scaffolds to be produced with vertical and horizontal direction pores. The moulds were comprised of aluminium grade 6082T6 base and PTFE moulds as shown in Figure 4.1. The mould designed to produce vertical orientation scaffolds will be mentioned in the thesis as “Mould-vertical” and the mould for horizontal orientation scaffolds will be mentioned as “Mould-horizontal”. For both moulds the PTFE walls were detachable to allow the easy removal of the scaffolds.

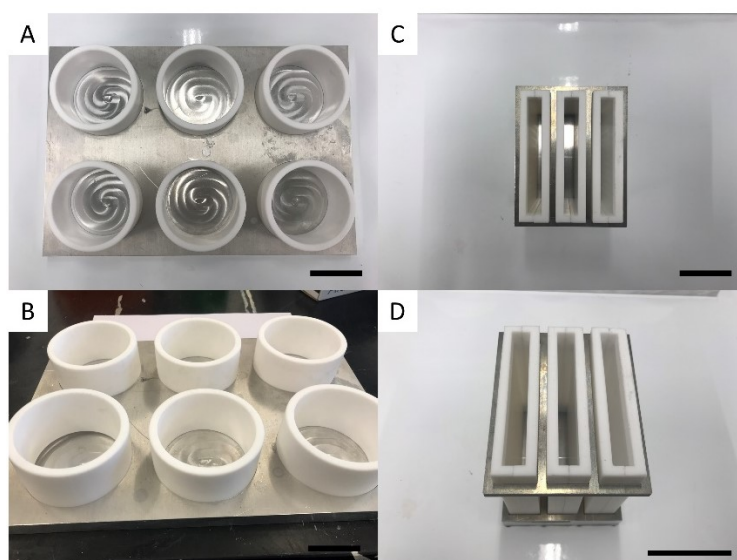


Figure 4.1. Inhouse designed moulds with aluminium base and PTFE walls for multiple orientation scaffold fabrication. (A) Top view of the mould-vertical, (B) side view of mould-vertical, (C) top view of mould-horizontal and (D) side view of mould-horizontal. Scale bar is 5 cm.

### 4.2.2.2.2. Controlled orientation PGSU scaffolds

The fabrication method is similar to the method described in Chapter 3: Section 3.2.2.2.2 except the mould that the PGSU solution was cast in was either mould-vertical or mould-horizontal dependent on the desired porous architecture, and the polymer concentration was kept at 10% (w/v) only. This polymer concentration was decided for two reasons; first the microstructure properties of these scaffolds logically

will be between 5% and 15% (w/v) polymer concentrations which may indicate the range of microfeatures that can be achieved; and second was due to the potential application of these scaffolds it may require stiffer mechanical properties than the PGSU-5% scaffolds had in Chapter 3. Therefore, the scaffolds with vertical pore orientation will be mentioned as “PGSU-vertical” and the scaffolds with horizontal orientation as “PGSU-horizontal”.

### **4.2.2.2.3. Multilayer PGSU scaffolds**

The multilayer scaffolds are composed from layers that have different pore sizes and porosities. The PGSU synthesis was performed as previously described in Chapter 3: Section 3.2.2.2.2 using the three different polymer concentrations (5%, 10% and 15%). The fabrication was done by building the scaffold layer by layer.

Two double-layer scaffolds were produced, the first one was composed from two layers PGSU-10% and PGSU-15% (will be referred as PGSU-bilayer); and the second scaffold was composed from PGSU-5% and a thin film (that resembles a basement membrane), will be referred as PGSU-BM.

To fabricate the PGSU-bilayer, both PGSU-10% and PGSU-15% were synthesised with 2 hours delay between them. Firstly, PGSU-10% was cast into mould-random and left to freeze at -50 °C for 2 hours inside the freeze drier. After 2 hours, the solution was completely frozen and PGSU-15% was ready to be casted on top of the frozen PGSU-10%, however before casting, the temperature of the solution was reduced from 55 °C to 15 °C (just before 1,4-dioxane melting point: 11.7 °C) and then it was cast on top of the already frozen base layer (PGSU-10%) allowing the surface of it to defrost and immediately freeze back. The mould was then placed back into the freeze drier and the freeze drying cycle shown in Chapter 3: Figure 3.4 was applied.

## Chapter 4

To fabricate PGSU-BM, PGSU-5% scaffold was synthesised and freeze dried as in Chapter 3: Section 3.2.2.2.2. To add the second layer, PGSU-5% was synthesised and instead of casting it on top of the base layer, a fabrication technique called airbrushing was utilised. For this technique an air spray gun was used to spray 1 or 2 ml of PGSU solution on top of the PGSU-5% scaffold to produce a second thin layer. Using published methods [152] with slight modifications to produce a film instead of fibres, the PGSU-5% solution was fed into a gravity fed cup of a double action/internal mixing spray gun with a nozzle size of 600  $\mu\text{m}$  and the polymer solution was ejected from a 15 cm distance at a steady air pressure using an air compressor (lowest setting used; unknown air pressure). To determine how the second layer should be fabricated (Table 4.1) three methods were investigated:

- i) the scaffold was frozen at  $-20\text{ }^{\circ}\text{C}$  and then freeze dried
- ii) the scaffold was frozen in liquid nitrogen and then freeze dried
- iii) or the scaffold was left inside the fume cabinet for 48 hours to air dry, and then placed in the vacuum oven for another 24 hours at  $40^{\circ}\text{C}$ .

Table 4.1: PGSU-BM airbrushing conditions.

Condition	Polymer solution volume	Scaffold name
$-20\text{ }^{\circ}\text{C}$	1 ml	PGSU-BM(1)
Liquid nitrogen	1 ml	PGSU-BM(2)
	2 ml	PGSU-BM(3)
Air dried	1 ml	PGSU-BM(4)
	2 ml	PGSU-BM(5)

One three-layer scaffold was also fabricated with different pore size, porosity and a thin film on top (to resemble a basement membrane). This trilayer scaffold was built from base to top, composed from PGSU-5%, PGSU-10% and thin film respectively, and it will be referred to as PGSU-trilayer. To fabricate this scaffold PGSU-5% was synthesised, cast into mould-random and frozen at  $-50^{\circ}\text{C}$  for 2 hours. PGSU-10% was then synthesised and the solution's temperature was reduced to  $15^{\circ}\text{C}$  and immediately cast on top of the frozen PGSU-5% solution. The now 2-layer scaffold was freeze dried following the freeze drying cycle shown at Figure 3.4. The top thin film was fabricated using the airbrushing technique mentioned above (PGSU solution volume = 1 ml). The PGSU-trilayer scaffold was then left to dry for 48 hours and then placed in the vacuum oven for another 24 hours at  $40^{\circ}\text{C}$ .

All scaffolds were washed with ethanol to remove any unreacted substances from its construct. The washing was done by submerging the scaffold in 100%, 70% and 50% Ethanol for 2 hours each, and then immersed in distilled water overnight. Shaking was also applied on the scaffolds while washing.

#### **4.2.2.2.4. Mould characterisation – polymer solution freezing rate**

The temperature gradient of the PGSU solution (10 % w/v) during the pre-freeze stage was recorded using a temperature probe at three different locations for all three moulds. For the mould-random and mould-vertical, a temperature probe was placed inside the PGSU solution at positions 0 mm (top), 5 mm (middle) and 10 mm (bottom) as soon as the pre-freeze stage began, and the temperature was recorded every minute for a total of 3 h. For the mould-horizontal a temperature probe was placed at 0 mm (bottom), 20 mm (middle) and 40 mm (top). The nucleation event was defined as the temperature point where the solution reached before latent heat was released and the temperature jumped back to a higher temperature [194]. The time at equilibrium was

defined as the two points that the temperature remained almost constant after the nucleation event and before dropping again.

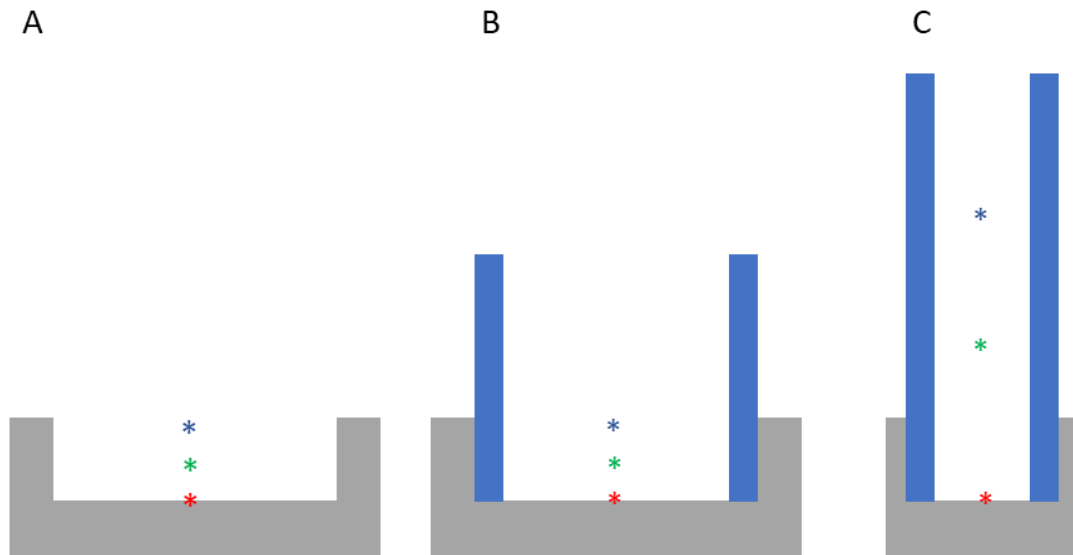


Figure 4.2: Schematic showing the moulds and the locations that the temperature probes were placed to quantify the freezing rate of the polymer solution. A) is the mould-random (asterisk: red = 0 mm, green = 5 mm, blue = 10 mm), B) is the mould-vertical (asterisk: red = 0 mm, green = 5 mm, blue = 10 mm) and C) is the mould-horizontal (asterisk: red = 0 mm, green = 20 mm, blue = 40 mm). The schematic is not scaled.

### 4.2.2.2.5. Multilayer scaffold characterisation

The scaffolds were characterised for their microstructure and pore size using SEM; and their permeability following the methods described in Chapter 2: Sections 2.2.2.5.2 and 2.2.2.5.7 respectively.

### 4.2.2.3. Oral mucosa *in vitro* cell culture experiments

#### 4.2.2.3.1. OKF6 cell culture

Immortalised human oral keratinocytes were grown using Keratinocyte – SFM (KSFM) media and cultured the same way as L929 cells described in Chapter 2: Section 2.2.2.6.1 above. OKF6/TERT2 cells were originally produced in Dickson et al. [214] and were obtained from Professor Martin Thornhill (School of Clinical Dentistry, University of Sheffield).

### 4.2.2.3.2. Normal oral keratinocytes cell culture

Normal oral keratinocytes (NOK) were isolated from oral mucosa biopsies from consenting human volunteers (according to our protocol approved by the University of Sheffield Research Ethics Committee, ethical approval number: 09/H1308/66). The biopsies were incubated overnight in 0.1% (w/v) Difco trypsin solution at -4 °C. Using sterile scalpel and forceps the epithelium was peeled off the connective tissue layer and then the keratinocytes were scraped from the epithelium and the top side of the connective tissue. The Difco trypsin and epithelium were then transferred into a universal and centrifuged for 5 min at 1000 rpm. The supernatant was then removed and the pellet was resuspended in Green's media, consisting of DMEM and Ham's F12 medium in a 3:1 (v/v) ratio supplemented with 10% (v/v) FCS, 0.1 µM cholera toxin, 10 ng/ml epidermal growth factor, 0.4 µg/ml hydrocortisone, 0.18 mM adenine, 5 µg/ml insulin, 5 µg/ml transferrin, 2 mM glutamine, 0.2 µM triiodothyronine, 0.625 µg/ml amphotericin B, 100 IU/ml penicillin and 100 µg/ml streptomycin. To culture the NOK, flasks previously seeded with irradiated mouse fibroblasts (i3T3) were used to seed on top. These cells act as a feeder cell layer by secreting growth factors important to allow good proliferation of keratinocytes and delaying their terminal differentiation [215] The media was changed as necessary, usually within 3 days, and not passaged before 80% confluency. To passage, the media was removed, and the flask was washed with PBS, then 5 ml of 0.02% EDTA solution was added for 5 min to detach i3T3 cells, washed with PBS, and then using trypsin for approximately 5 min the NOK were detached, collected, centrifuged and passaged into more flasks again on top of fresh i3T3. Prior to seeding the methods described for cell counting in Chapter 2: Section 2.2.2.6.1 were used here as well. NOKs were used between passages 1-3.

### **4.2.2.3.3. Normal tonsil fibroblasts cell culture**

Normal oral fibroblasts isolation was attempted from the biopsies used in Section 4.2.2.3.2, however due to low number of cells isolated they could not grow into an adequate cell number to use for this chapter. Therefore, normal tonsil fibroblasts (NTF) were isolated from waste tissue from surgery (according to our protocol approved by the NHS Research Ethics Committee 09/H1308/66) and cultured in Green's media as for NOK and were cultured the same way as L929 cells in Chapter 2: Section 2.2.2.6.1 above. Prior to seeding the methods described for cell counting in Chapter 2: Section 2.2.2.6.1 were used here as well. NTF cells were used between passages 3-8.

### **4.2.2.3.4. Oral cells co-culture**

#### **4.2.2.3.4.1. OKF6 attachment on PGSU-film**

PGSU-films were punched (10 mm diameter) and sterilised using 70% ethanol overnight and then washed in sterile PBS. The films were then placed in a 12 well plate and fixed with a surgical stainless-steel ring (10 mm inner diameter) to facilitate with cell seeding. OKF6 cells were then seeded at a  $1.0 \times 10^6$  cells/scaffold and left to attach for 24 hours. The next day the surgical stainless-steel rings were removed and the samples were transferred to a fresh well plate, and cultured for 9 days, performing resazurin assay every 3 days following the methods described in Chapter 2: Section 2.2.2.6.3.2. Cells seeded on TCP and acellular PGSU-film served as positive and negative controls respectively. The experiment was repeated 3 times and each repeat was in triplicates.

#### **4.2.2.3.4.1.1. Live/Dead staining**

Live/dead assay consists of SYTO<sup>®</sup>9, which has green fluorescence and propidium iodide (PI), which has the red fluorescence and both stain the nucleic acid. SYTO<sup>®</sup>9



is an intercalating membrane permeant stain that stains both live and dead cells, whereas the PI can only bind to dead cells, and it because it has stronger affinity for nucleic acid it displaces the SYTO<sup>®</sup>9 and the cell will fluorescence in red [216]. Therefore, live cells are stained green and dead cells are stained red.

The samples were washed with PBS and live/dead working solution was added to the samples, covered with aluminium foil and left at room temperature for 30 min while shaking. The working solution used was commercially available and consisted of 1:1000 dilution of SYTO<sup>®</sup>9 (0.001% (v/v)) and a 1:100 dilution of PI (0.0015% (v/v)). After 30 min the samples were washed with PBS and submerged again in PBS and visualised using fluorescence microscopy.

#### **4.2.2.3.4.2. NOK attachment on PGSU-film**

The same methods as Section 4.2.2.3.4.1 were used to examine the NOK attachment on PGSU-films, with the addition of i3T3 cells were seeded the day before the experiment. Prior to resazurin assay, the samples were moved to a fresh well plate for the assay and then back to their original plate (with i3T3).

#### **4.2.2.3.4.3. PGSU-BM sample preparation**

All samples were prepared as in Chapter 3: Section 3.2.2.4.1, with inner diameter 10 mm and 3 mm thickness. The samples were placed in a 12 well-plate inside a surgical stainless-steel ring with the sprayed BM mimic on the bottom of the well and the porous PGSU scaffold exposed. A 200  $\mu$ l cell suspension containing  $5.0 \times 10^5$  of NTF was seeded using a dynamic seeding technique, following the methods established by [217] with some modifications. Briefly, after overlaying the samples with the cell suspension, the well-plate was placed in sterile plastic bag with syringe and syringe filter, moved into a vacuum desiccator and the cells were seeded by reducing the

## Chapter 4

pressure up to 0.1 bar followed by a rapid ventilation to atmospheric pressure, the cycle was repeated 6 times, shown in Figure 4.3. The samples with NTF were then incubated and cultured overnight. On the next day, the samples were turned 180° so the BM mimic was now on top while keeping them inside the ring. NOK were then passively seeded in a 200 µl cell suspension containing  $5.0 \times 10^5$  cells. The media was then topped up to 2 ml and incubated for 2 more days. On day 3, the PGSU-BM samples were placed on a stainless-steel grid and lifted to an air-liquid interface (ALI), ensuring that the bottom layer of the scaffold was covered with media and the top exposed to air to promote the epithelial stratification. The samples were cultured for another 12 days at the ALI. The experiment was repeated three times in triplicates.



Figure 4.3: Image showing the PGSU-BM ready for dynamic seeding. The scaffolds are fixed in a surgical stainless-steel ring and overlaid with cell/media suspension. The well-plate was then placed in a sterile plastic bag with a syringe and a syringe filter to sterilise the returning air while ventilating.

### 4.2.2.3.4.4. Preparation of de-epithelialised dermis

De-epithelialised dermis was pre-prepared as described in Colley et al. [2], from human skin collected from contenting patients following routine surgical procedures

(according to our protocol approved by the NHS Research Ethics Committee 15/YH/0177). On the day of seeding, sterile DED was cut into squares (~12 x 12 mm) and placed in a 6 well-plate submerged in Green's media. Surgical stainless-steel rings were pushed onto the DED to provide a tight seal with inner diameter of 10 mm. The samples were seeded with 1 ml cell suspension containing  $5.0 \times 10^5$  NTF and  $5.0 \times 10^5$  NOK, at this point Green's media was added outside the ring to stop cells leaking out of the ring. After 2 days half the media inside the ring was replaced with fresh Green's media. On day 3, the DED was placed onto a stainless-steel grid and raised to ALI, making sure that the bottom of the DED was in contact with the media and the top exposed to air to enhance the epithelial stratification and cultured for another 12 days. The experiment was repeated three times in triplicates.

#### **4.2.2.3.5. Histology**

Histology was performed as mentioned in Chapter 3: Section 3.2.2.5.

#### **4.2.2.3.6. Immunohistochemistry**

Cytokeratin AE1/AE3 antibodies were used to characterise the epithelium of the tissue engineered oral mucosa cultured on PGSU-BM and DED. Paraffin embedded (5  $\mu$ m) sections were dewaxed with xylene and rehydrated through a series of ethanol dilutions. The endogenous peroxidase was neutralised with 0.3% hydrogen peroxide for 30 min. The sections were then washed in PBS for 5 min. For antigen retrieval the sections were submerged in pre-warmed 0.01M tri-dofium citrate buffer (pH 6) and placed in a microwave at medium heat for 8 min. The samples were then washed again in stirring tap water for 5 min. The sections were then blocked with blocking serum mixture from Vectastain elite ABC kit for 20 min at room temperature. The cytokeratin AE1/AE3 antibodies were prepared as shown in the table below. A drop of the antibodies was placed on the slides ensuring the whole section was covered and

left for 1 h at room temperature. The slides were washed for 5 min in PBS. Then biotinulated secondary antibody solution was added for 30 min and incubated at 37°C and 5% CO<sub>2</sub> and washed again for 5 min in PBS. The slides were then again incubated with Vectastain Elite ABC reagent mixture for 30 min. The samples were again washed for 5 min in PBS. Finally, DAB solution was prepared and mixed well, and then added on the slides for 2-10 min, depending on the staining intensity required, therefore the samples were monitored under the microscope until the desired staining was obtained. The samples were then washed and counter-stained with haematoxylin following the methods described in Chapter 3: Section 3.2.2.5.

Table 4.2: Antibodies and antigen retrieval conditions used in this study.

Marker	Antibody clone	Dilution/final concentration (in PBS)	Antigen retrieval	Source
AE1/AE3	AE1/AE3	1 : 100	0.01 M sodium citrate buffer	Dako

#### 4.2.2.4. Statistical analysis

The statistical analysis was performed as in Chapter 2: Section 2.2.2.7.

### 4.3. Results

#### 4.3.1. Mould characterisation – polymer solution freezing rate

The thermal profile of the in-house build moulds was characterised to understand how each mould and its design can affect the freezing behaviour of the PGSU solution (10% (w/v)) therefore the pore architecture of the PGSU scaffolds.

In view of mould-random, the nucleation event of the PGSU solution happened first at the 0 mm then 10 mm and last at 5 mm (see Figure 4.4), indicating that the solution froze from the two outer surfaces to the inside. However, the 5 mm that froze last had

the highest nucleation temperature, 14°C at 10 min, demonstrating that the solution froze within the first 10 min. This temperature is also above the melting point of 1,4-dioxane ( $T_m$ ). The other two nucleation events occurred at the same temperature, 11°C, but different time points, 3 min for the 0 mm and 5 min for the 10 mm. The time at equilibrium, at the 0 mm position was less than 1 min and it could not be measured precisely using the methods of this thesis, but 5 mm and 10 mm were at equilibrium for 5 min and 6 min respectively.

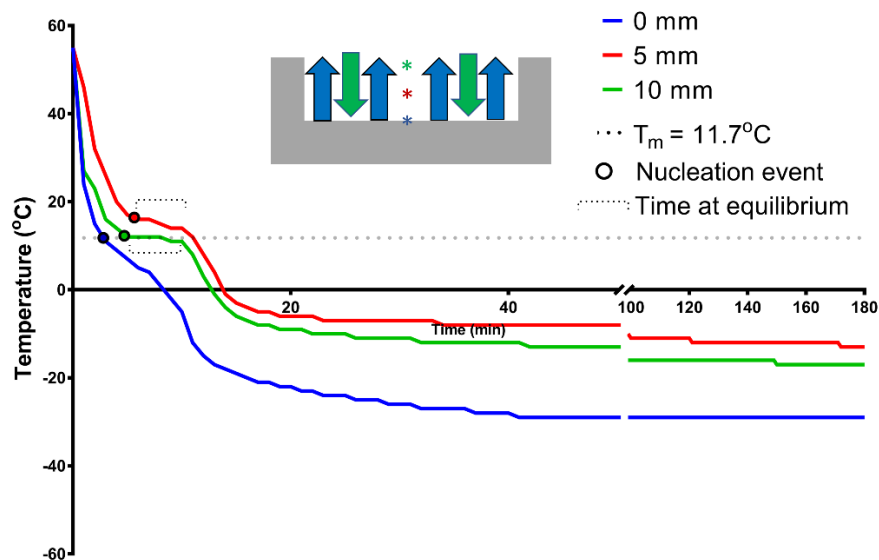


Figure 4.4: Thermal profile of the PGSU/1,4-dioxane solution during freezing using the mould-random.  $T_m$  = melting point of 1,4-dioxane. The schematic represents the mould and the freezing direction of the polymer solution (schematic is not scaled).

Regarding the mould-vertical, the nucleation event happened first at the 0 mm point, 12°C at 6 min, and then second was the 5 mm position, 12°C at 10 min, and last the 10 mm, 17°C at 12 min (see Figure 4.5). This means that the PGSU solution froze from the bottom to the top, as expected. Additionally, the whole solution froze within the first 12 min, with only 6 min separating the first nucleation event to the last. The time at equilibrium was again very small (<1 min) for the 10 mm that could not be

measured, but the 5 mm was at equilibrium for 11 min and the 0 mm was at equilibrium for 13 min.

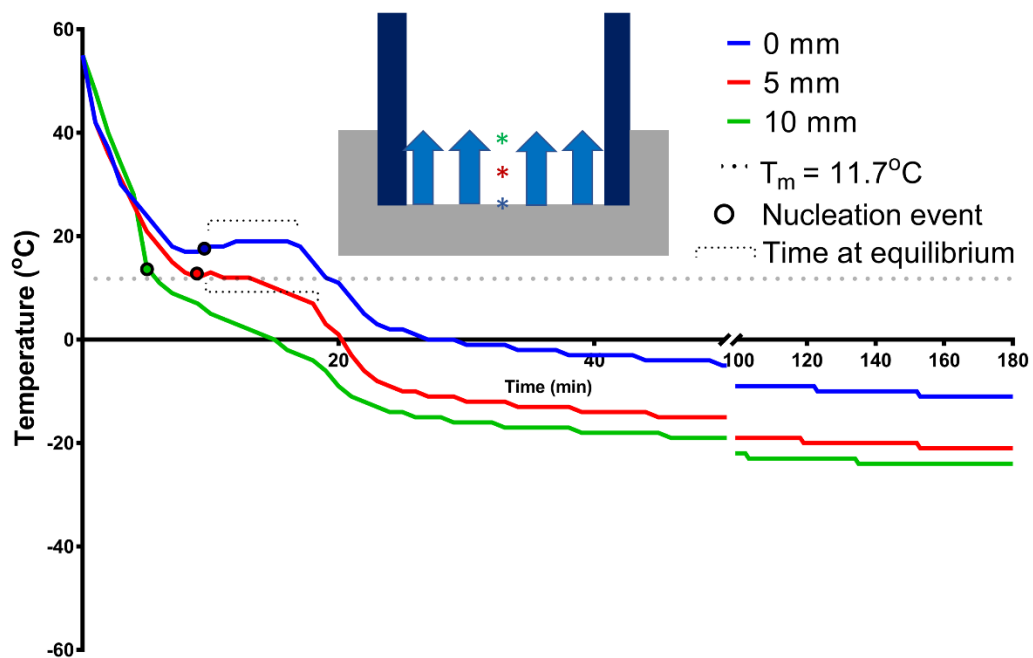


Figure 4.5: Thermal profile of the PGSU/1,4-dioxane solution during freezing using the mould-vertical.  $T_m$  = melting point of 1,4-dioxane. The schematic represents the mould and the freezing direction of the polymer solution (schematic is not scaled).

The thermal profile was recorded from the mould-horizontal and is shown in Figure 4.6. The bottom of the solution, at 0 mm, had its nucleation point 8 minutes after the start of the experiment, at 3°C, followed by the top part of the solution at 40 mm after 62 minutes, at 12°C. However, the nucleation point could not be identified for the midpoint, at 20 mm, but a linear negative gradient was observed until it reached its lowest temperature. Therefore, the solution froze first from the bottom and slowly moved upwards and, the nucleation events had 54 min difference between them. The time at equilibrium could only be identified for the 40 mm and it was equal to 34 min.

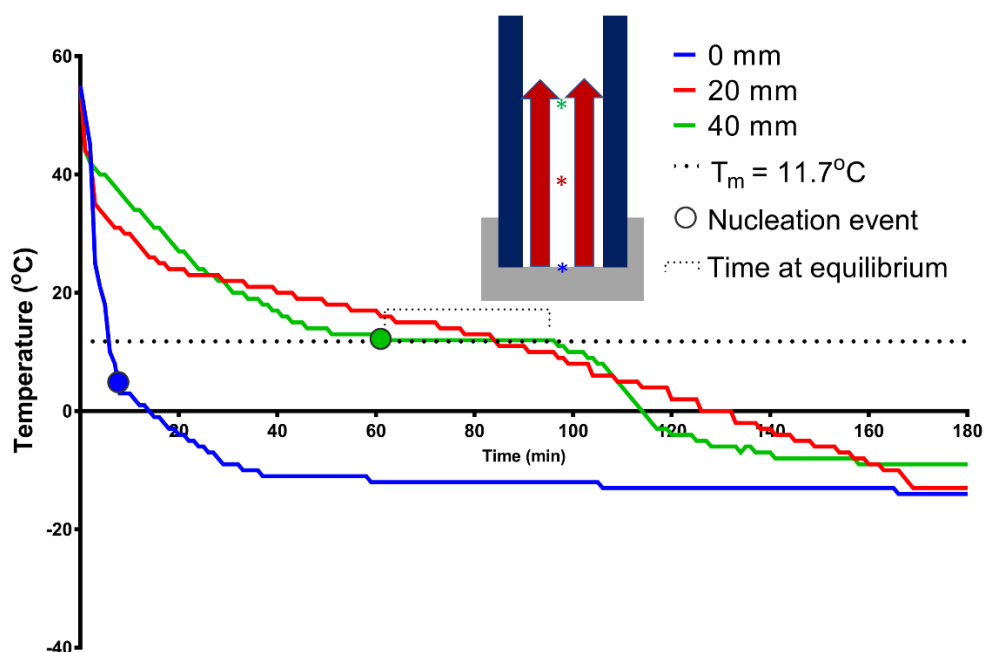


Figure 4.6: Thermal profile of the PGSU/1,4-dioxane solution during freezing using the mould-horizontal.  $T_m$  = melting point of 1,4-dioxane. The schematic represents the mould and the freezing direction of the polymer solution (schematic is not scaled).

### 4.3.2. Microstructure of PGSU scaffolds

SEM was used to visualise the microstructure of the PGSU scaffolds. Figure 4.7 show the images from the PGSU-random scaffold fabricated using mould-random. This scaffold was fabricated the same way as the scaffolds in Chapter 3. There was a difference in pore structure found between the top and bottom sections. The top section had a random pore structure, some pores are circular, and others are ovoid. Regarding the bottom section, circular pores were found but at a lower density compared to the rest of the scaffold. The cross section shows an ovoid shaped pore structure.

The pore size and permeability of this scaffold was calculated in Chapter 3 and is shown in Figure 3.6 and Figure 3.10 respectively. Briefly, the pore size of the scaffold ranged from 12  $\mu\text{m}$  to 28  $\mu\text{m}$  dependent on the depth of the scaffold. The water permeability of the scaffold was very high, and it was equal to  $3.8 \times 10^{-3} \text{ m}^2$ .

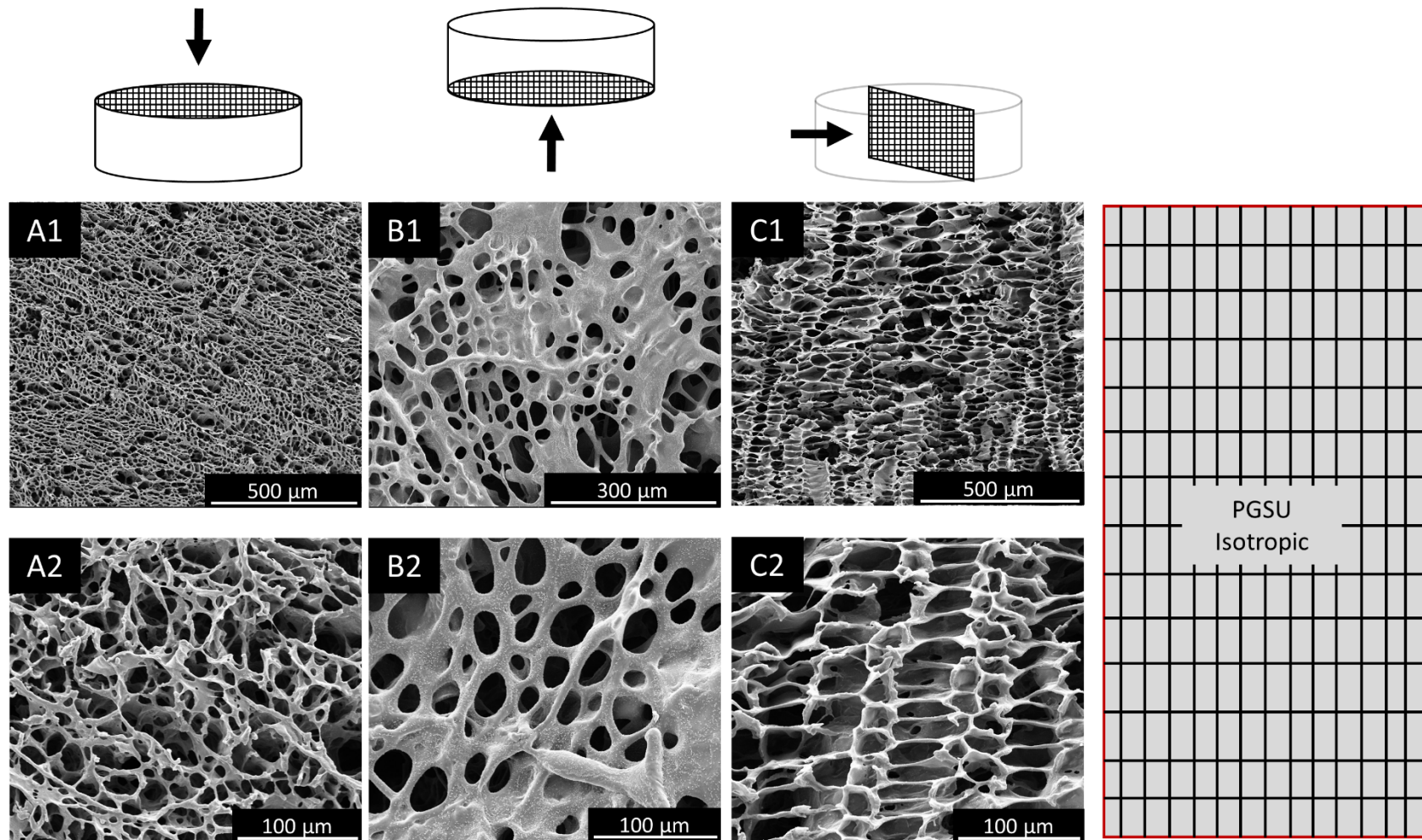


Figure 4.7: SEM images of the PGSU-random scaffolds. A1-2) Top section, B1-2) bottom section and C1-2) cross section. The schematic demonstrates the plywood structure of the scaffold.



Figure 4.8 shows the SEM images from the PGSU-vertical scaffolds fabricated using mould-vertical. As expected this scaffold had a unidirectional pore structure moving from the bottom to top (vertical) forming porous channels that interconnect to the top part of the scaffold.

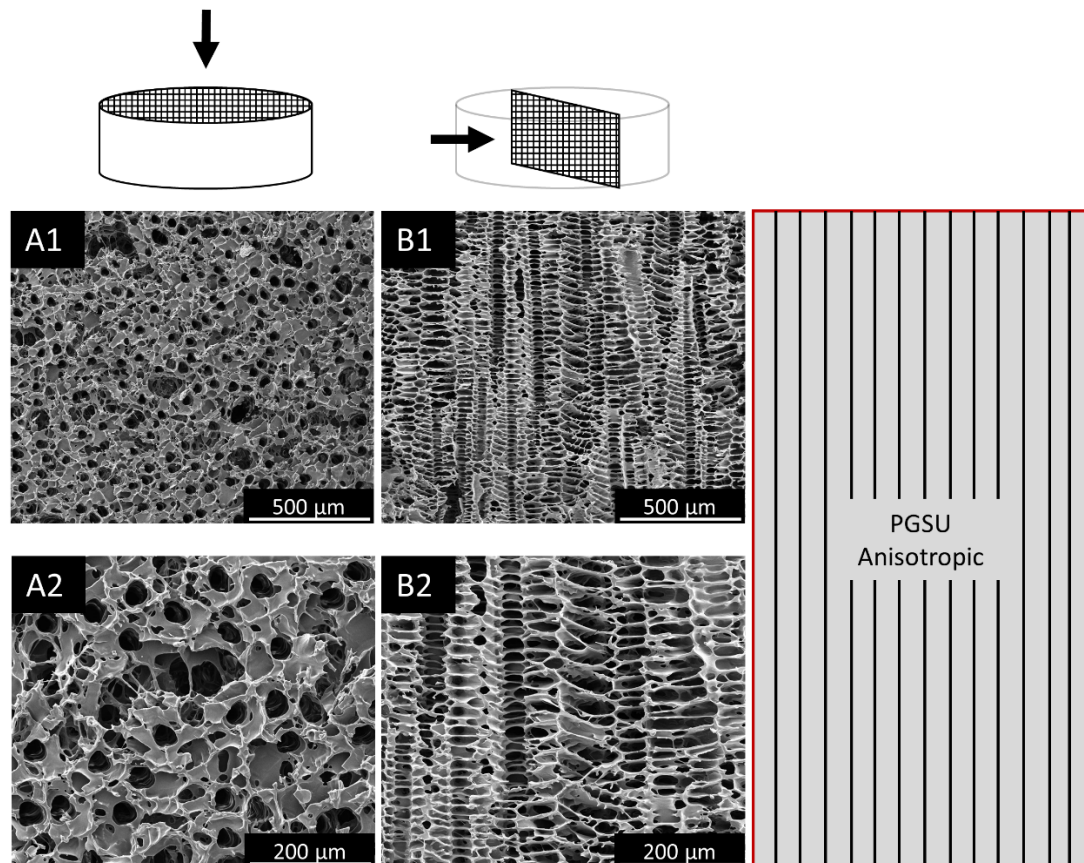


Figure 4.8: SEM images of PGSU-vertical. A1-2) Top section and B1-2) cross section. The schematic demonstrates the plywood structure of the scaffold.

The pore size of the PGSU-vertical, Figure 4.9, is significantly different between its cross section and top section with pore sizes of  $34.1 \pm 2.1$  and  $40.3 \pm 1.0$  μm respectively. The water permeability of the PGSU-vertical was measured parallel and perpendicular to the pore direction, as shown in Figure 4.10. High permeability was observed from both directions ( $4.2 \times 10^{-3}$  and  $3.7 \times 10^{-3}$  m<sup>2</sup>) and no significant difference was found between them.

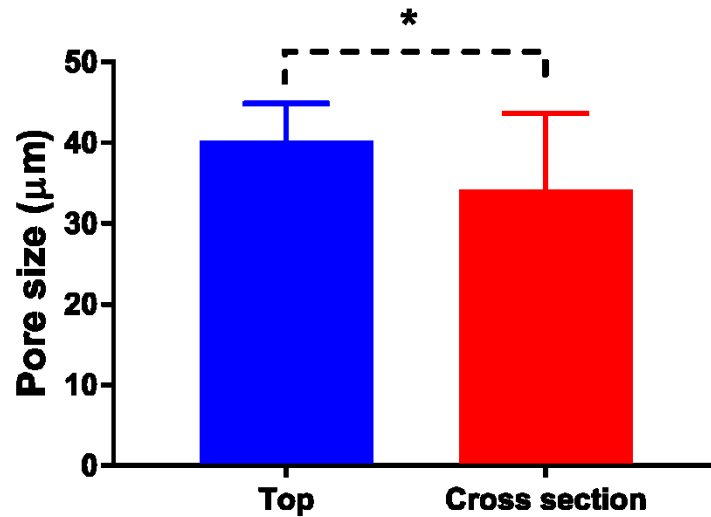


Figure 4.9: PGSU-vertical pore size measured from the top and cross section. Results are shown as mean  $\pm$  standard deviation,  $n=50$ , \* when  $p < 0.05$ .

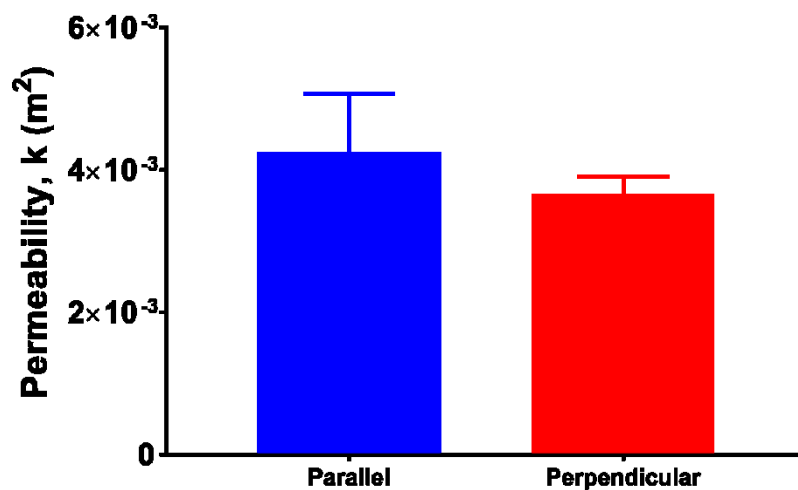


Figure 4.10: Water permeability of the PGSU-vertical. The anisotropic structure of the scaffold was examined by measuring the permeability parallel (longitudinal) and perpendicular to the pore direction. Results are shown as mean  $\pm$  standard deviation,  $n=3$ .

The SEM images of the PGSU-horizontal scaffold are shown in Figure 4.11. In this case the resulting scaffold had a rectangular parallelepiped shape and the pore direction was unidirectional from the left to right. A very uniform structure is observed

with porous channels formed along the horizontal axis. When it was examined for its cross section, open pores are found throughout the scaffold.

The uniformity of the pore structure is also demonstrated from the pore size measurements shown in Figure 4.12. The PGSU-horizontal scaffold had no significant difference in pore size between the top, cross and bottom sections and its pore sizes ranged from  $67.8 \pm 20.0$  to  $78.8 \pm 24.2$   $\mu\text{m}$ . Figure 4.13 shows the permeability of the PGSU-horizontal. It was found to have the highest water permeability from all scaffolds fabricated in this study ranging between  $8.7 \times 10^{-3} \text{ m}^2$  to  $1.1 \times 10^{-2} \text{ m}^2$ . Furthermore, there was significant difference ( $p < 0.001$ ) found when the permeability was measured parallel to the pore direction compared to perpendicular demonstrating the anisotropic structure of this scaffold.

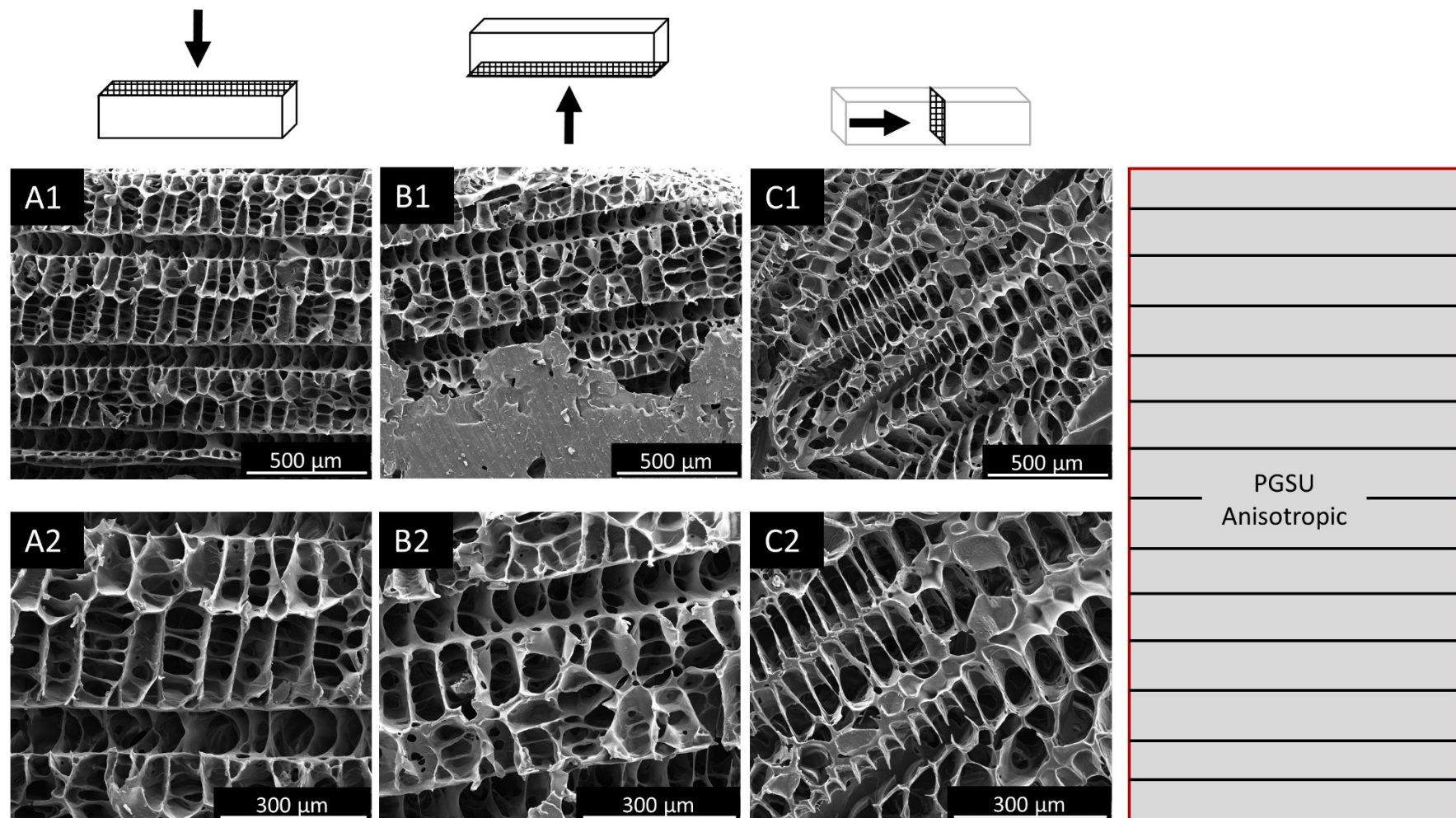


Figure 4.11: SEM images of PGSU-horizontal. A1-2) Top section, B1-2) bottom section and C1-2) cross section. The schematic demonstrates the plywood structure of the scaffold.

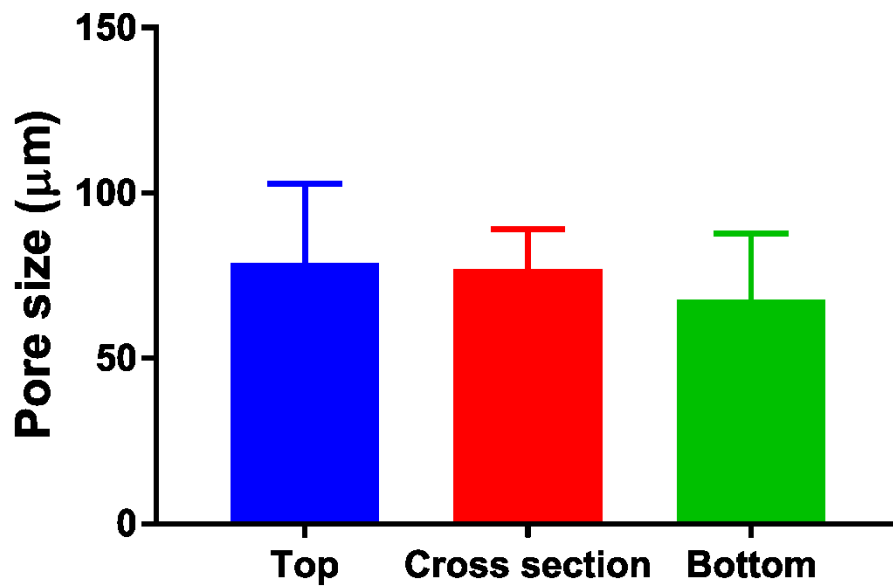


Figure 4.12: PGSU-horizontal pore size measured from the top, cross section and bottom of the scaffold. Results are shown as mean  $\pm$  standard deviation,  $n=50$ .

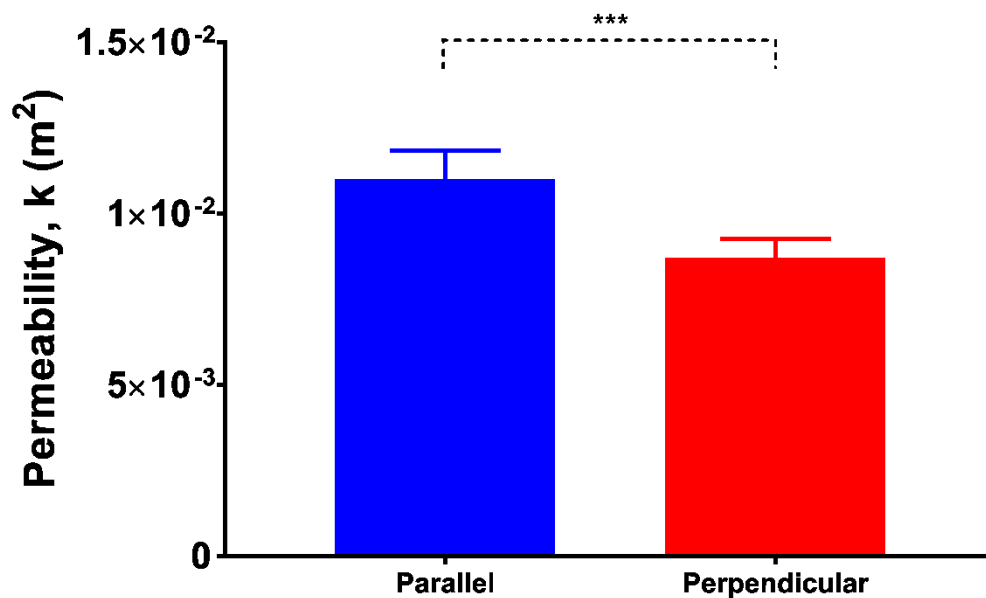


Figure 4.13: Water permeability of PGSU-horizontal. The anisotropic structure was examined by measuring the permeability parallel (longitudinal) and perpendicular to the pore direction. Results are shown as mean  $\pm$  standard deviation,  $n=3$ , \*\*\* when  $p < 0.001$ .

## Chapter 4

Below, Figure 4.14 the PGSU-bilayer is illustrated. In this case top layer was made from PGSU-15% and bottom layer from PGSU-10%, thus there is a difference in pore structure when looking from the cross section. It is clear where the layers meet and a good attachment between them is also evident. However, the pore structure was similar when imaging the scaffold from its top and bottom section.

Following the results from Chapter 3 it was expected the pore size to vary between sections and layers of the PGSU-bilayer. To examine this the pore sizes of the PGSU-bilayer were measured and plotted in Figure 4.15. Multiple pore sizes were found depending on the layer and the section. Considering each layer individually, there was significant difference found between the pore size of the top layer (PGSU-15%) when comparing its top and cross section. Similar observation was found from the bottom layer (PGSU-10%). Most importantly there was a significant difference found when comparing the pore size between the layers, especially in cross section. The pore size for the PGSU-15% layer was  $26.2 \pm 9.7 \mu\text{m}$  and the pore size for the PGSU-10% layer was  $74.0 \pm 4.9 \mu\text{m}$ , which is approximately a 3-fold difference. The water permeability was measured in the longitudinal direction and high permeability was found ( $1.1 \times 10^{-3} \text{ m}^2$ ), shown in Figure 4.16.

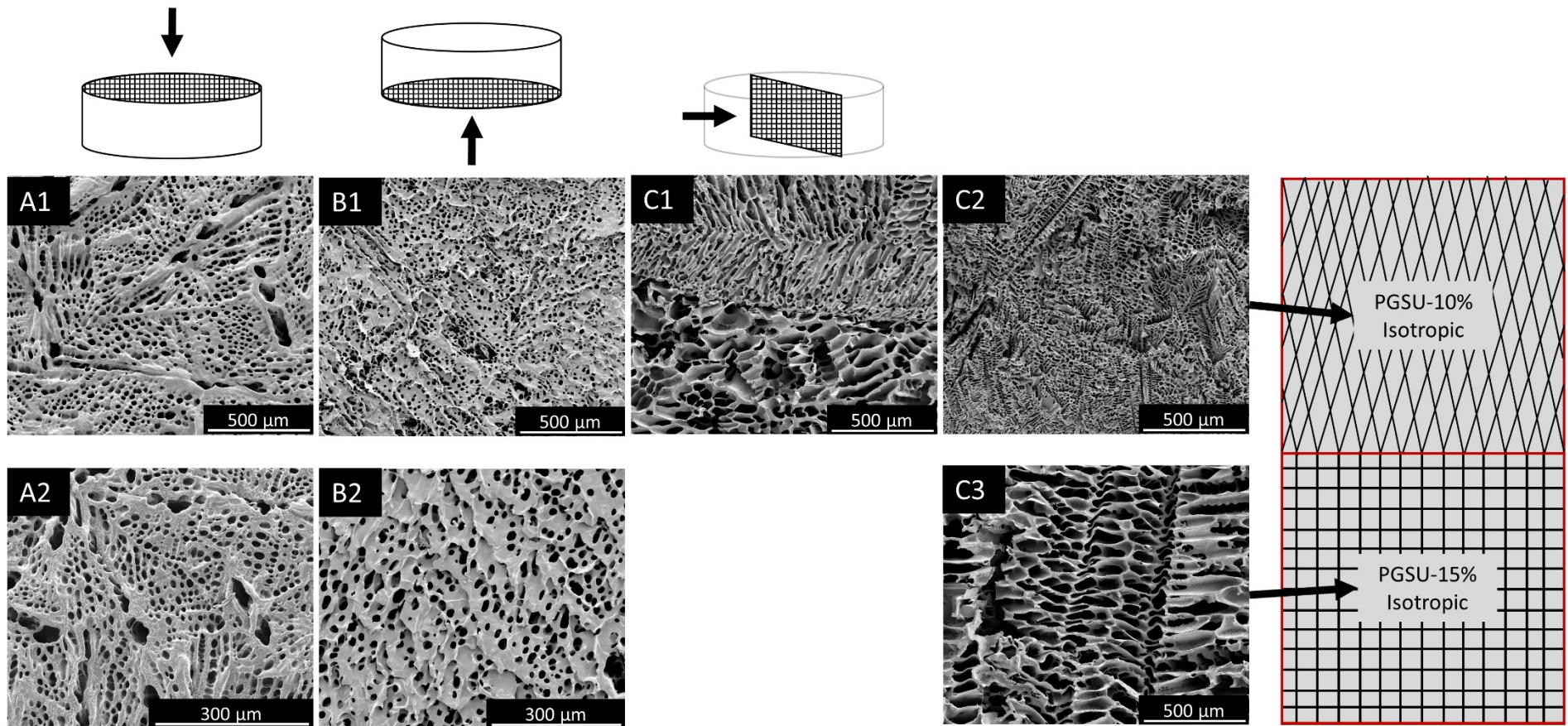


Figure 4.14: SEM images of PGSU-bilayer. A1-2) Top section, B1-2) bottom section and C1-3) cross section (C2 = PGSU-15% and C3 = PGSU-10%). The schematic demonstrates the plywood structure of the scaffold.

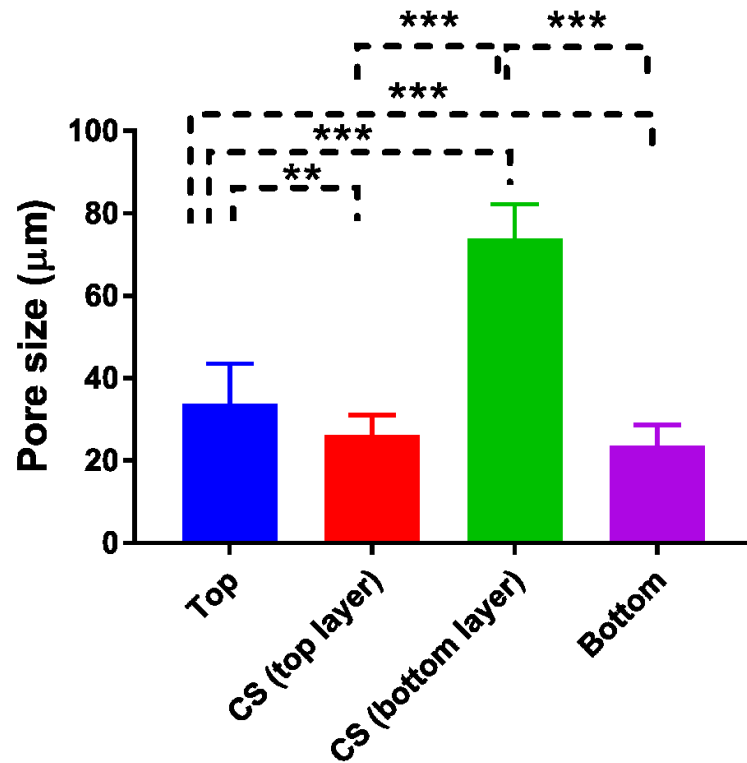


Figure 4.15: PGSU-bilayer pore size measured from the top, cross section (CS) and bottom. Since it is consisted of two layers the top and bottom layers of the scaffold were measured separately. Results are shown as mean  $\pm$  standard deviation, n=50, \*\*\* when  $p < 0.001$ .

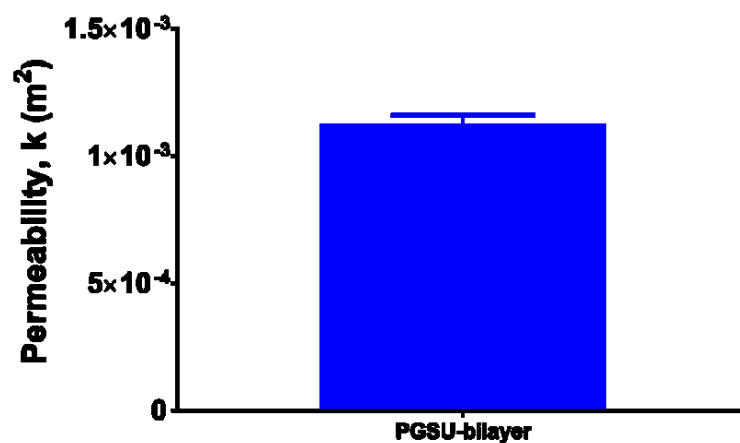


Figure 4.16: Water permeability of PGSU-bilayer measured longitudinal to the scaffold. Results are shown as mean  $\pm$  standard deviation, n=3.



To fabricate PGSU-BM the freeze drying technique was combined with airbrushing. To characterise the methods for airbrushing we used 2 different polymer solution volumes (1 and 2 ml) and either frozen the sample at  $-20\text{ }^{\circ}\text{C}$ , in liquid nitrogen or left it to air dry in room temperature. The results from these scaffolds are shown in Figure 4.17. The PGSU-BM that had 1 ml of polymer solution sprayed on it and then frozen at  $-20\text{ }^{\circ}\text{C}$  (Figure 4.17 (A1-2)) had a porous top layer, and the polymer solution was absorbed inside the scaffold filling some of the pre-existing pores making them less porous. For the same polymer solution but frozen in liquid nitrogen the polymer solution was not absorbed within the scaffold and a non-porous layer ( $61.2 \pm 19.0\text{ }\mu\text{m}$  thick) was formed (Figure 4.17 (B1-2)). Similar observations were seen for the PGSU-BM that had 1 ml of polymer solution sprayed on it and then left in room temperature to dry the solvent (Figure 4.17 (C1-2)), but it had a significantly lower thickness ( $36.0 \pm 14.7\text{ }\mu\text{m}$ ,  $p < 0.001$ ). When the polymer solution volume increased from 1 ml to 2 ml it was found that the polymer solution was absorbed deeper into the scaffold for the sample that was frozen in liquid nitrogen (Figure 4.17 (D1-2)) and in the case of air drying at room temperature a significantly thicker layer ( $202.2 \pm 103.7\text{ }\mu\text{m}$ ,  $p < 0.001$ ) was formed on top of the scaffold (Figure 4.17 (E1-2)). It was therefore decided to proceed with the PGSU-BM fabricated using 1 ml polymer solution and letting it air dry in room temperature because the thinnest BM was achieved compared to the other methods and simpler steps were involved in the fabrication procedure (no additional freezing and freeze drying), shown in Figure 4.17 (C1-2).

The selected PGSU-BM scaffold is shown in Figure 4.18, where a thin layer of low porosity was formed on the top section of a PGSU-5% scaffold to replicate a BM. The results show the formation of a thin BM found on the top section and a porous structure

from the bottom section. Additionally, it was important to ensure that the two layers were connected together, and it is demonstrated in Figure 4.18 (C1).

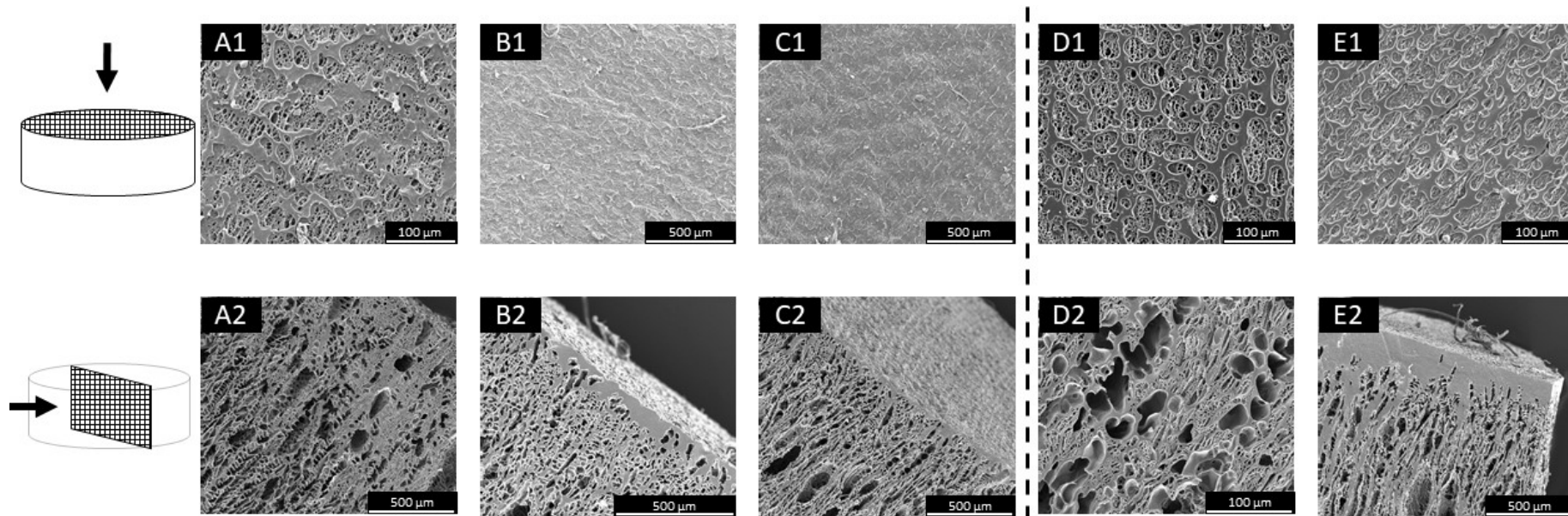


Figure 4.17: PGSU-BM fabricated with different airbrushing techniques. (A1-2) 1 ml of polymer solution was sprayed and frozen at  $-20\text{ }^{\circ}\text{C}$  before freeze drying (PGSU-BM(1)), (B1-2) 1 ml polymer solution was sprayed and frozen in liquid nitrogen before freeze drying (PGSU-BM(2)), (C1-2) 1 ml of polymer solution was sprayed and left in room temperature to dry (PGSU-BM(4)), (D1-2) 2 ml of polymer solution was sprayed and frozen in liquid nitrogen before freeze drying (PGSU-BM(3)) and (E1-2) 2 ml of polymer solution was sprayed and left in room temperature to dry (PGSU-BM(5)). The schematic demonstrates the plywood structure of the scaffold.

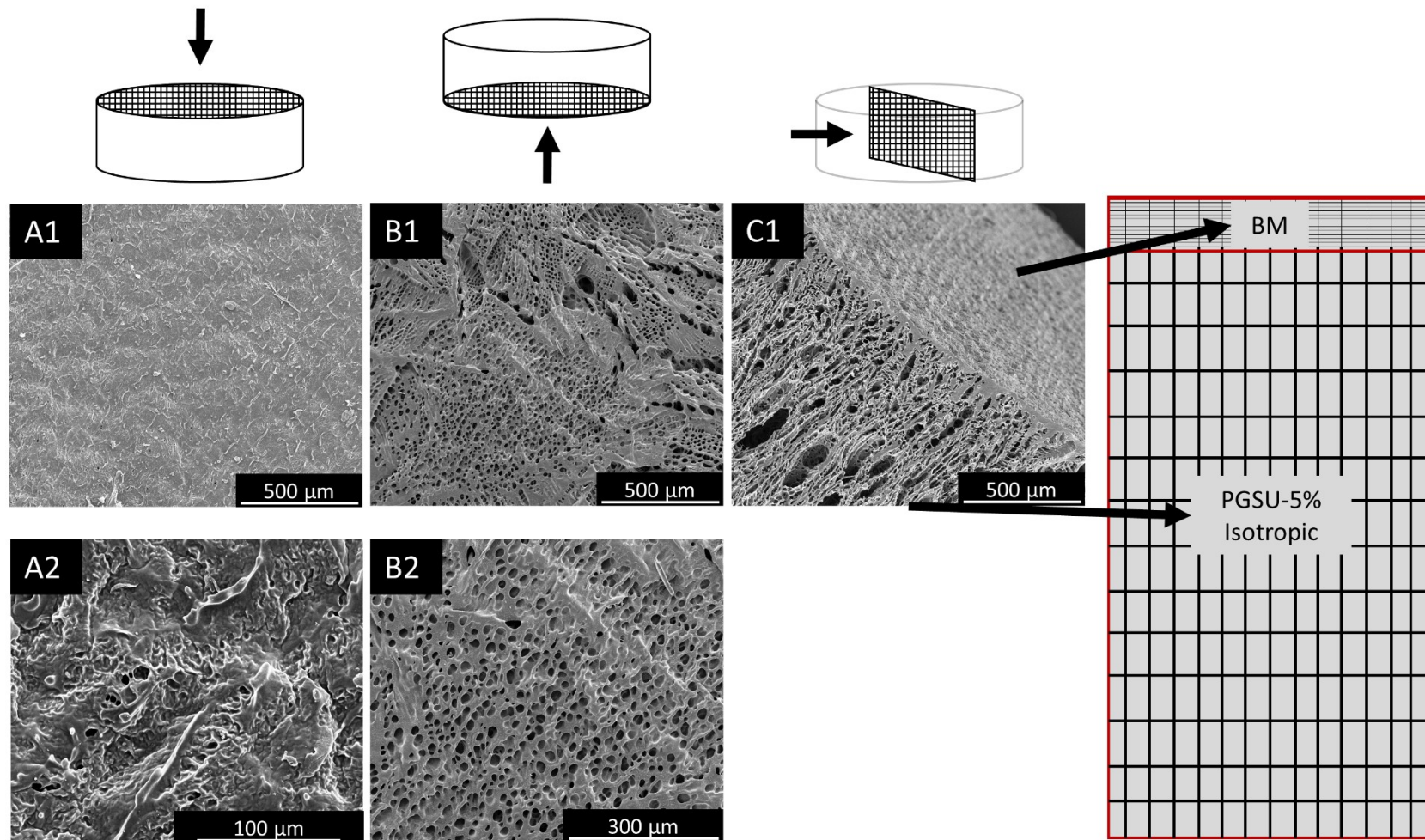


Figure 4.18: SEM images of PGSU-BM(4). A1-2) Top section, B1-2) Bottom section and C1) cross section. The schematic demonstrates the plywood structure of the scaffold.

## Chapter 4

The pore size of the PGSU-BM scaffold (Figure 4.19) is  $20.2 \pm 1.9 \mu\text{m}$  at its cross section and  $20.4 \pm 0.7 \mu\text{m}$  at its bottom section and there was no significant difference between them. Even though a low porosity film was fabricated on top of the scaffold the permeability of the scaffold (Figure 4.20) was still very high ( $5.6 \times 10^{-3} \text{ m}^2$ ) showing that water can still pass through the dense layer which is extremely important in tissue development because it allows for gas and nutrient exchange.

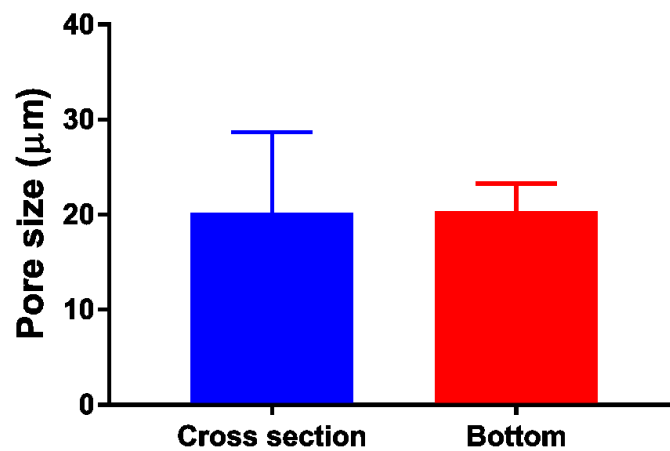


Figure 4.19: PGSU-BM pore size was measured from the cross section and bottom of the scaffold. Results are shown as mean  $\pm$  standard deviation,  $n=50$ .

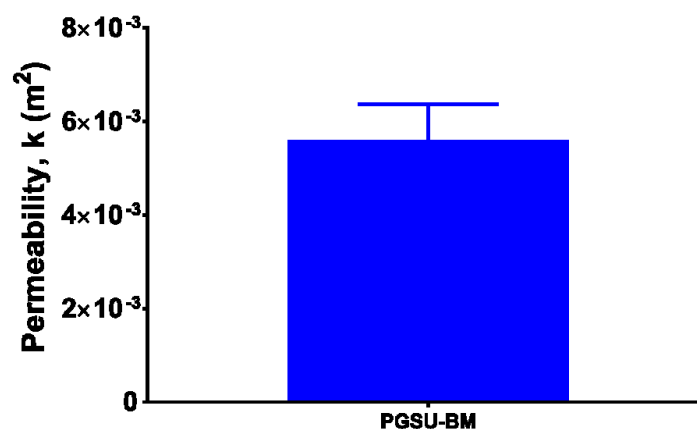


Figure 4.20: Water permeability of the PGSU-BM measured longitudinal to the scaffold. Results are shown as mean  $\pm$  standard deviation,  $n=3$ .

## Chapter 4

The last scaffold that was fabricated was PGSU-trilayer and the results are shown in Figure 4.21. In this case the top layer acts as a BM with low porosity, and at the same time the bottom section has an open pore structure. The connection of all three layers is also shown, which confirms that one solid scaffold can be fabricated from three different layers that can be distinguished by their difference in pore structure and porosities.

As expected the pore size was significantly different between the layers of the scaffold (Figure 4.22), with the top layer demonstrating a pore size of  $20.3 \pm 5.0 \mu\text{m}$  and the bottom layer demonstrating a pore size of  $49.2 \pm 10.8 \mu\text{m}$ . This demonstrates that by changing the polymer concentration different pore sizes can be achieved, as in Chapter 3, and that by stacking these scaffolds on top of each other, the same scaffold can exhibit multiple pore sizes. The water permeability of the PGSU-trilayer (Figure 4.23) was the lowest from all the scaffolds of this study,  $7.3 \times 10^{-4} \text{ m}^2$ , which can be explained by the dense PGSU-15% layer of the scaffold in addition with the BM ( $99.2 \pm 34.2 \mu\text{m}$  thickness) on top of the scaffold, which is significantly thicker ( $p < 0.001$ ) than the BM ( $36.0 \pm 14.7 \mu\text{m}$  thickness) for the PGSU-BM scaffold.

Finally, in Table 4.3, a summary of the scaffolds fabricated in this chapter are shown. Multiple pore structures, pore orientations, pore sizes and permeabilities were obtained using PGSU, freeze drying, moulding technology and airbrushing.

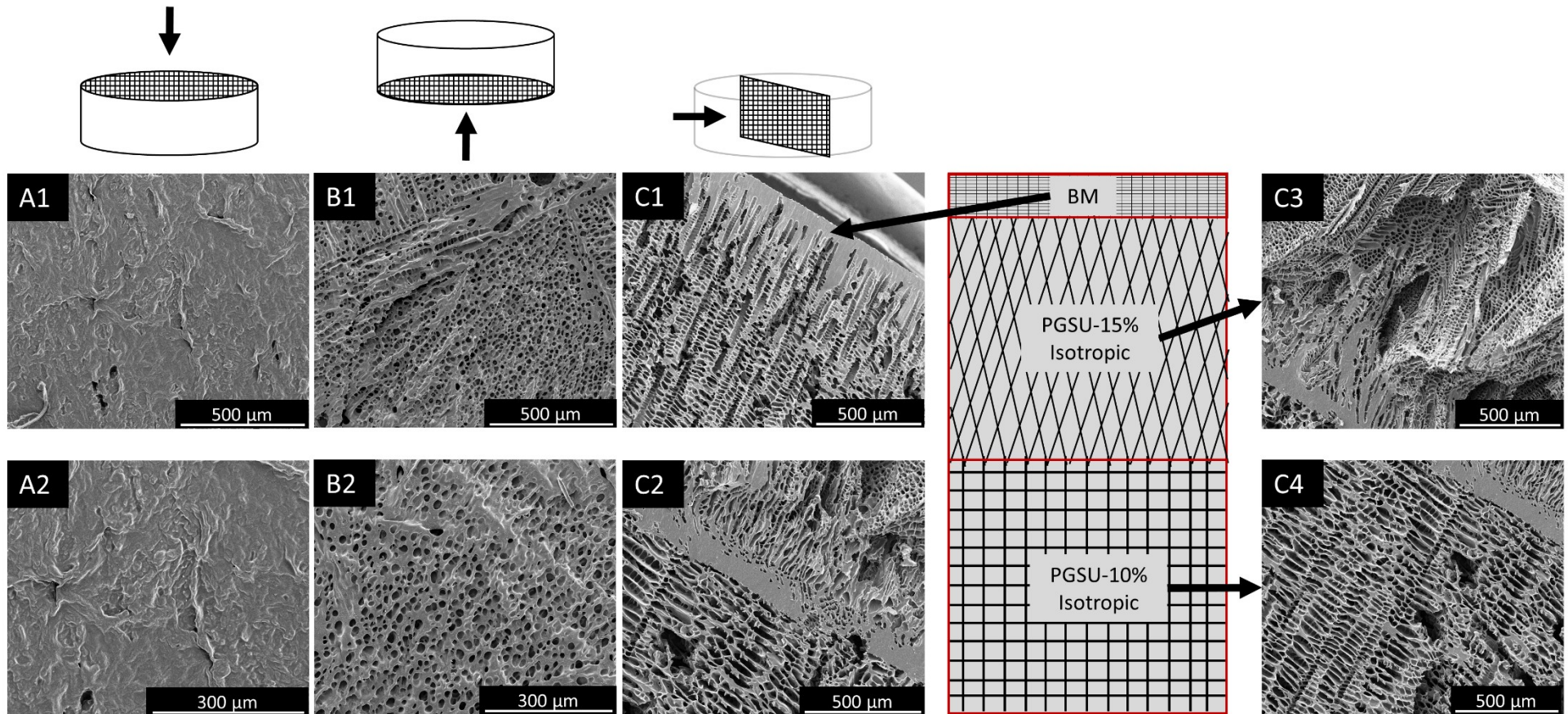


Figure 4.21: SEM images of PGSU-trilayer. A1-2) Top section, B1-2) Bottom section and C1-4) cross section. (C3 = PGSU-15% and C4 = PGSU-10%). The schematic demonstrates the plywood structure of the scaffold.

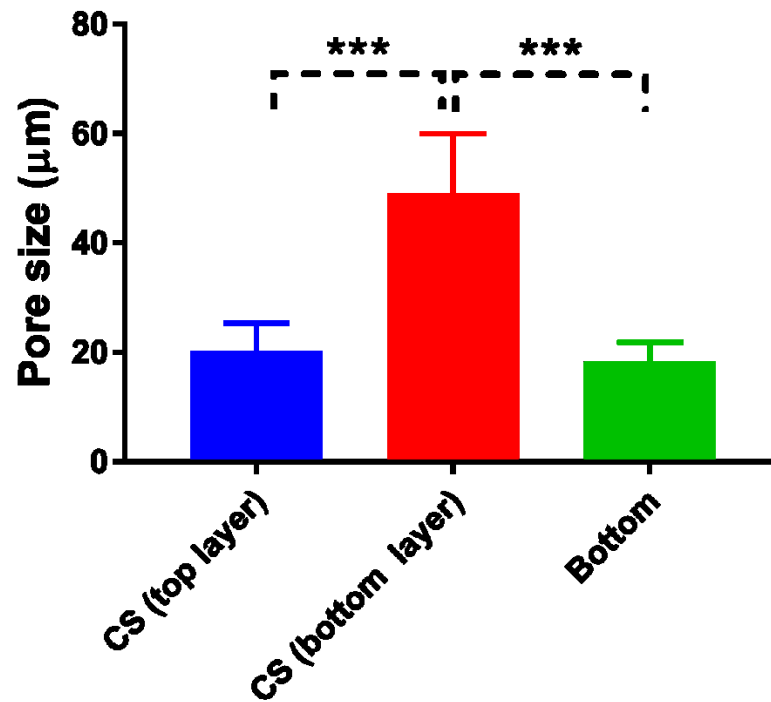


Figure 4.22: PGSU-trilayer pore size was measured from the cross section (CS) and bottom. Since the scaffold is consisted of three layers and the first layer is low porosity, the other two layers were measured and plotted separately. CS = cross section. Results are shown as mean  $\pm$  standard deviation,  $n=50$ , \*\*\* when  $p < 0.001$ .

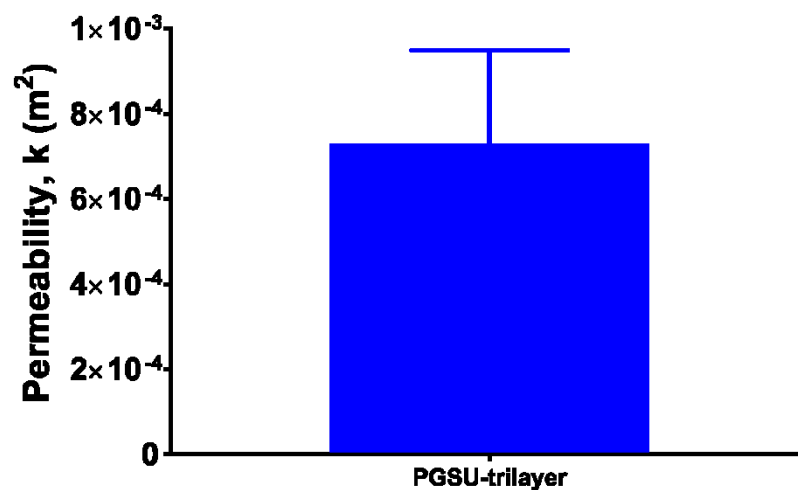


Figure 4.23: Water permeability of the PGSU-trilayer measured longitudinal to the scaffold. Results are shown as mean  $\pm$  standard deviation,  $n=3$ .



Table 4.3: Summary of the different moulds and scaffolds demonstrated in this chapter.

Moulds	Thermal profile	Pore structure	Scaffold	Range of pore size (µm)		Permeability
Mould-random	From the bottom and top to the inside	Isotropic	PGSU-random	12.3 – 28.2		<p>Figure 4.24: Water permeability of all PGSU scaffolds fabricated for this chapter. Statistical significance was found in all multiple comparison cases, except PGSU-trilayer vs PGSU-bilayer. Results are shown as mean ± standard deviation, n=3, *** when p&lt;0.001.</p>
			PGSU-bilayer	<u>Top layer</u>	<u>Bottom layer</u>	
				26.2 ± 9.7	74.0 ± 4.9	
			PGSU-BM	20.2 – 20.4		
			PGSU-trilayer	<u>Mid layer</u>	<u>Bottom layer</u>	
				20.3 ± 5.0	49.2 ± 10.8	
Mould-vertical	From the bottom to the top	Anisotropic	PGSU-vertical	34.1 – 40.3		
Mould-horizontal	From the bottom to the top	Anisotropic	PGSU-horizontal	67.8 – 78.8		

### **4.3.3. Oral mucosa *in vitro* cell culture**

For OMTE, the PGSU-BM scaffold was chosen, shown in Figure 4.18, as it had the thinnest low porosity layer that was expected to act as basement membrane to keep the keratinocytes from penetrating the inner porous structure of the scaffold (the area where fibroblasts are expected to reside). The aim of this part of the work was to demonstrate our ability to produce a scaffold with biomimetic microstructure that had a second layer which functions as a cell barrier but allows cell communication and gas/nutrient exchange. We approached this study systematically and it began with studying the ability of oral keratinocytes to adhere on the scaffold and to be metabolically active.

#### **4.3.3.1. OKF6 cell attachment on PGSU-film**

PGSU-films were seeded with OKF6 cells ( $1.0 \times 10^6$  cells) to characterise the ability of the cells to adhere on the surface of the film. Cells cultured on TCP were considered as the positive control. Resazurin assay over 9 days showed a significant increase in metabolic activity between days 3 – 9 and days 6 – 9 indicating that the OKF6 cells adhered on the PGSU films and were metabolically active (Figure 4.25 (A)). When normalised against the positive control a significant decrease in metabolic activity was found between days 3 and 6, which then a significant increase was observed reaching approximately ~20% of the TCP, Figure 4.25 (B). The samples were also imaged after every resazurin assay, shown in Figure 4.26, to quantify the staining progression on the PGSU-films. It was observed that the staining intensity increased between days which indicates higher cell activity by the OKF6.

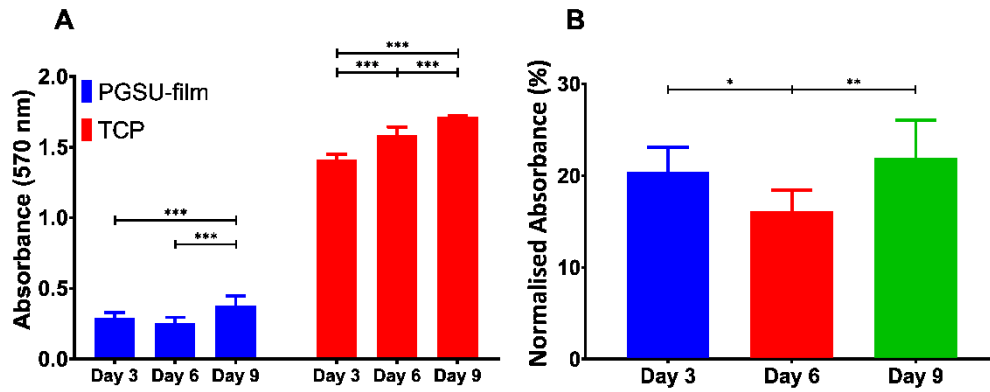


Figure 4.25: PGSU films seeded with OKF6. (A) The absorbance obtained from OKF6 cultured on PGSU films and TCP which served as the positive control; (B) Normalised absorbance against the positive control (TCP) of the resazurin assay for all 9 days, Results are shown as mean  $\pm$  standard deviation, n=3 in triplicates, \*\*\* when  $p < 0.001$ .

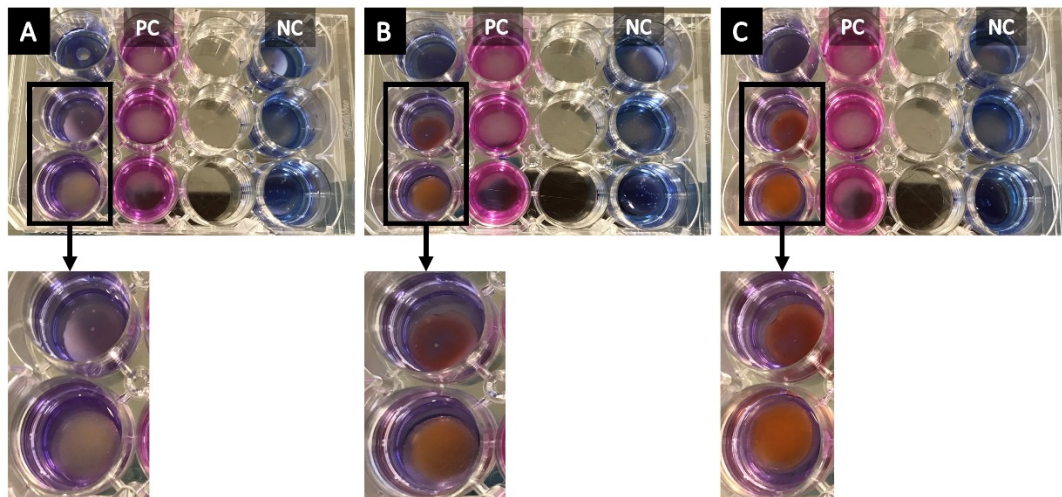


Figure 4.26: Images taken from the samples after resazurin assay at each time point. A) day 3, B) day 6 and C) day 9. PC = positive control, cells cultured on TCP; NC = negative control, acellular films.

The samples were also stained with live/dead to determine the ratio between live and dead cells. The samples were visualised using a brightfield microscope and a fluorescence microscope. Looking at the positive control (cells cultured on TCP), Figure 4.27 (A1-2), most of the cells were alive at a high confluency with a very small number of dead cells. In the case of PGSU-film, the cells were visible when brightfield was used, see (B1), but the live/dead resulted in a higher level of background staining

on the PGSU material and it was not possible to visualise the cells under the fluorescence microscope. To confirm that this was an issue from the PGSU-film material and cells were not dead, we performed the same assay on acellular PGSU-films in which case it should not have any dye attached to it, but it can be seen in (C2) that the sample is again completely covered with the red dye. Furthermore, the autofluorescence of the PGSU-film was examined and compared with the autofluorescence of TCP, shown in Figure 4.27 (D1-2 and E1-2). A slight autofluorescence is observed from the PGSU-film, however not as evident as the acellular PGSU-film shown in Figure 4.27 (C2).

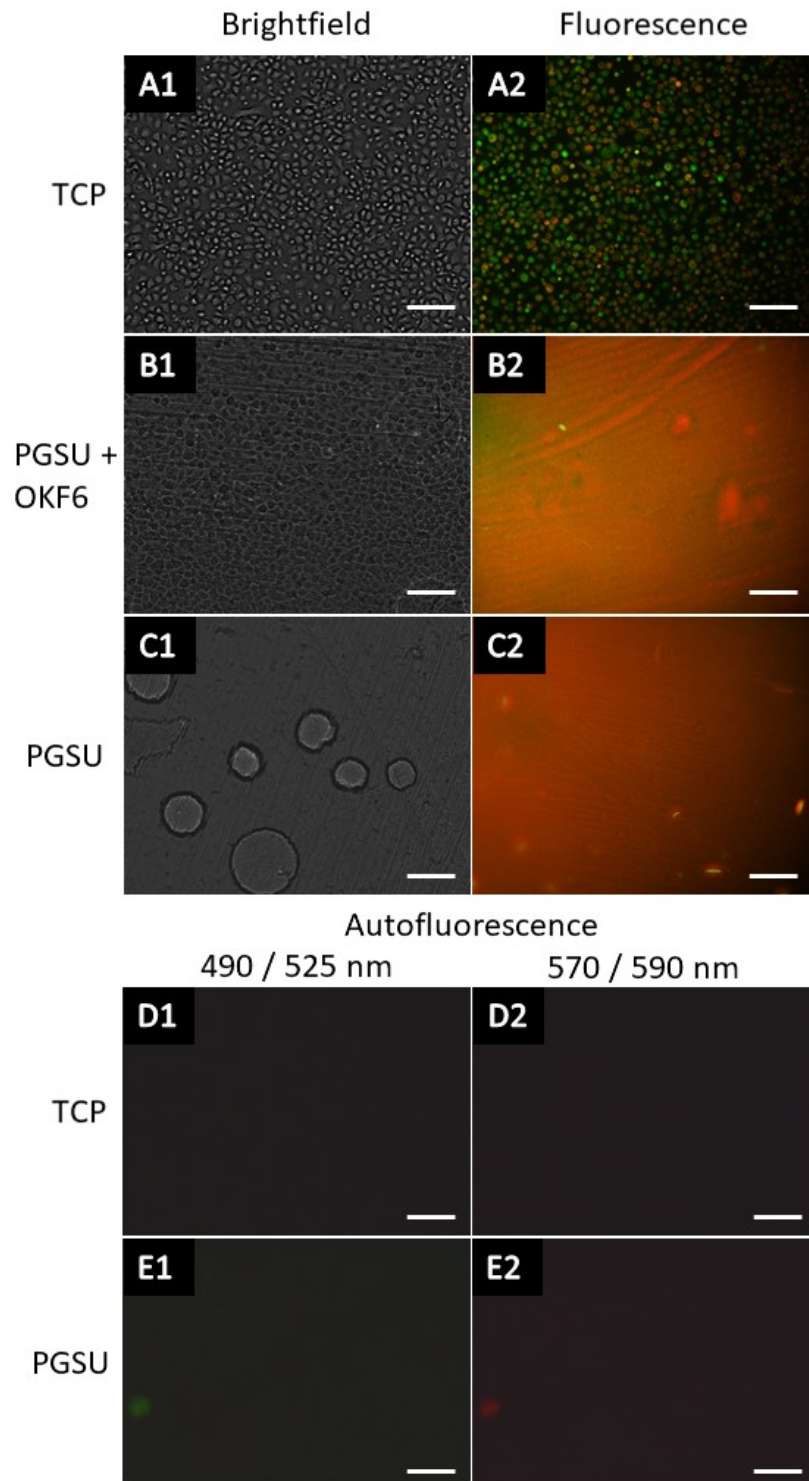


Figure 4.27: OKF6 cells cultured on PGSU-film for 9 days and stained with live/dead assay. A1-2) TCP, B1-2) PGSU-film, C1-2) NC, D1-2) autofluorescence of TCP and E1-2) autofluorescence of PGSU with the corresponding excitation/emission wavelengths. The scale bars are 200  $\mu$ m.

#### 4.3.3.2. NOK attachment on PGSU-films

Similar behaviour to the OKF6 was noticed for the NOK cell attachment study. It was found that the NOKs were metabolically active on the PGSU-films and a significant increase was found between days 3 – 9 and days 6 – 9, Figure 4.28 (A). When the results were normalised against the positive control, again a significant increase was found between day 3 – 9 and days 6 - 9 however the activity was not as high as the TCP control, reaching slightly over ~22% at day 9 (Figure 4.28 (B)).

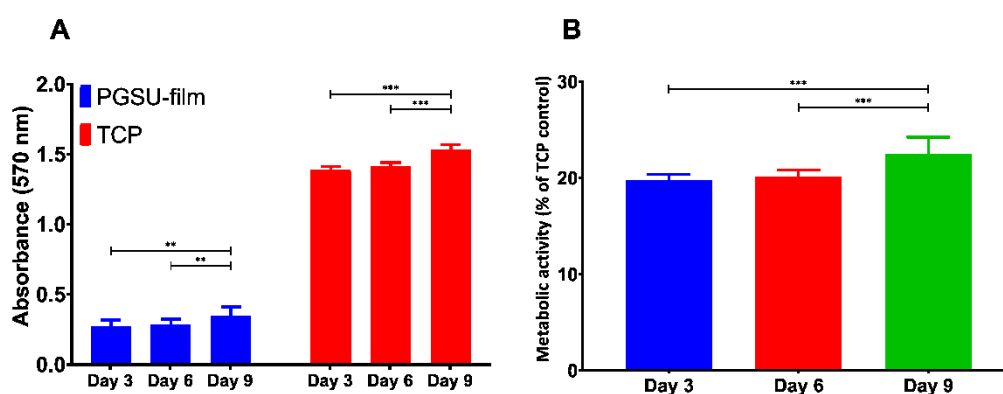


Figure 4.28: PGSU films seeded with NOK cells. (A) The absorbance obtained from NOK cultured on PGSU films and TCP which served as the positive control; (B) Normalised absorbance against the positive control (TCP) of the resazurin assay for all 9 days, Results are shown as mean  $\pm$  standard deviation,  $n=3$  in triplicates, \*\*\* when  $p < 0.001$ .

#### 4.3.3.3. Dynamic seeding

An issue we had when passively seeding the PGSU-scaffolds was that the cells were not penetrating the internal area of the sample, see Figure 3.14. This is thought to be due to the hydrophobicity (water contact angle =  $106.7 \pm 4.5^\circ$  for the PGSU-2.5% scaffold, shown in Figure 2.21) of the PGSU and the lack of stimuli encouraging cell penetration. Therefore, dynamic seeding was used which was a method through which cells could be pushed inside the scaffold. Comparing the histological images from Figure 4.29, it can be seen that a lower number of cells were found in the PGSU

scaffolds that were passively seeded (Figure 4.29 (A1, 2)) compared to the dynamically seeded (Figure 4.29 (B1, 2)). Additionally, a better cell distribution was observed with cells distributed all over the internal structure of the PGSU-5% scaffold.

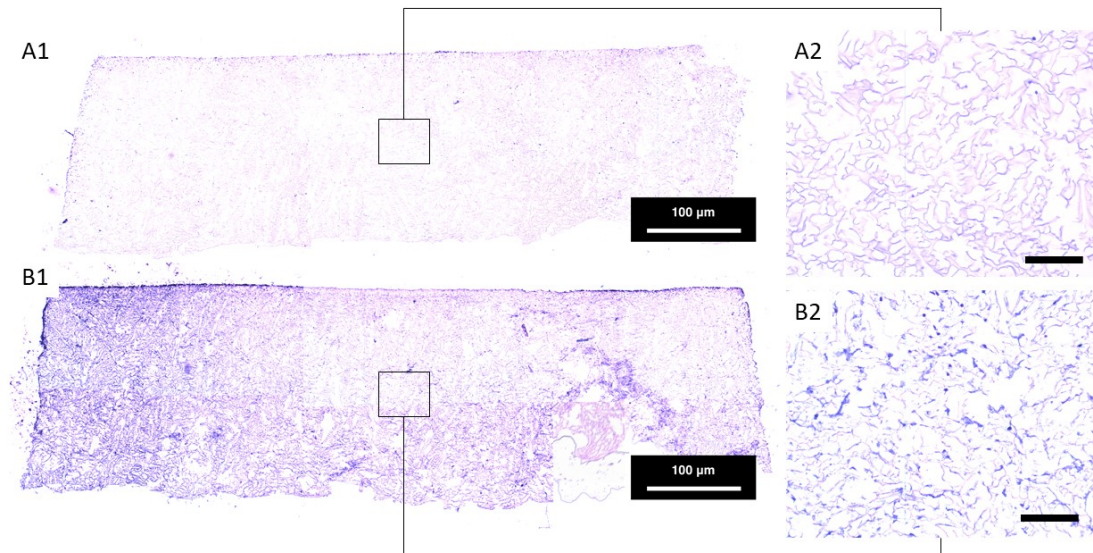


Figure 4.29: Histology (H&E) of PGSU-10% scaffolds seeded with L929 fibroblasts using (A1 and A2) Static (B1 and B2) Vacuum seeding. Scale bar is 50 µm. n=3.

Sirius red was also used to investigate the effect that the cell seeding method had on the collagen production, Figure 4.30. No significant difference was found between them, concluding to that the cell seeding efficiency and distribution did not affect the collagen production.

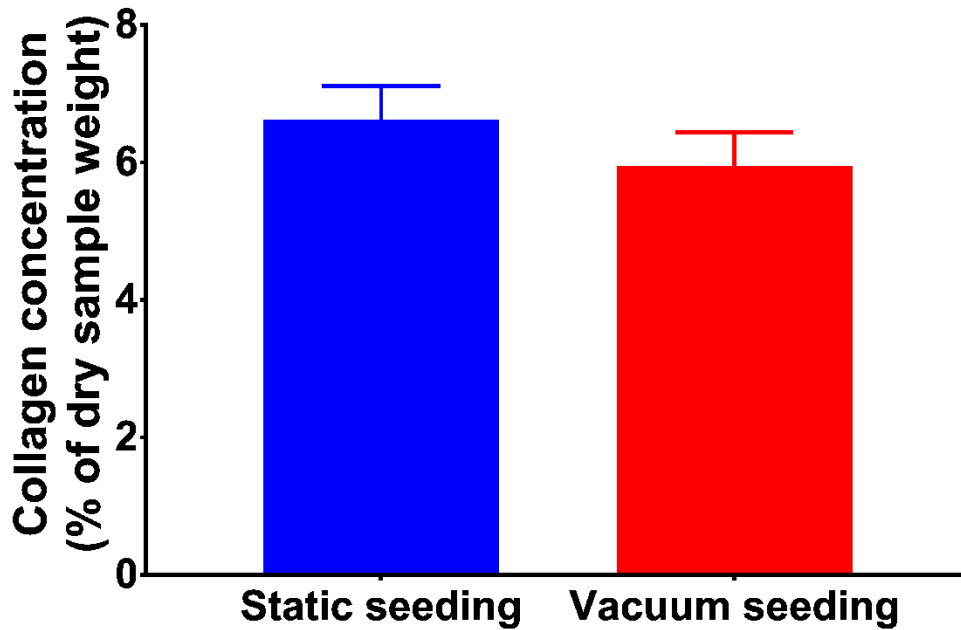


Figure 4.30: Collagen produced on the scaffolds measured using Sirius red and standardised using the standard curve in chapter 3. The results are demonstrated as a percentage of collagen mass per dry sample's mass. Results are shown as mean  $\pm$  standard deviation, n=3.

#### 4.3.3.4. Human oral cells co-culture

With the results described above, it was confirmed that oral keratinocytes can adhere on the PGSU-film and dynamic seeding leads to better cell seeding efficiency and distribution. Therefore, the final experiment performed for this study was to seed human oral cells in co-culture on PGSU-BM scaffolds for 15 days. Sirius red was used to quantify collagen production and immunohistochemistry was used to stain the cytokeratin which are keratin proteins found inside the intracytoplasmic cytoskeleton of epithelial cells.

Figure 4.31, shows the collagen produced within the scaffolds during the 15 days culture compared to PGSU-5% (from Chapter 3) and DED (which is predominantly made from collagen). As expected the DED ( $54.4 \pm 6.5$  %) resulted to a significantly higher collagen concentration compared to both PGSU-BM ( $15.7 \pm 0.6$  %) and PGSU-



5% ( $7.5 \pm 2.6$  %), however no significant difference was found between the PGSU-BM and PGSU-5% scaffolds.

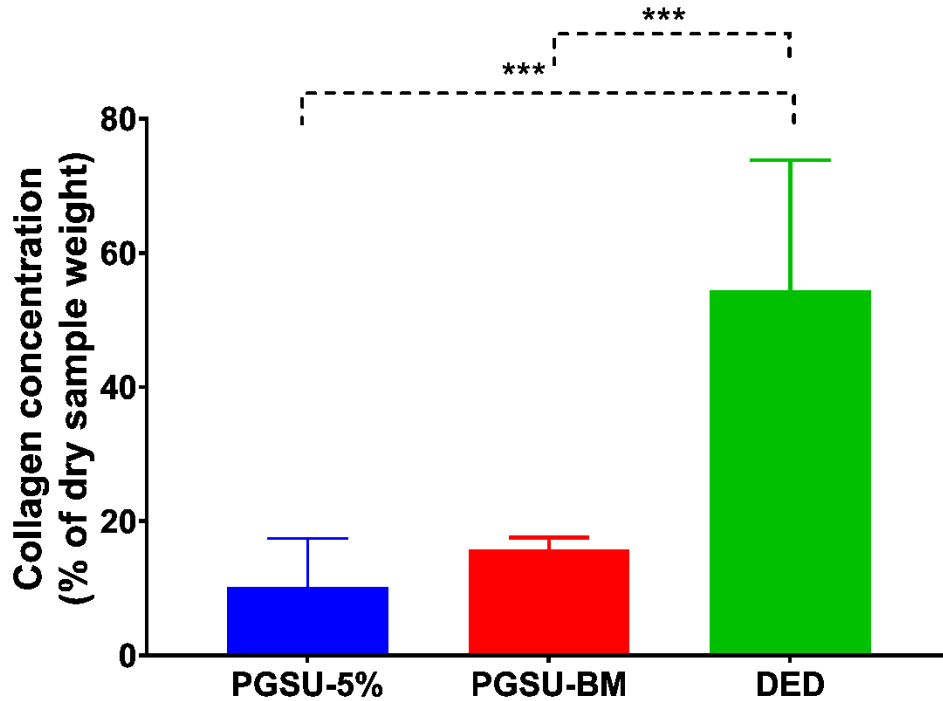


Figure 4.31: Collagen produced on the scaffolds measured using Sirius red and standardised using the standard curve in Chapter 3. The results are demonstrated as percentage of collagen mass against the scaffolds dry mass. PGSU-5% is from Chapter 3 and is there for comparison reasons. Results are shown as mean  $\pm$  standard deviation,  $n=3$ , \*\*\* when  $p < 0.001$ .

Figure 4.32 (A1-2), show the H&E stained samples with multiple layers of cells found on the BM of the scaffold and a good distribution of cells dispersed in the porous part of scaffold. When the cytokeratin antibody was used (AE1/3) it showed that the NOK cells migrated and proliferated laterally over the BM surface with limited cytokeratin found within the porous part of the scaffold suggesting NOK cells could not infiltrate.

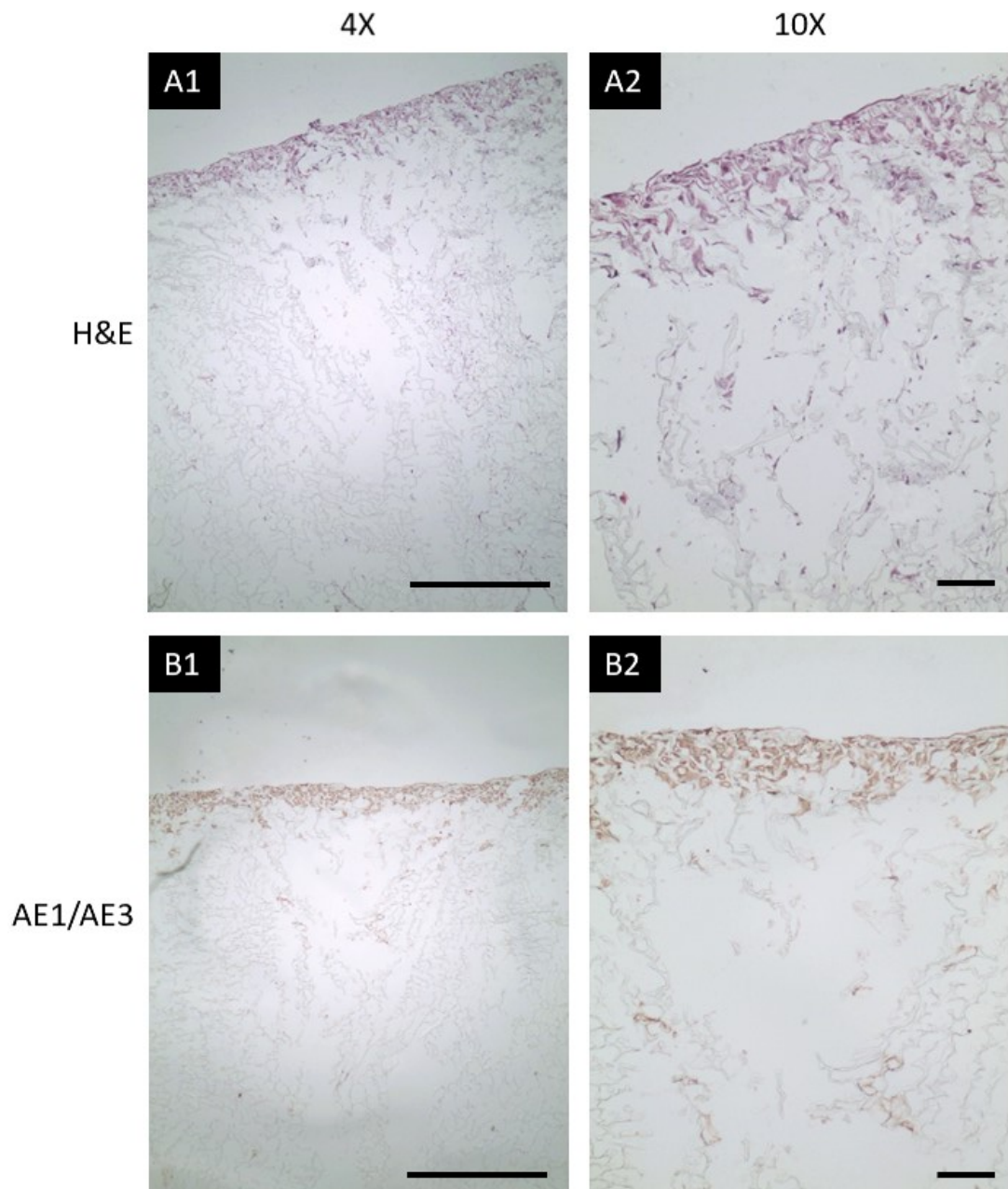


Figure 4.32: Representative sections from PGSU-BM samples after cell co-culture with NTF and NOK. A1-2) are PGSU-BM stained with H&E, B1-2) immunohistochemically stained PGSU-BM with AE1/AE3. n=3. Scale bar is 100  $\mu\text{m}$ .

#### 4.4. Discussion

The aim of this chapter was to identify tissues with different microstructures and to fabricate PGSU scaffolds using ice templating, airbrushing and mould technology techniques. Through a thorough literature review we identified four tissues with

special ECM microstructures (isotropic, anisotropic and multilayer) and we utilised the techniques mentioned above to mimic their native architecture. Since the main objective of this thesis was to fabricate PGSU scaffolds for OMTE, we concluded this chapter with results demonstrating the development of PGSU scaffolds for OMTE with a structured scaffold which could support cell co-culture while providing an environment that promotes tissue generation.

The objective of ice templating (also known as modified thermal induced phase separation (mTIPS)) is to control the microstructure of the scaffold by controlling the ice crystal formation. Ice templating is not a new technology, and there are numerous studies that used it to fabricate anisotropic scaffolds for a range of applications, including cartilage, skeletal muscle, tendons and neurons [211, 218, 219]. To characterise the ice templating and mould technology we investigated the thermal profiles of the in-house moulds. These moulds were carefully designed to allow heat to enter the polymer solution in an isotropic or anisotropic manner dependent on the end product. These different moulds enabled (i) the polymer solution to freeze uniformly, with heat distributed evenly from multiple directions within the polymer solution to create a uniform isotropic (random) structure; and (ii) the polymer solution to freeze from only one direction, with heat distributed evenly but from one direction to create a uniform anisotropic (oriented) structure. Most of the ice templating methods used in previous studies involved a glass tube where it is lowered into liquid nitrogen at a control rate which results in unidirectional freezing [211, 218]. This methodology results in good anisotropic structures however it requires more steps and more equipment, such as a moving platform for lowering the glass tube inside the liquid nitrogen bath. Additionally, the temperature of the bath cannot be controlled unless a cooling bath is used. In our case, we only required the freeze drier to freeze and control

the temperature; and in combination with the mould we directed the heat transfer in a uniform anisotropic or isotropic direction. For example, the polymer solution in mould-random froze at its bottom and top with only 2 min difference meaning that ice crystals were growing upwards and downwards almost simultaneously and within 5 minutes the middle area of the solution was completely frozen. This isotropic heat transfer then converts to a uniform isotropic scaffold (Figure 4.7). However, when the walls of the mould were isolated using PTFE (low thermal conductivity) the polymer solution froze from the bottom to top, resulting in an anisotropic heat transfer therefore anisotropic scaffold microstructure (Figure 4.9 and Figure 4.12). The terms isotropic and anisotropic do not only refer to structural properties. The isotropic structure means that the scaffold exhibits the same properties (structural, mechanical, permeability properties etc.) when viewed from any direction, while anisotropic distributes the structural, mechanical and permeability properties to a specific direction (longitudinal to the pore alignment). In this study the mechanical properties of the anisotropic scaffolds were not characterised due to time limit, however we visualised their anisotropic structure using SEM and demonstrated their anisotropic behaviour by characterising their water permeability. Visually, the scaffolds exhibited the structure we expected, and reflected the results from the heat transfer results.

Regarding the water permeability, we found significant difference when the scaffold was tested longitudinal to the pore alignment as opposed to transversely. This means that the permeability properties are anisotropic and that the gas/nutrient exchange is enhanced in the more permeable direction, which could direct the tissue development in the more permeable direction. We observed very high permeability for all the scaffolds. We found that all the scaffolds that were fabricated in this study were at least an order of magnitude higher than scaffolds that were successfully used

in tissue engineering [183]. We believe this is due to the highly porous structure, with pores interconnected through mesopores forming a complex microstructure. These results demonstrate PGSU scaffolds are able to ensure an adequate transport of nutrients and waste during *in vitro* and *in vivo* cell culture. The isotropic and anisotropic PGSU scaffolds (PGSU-random, PGSU-vertical and PGSU-horizontal) are structured and could be used for one layer tissues such as adipose, tendon and nerve tissues, and they can also display anisotropic mechanical properties to promote guided tissue generation. These scaffolds should be further characterised specifically for each tissue. The mechanical properties found in previous chapters suggests PGSU is likely to be more suitable for tissues which have lower mechanical requirements such as adipose tissue compared to tissues such as tendon.

Multilayer ECM structures are found when a tissue is composed from multiple cell types and functionalities. Such tissues could be skin and oral mucosa. These tissues have different tissue layers and are separated with a BM, which as mentioned earlier, functions by separating the tissue layers while allowing gas/nutrient exchange and cell communication. Research in fabricating multilayer scaffolds has been successful in the past, using multiple materials (collagen, PCL, PLGA) and fabrication techniques (porogen leaching, electrospinning, freeze drying, 3D printing) [220-222]. The aim of all these studies including this thesis is to mimic the complex hierarchical multilayer characteristics of native ECM which has been shown to guide tissue development and stem cell differentiation. Tissue development was enhanced mainly due to difference in pore size, porosity and mechanical properties. For example, in cartilage tissue engineering a bilayer scaffold was fabricated with PLGA and collagen [223]. These scaffolds were then seeded with mesenchymal stem cells (MSCs) and 4 months after implantation into a 1-year-old beagle, osteochondral tissue was regenerated with

cartilage and bone like tissues in each respective layer [223]. Here we propose a similar approach, but to fabricate the hierarchical multilayer scaffolds we combined two fabrication techniques, freeze drying and airbrushing, using the same polymer. The combination of these techniques allowed to design novel PGSU scaffolds that either exhibited a thin low porosity layer (BM like structure) or multiple porous layers with different pore structure, size and porosities. As the previous study the difference in pore structure, size and porosities is there to provide the appropriate structure for either MSCs to differentiate to localised specific cells or for those specific cells to be seeded individually and reside within a biomimetic environment. The BM like structure, as second or third layer of the scaffold is there to restrict the epithelial cells from penetrating to the porous section of the scaffold where fibroblasts are supposed to reside. It was found that any loss of full thickness skin that is more than 4 cm in diameter will not regenerate well without a graft, and when substantial amount of skin is needed autologous skin cannot be used to reconstruct the defect [116]. Probably, PGSU-trilayer could be used to co-culture cells to develop a hypodermis (bottom layer), dermis (middle layer, and epidermis (on top of BM-layer). It was important though to make sure that the transportation for gas and nutrients was sufficient to allow cell survival and cell communication since epithelial cells require signals, in the form of growth factors, to attach and be metabolically active. For this reason, we characterised the permeability of the scaffolds with BM (PGSU-BM and PGSU-trilayer) to determine if the non-porous film would allow sufficient water transport. We found that the PGSU-BM had high water permeability and it was significantly higher than all the other scaffolds in this chapter except the PGSU-horizontal, even higher than the PGSU-vertical which was not expected since it is a one layer porous scaffold. This probably occurred because the PGSU-vertical was made from PGSU-

10% but the PGSU-BM was made using PGSU-5% despite the fact that it had a low porosity film as a second layer. However, the PGSU-trilayer had the lowest water permeability than all other scaffolds but had the same BM layer with the PGSU-BM which indicates that as long as the BM is thin, the porous structure afterwards is what determines the permeability of the scaffold.

Unfortunately, oral mucosa was never characterised for its BM thickness but as mentioned earlier, oral mucosa and skin have many similarities. Natively, human skin BM has a thickness of 0.5 – 1.0  $\mu\text{m}$  [224], which is significantly thinner than the BM-like layer of the PGSU-BM ( $36.0 \pm 14.7 \mu\text{m}$ ). Hence, to fabricate a biomimetic BM like structure is extremely difficult.

With the SEM images and permeability results we were able to proceed with co-culturing oral mucosa cells on the PGSU-BM scaffolds and investigate its structural ability to separate the cell layers and assess the collagen production. A step by step approach was used to examine this. The oral mucosa is comprised from two cell types, keratinocytes and fibroblasts, and because of seeding issues found in the previous chapters we decided to assess first the keratinocyte adherence and then the fibroblast seeding efficiency individually prior to the co-culture. Ralston et al. studied the epidermal keratinocytes cell attachment with and without fibroblasts and found that fibroblasts are essential for keratinocytes attachment and proliferation [225]. They also showed that both cell types are required to maintain a BM [225]. Furthermore, a study by Vintermyr et al. has showed that fibroblasts are necessary for oral epithelial development and thickening in oral models [226]. Therefore, we began to assess the keratinocyte viability on PGSU-films using OKF6. The reason for using OKF6 was the fact that these cells do not require fibroblasts to be able to adhere and proliferate [227]. We found that the cells were able to adhere and have significant increase in

their metabolic activity over the 9 days culture, but not as metabolically active as the positive control. This is because of the seeding technique. It is extremely difficult to seed cells on a hydrophobic non-porous film without losing a large portion of cells to the TCP. Nevertheless, when the samples were imaged, cells were attached in a confluent layer on the PGSU-film which allowed us to move to the next step of this chapter. Another observation was that the live/dead stain was unsuitable for use with the PGSU-film. This is believed to be because of the propidium iodide was absorbed by the material itself, therefore masking the green dye, which was confirmed by the negative control without cells. We also assessed the metabolic activity of NOKs on PGSU-films and similar results as OKF6 were observed. These positive results allowed us to then move to optimising the fibroblast seeding technique.

In the previous chapters we showed that cell distribution was poor when cells were seeded passively, since passive seeding relies on the hydrophilicity of the material (which is low for PGSU) and gravity only to encourage cell infiltration. Previous work by Solchaga et al. [217] showed that dynamic seeding was able to improve cell distribution for 3D scaffolds and we modified their protocol to suit our scaffolds. Dynamic cell seeding works by placing the scaffold under vacuum to remove the air from the chamber and from the pores of the scaffold. The result is, when the air pressure returns to atmospheric pressure the returning air passes through the media/cell suspension that is overlaying the scaffold pushing it inside the pores of the scaffold. Repeating this vacuum/ventilation cycle resulted into a uniform cell distribution. As a results fibroblast cells were well distributed within the porous structure of the scaffold, which should result in better cell growth as cells have higher surface area to grow in. The success of the dynamic seeding technique used in this thesis relied on to the sterile plastic bag with the syringe and syringe filter (Figure 4.3).



This in-house, easy to make, sterile chamber functioned by sterilising the returning air entering the scaffold. During the first attempt of the dynamic seeding a sterile chamber was not used and caused a rapid contamination which killed all the cells.

During cell co-culture, using NOK and NTF, we managed to combine static seeding and dynamic seeding for each cell type respectively. We methodically seeded the scaffolds with NTF and NOK following published co-culture methods in engineering oral mucosa tissue equivalents using DED [2, 228, 229]. We quantified the collagen produced during co-culture and compared it against the DED and PGSU-5% (results from Chapter 3, Figure 3.16). As expected DED had significantly higher collagen concentration in comparison to the other two, because it is predominantly made out of collagen (skin collagen content is 60-80 % [197]). What was interesting from this experiment was the higher collagen produced from the PGSU-BM during co-culture (NOKs and NTFs) compared to PGSU-5% during monoculture (L929 cells). We believe this is because of different fibroblast cells used, but most importantly we believe the NOKs promoted NTF proliferation and production of ECM because of growth factors that keratinocytes secrete (platelet-derived growth factors) [230]. The PGSU-BM scaffolds facilitated a structural support for cell co-culture, by separating the cell layers restricting cell penetration while providing a surface for the NOK to develop an epithelium. The cytokeratin staining was observed throughout the epithelial layer demonstrating these cells maintained their phenotype however the intensity of staining observed did not increase in intensity in the lower third of the epithelium as in the work of Colley et al. [2]. This is possibly because cells were not cultured long enough at ALI or that the epithelium was not as mature cells grown on the dermal scaffold. The NOKs within the epithelial layer of the PGSU-BM had similar structure with the NOKs of the tissue engineered oral mucosa model in the

work of Colley et al. [2], but lower cell confluency and tissue development was also evident. This could be due to NOK variation between patients but we believe longer culture period is necessary to characterise the tissue development.

Further examination is required, however we managed to demonstrate our ability to fabricate synthetic scaffolds for, but not limited to, oral mucosa tissue engineering. With some improvements on fabrication and cell co-culture methods such scaffolds have the potential to be used as an oral mucosa tissue equivalent to measure toxicity, drug delivery and to model oral diseases (similar to [2, 228, 231]) but also for the purpose of regenerating oral mucosa tissue defects. DED has multiple advantages such as good durability, can retain its structural ability and low antigenicity, but lacks in fibroblast infiltration and there is limited availability [15]. Natural scaffolds used in OMTE such as gelatin-base scaffolds which promote epithelialisation; and collagen-based scaffolds which support excellent fibroblast growth; have the disadvantages of not being available in large quantities (limits their scalability), batch-to-batch variation (limits their reproducibility) and low range of physical properties (mechanical properties, degradation rate) [15]. The advantages of the above mentioned scaffolds could be achieved from the PGSU-BM scaffolds which allowed keratinocyte attachment, limited cell infiltration, an early development of epithelium and collagen production. Additionally, synthetic PGSU solves their disadvantages as well. In terms of: scalability, large quantities of PGSU can be synthesised and fabricated at a low cost; the scaffold is reproducible, with controlled chemical synthesis and freeze drying the reproducibility could be high; and physical properties, there are multiple ways to alter both the mechanical properties and degradation rates (change the reactant ratio, change polymer concentration). Furthermore, as demonstrated in this chapter, multiple hierarchical scaffold microstructures can be fabricated which literature has shown to

influence the differentiation of MSCs into specific localised cells [232], making the scaffold a potential candidate for stem cell delivery, acting as not just a cell carrier but also as a guide to stem cell differentiation. As mentioned in the literature review, the native basement membrane functions by orchestrating growth factor-mediated extracellular communication, cellular adhesion, migration and differentiation [10]. Despite the fact that this was not tested in this thesis, it is extremely difficult to fabricate a synthetic BM with the native functionality. However, it is possible to mimic the structure functionality of BM, which is to keep the two tissue layers separated while allowing cell communication. With this in mind, the PGSU-BM had some success in separating the cell layers by restricting cell infiltration, however more studies are necessary to fully characterise its ability to mimic the structure functionality of native BM.

## **4.5. Conclusion**

In this chapter we demonstrate that:

1. Combining freeze drying with mould technology produced uniform isotropic and anisotropic scaffolds.
2. Combining freeze drying with mould technology and airbrushing produced scaffolds with complex, hierarchical, multilayer scaffolds with different pore structure, pore sizes and porosities.
3. PGSU scaffolds can be fabricated with a second layer that resembles the cell separation functionality of BM (PGSU-BM).
4. The BM of PGSU-BM successfully acted as a cell barrier with limited cell infiltration from the epithelium layer.

5. PGSU scaffolds seeded with oral cells produced collagen indicating tissue generation and ECM production over 15 days.

In conclusion it was found that the in-house designed moulds could direct the heat transfer during pre-freeze stage concluding to anisotropic PGSU scaffolds. Potential applications of these scaffolds are tissues that exhibit anisotropic structure however these scaffolds were not characterised for their physical and biological properties and these scaffolds can be examined in future work. Furthermore, multilayer scaffolds were also fabricated, and PGSU-BM was used to co-culture oral cells focusing on assessing their ability to sustain cell growth and restrict cell infiltration. It was found that normal oral keratinocytes could grow on the surface of the PGSU and low cell infiltration was evident during immunohistochemistry. Additionally, the scaffold provided an environment for the fibroblast cells to start producing ECM. Nevertheless, more research is required into PGSU scaffolds to understand their potential in oral mucosa tissue engineering.

## **Chapter 5 Conclusions and suggestions for future work**

### **5.1. Conclusions**

The overall aim of this thesis was to develop PGSU scaffolds with a focus on specific microstructures and mechanical properties that are similar to the native oral mucosa tissue. In each individual chapter the key findings were identified and discussed. The major conclusions from each chapter are underlined below.

Before testing our first hypothesis, PGSU scaffolds were fabricated using different freeze drying cycles to try and achieve a uniform microstructure. For PGSU-2.5% this was not possible at any of the three freezing temperatures used, most probably due to the mould. However, we used these scaffolds to characterise the effect that the sterilisation method has on them. It was found that the scaffolds could be sterilised with all three methods used in Chapter 2 (70% Ethanol, 0.1% PAA and autoclave) without any significant difference between their chemical structure, mechanical properties and cell metabolic activity. This part of the thesis did not have a significant contribution into the science of TE, but since it was the first time that PGSU scaffolds were fabricated it was important to set a starting point in order to understand what had to be improved before testing the scaffold for OMTE. From Chapter 2 we concluded to that the scaffolds required an improvement on their microstructure (more uniform), mechanical properties (try to achieve biomimetic to oral mucosa's mechanical properties) and improve the cell culture techniques (seeding and culture).

To test our first hypothesis, we focused on improving the freeze drying protocol, improve the microstructure and mechanical properties of the scaffolds, and perform a longer more reproducible cell culture. The freeze drying protocol was improved by producing another mould (aluminium mould; to increase the thermal conductivity of

the mould) and changing the polymer concentration during synthesis. The polymer concentration also caused an increase on the mechanical properties of the scaffolds due to more material present within the scaffold and less void space. By reducing the void space (porosity), the pore size was also reduced which resulted into low cell infiltration, however it did not affect the cell metabolic activity. It did however affect the tissue generation by reducing the amount of collagen produced by the fibroblast cells. We also showed that the PGSU scaffolds (all three polymer concentrations) exhibited elastomeric properties with almost no loss in shape and mechanical strength during cyclic tensile loading. This property is an advantage over all the other synthetic materials used in OMTE, and it is needed if biomimicry is wished to be achieved. Therefore, considering our first hypothesis it can be concluded that it was found to be true, as adjusting the polymer concentration allowed us to adjust the microstructure, mechanical properties and degradation rate of the PGSU scaffolds. Our second hypothesis was also found to be partially true, as the scaffold microstructure affected protein production but did not affect cell metabolic activity. By the end of this chapter it was realised that PGSU-5% is a scaffold that might be a good candidate to be used in OMTE. The only limitation that was evident at this point was the mechanical properties of the PGSU-5% were significantly lower than oral mucosa. According to the definition of biocompatibility this might be an issue, however, collagen was found to be successful in OMTE and skin TE and in both cases collagen has significantly lower mechanical properties than both tissues. Having lower mechanical properties when the scaffold is implanted might be a disadvantage because it makes it susceptible to breaking and failing, but if the material can facilitate co-culture, degrades linearly allowing time for cells to produce their ECM the mechanical properties of the scaffold

may end up matching the ones of the native tissue that they are replacing, as in the case of collagen scaffolds.

We believed that the reason that lower collagen production was found from the higher polymer concentration scaffolds was mainly because of the lack of cell infiltration within the scaffold, which reduced the surface area that cells could work with and produce their ECM. Therefore, we used a vacuum seeding technique that significantly improved the seeding efficiency. However, after cell culture and Sirius red, the collagen produced was not significantly different between seeding techniques (static and vacuum seeding). Therefore, most probably the porosity of the scaffold that influences the protein production but does not affect the cell metabolic activity. Nevertheless, the vacuum seeding technique demonstrated in this thesis could be used with other scaffolds and cells as well. By adjusting the speed and number of the vacuum/ventilation cycles most scaffolds can be dynamically seeded with no need of advanced equipment.

Since freeze drying was used extensively in this thesis it was of interest to attempt in complicating the microstructure of the scaffolds aiming to fabricate PGSU scaffolds with a BM-like layer. Having a second layer which provides the structural functionality of the native BM was hypothesised to be beneficial by allowing cell co-culture without epithelial cells infiltrating the lamina propria area of the scaffold, or fibroblasts infiltrating into the epithelium. This infiltration issue was seen from collagen scaffolds, where epithelial islands were formed inside the porous area of the collagen scaffolds. During the exploitation of freeze drying it was realised that interesting scaffold microstructures could be achieved by using the knowledge gained from Chapter 3 (polymer concentration affects porosity and pore size) and directing the heat transfer. To show these findings, anisotropic and multilayer PGSU scaffolds

were fabricated with layers distinguished by their pore alignment or porosity/pore size. These scaffolds were not characterised fully, but they demonstrated a proof of concept and supported the second hypothesis of this thesis that stated that using freeze drying, multiple layer scaffolds can be fabricated to mimic the native tissue aiming to replace. These native tissues could be skin (PGSU-trilayer) and tendon (PGSU-horizontal), however these scaffolds should be characterised fully for their specific application before concluding to their TE impact. Furthermore, the fabrication techniques demonstrated in this thesis can be used with other materials, that have been shown to be optimum for their target tissue but are lacking the complex, hierarchical multilayer ECM structure that the native tissue exhibits.

Nevertheless, the aims and objectives of this work was about fabricating scaffolds for OMTE. Since epithelial cells do not require a porous structure, but a surface to adhere and proliferate, while fibroblasts require a porous structure to develop into a connective tissue, it was logical to fabricate a scaffold that exhibited a porous layer and a thin film on top. The porous layer was decided to be the one achieved from the PGSU-5% scaffold since the best biological results were achieved by it making it the best candidate for lamina propria development. However, a reproducible second thin layer was difficult to achieve using freeze drying alone, hence the use of airbrushing. Airbrushing was recently developed, and it was used to fabricate nanosized fibres. Since the native BM of oral mucosa is  $\sim 1 \mu\text{m}$  thick, airbrushing was assumed to be a good technique to achieve this. The  $1 \mu\text{m}$  thickness was not achieved in this thesis, but an approximately  $\sim 36 \mu\text{m}$  which is significantly thicker than the native BM of oral mucosa. This occurred because of the methods used during airbrushing and it can be improved and optimised in future works. When these scaffolds were used for oral cell co-culture it was found that the microstructure functioned accordingly by restricting



cell infiltration while early stages of epithelium development was evident. From these findings we can conclude that the third and final hypothesis of this thesis is true, but improvements are necessary to optimise the PGSU-BM scaffold. The results histological/immunohistochemical results were not completely resembling the native oral mucosa nor oral mucosa equivalents developed using EVPOME or DED, but with improvements into the fabrication, seeding and culture methods these results could improve and add to the development of synthetic scaffolds for OMTE.

The PGSU scaffold in general was found to be an interesting material for TE. It allowed to be fabricated with multiple microstructures, mechanical properties and degradation rates, and certainly the range can be expanded by changing freeze drying protocols and reactants molar ratio. This material also demonstrated that it can facilitate cell attachment and activity as well as collagen production, which are very important in the field of TE. While not being an advantage over other materials, these scaffolds have not been significantly investigated by the scientific community surrounding biomaterials and TE but results from this thesis support that it can be potentially used in soft tissue engineering. Furthermore, the freeze drying techniques developed and used in this thesis has shown the flexibility of freeze drying as a fabrication technique. All the freeze drying techniques as well as the mould technology used can be used with other materials too, for example collagen. Since collagen has attracted lots of attention for its use in TE trying to mimic the microstructure of the target tissue may be beneficial. Finally, this thesis has shown that airbrushing can be used to fabricate BM-like layer with PGSU, but generally speaking it can be used to fabricate any soluble biomaterial into a thin BM-like layer. While not a true biomimetic BM because of the biological complexity involved in the native BM, structure wise it can help during tissue regeneration, for example this BM-like layer

can be used to overlay a collagen scaffold which has shown to form epithelial islands within its connective tissue area to restrict the cell infiltration.

In conclusion, by identifying some specific limitations in OMTE and PGSU scaffolds we developed methods to address them in a methodical manner. The field of OMTE lacks from synthetic scaffolds that exhibit elastomeric properties with the ability to recover their shape and strength after loading. Therefore, we developed PGSU scaffolds that are elastomeric with recoverable shape and strength, degrade linearly, and exhibit specific physical features to allow cell culture and tissue development. These physical properties were the pore size, pore structure, permeability and oral mucosa biomimetic structure. It was demonstrated that the BM-like scaffold functioned by restricting the oral keratinocytes from infiltrating to the lamina propria. These scaffolds could have a great impact in OMTE because it solves multiple disadvantages that scaffolds exhibit in this field.

## **5.2. Future Work**

We believe PGSU scaffolds have a great potential in TE. Through this study we demonstrated that scaffolds can be fabricated with multiple pore size/porosities and different microstructure architectures that exhibit similar structure properties with oral mucosa, skin and other soft tissues. However, more characterisation and improvements are necessary to demonstrate PGSU's full potential in TE and this can be done in future work. Future research work should firstly address in improving the PGSU scaffold for OMTE, use sterilisation methods that are applied clinically and investigate the potential of PGSU in other soft TE applications.

Regarding PGSU in OMTE, the scaffold mechanical properties should be improved to match the mechanical properties of oral mucosa. This can be done by altering the

reactants molar ratio which according to literature the mechanical properties of PGSU increase approximately by 2-folds when the reactants molar ratio is altered from 1:0.6 (used in this thesis) to 1:1. Furthermore, a complete assessment should be done on the fabrication technique used to introduce a BM-like layer by assessing its microstructure using transmission electron microscopy (TEM) to visualise the BM-like layer at the nanoscale and characterise its nanostructure. The airbrushing technique should also be improved by changing the nozzle size, distance of spraying, volume and polymer concentration of the polymer solution in order to achieve a thinner more biomimetic 2<sup>nd</sup> layer. The optimised PGSU-BM scaffold should then be characterised for its tensile and compression properties as well as its suitability to culture oral keratinocytes and fibroblast cells. The oral mucosa tissue development should also be assessed using cell proliferation assays (DNA assay) and histology/immunohistochemistry. The sterilisation method may have tremendous effects on the scaffold's chemical structure, microstructure, mechanical properties and sometimes biological properties. For the purpose of using the optimised PGSU scaffolds clinically, conventional and approved clinical sterilisation methods should be examined, such as sterilisation by ethylene oxide and gamma irradiation. Establishing a solid clinically approved sterilisation method that has minimal or no effect on the scaffold's tissue engineering abilities will improve its potential for clinical use. Finally, these scaffolds should be examined in pre-clinical animal models to assess their *in vivo* biocompatibility, tissue development and angiogenesis.

Future research work may also involve developing PGSU scaffolds using the fabrication techniques of this thesis for other tissue applications. For example, the field of tendon tissue engineering is growing because of tendon's low regenerative capacity. Anisotropic PGSU scaffolds fabricated in this thesis can be used to culture tenocytes

and/or mesenchymal stem cells to engineer a tendon tissue for tendon therapy. Literature suggests that the anisotropic nature of the PGSU scaffolds will guide the tissue development to mimic the tendon tissue. For this specific application the PGSU-horizontal scaffolds can be fabricated and the mechanical properties of the scaffold will probably need to be enhanced by increasing the reactant ratio, and we believe the anisotropic structure of the scaffold will direct the mechanical properties along the mechanical loading axis. Furthermore, if mesenchymal stem cells are to be used, literature has shown that proteins such as bone-morphogenic protein-12 (BMP-12) can guide stem cell differentiation into tenocytes. Therefore, loading PGSU-horizontal with BMP-12 can be beneficial. For drug loading it is hypothesised that BMP-12 can be loaded into collagen nanoparticles to protect the protein during PGSU synthesis. Since drug release properties will be exhibited from the PGSU scaffolds, a complete characterisation into drug release kinetics should be performed.

Furthermore, cartilage is a more complex tissue with low regenerative capacity. The need for cartilage tissue engineering is increasing due to the increase in physical activities and longer life span, which renders it impossible for the cartilage to synchronise its regeneration with its degeneration. Trilayer PGSU scaffolds with different pore orientations can be used to mimic the native ECM of cartilage. Compression properties of these scaffolds should be characterised and optimised to function similar to cartilage tissue. The biomimetic microstructure and mechanical properties could provide guided stem cell differentiation into localised cells and tissue generation. Growth factors could also be loaded in the scaffolds with similar methods as suggested above to promote stem cell differentiation.

Finally, regenerating skin tissue can also be a future application of PGSU-BM. Histologically skin is very similar to oral mucosa and is consisted of two layers, the

epidermis and dermis. Reconstruction of full thickness burn injuries (more than 4 cm in diameter) is necessary as it will not heal well without surgical intervention. In this case PGSU-BM should be approached as suggested for OMTE but its mechanical properties and cell viability should be assessed to mimic the skin tissue.

## References

- [1] K. Izumi, S.E. Feinberg, A. Iida, M. Yoshizawa, Intraoral grafting of an ex vivo produced oral mucosa equivalent: a preliminary report, *Int J Oral Maxillofac Surg* 32(2) (2003) 188-97.
- [2] H.E. Colley, V. Hearnden, A.V. Jones, P.H. Weinreb, S.M. Violette, S. Macneil, M.H. Thornhill, C. Murdoch, Development of tissue-engineered models of oral dysplasia and early invasive oral squamous cell carcinoma, *British journal of cancer* 105(10) (2011) 1582-92.
- [3] S.Q. Liu, *Bioregenerative Engineering: Principles and Applications*, Wiley Interscience 2007.
- [4] G. Vunjak-Novakovic, R.I. Freshney, *Culture of cells for tissue engineering*, Wiley-Liss, Hoboken, N.J., 2006.
- [5] E.N. Marieb, K. Hoehn, *Human Anatomy & Physiology*, 8th ed., Pearson International Edition 2010.
- [6] B. Kinikoglu, O. Damour, V. Hasirci, Tissue engineering of oral mucosa: a shared concept with skin, *J Artif Organs* 18(1) (2015) 8-19.
- [7] C.A. Squier, M.J. Kremer, *Biology of Oral Mucosa and Esophagus*, JNCI Monographs 2001(29) (2001) 7-15.
- [8] T.A. Winning, G.C. Townsend, Oral mucosal embryology and histology, *Clinics in Dermatology* 18(5) (2000) 499-511.
- [9] M.A. Landay, H.E. Schroeder, Differentiation in normal human buccal mucosa epithelium, *Journal of anatomy* 128(Pt 1) (1979) 31-51.
- [10] M. Varkey, J. Ding, E.E. Tredget, Superficial dermal fibroblasts enhance basement membrane and epidermal barrier formation in tissue-engineered skin:

implications for treatment of skin basement membrane disorders, *Tissue engineering*. Part A 20(3-4) (2014) 540-552.

[11] J.R. Stanley, D.T. Woodley, S.I. Katz, G.R. Martin, Structure and Function of Basement Membrane, *Journal of Investigative Dermatology* 79(1, Supplement) (1982) 69-72.

[12] S. Inoue, Ultrastructure of Basement Membranes, in: G.H. Bourne, K.W. Jeon, M. Friedlander (Eds.), *International Review of Cytology*, Academic Press 1989, pp. 57-98.

[13] E. Pöschl, U. Schlötzer-Schrehardt, B. Brachvogel, K. Saito, Y. Ninomiya, U. Mayer, Collagen IV is essential for basement membrane stability but dispensable for initiation of its assembly during early development, *Development* 131(7) (2004) 1619.

[14] A. El Ghalbzouri, M.F. Jonkman, R. Dijkman, M. Ponc, Basement Membrane Reconstruction in Human Skin Equivalents Is Regulated by Fibroblasts and/or Exogenously Activated Keratinocytes, *Journal of Investigative Dermatology* 124(1) (2005) 79-86.

[15] K. Moharamzadeh, I.M. Brook, R. Van Noort, A.M. Scutt, M.H. Thornhill, Tissue-engineered oral mucosa: a review of the scientific literature, *Journal of dental research* 86(2) (2007) 115-24.

[16] S. Goktas, J.J. Dmytryk, P.S. McFetridge, Biomechanical behavior of oral soft tissues, *J Periodontol* 82(8) (2011) 1178-86.

[17] R.P. Lanza, R.S. Langer, J. Vacanti, *Principles of tissue engineering*, 3rd ed., Elsevier / Academic Press, Amsterdam ; Boston, 2007.

[18] T. Amemiya, T. Nakamura, T. Yamamoto, S. Kinoshita, N. Kanamura, Autologous Transplantation of Oral Mucosal Epithelial Cell Sheets Cultured on an

Amniotic Membrane Substrate for Intraoral Mucosal Defects, PLoS ONE 10(4) (2015) e0125391.

[19] U. Meyer, T. Meyer, J. Handschel, H.P. Wiesmann, *Fundamentals of Tissue Engineering and Regenerative Medicine*, Springer 2009.

[20] M. Ueda, I. Tohnai, H. Nakai, *Tissue Engineering Research in Oral Implant Surgery*, *Artificial Organs* 25(3) (2001) 164-171.

[21] F. Imaizumi, I. Asahina, T. Moriyama, M. Ishii, K. Omura, *Cultured Mucosal Cell Sheet with a Double Layer of Keratinocytes and Fibroblasts on a Collagen Membrane*, *Tissue Engineering* 10 (2004) 657-664.

[22] T. Okano, N. Yamada, H. Sakai, Y. Sakurai, *A Novel Recovery-System for Cultured-Cells using Plasma-Treated Polystyrene Dishes Grafted with Poly(N-Isopropylacrylamide)*, *Journal of Biomedical Materials Research* 27(10) (1993) 1243-1251.

[23] Y.P. Talmi, L. Sigler, E. Inge, Y. Finkelstein, Y. Zohar, *Antibacterial properties of human amniotic membranes*, *Placenta* 12(3) (1991) 285-8.

[24] E. Inge, Y.P. Talmi, L. Sigler, Y. Finkelstein, Y. Zohar, *Antibacterial properties of human amniotic membranes*, *Placenta* 12(3) (1991) 285-288.

[25] D. Murakami, M. Yamato, K. Nishida, T. Ohki, R. Takagi, J. Yang, H. Namiki, T. Okano, *Fabrication of transplantable human oral mucosal epithelial cell sheets using temperature-responsive culture inserts without feeder layer cells*, *J Artif Organs* 9(3) (2006) 185-91.

[26] M. Ueda, *Formation of epithelial sheets by serially cultivated human mucosal cells and their applications as a graft material*, *Nagoya J Med Sci* 58(1-2) (1995) 13-28.



- [27] G.M. Raghoobar, A.M. Tomson, J. Scholma, E.H. Blaauw, M.J. Witjes, A. Vissink, Use of cultured mucosal grafts to cover defects caused by vestibuloplasty: an in vivo study, *J Oral Maxillofac Surg* 53(8) (1995) 872-8; discussion 878-9.
- [28] M. Yoshizawa, S.E. Feinberg, C.L. Marcelo, V.M. Elner, Ex vivo produced human conjunctiva and oral mucosa equivalents grown in a serum-free culture system, *Journal of Oral and Maxillofacial Surgery* 62(8) (2004) 980-988.
- [29] A. Dongari-Bagtzoglou, H. Kashleva, Development of a highly reproducible three-dimensional organotypic model of the oral mucosa, *Nat. Protocols* 1(4) (2006) 2012-2018.
- [30] K. Moharamzadeh, I.M. Brook, R. Van Noort, A.M. Scutt, K.G. Smith, M.H. Thornhill, Development, optimization and characterization of a full-thickness tissue engineered human oral mucosal model for biological assessment of dental biomaterials, *J Mater Sci Mater Med* 19(4) (2008) 1793-801.
- [31] M. Alaminos, I. Garzon, M.C. Sanchez-Quevedo, G. Moreu, M. Gonzalez-Andrades, A. Fernandez-Montoya, A. Campos, Time-course study of histological and genetic patterns of differentiation in human engineered oral mucosa, *J Tissue Eng Regen Med* 1(5) (2007) 350-9.
- [32] W.M.W. Tra, J.W. van Neck, S.E.R. Hovius, G.J.V.M. van Osch, S. Perez-Amodio, Characterization of a Three-Dimensional Mucosal Equivalent: Similarities and Differences with Native Oral Mucosa, *Cells Tissues Organs* 195(3) (2012) 185-196.
- [33] Z. Zhang, B.B. Michniak-Kohn, Tissue engineered human skin equivalents, *Pharmaceutics* 4(1) (2012) 26-41.

- [34] R. Ophof, J.C. Maltha, A.M. Kuijpers-Jagtman, J.W. Von den Hoff, Implantation of tissue-engineered mucosal substitutes in the dog palate, *Eur J Orthod* 30(1) (2008) 1-9.
- [35] B. Kinikoglu, C. Auxenfans, P. Pierrillas, V. Justin, P. Breton, C. Burillon, V. Hasirci, O. Damour, Reconstruction of a full-thickness collagen-based human oral mucosal equivalent, *Biomaterials* 30(32) (2009) 6418-6425.
- [36] R.N. Lucier, O. Etienne, S. Ferreira, J.A. Garlick, G. Kugel, C. Egles, Soft-Tissue Alterations Following Exposure to Tooth-Whitening Agents, *Journal of Periodontology* 84(4) (2012) 513-519.
- [37] C.R. Chapple, S. MacNeil, Tissue Engineered Oral Mucosa for Urethroplasty: Past Experience and Future Directions, *The Journal of Urology* 187(5) (2012) 1533-1534.
- [38] U. Kriegebaum, M. Mildenerger, U.D. Mueller-Richter, U. Klammert, A.C. Kuebler, T. Reuther, Tissue engineering of human oral mucosa on different scaffolds: in vitro experiments as a basis for clinical applications, *Oral surgery, oral medicine, oral pathology and oral radiology* 114(5 Suppl) (2012) S190-8.
- [39] A. Simsek, A.J. Bullock, S. Roman, C.R. Chapple, S. Macneil, Developing improved tissue-engineered buccal mucosa grafts for urethral reconstruction, *Canadian Urological Association journal = Journal de l'Association des urologues du Canada* 12(5) (2018) E234-E242.
- [40] F. Groeber, M. Holeiter, M. Hampel, S. Hinderer, K. Schenke-Layland, Skin Tissue Engineering-In Vivo and In Vitro Applications, *Clin Plast Surg Clin Plast Surg* 39(1) (2012) 33-+.
- [41] J. Mansbridge, Skin tissue engineering, *J Biomat Sci-Polym E J Biomat Sci-Polym E* 19(8) (2008) 955-968.

- [42] K.A. Faraj, T.H. van Kuppevelt, W.F. Daamen, Construction of collagen scaffolds that mimic the three-dimensional architecture of specific tissues, *Tissue Eng* 13(10) (2007) 2387-94.
- [43] F. Groeber, M. Holeiter, M. Hampel, S. Hinderer, K. Schenke-Layland, Skin tissue engineering - In vivo and in vitro applications, *Advanced Drug Delivery Reviews* 63(4-5) (2011) 352-366.
- [44] J.N. Mansbridge, Tissue-engineered skin substitutes in regenerative medicine, *Current Opinion in Biotechnology* 20(5) (2009) 563-567.
- [45] A. El-Ghalbzouri, E.N. Lamme, C. van Blitterswijk, J. Koopman, M. Ponec, The use of PEGT/PBT as a dermal scaffold for skin tissue engineering, *Biomaterials* 25(15) (2004) 2987-96.
- [46] K.W. Ng, H.L. Khor, D.W. Hutmacher, In vitro characterization of natural and synthetic dermal matrices cultured with human dermal fibroblasts, *Biomaterials* 25(14) (2004) 2807-18.
- [47] E.W. Evans, Treating Scars on the Oral Mucosa, *Facial Plastic Surgery Clinics of North America* 25(1) (2017) 89-97.
- [48] D.W. Hutmacher, Scaffolds in tissue engineering bone and cartilage, *Biomaterials* 21(24) (2000) 2529-43.
- [49] N. L'Heureux, T.N. McAllister, L.M. de la Fuente, Tissue-Engineered Blood Vessel for Adult Arterial Revascularization, *New England Journal of Medicine* 357(14) (2007) 1451-1453.
- [50] F. Oberpenning, J. Meng, J.J. Yoo, A. Atala, De novo reconstitution of a functional mammalian urinary bladder by tissue engineering, *Nature Biotechnology* 17 (1999) 149.

- [51] E. Tziampazis, A. Sambanis, Tissue Engineering of a Bioartificial Pancreas: Modeling the Cell Environment and Device Function, *Biotechnology Progress* 11(2) (1995) 115-126.
- [52] A. Subramanian, U.M. Krishnan, S. Sethuraman, Development of biomaterial scaffold for nerve tissue engineering: Biomaterial mediated neural regeneration, *Journal of Biomedical Science* 16(1) (2009) 108.
- [53] L. Flynn, K.A. Woodhouse, Adipose tissue engineering with cells in engineered matrices, *Organogenesis* 4(4) (2008) 228-235.
- [54] D.F. Williams, On the mechanisms of biocompatibility, *Biomaterials* 29(20) (2008) 2941-2953.
- [55] B. Dhandayuthapani, Y. Yoshida, T. Maekawa, D.S. Kumar, Polymeric Scaffolds in Tissue Engineering Application: A Review, *International Journal of Polymer Science* 2011 (2011) 1-19.
- [56] B.D. Boyan, T.W. Hummert, D.D. Dean, Z. Schwartz, Role of material surfaces in regulating bone and cartilage cell response, *Biomaterials* 17(2) (1996) 137-146.
- [57] P. Roach, D. Eglin, K. Rohde, C.C. Perry, Modern biomaterials: a review—bulk properties and implications of surface modifications, *Journal of Materials Science: Materials in Medicine* 18(7) (2007) 1263-1277.
- [58] P. Roach, T. Parker, N. Gadegaard, M.R. Alexander, Surface strategies for control of neuronal cell adhesion: A review, *Surface Science Reports* 65(6) (2010) 145-173.
- [59] K.B. McClary, T. Ugarova, D.W. Grainger, Modulating fibroblast adhesion, spreading, and proliferation using self-assembled monolayer films of alkylthiolates on gold, *Journal of Biomedical Materials Research* 50(3) (2000) 428-439.

- [60] N. Faucheux, R. Schweiss, K. Lutzow, C. Werner, T. Groth, Self-assembled monolayers with different terminating groups as model substrates for cell adhesion studies, *Biomaterials* 25(14) (2004) 2721-2730.
- [61] R.N.S. Sodhi, Application of surface analytical and modification techniques to biomaterial research, *J Electron Spectrosc* 81(3) (1996) 269-284.
- [62] S. Halstenberg, A. Panitch, S. Rizzi, H. Hall, J.A. Hubbell, Biologically Engineered Protein-graft-Poly(ethylene glycol) Hydrogels: A Cell Adhesive and Plasmin-Degradable Biosynthetic Material for Tissue Repair, *Biomacromolecules* 3(4) (2002) 710-723.
- [63] A.M. Wojtowicz, A. Shekaran, M.E. Oest, K.M. Dupont, K.L. Templeman, D.W. Hutmacher, R.E. Guldberg, A.J. Garcia, Coating of biomaterial scaffolds with the collagen-mimetic peptide GFOGER for bone defect repair, *Biomaterials* 31(9) (2010) 2574-2582.
- [64] K. Eid, E. Chen, L. Griffith, J. Glowacki, Effect of RGD coating on osteocompatibility of PLGA-polymer disks in a rat tibial wound, *J Biomed Mater Res* 57(2) (2001) 224-31.
- [65] H.B. Lin, W. Sun, D.F. Mosher, C. Garcia-Echeverria, K. Schaufelberger, P.I. Lelkes, S.L. Cooper, Synthesis, surface, and cell-adhesion properties of polyurethanes containing covalently grafted RGD-peptides, *J Biomed Mater Res* 28(3) (1994) 329-42.
- [66] J.C. Schense, J. Bloch, P. Aebischer, J.A. Hubbell, Enzymatic incorporation of bioactive peptides into fibrin matrices enhances neurite extension, *Nature Biotechnology* 18 (2000) 415.
- [67] S.L. Bellis, Advantages of RGD peptides for directing cell association with biomaterials, *Biomaterials* 32(18) (2011) 4205-4210.

- [68] S. Sakiyama-Elbert, J. Hubbell, Functional Biomaterials: Design of Novel Biomaterials, *Annual Review of Materials Research* 31(1) (2001) 183-201.
- [69] J.J. Blaker, J.E. Gough, V. Maquet, I. Notingher, A.R. Boccaccini, In vitro evaluation of novel bioactive composites based on Bioglass-filled polylactide foams for bone tissue engineering scaffolds, *J Biomed Mater Res A* 67(4) (2003) 1401-11.
- [70] C.A. León y León, New perspectives in mercury porosimetry, *Advances in Colloid and Interface Science* 76-77 (1998) 341-372.
- [71] J.H. Brauker, V.E. Carr-Brendel, L.A. Martinson, J. Crudele, W.D. Johnston, R.C. Johnson, Neovascularization of synthetic membranes directed by membrane microarchitecture, *J Biomed Mater Res* 29(12) (1995) 1517-24.
- [72] I.V. Yannas, E. Lee, D.P. Orgill, E.M. Skrabut, G.F. Murphy, Synthesis and characterization of a model extracellular matrix that induces partial regeneration of adult mammalian skin, *Proc Natl Acad Sci U S A* 86(3) (1989) 933-7.
- [73] S.M. Lim, S.H. Oh, I.K. Park, J.H. Lee, Investigation of Pore Size Effect on Cell Compatibility Using Pore Size Gradient Chitosan Scaffold, *Key Engineering Materials* 342-343 (2007) 285-288.
- [74] J. Zeltinger, J.K. Sherwood, D.A. Graham, R. Müller, L.G. Griffith, Effect of Pore Size and Void Fraction on Cellular Adhesion, Proliferation, and Matrix Deposition, *Tissue Engineering* 7(5) (2001) 557-572.
- [75] A. Samourides, L. Browning, V. Hearnden, B. Chen, Biocompatible poly(glycerol sebacate urethane) scaffolds with controllable porous structures, mechanical properties, and excellent angiogenesis and tissue ingrowth., Submitted (2018).

- [76] A. Samourides, L. Browning, B. Chen, V. Hearnden, Porosity of poly(glycerol sebacate urethane) scaffolds controls angiogenic response and tissue ingrowth in vivo, TCES Conference Abstracts, eCM Online Periodical, 2018, p. 19.
- [77] M. Rumpler, A. Woesz, W.C. Dunlop John, T. van Dongen Joost, P. Fratzl, The effect of geometry on three-dimensional tissue growth, *Journal of The Royal Society Interface* 5(27) (2008) 1173-1180.
- [78] A.J. Salgado, O.P. Coutinho, R.L. Reis, Bone tissue engineering: state of the art and future trends, *Macromol Biosci* 4(8) (2004) 743-65.
- [79] H.K. Kleinman, G.R. Martin, Matrigel: Basement membrane matrix with biological activity, *Seminars in Cancer Biology* 15(5) (2005) 378-386.
- [80] C.S. Hughes, L.M. Postovit, G.A. Lajoie, Matrigel: a complex protein mixture required for optimal growth of cell culture, *Proteomics* 10(9) (2010) 1886-90.
- [81] J. Debnath, S.K. Muthuswamy, J.S. Brugge, Morphogenesis and oncogenesis of MCF-10A mammary epithelial acini grown in three-dimensional basement membrane cultures, *Methods* 30(3) (2003) 256-68.
- [82] L.E. O'Brien, M.M. Zegers, K.E. Mostov, Opinion: Building epithelial architecture: insights from three-dimensional culture models, *Nat Rev Mol Cell Biol* 3(7) (2002) 531-7.
- [83] T. Sato, H. Clevers, Growing self-organizing mini-guts from a single intestinal stem cell: mechanism and applications, *Science* 340(6137) (2013) 1190-4.
- [84] R. Cruz-Acuña, A.J. García, Synthetic Hydrogels Mimicking Basement Membrane Matrices to Promote Cell-Matrix Interactions, *Matrix biology : journal of the International Society for Matrix Biology* 57-58 (2017) 324-333.

- [85] S.R. Pullela, C. Andres, W. Chen, C. Xu, L. Wang, N.A. Kotov, Permselectivity Replication of Artificial Glomerular Basement Membranes in Nanoporous Collagen Multilayers, *The journal of physical chemistry letters* 2(16) (2011) 2067-2072.
- [86] A.S. Au - Pellowe, H.M. Au - Lauridsen, R. Au - Matta, A.L. Au - Gonzalez, Ultrathin Porated Elastic Hydrogels As a Biomimetic Basement Membrane for Dual Cell Culture, *JoVE* (130) (2017) e56384.
- [87] Y. Uchino, S. Shimmura, H. Miyashita, T. Taguchi, H. Kobayashi, J. Shimazaki, J. Tanaka, K. Tsubota, Amniotic membrane immobilized poly(vinyl alcohol) hybrid polymer as an artificial cornea scaffold that supports a stratified and differentiated corneal epithelium, *Journal of Biomedical Materials Research Part B: Applied Biomaterials* 81B(1) (2006) 201-206.
- [88] N.A. Peppas, Y. Huang, M. Torres-Lugo, J.H. Ward, J. Zhang, Physicochemical foundations and structural design of hydrogels in medicine and biology, *Annual review of biomedical engineering* 2 (2000) 9-29.
- [89] E.M. Ahmed, Hydrogel: Preparation, characterization, and applications: A review, *Journal of Advanced Research* 6(2) (2015) 105-121.
- [90] K.H. Schmedlen, K.S. Masters, J.L. West, Photocrosslinkable polyvinyl alcohol hydrogels that can be modified with cell adhesion peptides for use in tissue engineering, *Biomaterials* 23(22) (2002) 4325-4332.
- [91] D.S. Puperi, L.R. Balaoing, R.W. O'Connell, J.L. West, K.J. Grande-Allen, 3-Dimensional spatially organized PEG-based hydrogels for an aortic valve co-culture model, *Biomaterials* 67 (2015) 354-364.
- [92] L.A. Hockaday, K.H. Kang, N.W. Colangelo, P.Y.C. Cheung, B. Duan, E. Malone, J. Wu, L.N. Girardi, L.J. Bonassar, H. Lipson, C.C. Chu, J.T. Butcher, Rapid



3D printing of anatomically accurate and mechanically heterogeneous aortic valve hydrogel scaffolds, *Biofabrication* 4(3) (2012).

[93] W. Lee, J.C. Debasitis, V.K. Lee, J.H. Lee, K. Fischer, K. Edminster, J.K. Park, S.S. Yoo, Multi-layered culture of human skin fibroblasts and keratinocytes through three-dimensional freeform fabrication, *Biomaterials* 30(8) (2009) 1587-1595.

[94] F.J. Bye, L. Wang, A.J. Bullock, K.A. Blackwood, A.J. Ryan, S. MacNeil, Postproduction Processing of Electrospun Fibres for Tissue Engineering, *Journal of Visualized Experiments : JoVE* (66) (2012) 4172.

[95] R. Langer, J.P. Vacanti, Tissue Engineering, *American Association for the Advancement of Science* 260 (1993) 920-926.

[96] J.C. Middleton, A.J. Tipton, Synthetic biodegradable polymers as orthopedic devices, *Biomaterials* 21(23) (2000) 2335-46.

[97] D.S. Katti, S. Lakshmi, R. Langer, C.T. Laurencin, Toxicity, biodegradation and elimination of polyanhydrides, *Adv Drug Deliv Rev* 54(7) (2002) 933-61.

[98] W.P. Ye, F.S. Du, W.H. Jin, J.Y. Yang, Y. Xu, In vitro degradation of poly(caprolactone), poly(lactide) and their block copolymers: influence of composition, temperature and morphology, *Reactive and Functional Polymers* 32(2) (1997) 161-168.

[99] D. Williams, Revisiting the definition of biocompatibility, 14(8) (2003) 10-3.

[100] F.N. Kenny, Z. Drymoussi, R. Delaine-Smith, A.P. Kao, A.C. Laly, M.M. Knight, M.P. Philpott, J.T. Connelly, Tissue stiffening promotes keratinocyte proliferation through activation of epidermal growth factor signaling, *Journal of Cell Science* 131(10) (2018).

- [101] E. Hadjipanayi, V. Mudera, R.A. Brown, Close dependence of fibroblast proliferation on collagen scaffold matrix stiffness, *Journal of Tissue Engineering and Regenerative Medicine* 3(2) (2008) 77-84.
- [102] C. Politis, J. Schoenaers, R. Jacobs, J.O. Agbaje, Wound Healing Problems in the Mouth, *Frontiers in Physiology* 7 (2016) 507.
- [103] F.J. O'Brien, Biomaterials & scaffolds for tissue engineering, *Materials Today* 14(3) (2011) 88-95.
- [104] S. Stratton, N.B. Shelke, K. Hoshino, S. Rudraiah, S.G. Kumbar, Bioactive polymeric scaffolds for tissue engineering, *Bioactive materials* 1(2) (2016) 93-108.
- [105] B.S. Kim, C.E. Baez, A. Atala, Biomaterials for tissue engineering, *World J Urol* 18(1) (2000) 2-9.
- [106] M.E. Nimni, D. Cheung, B. Strates, M. Kodama, K. Sheikh, Chemically modified collagen: a natural biomaterial for tissue replacement, *J Biomed Mater Res* 21(6) (1987) 741-71.
- [107] T. Koide, M. Daito, Effects of Various Collagen Crosslinking Techniques on Mechanical Properties of Collagen Film, *Dental Materials Journal* 16(1) (1997) 1-9,109.
- [108] A.V. Vashi, K.M. Abberton, G.P. Thomas, W.A. Morrison, A.J. O'Connor, J.J. Cooper-White, E.W. Thompson, Adipose tissue engineering based on the controlled release of fibroblast growth factor-2 in a collagen matrix, *Tissue Eng* 12(11) (2006) 3035-43.
- [109] I.R. Williams, Fibroblasts, in: P.J. Delves (Ed.), *Encyclopedia of Immunology* (Second Edition), Elsevier, Oxford, 1998, pp. 905-909.

- [110] Y. Xu, D. Xia, J. Han, S. Yuan, H. Lin, C. Zhao, Design and fabrication of porous chitosan scaffolds with tunable structures and mechanical properties, *Carbohydrate Polymers* 177 (2017) 210-216.
- [111] H. Liu, E.B. Slamovich, T.J. Webster, Less harmful acidic degradation of poly(lactic-co-glycolic acid) bone tissue engineering scaffolds through titania nanoparticle addition, *International Journal of Nanomedicine* 1(4) (2006) 541-545.
- [112] J.H. Choi, J.M. Gimble, K. Lee, K.G. Marra, J.P. Rubin, J.J. Yoo, G. Vunjak-Novakovic, D.L. Kaplan, Adipose Tissue Engineering for Soft Tissue Regeneration, *Tissue Eng Part B-Re Tissue Eng Part B-Re* 16(4) (2010) 413-426.
- [113] C.A. Harper, Handbook of plastics, elastomers, and composites, 4th ed., McGraw-Hill, New York, 2002.
- [114] C. Legnani, A. Ventura, C. Terzaghi, E. Borgo, W. Albisetti, Anterior cruciate ligament reconstruction with synthetic grafts. A review of literature, *International orthopaedics* 34(4) (2010) 465-71.
- [115] B. Veleirinho, D.S. Coelho, P.F. Dias, M. Maraschin, R. Pinto, E. Cargin-Ferreira, A. Peixoto, J.A. Souza, R.M. Ribeiro-do-Valle, J.A. Lopes-da-Silva, Foreign body reaction associated with PET and PET/chitosan electrospun nanofibrous abdominal meshes, *PLoS One* 9(4) (2014) e95293.
- [116] S. MacNeil, Progress and opportunities for tissue-engineered skin, *Nature* 445 (2007) 874.
- [117] D.F. Williams, There is no such thing as a biocompatible material, *Biomaterials* 35(38) (2014) 10009-10014.
- [118] M. Frydrych, B. Chen, Large three-dimensional poly(glycerol sebacate)-based scaffolds – a freeze-drying preparation approach, *Journal of Materials Chemistry B* 1(48) (2013) 6650-6661.

- [119] R. Rai, M. Tallawi, A. Grigore, A.R. Boccaccini, Synthesis, properties and biomedical applications of poly(glycerol sebacate) (PGS): A review, *Progress in Polymer Science* 37(8) (2012) 1051-1078.
- [120] Y. Wang, G.A. Ameer, B.J. Sheppard, R. Langer, A tough biodegradable elastomer, *Nat Biotech* 20(6) (2002) 602-606.
- [121] Y. Li, G.A. Thouas, H. Shi, Q. Chen, Enzymatic and oxidative degradation of poly(polyol sebacate), *J Biomater Appl* 28(8) (2014) 1138-50.
- [122] A.B.W. Brochu, S.L. Craig, W.M. Reichert, Self-healing biomaterials, *Journal of Biomedical Materials Research Part A* 96A(2) (2011) 492-506.
- [123] A.R. Webb, J. Yang, G.A. Ameer, Biodegradable polyester elastomers in tissue engineering, *Expert Opin Biol Th Expert Opin Biol Th* 4(6) (2004) 801-812.
- [124] Q.Z. Chen, A. Bismarck, U. Hansen, S. Junaid, M.Q. Tran, S.E. Harding, N.N. Ali, A.R. Boccaccini, Characterisation of a soft elastomer poly(glycerol sebacate) designed to match the mechanical properties of myocardial tissue, *Biomaterials* 29(1) (2008) 47-57.
- [125] W.L. Neeley, S. Redenti, H. Klassen, S. Tao, T. Desai, M.J. Young, R. Langer, A microfabricated scaffold for retinal progenitor cell grafting, *Biomaterials* 29(4) (2008) 418-426.
- [126] Y. Wang, Y.M. Kim, R. Langer, In vivo degradation characteristics of poly(glycerol sebacate), *Journal of Biomedical Materials Research Part A* 66A(1) (2003) 192-197.
- [127] S.L. Liang, X.Y. Yang, X.Y. Fang, W.D. Cook, G.A. Thouas, Q.Z. Chen, In Vitro enzymatic degradation of poly (glycerol sebacate)-based materials, *Biomaterials* 32(33) (2011) 8486-8496.

- [128] X.J. Loh, A. Abdul Karim, C. Owh, Poly(glycerol sebacate) biomaterial: synthesis and biomedical applications, *J. Mater. Chem. B* 3(39) (2015) 7641-7652.
- [129] C.A. Sundback, J.Y. Shyu, Y.D. Wang, W.C. Faquin, R.S. Langer, J.P. Vacanti, T.A. Hadlock, Biocompatibility analysis of poly(glycerol sebacate) as a nerve guide material, *Biomaterials* 26(27) (2005) 5454-5464.
- [130] P.M. Crapo, Y.D. Wang, Physiologic compliance in engineered small-diameter arterial constructs based on an elastomeric substrate, *Biomaterials* 31(7) (2010) 1626-1635.
- [131] S. Sant, C.M. Hwang, S.H. Lee, A. Khademhosseini, Hybrid PGS-PCL microfibrillar scaffolds with improved mechanical and biological properties, *Journal of Tissue Engineering and Regenerative Medicine* 5(4) (2011) 283-291.
- [132] C.J. Bettinger, B. Orrick, A. Misra, R. Langer, J.T. Borenstein, Microfabrication of poly (glycerol–sebacate) for contact guidance applications, *Biomaterials* 27(12) (2006) 2558-2565.
- [133] F. Yi, D.A. Lavan, Poly(glycerol sebacate) nanofiber scaffolds by core/shell electrospinning, *Macromolecular Bioscience* 8(9) (2008) 803-806.
- [134] G.C. Engelmayr, M.Y. Cheng, C.J. Bettinger, J.T. Borenstein, R. Langer, L.E. Freed, Accordion-like honeycombs for tissue engineering of cardiac anisotropy, *Nature Materials* 7(12) (2008) 1003-1010.
- [135] M. Kharaziha, M. Nikkhah, S.R. Shin, N. Annabi, N. Masoumi, A.K. Gaharwar, G. Camci-Unal, A. Khademhosseini, PGS:Gelatin nanofibrillar scaffolds with tunable mechanical and structural properties for engineering cardiac tissues, *Biomaterials* 34(27) (2013) 6355-66.

- [136] E.M. Jeffries, R.A. Allen, J. Gao, M. Pesce, Y. Wang, Highly elastic and suturable electrospun poly(glycerol sebacate) fibrous scaffolds, *Acta Biomater* 18 (2015) 30-9.
- [137] B. Xu, B. Rollo, L.A. Stamp, D.C. Zhang, X.Y. Fang, D.F. Newgreen, Q.Z. Chen, Non-linear elasticity of core/shell spun PGS/PLLA fibres and their effect on cell proliferation, *Biomaterials* 34(27) (2013) 6306-6317.
- [138] R. Maidhof, A. Marsano, E.J. Lee, G. Vunjak-Novakovic, Perfusion Seeding of Channeled Elastomeric Scaffolds with Myocytes and Endothelial Cells for Cardiac Tissue Engineering, *Biotechnology Progress* 26(2) (2010) 565-572.
- [139] M. Radisic, H. Park, T.P. Martens, J.E. Salazar-Lazaro, W.L. Geng, Y.D. Wang, R. Langer, L.E. Freed, G. Vunjak-Novakovic, Pre-treatment of synthetic elastomeric scaffolds by cardiac fibroblasts improves engineered heart tissue, *Journal of Biomedical Materials Research Part A* 86A(3) (2008) 713-724.
- [140] S. Redenti, W.L. Neeley, S. Rompani, S. Saigal, J. Yang, H. Klassen, R. Langer, M.J. Young, Engineering retinal progenitor cell and scrollable poly(glycerol-sebacate) composites for expansion and subretinal transplantation, *Biomaterials* 30(20) (2009) 3405-3414.
- [141] C. Fidkowski, M.R. Kaazempur-Mofrad, J. Borenstein, J.P. Vacanti, R. Langer, Y.D. Wang, Endothelialized microvasculature based on a biodegradable elastomer, *Tissue Engineering* 11(1-2) (2005) 302-309.
- [142] A. Jean, G.C. Engelmayr, Finite element analysis of an accordion-like honeycomb scaffold for cardiac tissue engineering, *Journal of Biomechanics* 43(15) (2010) 3035-3043.

- [143] J.M. Kemppainen, S.J. Hollister, Tailoring the mechanical properties of 3D-designed poly(glycerol sebacate) scaffolds for cartilage applications, *Journal of Biomedical Materials Research Part A* 94A(1) (2010) 9-18.
- [144] C.L.E. Nijst, J.P. Bruggeman, J.M. Karp, L. Ferreira, A. Zumbuehl, C.J. Bettinger, R. Langer, Synthesis and Characterization of Photocurable Elastomers from Poly(glycerol-co-sebacate), *Biomacromolecules* 8(10) (2007) 3067-3073.
- [145] S. Pashneh-Tala, R. Owen, H. Bahmaee, S. Rekštytė, M. Malinauskas, F. Claeysens, Synthesis, Characterization and 3D Micro-Structuring via 2-Photon Polymerization of Poly(glycerol sebacate)-Methacrylate—An Elastomeric Degradable Polymer, *Frontiers in Physics* 6(41) (2018).
- [146] M. Frydrych, S. Roman, S. MacNeil, B. Chen, Biomimetic poly(glycerol sebacate)/poly(L-lactic acid) blend scaffolds for adipose tissue engineering, *Acta biomaterialia* 18 (2014) 40-49.
- [147] M.J. Pereira, B. Ouyang, C.A. Sundback, N. Lang, I. Friehs, S. Mureli, I. Pomerantseva, J. McFadden, M.C. Mochel, O. Mwizerwa, P. Del Nido, D. Sarkar, P.T. Masiakos, R. Langer, L.S. Ferreira, J.M. Karp, A highly tunable biocompatible and multifunctional biodegradable elastomer, *Adv Mater* 25(8) (2013) 1209-15.
- [148] M. Frydrych, B. Chen, Fabrication, structure and properties of three-dimensional biodegradable poly(glycerol sebacate urethane) scaffolds, *Polymer* 122 (2017) 159-168.
- [149] K. Scoffin, *Scalling the Scaffolds: Control of Pore Size in Tissue Engineering Scaffolds*, (2011).
- [150] G. Chen, T. Ushida, T. Tateishi, *Scaffold Design for Tissue Engineering*, *Macromolecular Bioscience* 2 (2002) 67-77.

- [151] K. Whang, K.E. Healy, D.R. Elenz, E.K. Nam, D.C. Tsai, C.H. Thomas, G.W. Nuber, F.H. Glorieux, R. Travers, S.M. Sprague, Engineering bone regeneration with bioabsorbable scaffolds with novel microarchitecture, *Tissue Eng* 5(1) (1999) 35-51.
- [152] A. Abdal-ha, S. Hamlet, S. Ivanovski, Fabrication of a thick three-dimensional scaffold with an open cellular-like structure using airbrushing and thermal cross-linking of molded short nanofibers, *Biofabrication* 11(1) (2018) 015006.
- [153] A. Abdal-hay, F.A. Sheikh, J.K. Lim, Air jet spinning of hydroxyapatite/poly(lactic acid) hybrid nanocomposite membrane mats for bone tissue engineering, *Colloids and surfaces. B, Biointerfaces* 102 (2013) 635-43.
- [154] A. Abdal-Hay, A.S. Hamdy, K.A. Khalil, J.H. Lim, A novel simple one-step air jet spinning approach for deposition of poly(vinyl acetate)/hydroxyapatite composite nanofibers on Ti implants, *Materials science & engineering. C, Materials for biological applications* 49 (2015) 681-690.
- [155] A. Abdal-Hay, N.A.M. Barakat, J.K. Lim, Novel Technique for Polymeric Nanofibers Preparation: Air Jet Spinning, *Science of Advanced Materials* 4(12) (2012) 1268-1275.
- [156] A. Abdal-Hay, K.H. Hussein, L. Casettari, K.A. Khalil, A.S. Hamdy, Fabrication of novel high performance ductile poly(lactic acid) nanofiber scaffold coated with poly(vinyl alcohol) for tissue engineering applications, *Materials science & engineering. C, Materials for biological applications* 60 (2016) 143-150.
- [157] C. Agarwal, B.T. Kumar, D.S. Mehta, An acellular dermal matrix allograft (Alloderm(®)) for increasing keratinized attached gingiva: A case series, *Journal of Indian Society of Periodontology* 19(2) (2015) 216-220.



- [158] N. Masoumi, A. Jean, J.T. Zugates, K.L. Johnson, G.C. Engelmayer, Laser Microfabricated Poly(glycerol Sebacate) Scaffolds for Heart Valve Tissue Engineering, *Journal of biomedical materials research. Part A* 101(1) (2013) 104-114.
- [159] Z. Dai, J. Ronholm, Y. Tian, B. Sethi, X. Cao, Sterilization techniques for biodegradable scaffolds in tissue engineering applications, *Journal of Tissue Engineering* 7 (2016) 2041731416648810.
- [160] T. Wu, M. Frydrych, K. O'Kelly, B. Chen, Poly(glycerol sebacate urethane) - Cellulose Nanocomposites with Water-Active Shape-Memory Effects, *Biomacromolecules* 15 (2014) 2663-2671.
- [161] N.P. Cheremisinoff, 1 - CHROMATOGRAPHIC TECHNIQUES, *Polymer Characterization*, William Andrew Publishing, Westwood, NJ, 1996, pp. 1-15.
- [162] P.R. Lewis, C. Gagg, 2 - Examination and analysis of failed components, *Forensic Polymer Engineering*, Woodhead Publishing 2010, pp. 42-88.
- [163] Q.L. Loh, C. Choong, Three-Dimensional Scaffolds for Tissue Engineering Applications: Role of Porosity and Pore Size, *Tissue Engineering. Part B, Reviews* 19(6) (2013) 485-502.
- [164] S.-L. Liang, X.-Y. Yang, X.-Y. Fang, W.D. Cook, G.A. Thouas, Q.-Z. Chen, In Vitro enzymatic degradation of poly (glycerol sebacate)-based materials, *Biomaterials* 32(33) (2011) 8486-8496.
- [165] A. Buettner, Influence of Human Salivary Enzymes on Odorant Concentration Changes Occurring in Vivo. 1. Esters and Thiols, *Journal of Agricultural and Food Chemistry* 50(11) (2002) 3283-3289.
- [166] Y. Gargouri, G. Pieroni, C. Riviere, J.F. Saunier, P.A. Lowe, L. Sarda, R. Verger, Kinetic assay of human gastric lipase on short- and long-chain triacylglycerol emulsions, *Gastroenterology* 91(4) (1986) 919-25.

- [167] S. Jasdanwala, M. Babyatsky, A critical evaluation of serum lipase and amylase as diagnostic tests for acute pancreatitis, *Integrative Molecular Medicine* 2(3) (2015).
- [168] W. Wang, G. Caetano, W.S. Ambler, J.J. Blaker, M.A. Frade, P. Mandal, C. Diver, P. Bártolo, Enhancing the Hydrophilicity and Cell Attachment of 3D Printed PCL/Graphene Scaffolds for Bone Tissue Engineering, *Materials (Basel, Switzerland)* 9(12) (2016) 992.
- [169] F. Pennella, G. Cerino, D. Massai, D. Gallo, G. Falvo D'Urso Labate, A. Schiavi, M.A. Deriu, A. Audenino, U. Morbiducci, A Survey of Methods for the Evaluation of Tissue Engineering Scaffold Permeability, *Annals of Biomedical Engineering* 41(10) (2013) 2027-2041.
- [170] T.L. Riss, R.A. Moravec, A.L. Niles, H.A. Benink, T.J. Worzella, L. Minor, Cell Viability Assays, in: G.S. Sittampalam, N.P. Coussens, H. Nelson, M. Arkin, D. Auld, C. Austin, B. Bejcek, M. Glicksman, J. Inglese, P.W. Iversen, Z. Li, J. McGee, O. McManus, L. Minor, A. Napper, J.M. Peltier, T. Riss, O.J. Trask, Jr., J. Weidner (Eds.), *Assay Guidance Manual*, Bethesda (MD), 2004, pp. 1-31.
- [171] J. O'Brien, I. Wilson, T. Orton, F. Pognan, Investigation of the Alamar Blue (resazurin) fluorescent dye for the assessment of mammalian cell cytotoxicity *European Journal of Biochemistry* Volume 267, Issue 17, *European Journal of Biochemistry*, 2000, pp. 5421-5426.
- [172] I.H. Jaafar, M.M. Ammar, S.S. Jedlicka, R.A. Pearson, J.P. Coulter, Spectroscopic evaluation, thermal, and thermomechanical characterization of poly(glycerol-sebacate) with variations in curing temperatures and durations, *Journal of Materials Science* 45(9) (2010) 2525-2529.
- [173] L.L. Liu, F.C. Yi, W. Cai, Synthesis and Shape Memory Effect of Poly (glycerol-sebacate) Elastomer, *Adv Mater Res-Switz* 476-478 (2012) 2141-+.

- [174] K. Vizárová, D. Bakoš, M. Reháková, M. Petříková, E. Panáková, J. Koller, Modification of layered atelocollagen: enzymatic degradation and cytotoxicity evaluation, *Biomaterials* 16(16) (1995) 1217-1221.
- [175] G.R. da Silva, A. da Silva-Cunha, F. Behar-Cohen, E. Ayres, R.L. Oréfice, Biodegradation of polyurethanes and nanocomposites to non-cytotoxic degradation products, *Polymer Degradation and Stability* 95(4) (2010) 491-499.
- [176] H.J. Wang, J. Pieper, F. Peters, C.A. van Blitterswijk, E.N. Lamme, Synthetic scaffold morphology controls human dermal connective tissue formation, *Journal of Biomedical Materials Research Part A* 74A(4) (2005) 523-532.
- [177] Y. Fukano, M.L. Usui, R.A. Underwood, S. Isenath, A.J. Marshall, K.D. Hauch, B.D. Ratner, J.E. Olerud, P. Fleckman, Epidermal and dermal integration into sphere-templated porous poly(2-hydroxyethyl methacrylate) implants in mice, *Journal of Biomedical Materials Research Part A* 94A(4) (2010) 1172-1186.
- [178] N. Davidenko, T. Gibb, C. Schuster, S.M. Best, J.J. Campbell, C.J. Watson, R.E. Cameron, Biomimetic collagen scaffolds with anisotropic pore architecture, *Acta Biomaterialia* 8(2) (2012) 667-676.
- [179] S.H. Oh, T.H. Kim, G.I. Im, J.H. Lee, Investigation of Pore Size Effect on Chondrogenic Differentiation of Adipose Stem Cells Using a Pore Size Gradient Scaffold, *Biomacromolecules* 11(8) (2010) 1948-1955.
- [180] D.J. Griffon, M.R. Sedighi, D.V. Schaeffer, J.A. Eurell, A.L. Johnson, Chitosan scaffolds: Interconnective pore size and cartilage engineering, *Acta Biomaterialia* 2(3) (2006) 313-320.
- [181] B.B. Mandal, S.C. Kundu, Cell proliferation and migration in silk fibroin 3D scaffolds, *Biomaterials* 30(15) (2009) 2956-2965.

- [182] K.M. Pawelec, H.A. van Boxtel, S.G.J.M. Kluijtmans, Ice-templating of anisotropic structures with high permeability, *Materials Science and Engineering: C* 76 (2017) 628-636.
- [183] X. Song, C.H. Zhu, D.D. Fan, Y. Mi, X. Li, R.Z. Fu, Z.G. Duan, Y. Wang, R.R. Feng, A Novel Human-Like Collagen Hydrogel Scaffold with Porous Structure and Sponge-Like Properties, *Polymers-Basel* 9(12) (2017).
- [184] H. Shearer, M.J. Ellis, S.P. Perera, J.B. Chaudhuri, Effects of common sterilization methods on the structure and properties of poly(D,L lactic-co-glycolic acid) scaffolds, *Tissue Eng* 12(10) (2006) 2717-27.
- [185] F.R. Rozema, R.R. Bos, G. Boering, J.A. van Asten, A.J. Nijenhuis, A.J. Pennings, The effects of different steam-sterilization programs on material properties of poly(L-lactide), *Journal of applied biomaterials : an official journal of the Society for Biomaterials* 2(1) (1991) 23-8.
- [186] F.J. O'Brien, B.A. Harley, I.V. Yannas, L.J. Gibson, The effect of pore size on cell adhesion in collagen-GAG scaffolds, *Biomaterials* 26(4) (2005) 433-41.
- [187] T.G. van Tienen, R.G.J.C. Heijkants, P. Buma, J.H. de Groot, A.J. Pennings, R.P.H. Veth, Tissue ingrowth and degradation of two biodegradable porous polymers with different porosities and pore sizes, *Biomaterials* 23(8) (2002) 1731-1738.
- [188] S.J. Hollister, Porous scaffold design for tissue engineering, *Nat Mater* 4(7) (2005) 518-24.
- [189] H. Tullberg-Reinert, G. Jundt, In situ measurement of collagen synthesis by human bone cells with a sirius red-based colorimetric microassay: effects of transforming growth factor beta2 and ascorbic acid 2-phosphate, *Histochemistry and cell biology* 112(4) (1999) 271-6.

- [190] T. Huynh, G. Abraham, J. Murray, K. Brockbank, P.-O. Hagen, S. Sullivan, Remodeling of an acellular collagen graft into a physiologically responsive neovessel, *Nat Biotech* 17(11) (1999) 1083-1086.
- [191] F.J. O'Brien, B.A. Harley, M.A. Waller, I.V. Yannas, L.J. Gibson, P.J. Prendergast, The effect of pore size on permeability and cell attachment in collagen scaffolds for tissue engineering, *Technol Health Care* 15(1) (2007) 3-17.
- [192] B. Elvers, G. Bellussi, *Ullmann's encyclopedia of industrial chemistry*, 7th, completely rev. ed., Wiley-VCH, Weinheim, 2011.
- [193] K.M. Pawelec, A. Husmann, S.M. Best, R.E. Cameron, A design protocol for tailoring ice-templated scaffold structure, *J R Soc Interface* 11(92) (2014) 20130958.
- [194] K.M. Pawelec, A. Husmann, S.M. Best, R.E. Cameron, Altering crystal growth and annealing in ice-templated scaffolds, *Journal of Materials Science* 50(23) (2015) 7537-7543.
- [195] Q. Hou, D.W. Grijpma, J. Feijen, Preparation of interconnected highly porous polymeric structures by a replication and freeze-drying process, *J Biomed Mater Res B Appl Biomater* 67(2) (2003) 732-40.
- [196] F.H. Silver, D.L. Christiansen, C.M. Buntin, Mechanical properties of the aorta: a review, *Critical reviews in biomedical engineering* 17(4) (1989) 323-58.
- [197] G. Holzapfel, *Biomechanics of Soft Tissue*, 2001, pp. 1049-1063.
- [198] Y.C. Yeh, C.B. Highley, L. Ouyang, J.A. Burdick, 3D printing of photocurable poly(glycerol sebacate) elastomers, *Biofabrication* 8(4) (2016) 045004.
- [199] H. Azevedo, R. Reis, *Understanding the Enzymatic Degradation of Biodegradable Polymers and Strategies to Control Their Degradation Rate*, *Biodegradable Systems in Tissue Engineering and Regenerative Medicine*, CRC Press 2004, pp. 177-197.

- [200] W. Cui, X. Li, X. Zhu, G. Yu, S. Zhou, J. Weng, Investigation of drug release and matrix degradation of electrospun poly(DL-lactide) fibers with paracetamol inoculation, *Biomacromolecules* 7(5) (2006) 1623-9.
- [201] J. Sottile, D.C. Hocking, P.J. Swiatek, Fibronectin matrix assembly enhances adhesion-dependent cell growth, *Journal of Cell Science* 111 (1998) 2933-2943.
- [202] R.A. Freitas, *Nanomedicine*, Landes Bioscience, Austin, TX, 1999.
- [203] S. Sant, D. Iyer, A.K. Gaharwar, A. Patel, A. Khademhosseini, Effect of biodegradation and de novo matrix synthesis on the mechanical properties of valvular interstitial cell-seeded polyglycerol sebacate-polycaprolactone scaffolds, *Acta Biomater* 9(4) (2013) 5963-73.
- [204] S. Roman, A. Mangera, N.I. Osman, A.J. Bullock, C.R. Chapple, S. MacNeil, Developing a tissue engineered repair material for treatment of stress urinary incontinence and pelvic organ prolapse-which cell source?, *Neurourol Urodyn* 33(5) (2014) 531-7.
- [205] C. Frantz, K.M. Stewart, V.M. Weaver, The extracellular matrix at a glance, *Journal of Cell Science* 123 (2010) 4195-4200.
- [206] S. Pal, *Design of Artificial Human Joints & Organs*, Springer US2014.
- [207] J.H.C. Wang, F. Jia, T.W. Gilbert, S.L.Y. Woo, Cell orientation determines the alignment of cell-produced collagenous matrix, *Journal of Biomechanics* 36(1) (2003) 97-102.
- [208] S. Deville, E. Saiz, A.P. Tomsia, Freeze casting of hydroxyapatite scaffolds for bone tissue engineering, *Biomaterials* 27(32) (2006) 5480-9.
- [209] M.C. Gutierrez, Z.Y. Garcia-Carvajal, M. Jobbagy, T. Rubio, L. Yuste, F. Rojo, M.L. Ferrer, F. del Monte, Poly(vinyl alcohol) scaffolds with tailored morphologies for drug delivery and controlled release, *Adv Funct Mater* 17(17) (2007) 3505-3513.

- [210] X.X. Hu, H. Shen, F. Yang, J.Z. Bei, S.G. Wang, Preparation and cell affinity of microtubular orientation-structured PLGA(70/30) blood vessel scaffold, *Biomaterials* 29(21) (2008) 3128-3136.
- [211] X. Wu, Y. Liu, X. Li, P. Wen, Y. Zhang, Y. Long, X. Wang, Y. Guo, F. Xing, J. Gao, Preparation of aligned porous gelatin scaffolds by unidirectional freeze-drying method, *Acta Biomaterialia* 6(3) (2010) 1167-1177.
- [212] R.A. Neal, A. Jean, H. Park, P.B. Wu, J. Hsiao, G.C. Engelmayr, R. Langer, L.E. Freed, Three-Dimensional Elastomeric Scaffolds Designed with Cardiac-Mimetic Structural and Mechanical Features, *Tissue Engineering Part A* 19(5-6) (2012) 793-807.
- [213] M.J.W. Koens, K.A. Faraj, R.G. Wismans, J.A. van der Vliet, A.G. Krasznai, V.M.J.I. Cuijpers, J.A. Jansen, W.F. Daamen, T.H. van Kuppevelt, Controlled fabrication of triple layered and molecularly defined collagen/elastin vascular grafts resembling the native blood vessel, *Acta Biomaterialia* 6(12) (2010) 4666-4674.
- [214] M.A. Dickson, W.C. Hahn, Y. Ino, V. Ronfard, J.Y. Wu, R.A. Weinberg, D.N. Louis, F.P. Li, J.G. Rheinwald, Human Keratinocytes That Express hTERT and Also Bypass a p16(INK4a)-Enforced Mechanism That Limits Life Span Become Immortal yet Retain Normal Growth and Differentiation Characteristics, *Molecular and Cellular Biology* 20(4) (2000) 1436-1447.
- [215] F. Bisson, E. Rochefort, A. Lavoie, D. Larouche, K. Zaniolo, C. Simard-Bisson, O. Damour, F.A. Auger, S.L. Guérin, L. Germain, Irradiated human dermal fibroblasts are as efficient as mouse fibroblasts as a feeder layer to improve human epidermal cell culture lifespan, *International journal of molecular sciences* 14(3) (2013) 4684-4704.
- [216] S.M. Stocks, Mechanism and use of the commercially available viability stain, BacLight, *Cytometry Part A* 61A(2) (2004) 189-195.

- [217] L.A. Solchaga, E. Tognana, K. Penick, H. Baskaran, V.M. Goldberg, A.I. Caplan, J.F. Welter, A Rapid Seeding Technique for the Assembly of Large Cell/Scaffold Composite Constructs, *Tissue engineering* 12(7) (2006) 1851-1863.
- [218] H. Zhang, I. Hussain, M. Brust, M.F. Butler, S.P. Rannard, A.I. Cooper, Aligned two- and three-dimensional structures by directional freezing of polymers and nanoparticles, *Nature Materials* 4 (2005) 787.
- [219] S. Jana, S.K.L. Levengood, M.Q. Zhang, Anisotropic Materials for Skeletal-Muscle-Tissue Engineering, *Adv Mater* 28(48) (2016) 10588-10612.
- [220] B.J. Papenburg, J. Liu, G.A. Higuera, A.M.C. Barradas, J. de Boer, C.A. van Blitterswijk, M. Wessling, D. Stamatialis, Development and analysis of multi-layer scaffolds for tissue engineering, *Biomaterials* 30(31) (2009) 6228-6239.
- [221] T.J. Levingstone, A. Matsiko, G.R. Dickson, F.J. O'Brien, J.P. Gleeson, A biomimetic multi-layered collagen-based scaffold for osteochondral repair, *Acta Biomaterialia* 10(5) (2014) 1996-2004.
- [222] T. Knight, J. Basu, E.A. Rivera, T. Spencer, D. Jain, R. Payne, Fabrication of a multi-layer three-dimensional scaffold with controlled porous micro-architecture for application in small intestine tissue engineering, *Cell Adhesion & Migration* 7(3) (2013) 267-274.
- [223] G. Chen, T. Sato, J. Tanaka, T. Tateishi, Preparation of a biphasic scaffold for osteochondral tissue engineering, *Materials Science and Engineering: C* 26(1) (2006) 118-123.
- [224] L.S. Chan, Human skin basement membrane in health and in autoimmune diseases, *Frontiers in Bioscience* (1093-9946 (Print)) (1997).



- [225] Ralston, Layton, Dalley, Boyce, Freedlander, M.A.C. Neil, The requirement for basement membrane antigens in the production of human epidermal/dermal composites in vitro, *British Journal of Dermatology* 140(4) (1999) 605-615.
- [226] O.K. Vintermyr, D.E. Costea, L.L. Loro, E.A.O. Dimba, A.C. Johannessen, Crucial Effects of Fibroblasts and Keratinocyte Growth Factor on Morphogenesis of Reconstituted Human Oral Epithelium, *Journal of Investigative Dermatology* 121(6) (2003) 1479-1486.
- [227] G. Goessel, M. Quante, W.C. Hahn, H. Harada, S. Heeg, Y. Suliman, M. Doebele, A. von Werder, C. Fulda, H. Nakagawa, A.K. Rustgi, H.E. Blum, O.G. Opitz, Creating oral squamous cancer cells: A cellular model of oral–esophageal carcinogenesis, *Proceedings of the National Academy of Sciences of the United States of America* 102(43) (2005) 15599-15604.
- [228] J. Walladbegi, S.A. Smith, A.K. Grayson, C. Murdoch, M. Jontell, H.E. Colley, Cooling of the oral mucosa to prevent adverse effects of chemotherapeutic agents: An in vitro study, *Journal of Oral Pathology & Medicine* 0(0) (2018).
- [229] V. Hearnden, H. Lomas, S. Macneil, M. Thornhill, C. Murdoch, A. Lewis, J. Madsen, A. Blanzs, S. Armes, G. Battaglia, Diffusion studies of nanometer polymersomes across tissue engineered human oral mucosa, *Pharmaceutical research* 26(7) (2009) 1718-28.
- [230] A.M. Wojtowicz, S. Oliveira, M.W. Carlson, A. Zawadzka, C.F. Rousseau, D. Baksh, The importance of both fibroblasts and keratinocytes in a bilayered living cellular construct used in wound healing, *Wound Repair and Regeneration* 22(2) (2014) 246-255.
- [231] L.R. Jennings, H.E. Colley, J. Ong, F. Panagakos, J.G. Masters, H.M. Trivedi, C. Murdoch, S. Whawell, Development and Characterization of In Vitro Human Oral

Mucosal Equivalents Derived from Immortalized Oral Keratinocytes, *Tissue Eng Part C-Me* 22(12) (2016) 1108-1117.

[232] N.D. Evans, E. Gentleman, J.M. Polak, Scaffolds for stem cells, *Materials Today* 9(12) (2006) 26-33.